UNIVERSITY OF SOUTHAMPTON

Faculty of Natural and Environmental Sciences

School of Ocean and Earth Science

Assessing the magnitude of anthropogenic ocean warming and ocean acidification using the novel Li/Mg-SST and δ^{11}B-pH proxies in the Caribbean coral *Siderastrea siderea*

by

Sara E. Fowell

Thesis for the degree of Doctor of Philosophy

September 2016

“We have become frighteningly effective at altering nature”

Sylvia Earle

UNIVERSITY OF SOUTHAMPTON

ABSTRACT

FACULTY OF NATURAL AND ENVIRONMENTAL SCIENCES

SCHOOL OF OCEAN AND EARTH SCIENCE

Thesis for the degree of Doctor of Philosophy

ASSESSING THE MAGNITUDE OF ANTHROPOGENIC OCEAN WARMING AND OCEAN ACIDIFICATION USING THE NOVEL Li/Mg-SST AND δ^{11}B-pH PROXIES IN THE CARIBBEAN CORAL *SIDERASTREA SIDEREA*

Sara Elisabeth Fowell

Coral reefs are highly sensitive ecosystems becoming increasingly damaged by anthropogenic climate change and pollution, particularly in the form of ocean warming, ocean acidification, and chronic sedimentation. In order for us to project how coral reefs will respond to future climate change, it is imperative to determine how they have responded to anthropogenic changes to date. This is a difficult task given that *in situ* observations of sea surface temperature (SST) and pH ($-\log_{10}[H]^{+}$) are short and sparse prior to recent decades. However, coral skeletons are archives of historic climate and environmental conditions, storing over century-long records at sub-annual resolutions. These archives can be unlocked by calibrating geochemical proxies against modern *in situ* observations. For instance, the Sr/Ca ratios of tropical coral skeletons are traditionally used to reconstruct historic SST changes, yet the accuracy of this proxy is debated, leading to recent investigations into the Li/Mg-SST proxy which has produced promising results. However, by investigating this proxy for the first time in the Caribbean reef-building coral *Siderastrea siderea*, it has been found that the Li/Mg ratio of colonies from the forereef zone are three times more sensitive to changes in SST than their backreef coral counterparts. This resulted in accurate reconstructions of SST in the forereef, but unfeasible SSTs in the backreef, suggesting a secondary influence on both the Li/Mg- and Sr/Ca-SST proxies. A combined field and laboratory study confirmed that these ratios are also sensitive to pH change, but the full variability in Li/Mg and Sr/Ca is not described by pH and SST change combined.

Long-term records of seawater pH in Belize reconstructed from the boron isotopic composition (δ^{11}B) of *S. siderea* showed that forereef corals, which have declining skeletal extension rates, have not been exposed to significant long-term ocean acidification. This contrasts with the ~0.15 pH unit decrease observed in the backreef since the 1920s, despite a lack of evidence of declining extension in this reef zone. Sub-annual δ^{11}B records revealed that seasonal pH cycles in these two reef zones are controlled by two different parameters.

Chronic and increasing sedimentation in the forereef from terrestrial sources implies that nutrification in this region is stimulating macroalgae production, and thus buffering against ocean acidification.

Corals are therefore suitable archives of historic climate that can be used to reconstruct multiple environmental parameters such as sea surface temperature and pH. The structure and longevity of coral skeletons allows changes in these environmental parameters to be assessed at monthly to century-long scales. However, although it is possible to use geochemical proxies from coral, the full extent of additional influences on such proxies are not yet fully quantified and therefore may not be suitable to use in all coral reefs.

Table of Contents

List of Tables

List of Figures

DECLARATION OF AUTHORSHIP

I, Sara Elisabeth Fowell, declare that this thesis "Assessing the magnitude of anthropogenic ocean warming and ocean acidification using the novel Li/Mg-SST and δ^{11}B-pH proxies in the Caribbean coral *Siderastrea siderea*" and the work presented in it are my own and has been generated by me as the result of my own original research.

I confirm that:

1. This work was done wholly or mainly while in candidature for a research degree at this University;
2. Where any part of this thesis has previously been submitted for a degree or any other qualification at this University or any other institution, this has been clearly stated;
3. Where I have consulted the published work of others, this is always clearly attributed;
4. Where I have quoted from the work of others, the source is always given. With the exception of such quotations, this thesis is entirely my own work;
5. I have acknowledged all main sources of help;
6. Where the thesis is based on work done by myself jointly with others, I have made clear exactly what was done by others and what I have contributed myself;
7. None of this work has been published before submission

Signed: .....

Date: .....

Acknowledgements

Firstly, I would like to thank my supervisor Gavin Foster for giving me the opportunity to study this PhD after excitedly turning up at his office immediately after seeing the advert to study the geochemistry of corals from Belize, a country that captured my heart years before embarking on this project. In particular, I have appreciated Gavin's patience, constructive advice, and personality. I would also like to thank the rest of my supervisors Justin Ries, Karl Castillo, Andrew Yool, Martin Palmer and Toby Tyrrell for their insight and encouragement. I would also like to thank my examiners Joerg Weidenmann and Ed Hathorne for being so accommodating with my tight schedule! I have been very fortunate to receive funding from NERC and GSNOCS for this PhD, but also from the Geochemistry Group and the University of Washington for travel grants to various conferences.

I have been extremely fortunate to be part of a large geochemistry group at NOC, and in particular, part of the infamous B-Team. The wealth of knowledge I gained from the B-Team is priceless, and without their support and reassurance I never would have got to the point of writing this acknowledgement section! I would like to thank Joe Stewart for taking on the challenge of mentoring me in the clean labs and data processing; Eleni Anagnostou for quality control and providing a 24 hour mass spec hotline; Hannah Donald for emotional support, and a helping hand with a smiling face when I overstretched myself; Elwyn de la Vega for help measuring samples and providing good company in the lab. I'd also like to thank past members Rosanna, Michael and Tom for help in the early days. Thanks to Kate for being a brilliant Masters student. I'd like to thank Andy Milton (mass spec wizard!) for all his time and patience teaching me to use the Element, and his monumental effort in keeping the mass spec lab functioning; likewise to Matt Cooper and Agnes Michalik in the clean labs.

During my time at NOC I have truly made friends for life, and I couldn't have wished to meet a better group of people: Padwell Rd. crew, Tim, Pierre - thanks for the laughs and banter, the cuddles, the company and the cans. "And that's not all!". Special thanks to James Fielding who has put up with me over the last couple of years, you've done a great job of looking after me, and I'll never forget the time dinner was waiting on the table for me after a 2 am Neptune finish.

Thanks to the staff at BIOS for helping to organise and implement my Bermuda coral sampling mission – Sam de Putron, Dready, Tim Noyes, and Nick Bates. Thanks to Bob, John and Dan (DD) for their help with choosing a drill and a core bit. Thanks to Darren

Rayner for taking me on the RAPID cruise - I appreciated both the change of scenery and the chance to learn new skills.

Thanks to all the unwitting suspects who have read various parts of this thesis – Stu, Tom, Kelsey, Colleen, James, Laura. Finally, I need to thank my family for providing ears at the end of the phone, chocolate packages in the post, and my sister for help and humour at the other end of an email.

Chapter 1: Introduction to climate change, coral reefs and palaeoproxies

Coral reefs are the largest and most vulnerable bioconstruction in the world (Figure 1-1) and have been shown to accumulate at a mean rate of 3-6 kg $CaCO_3$ m^{-2} y^{-1} (*Barnes and Devereux*, 1984). They cover an area of 284,300 km^2 (0.1% of the ocean floor; *Spalding et al.*, 2001) which hundreds of thousands of species call home (~25% of all marine species; *Hoegh-Guldberg*, 1999, *Burke et al.*, 2011). Coral reefs provide numerous ecosystem services including coastal protection, fisheries enhancement, and recreational use, all of which are estimated to directly contribute almost US$30 billion y^{-1} to the global economy (*Cesar et al.*, 2003), indirectly supporting and protecting ~500 million people, 30 million of whom are fully dependent on such ecosystem services (*Wilkinson*, 2008). By 2008, a minimum of 27% of coral had been lost, with an additional 30% of coral species facing extinction (*Cesar et al.*, 2003; *Carpenter et al.*, 2008; *Wilkinson*, 2008), and some coral reefs are losing 2% of their cover each year (*Bruno and Selig*, 2007). Allowing the loss and destruction of coral reefs to anthropogenic climate change, unsustainable fishing and land-based pollution is damaging to both the environment and the economy. *Bryant et al.*, (1998) estimated that losing 58% of the world's total coral reefs would cause a loss of $90 billion in the tourist sector alone.

Figure 1-1. Eagle ray swimming over the coral reef at Long Caye, Belize. Image credit: XL Catlin Seaview Survey.

The synergistic effects of anthropogenic stressors such as climate change, pollution, over-fishing and land-based activities are degrading the remaining coral reefs in terms of reef structure, species diversity and species abundance. Western Atlantic reefs are currently displaying the highest levels of degradation of up to 80%, although all reefs worldwide have been negatively impacted (Figure 1-2; *Pandolfi et al.*, 2011).

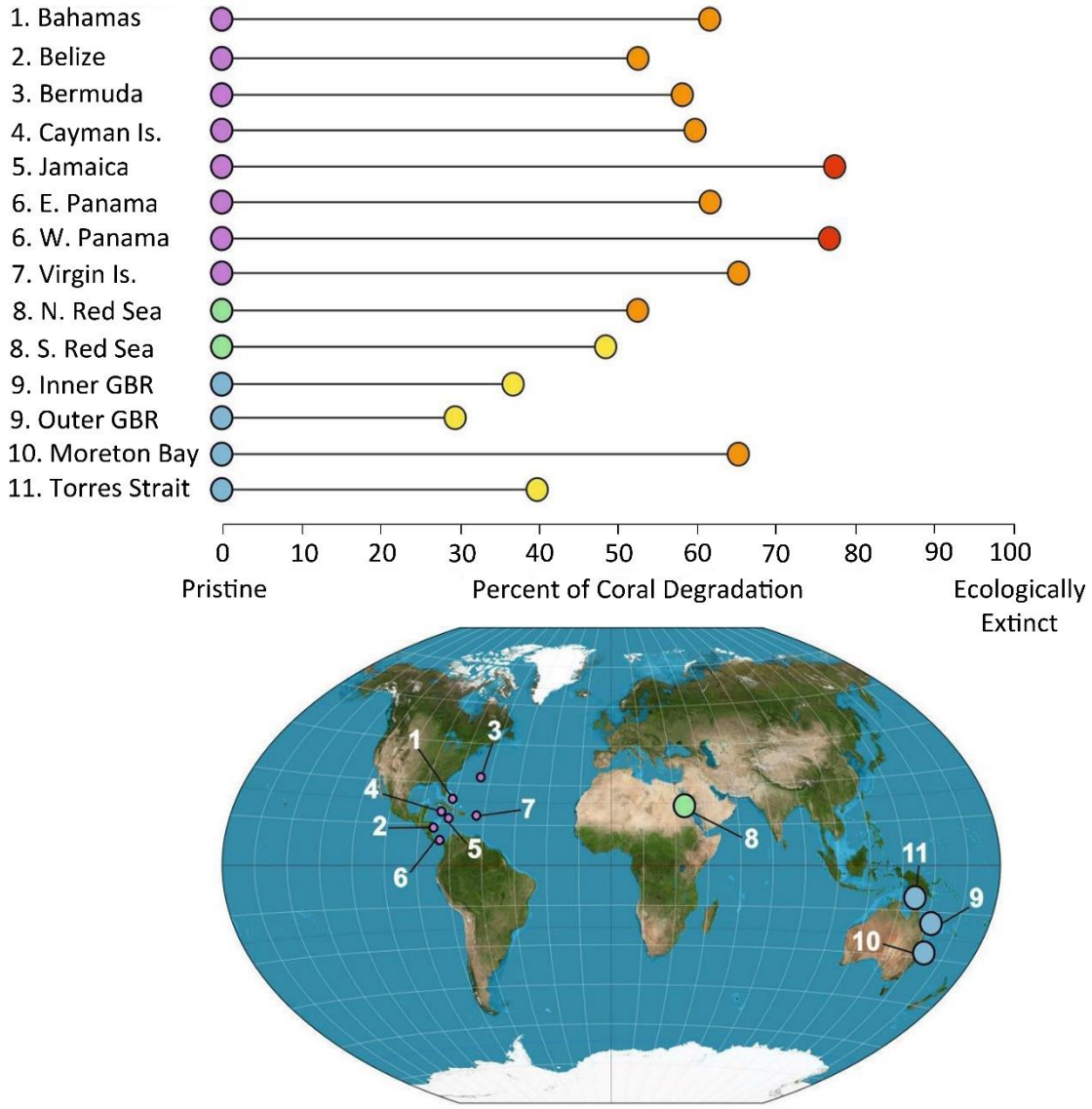

Figure 1-2. Range of reef degradation (as of 2003) across 14 regions; shown by the percentage of coral degradation in each area. The number before each region corresponds to their location on the world map. The colours in the left hand circles represent the location of each region: western Atlantic (purple); Red Sea (green); Australia (Great Barrier Reef (GBR); blue). The severity of coral degradation has also been colour coded in the right hand circles: 0-50% (yellow); 51-75% (orange); 76-100% (red). Adapted from *Pandolfi et al.*, (2003).

1.1 Global climate change

In order to fully assess and quantify the extent of the damage inflicted on delicately balanced ocean processes and ecosystems by anthropogenic climate change, a multinational research effort is under-way. Pre-industrial global mean atmospheric carbon dioxide concentrations were 280 ppm (*Raupach et al.*, 2007), but by the year 2013 they had reached 400 ppm (*Cubasch et al.*, 2013) for the first time in at least the last 800,000 years (*Lüthi et al.*, 2008), or even the last 3 million years (*Martínez-Botí et al.*, 2015). The rate of change in atmospheric CO_2 concentrations in the twentieth century was an order of magnitude greater than any observed variation in the last 22,000 years (*Steinacher et al.*, 2009) and indeed for much of geological time (*Zeebe et al.*, 2016). During this time, average combined ocean and land surface temperatures have risen by 0.85ºC (*Rhein et al.*, 2013), but different regions have warmed between 0.07 and 1.07ºC per century since 1800 AD (*Abram et al.*, 2016). Between 1971 and 2010 the global average warming in the top 75 m of the ocean was 0.11ºC per decade, but tropical regions have warmed at a faster rate of ~0.2ºC per decade (Figure 1-3; *Rhein et al.*, 2013). In extreme business-as-usual greenhouse gas emission scenarios, atmospheric CO_2 levels could rise to between 750 ppm (IPCC scenario IS92a; *IPCC*, 2007) and 1250 ppm (Representative Concentration Pathway 8.5 scenario) by the end of this century (*Keywan et al.*, 2011; *Wilcox et al.*, 2012). As a consequence of this, global climate change is having two major impacts on our oceans, both of which will be discussed in more detail: ocean warming (section 1.1.1), and ocean acidification (section 1.1.2).

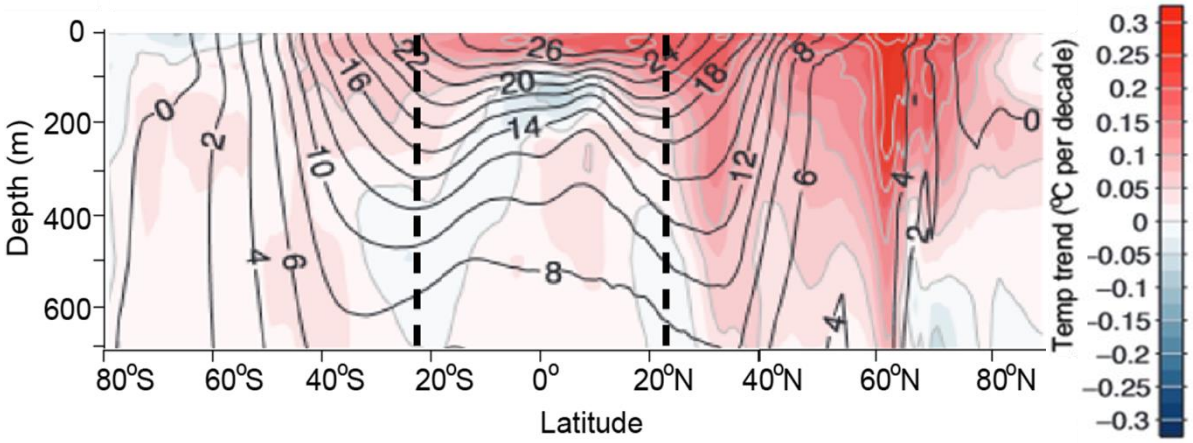

Figure 1-3. Averaged upper ocean temperature increased by an average of 0.11ºC per decade between 1971 and 2010. Zonally averaged mean temperature is shown by the black contours. With a 0.2ºC increase per decade, tropical oceans between the dashed lines experienced surface temperature changes double the mean global average. Figure adapted from *Rhein et al.*, (2013).

1.1.1 Ocean warming

Coral reefs grow in tropical and sub-tropical areas (Figure 1-4a) where the minimum sea surface temperature (SST) exceeds 18°C (*Achituv and Dubinsky*, 1990) and the typical SST range experienced by corals is 21 to 29°C (Figure 1-4b), although, some exceptional *Porites sp*. in the Persian/Arabian Gulf can withstand temperatures of up to 36°C (*Riegl et al.*, 2011; *Hume et al.*, 2013). The ocean has absorbed ~93% of the excess heat trapped by rising greenhouse gasses since 1955 resulting in a mean warming in that time of 0.18°C (*Levitus et al.*, 2012). Tropical regions experience amplified SST warming, with an increase of as much as 0.3 to 0.4°C over the last 20 to 30 years (*Kleypas et al.*, 2008). This amplification is owed to increasing atmospheric temperatures causing vertical atmospheric overturning circulation to slow down alongside a decrease in trade winds and sea level pressure gradient between the eastern and western pacific, reducing the amount of upwelling which usually cools the faster warming surface waters around the Pacific equator (Bjerknes Feedback; *Collins et al.*, 2010). While maximum SSTs in the tropics have increased by an average of 0.3–0.4°C, the warmest parts of the open ocean (where average SST > 29°C) have increased by only half that amount.

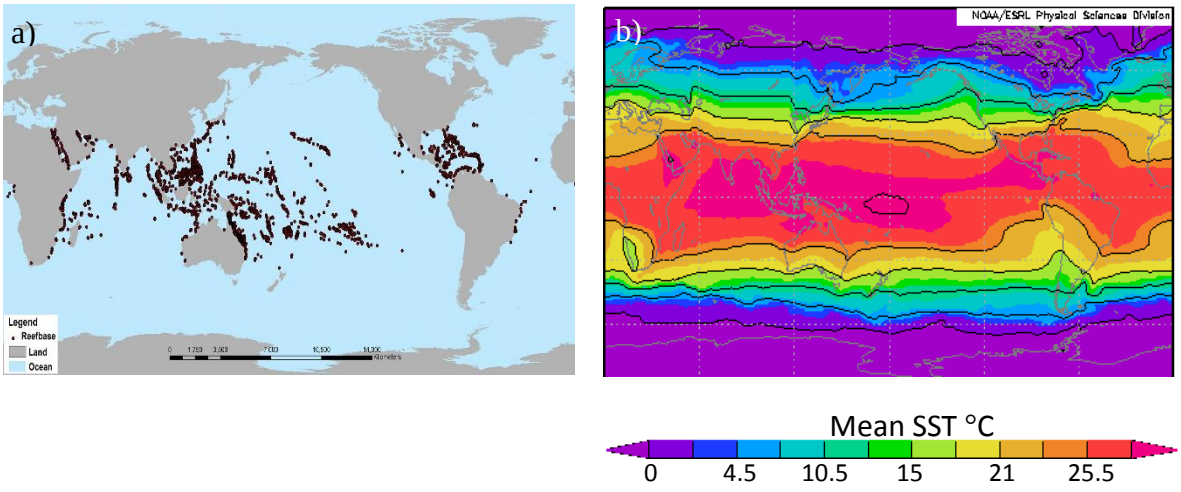

Figure 1-4. a) Global distribution of coral reefs (Image credit NOAA Ocean Service http://oceanservice.noaa.gov/facts/coralwaters.html). b) Mean annual sea surface temperatures in 2015 from the NOAA Optimum Interpolation SST V2 data set. *(Image credit Physical Sciences Division, Earth System Research Laboratory, NOAA, Boulder, Colorado, produced from* http://www.esrl.noaa.gov/psd/*).*

The major impact of ocean warming on corals is coral bleaching, which primarily occurs during periods of excessive heat and light intensity whereby the thermal tolerance of both coral and their symbiotic dinoflagellate algae (*Symbiodinium*) is exceeded (*Muscatine*, 1990; *Hoegh-Guldberg*, 1999). Coral bleaching is a process in which scleractinian coral polyps expel their symbionts (e.g.*Tchernov et al.*, 2011; *Lewis et al.*, 2016), which become toxic (e.g. by producing H_2O_2; *Shick et al.*, 1996, *Smith et al.*, 2005), causing an observed loss in colour (Figure 1-5, Figure 1-6). Corals commonly lose between 60% and 90% of their symbionts during bleaching, and the *Symbiodinium* themselves can lose between 50% and 80% of their photosynthetic pigment (*Glynn*, 1996). Without *Symbiodinium*, coral loses up to 95% of its total energy, which is usually gained through photosynthesis (*Muscatine et al.*, 1981; *Edmunds and Davies*, 1986), making it too energetically costly to calcify (*Goreau and Macfarlane*, 1990; *Leder et al.*, 1991) or reproduce (Figure 1-6; e.g. *Szmant and Gassman*, 1990). Although photosynthesis produces the carbon (carbohydrates) required to grow, coral growth is also dependant on compounds that cannot be produced by photosynthesis, such as nutrients (e.g. nitrogen, phosphorous) and proteins (amino acids) (*Muscatine and Porter*, 1977). These are gained via heterotrophic feeding by ingesting bacteria, plankton and detritus, and such heterotrophy accounts for up to 100% of carbon input when a coral is bleached (*Houlbrèque and Ferrier-Pagès*, 2009) . Each week SSTs are up to 1ºC higher than the local summer maximum is termed a 'degree heating week' (DHW). Bleaching generally occurs after four DHW (*Liu et al.*, 2003), and if DHW is prolonged for more than 8 weeks the coral can die (*Baird and Marshall*, 2002), suffer decreased colony growth, exhibit lower reproduction amongst the remaining coral (*Mendes and Woodley*, 2002) and increased susceptibility to disease (*Bruno et al.*, 2007; *Muller et al.*, 2008). Using Australia as an example, Figure 1-7 shows the correlation between SST anomalies and DHW because where the SST anomalies in Eastern Australia exceed 2°C (Figure 1-7a), the number of DHW reached up to 16 (Figure 1-7b). Once average SSTs return, corals which have not starved will become repopulated by their symbionts (providing some of the population remained in the coral during the bleaching event), and the corals will regain their colour between 4 and 74 days (*Glynn*, 1996).

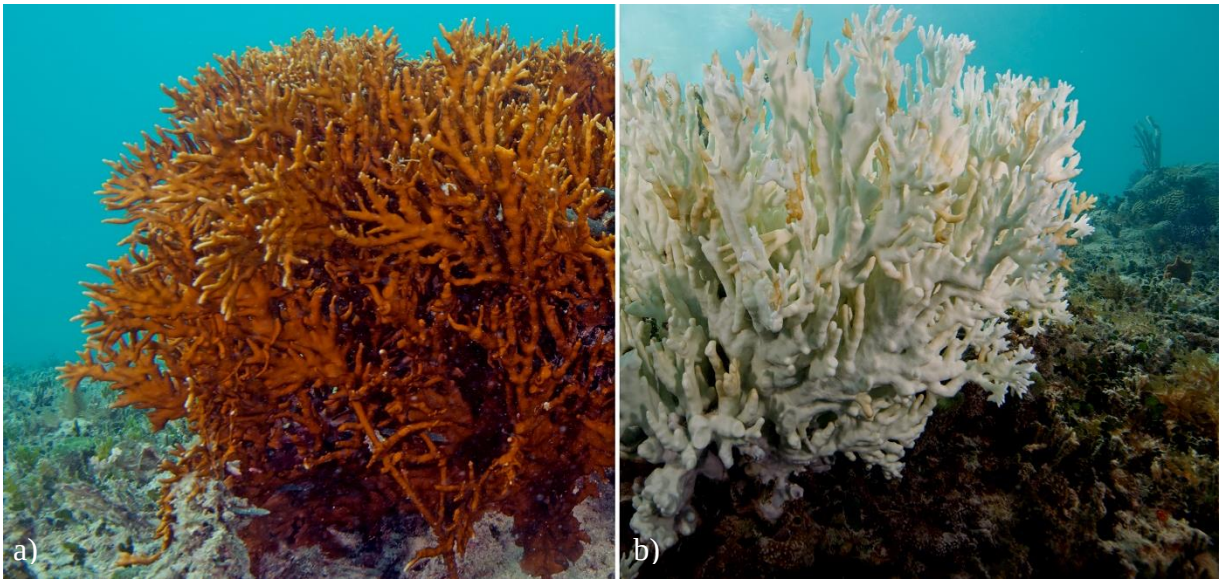

Figure 1-5. a) Healthy coral hosts coloured *Symbiodinium* dinoflagellate symbionts. b) When corals exceed their thermal tolerance, they expel these algae from the tissue layer and the white skeleton underneath can be seen . Image credit: XL Catlin Seaview Survey.

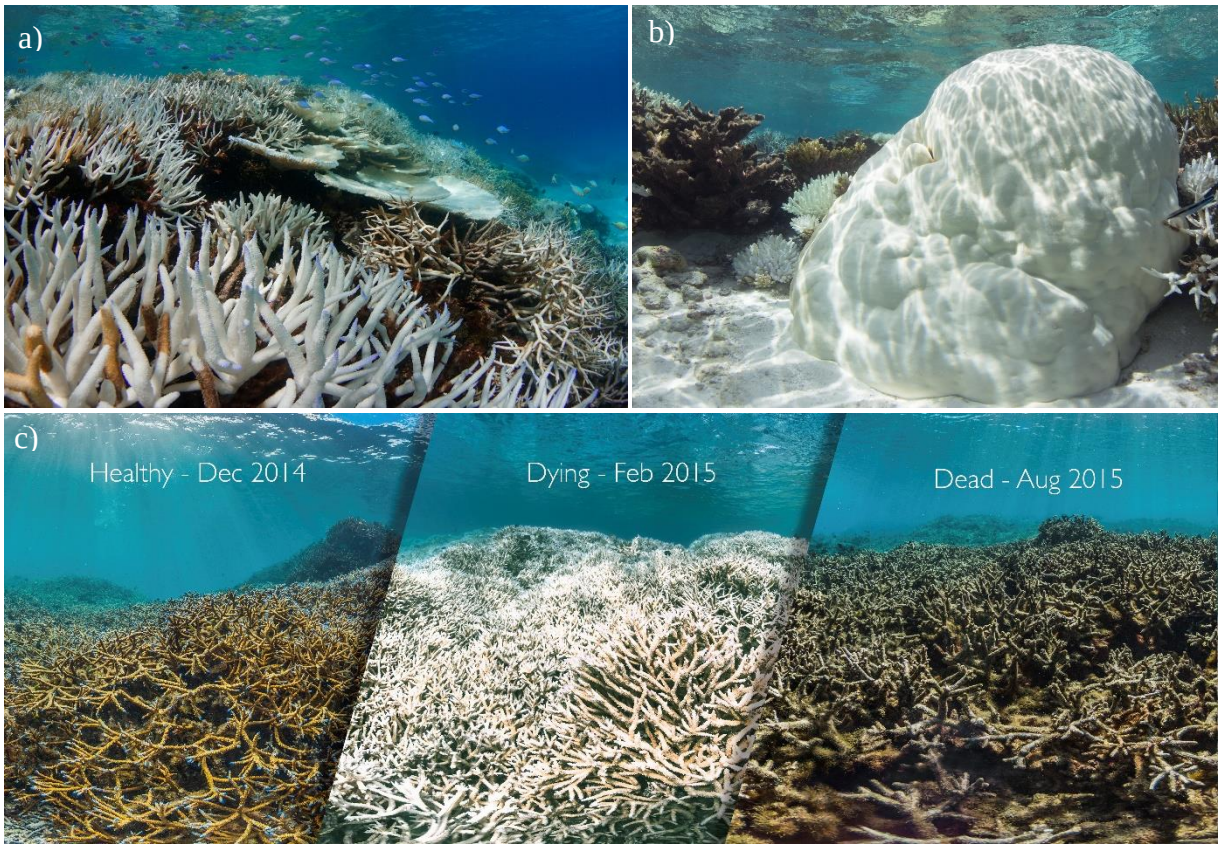

Figure 1-6. Bleached corals lose their brown symbiotic algae and become white. Branching corals, table-top corals (top left) and massive corals (top right) have all become bleached on this Maldivian reef during the 2016 bleaching event. The bottom image depicts the transformation from a healthy branching coral reef in American Samoa, to a bleached reef and finally to a dead reef covered in fleshy algae within the space of a few months. Image credits: XL Catlin Seaview Survey in May 2016.

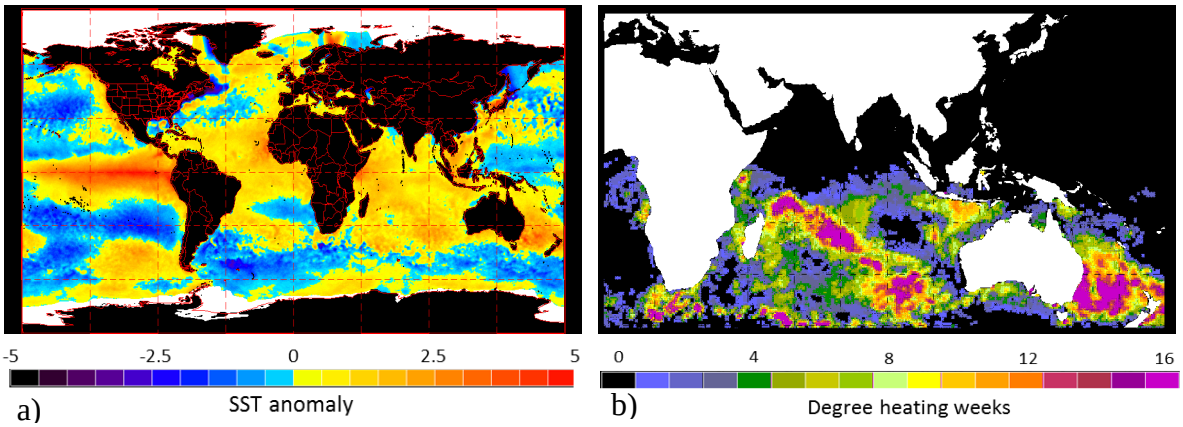

Figure 1-7. a) Satellite only sea surface temperature anomalies during the coral bleaching event in February 1998 show greater than 2°C temperature anomalies in the Australian and Indonesian summer time. b) Number of degree heating weeks from January to March 1998 show some areas of Australia experienced up to 16 degree heating weeks. Images adapted from NOAA/NESDIS.

Coral bleaching has happened across coral reefs globally, with major mass bleaching events in 1998, 2005 and 2015-2016, and smaller events in 1995 and 2010. This year (2016), the worst and longest coral bleaching event in history is occurring on a global scale as a result of climate change being exacerbated by a strong El Niño. El Niño events coupled with unusually high Pacific Ocean SSTs with a weakening or reversal of easterly winds, prevent cold water from upwelling at the equator, forcing the warm pool of Eastern Pacific water to expand and circulate westwards. El Niño events can happen abruptly and increase SSTs to 3 to 4°C above the average summer maximum (Figure 1-8; *McPhaden*, 1999), bringing additional heat and light stress to corals already struggling to adapt to rapidly increasing baseline temperatures. In 2016, up to 93% of the Great Barrier Reef has been bleached, with mortality rates ranging from 0% to >50% across the reef (Figure 1-9), culminating in a total mortality of 22% (AIMS press release). Higher mortality rates have also been observed at Jarvis Island, USA, which has become barren following the death of 90% of the coral reef (*Cohen, in progress*). The 2005 bleaching event in the Caribbean was caused by the change in storm tracks, meaning that the storms did not pass close enough to coral inhabited areas to cool them, causing the corals to exceed their thermal tolerance, resulting in 90% of corals bleaching with a 60% mortality rate (*Wilkinson*, 2008).

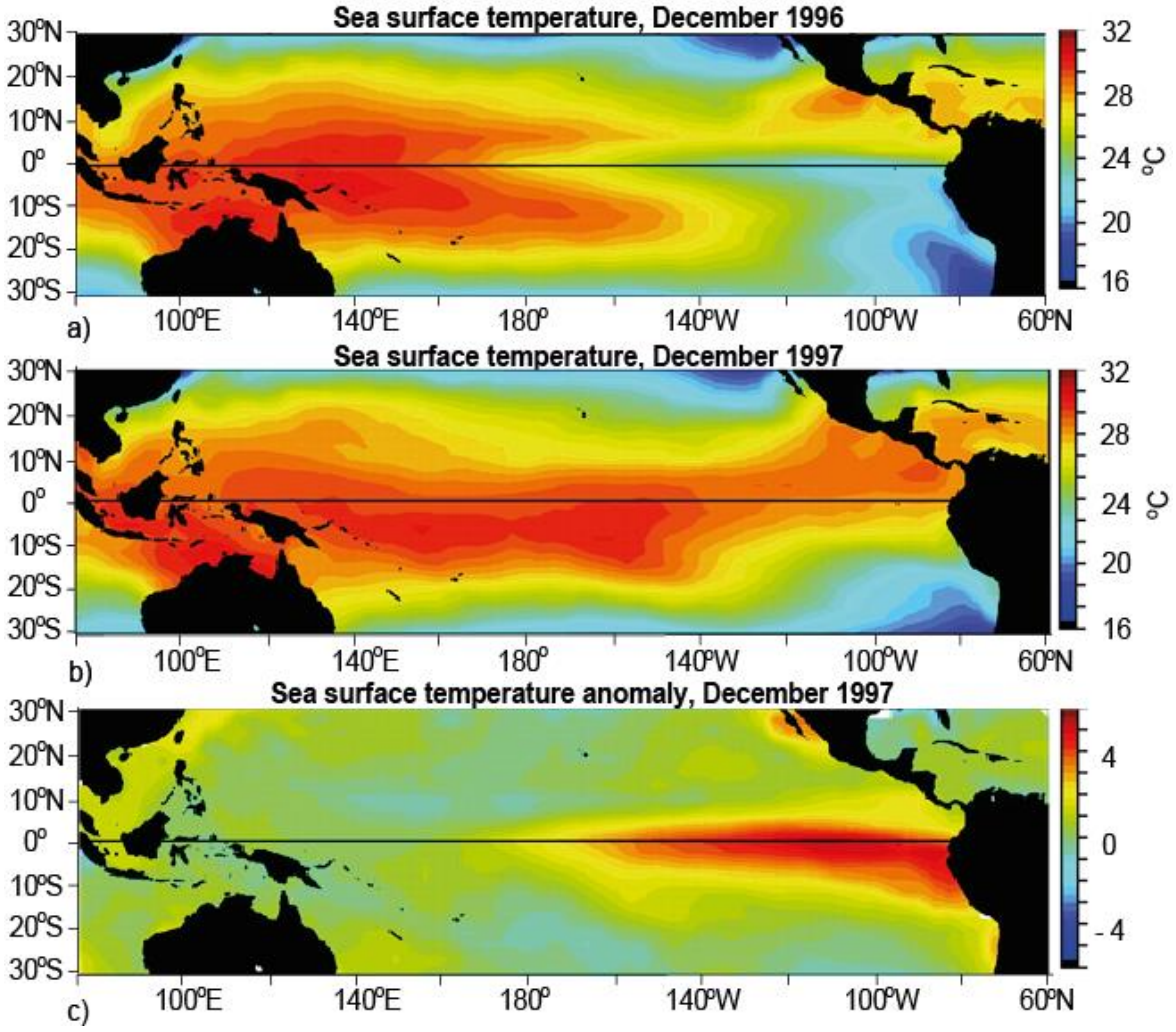

Figure 1-8. Monthly averaged sea surface temperature for December 1996 (normal) and December 1997 (El Niño). Monthly average SST anomalies for December 1997 show up to 4ºC increase in the Eastern Equatorial Pacific. Figure adapted from *McPhaden*, (1999).

Coral bleaching events such as these are predicted to become more frequent, possibly to even occur annually, and increase in both scale and severity given the likely trajectory of ocean warming (*Hoegh-Guldberg*, 1999; *Donner et al.*, 2007; *Hoegh-Guldberg et al.*, 2007; *Baker et al.*, 2008). Some estimates even suggest that all reefs will become affected by bleaching by the year 2040 (*Van Hooidonk et al.*, 2013). It can take around 15 years for coral reefs to completely recover from coral bleaching events, so the increase in frequency is going to make it nearly impossible for reefs to make a full recovery between such events (*Graham et al.*, 2015).

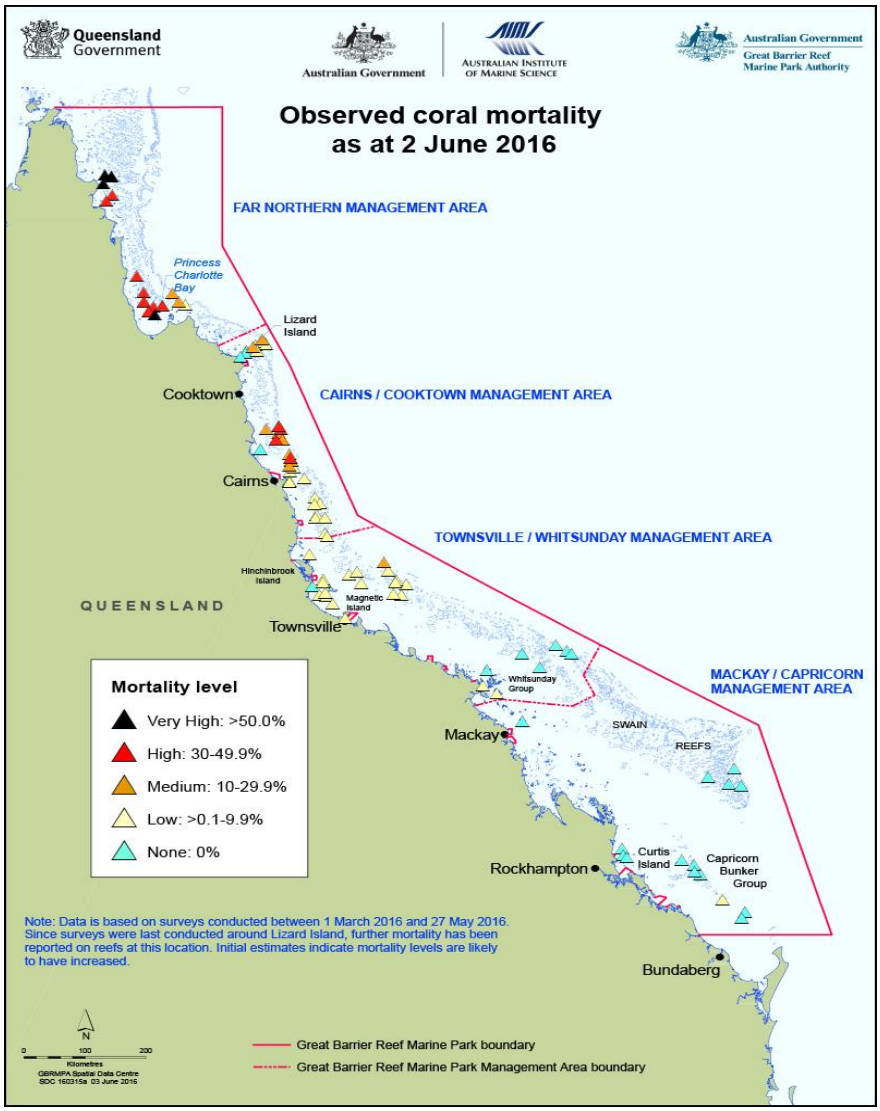

Figure 1-9. Observed coral mortality percentages as a result of the 2015-2016 coral bleaching event in the Great Barrier Reef. Image credit: Great Barrier Reef Marine Park Authority (*GBRMPA*, 2016).

The average 0.4°C increase in the tropics over the last three decades has been implicated in a decline in coral calcification (*Kleypas et al.*, 2008). Calcification is the term used to describe the process of corals forming hard calcium carbonate skeletons (described in detail in section 1.3.4) and can be quantified by either the extension rate (cm y^{-1}), which is how much the skeleton has grown along its growth axis, or calcification rate (g cm^{-2} y^{-1}), which is a function of density and linear extension and quantifies the mass of skeleton deposited per unit area. In the Caribbean, the region this thesis is focused on, the maximum SST has reached 32°C (September 2010), contributing to an 80% decrease in the total reef calcification rate (*Eakin et al.*, 2010). The extension rate of the Caribbean reef-building coral *Siderastrea siderea* has declined by ~35% in the forereef of the Mesoamerican Barrier Reef,

and is thought to have been caused by a >1°C SST increase since the 1900s and a lack of natural resilience in comparison to their backreef counterparts (*Castillo et al.*, 2012). Similar responses are also seen elsewhere, for instance, growth of the coral *Diploastrea heliopora* in the Red Sea has declined by 30% since the 1998 bleaching event because the waters failed to cool sufficiently to allow a full recovery. Indeed, it is predicted that by 2070, high temperatures will prevent this coral from growing at all in its present location (*Cantin et al.*, 2010).

1.1.2 Ocean acidification

The ocean has absorbed ~25% of anthropogenic CO_2 emitted since 1850 (*Le Quéré et al.*, 2010), equivalent to ~2.2 Pg C y^{-1} (*Canadell et al.*, 2007), forcing oceanic pCO_2 to increase by ~19 μatm per decade (*Takahashi et al.*, 2014). Atmospheric CO_2 dissolves into seawater and causes significant shifts in seawater carbonate chemistry (Figure 1-10), mainly due to the formation of carbonic acid (H_2CO_3), which releases hydrogen ions (H^+) that cause a decrease in seawater pH (pH_{sw}) in a process known as ocean acidification (OA).

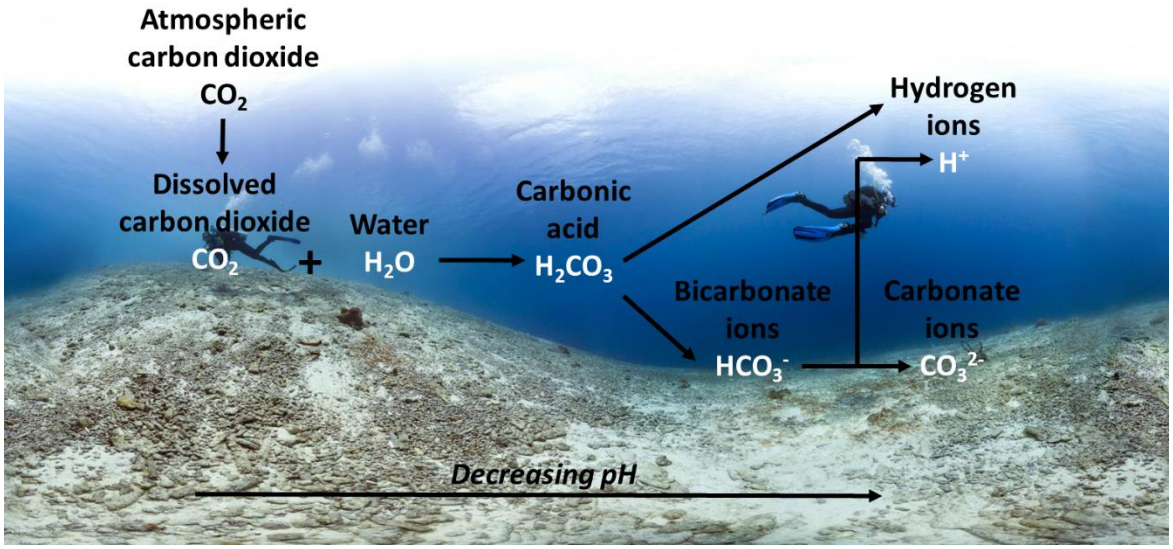

Figure 1-10. Carbon chemistry of ocean acidification. Atmospheric CO_2 dissolves into seawater, forming carbonic acid which decreases pH by directly releasing H^+ ions. Background image: Coral Deadzone, Bonaire, XL Catlin Seaview Survey.

Open ocean surface water pH ranges from 7.9 to 8.2, with the highest values representing the spring-summer phytoplankton blooms in the sub-polar and polar regions

(*Takahashi et al.,* 2014). The pH surrounding coral reefs can range from 7.65 to 8.4 (*Kayanne et al.,* 2002; *Manzello,* 2010; *Santos et al.,* 2011) and is dynamic even on a daily scale, with some reefs exhibiting a range of 0.5 pH units over a diurnal cycle (*Kayanne et al.,* 2002). Absorption of anthropogenic atmospheric CO_2 by the ocean has caused an estimated decrease in average surface seawater pH from 8.2 to 8.1 since the Industrial Revolution (*Doney et al.,* 2009), corresponding to a 30% increase in acidity (*Albright et al.,* 2015). Time-series data from the Bermuda Atlantic Time Series (BATS) has measured a decrease of ~0.045 pH units between 1983 and 2012 (*Bates et al.,* 2014). Collectively, BATS, the Hawaiian Ocean Time-series (HOT), the Drake Passage, and European Station for Time-series in the Ocean Canary Islands (ESTOC), indicate that seawater pH has been declining at an average rate of 0.02 pH units per decade (*Takahashi et al.,* 2014). With business as usual emission scenarios, by 2100 surface ocean pH is expected to have decreased by 0.3-0.5 pH units from pre-industrial levels (*Caldeira and Wickett,* 2003; *Orr et al.,* 2005).

A further decrease of 0.6 units over the next few centuries predicted by *Ridgwell and Zeebe,* (2005) is equivalent to the maximum ocean pH reduction observed over the last 300 million years according to geological records (*Caldeira and Wickett,* 2003). The geochemical models derived by *Caldeira and Wickett,* (2003) present the most extreme estimate of 1,900 ppm atmospheric CO_2 causing a reduction of 0.77 pH units in surface seawater by 2300. *Provoost et al.,* (2010) suggest that the mean global open ocean predictions may also be an underestimate for some parts of the oceans, particularly in coastal and shelf areas. To put these figures into the context of coral reefs, one can consider the prediction made by *Silverman et al.,* (2009), who estimate that coral reefs in the Red Sea will become zones of net dissolution as opposed to net calcification at just 560 ppm atmospheric CO_2.

Although coral reefs experience pH changes on multiple timescales, the magnitude of OA needs further study because its ultimate scale, and the extent of the resulting impacts on the carbonate system are not yet fully determined. It is however generally accepted that OA will cause an array of positive and negative impacts to both calcifying and non-calcifying organisms (*Orr et al.,* 2005; *Iglesias-Rodriguez et al.,* 2008) with global consequences that will directly affect human society. In particular, OA will reduce global fish stocks (which currently provide ~17% of the global population's intake of animal protein; *FAO,* 2012) due to degradation in coral reefs, and bring alterations of plankton communities (*Gattuso et al.,* 2015). In terms of the environment, OA can reduce the rate at which CO_2 is absorbed from

the atmosphere (*Sabine et al.*, 2004), and also alter the rates of carbon burial (*Feely et al.*, 2004; *Doney et al.*, 2009).

In addition to water temperature constraints (Figure 1-4), coral reefs are restricted to waters with an aragonite saturation (Ω_{arag}) of at least 3.3 Ω_{arag} (Figure 1-11). Deep water corals however, are able to survive in less saturated water, and some species even survive in undersaturated waters (Ω_{arag} <1; *Orr et al.*, 2005a). Ω_{arag} is defined as:

$$\Omega_{arag} = \frac{[Ca^{2+}] \times [CO_3^{2-}]}{K_{sp}} \qquad \text{Equation 1-1}$$

where K_{sp} is the solubility of precipitated aragonite polymorph of $CaCO_3$. When Ω_{arag} is >1 (supersaturation), precipitation is possible, whereas when Ω_{arag} is <1 (undersaturation), dissolution is favoured (*Feely et al.*, 2004).

Ocean acidification has caused the aragonite saturation state to diminish by decreasing the concentration of carbonate ions ($[CO_3^{2-}]$). A lower saturation state hinders calcification and therefore inhibits new skeletal growth, although an exact mechanisitic understanding applicable to all calcifiers is currently lacking. Before the Industrial Revolution, average saturation in the tropics was 4.2 Ω_{arag}, but it is estimated that by 2100 the average will be 2.3 Ω_{arag} (*Kleypas et al.*, 2005). When atmospheric CO_2 levels reach 500 ppm, it is calculated that global mean Ω_{arag} will drop to 3, resulting in Ω_{arag} < 3 for >70% of the summer in Puerto Rico (*Gray et al.*, 2012b). Alarmingly, by 2040 the Great Barrier Reef will experience marginal saturation levels (just above saturation point, Ω_{arag} =1) and *Steinacher et al.*, (2009) predicted that waters with Ω_{arag} >3 will disappear by 2070, forcing a state of net dissolution (*Wollast et al.*, 1980; *Andersson et al.*, 2003; *Morse et al.*, 2006; *Andersson et al.*, 2009). If the assumption is made that reef waters are acidifying at the same rate as the open ocean, the ocean acidification models of *Hoegh-Guldberg et al.*, (2007) and *Silverman et al.*, (2009) predict that biogeochemical conditions will become unsuitable for all coral reef growth by 2050.

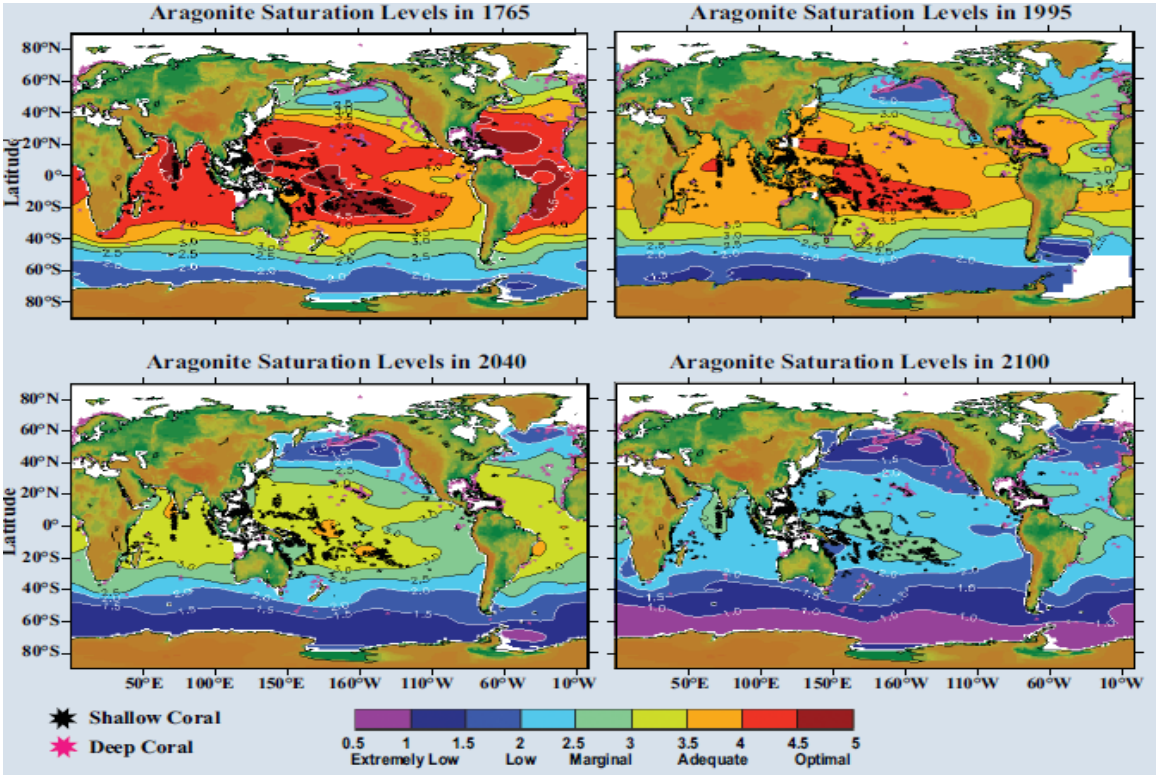

Figure 1-11. Changes in aragonite saturation state between 1765 and 1994, and predicted saturation levels for the years 2040 and 2100. Coral reefs are shown by the black markers, and are located in the most saturated areas, and cold water corals are indicated by the pink markers are able to grow in less saturated waters. In 1764, almost all coral reefs had aragonite >3.5, but are predicted to be found with <3 by 2100, although some areas will decrease at a faster rate, such as the Great Barrier Reef. Figure from *Kleypas et al.*, (2005).

From a multitude of experimental studies and field observations, it is widely acknowledged that ocean acidification can have a negative effect on coral calcification (e.g., *Gattuso et al.*, 1999; *Marubini and Atkinson*, 1999; *Marubini et al.*, 2008; *Bates et al.*, 2010) as a consequence of decreased carbonate ion availability and hence a lower aragonite saturation state (Equation 1-1) (*Langdon and Atkinson*, 2005). *Broecker et al.*, (2001) suggested that coral calcification declined linearly with decreasing Ω_{arag}, reaching 0 when Ω_{arag} is equal to 1. The coral reefs of Bermuda are compared to the "canaries in the coal mine", since they are already growing at the limits of low aragonite saturation levels and could be the earliest reactors to changing conditions. The calcification rate of *Diploria labyrinthiformis* in Bermuda is documented to have decreased by >50% compared to pre-industrial rates (*Bates et al.*, 2010). Over the last 20 years, OA has already caused a 20% decrease in calcification rates in the GBR (*Kline et al.*, 2012), and *Broecker et al.*, (2001) predict an 83% decline in GBR calcification by 2065. Despite the wealth of evidence to suggest some corals express a negative calcification response to lower aragonite or pH, the response of coral calcification to OA is greatly variable between coral species and locations

(e.g. *Doney et al.*, 2009). Some experimental studies even showed some corals do not respond negatively, or at least non-linearly, to lower pH (*Marubini and Atkinson*, 1999; *Marubini et al.*, 2001; *Langdon and Atkinson*, 2005; *Schneider and Erez*, 2006; *Holcomb et al.*, 2010; *Ries et al.*, 2010; *Comeau et al.*, 2014).

1.1.3 Combined impacts of ocean warming and acidification on coral reefs

Over geological history, four of the five largest "reef crises", whereby coral reefs experienced huge losses of biodiversity and reduced or even a cessation of biomineralisation, occurred during times of combined rapid warming and acidification. Two of these events included the end-Phanerozoic mass extinctions, more commonly known as the Permo-Triassic (251 Ma), and the end-Triassic extinction (200 Ma; *Kiessling and Simpson*, 2011). The most recent reef crisis occurred during the Paleocene-Eocene Thermal Maximum (55.8 Ma), through which there was a simultaneous rapid increase in SST alongside an increase in atmospheric CO_2, and decrease of ~0.3 pH units in seawater, partially analogous to modern conditions (*Pandolfi et al.*, 2011; *Penman et al.*, 2014).

Ocean warming and acidification will affect reef systems simultaneously. The combined impacts of multiple stressors on coral reefs are however less well-documented than single stressor experiments (*Schmidt et al.*, 2014), but it is rapidly becoming imperative to study the possibility and potential for ocean warming and ocean acidification to work in synergy against coral reef health. Such studies are becoming more common and this combination was studied in corals (*Reynaud et al.*, 2003; *Anthony et al.*, 2008a; *Rodolfo-Metalpa et al.*, 2011), bryozoan, molluscs (*Rodolfo-Metalpa et al.*, 2011), and coralline algae (*Anthony et al.*, 2008; *Diaz-Pulido et al.*, 2012). *Rodolfo-Metalpa et al.*, (2011) found that live colonies of *C. caespitosa* and *B. europaea* are able to calcify at pH 7.4 under ambient SSTs, but when they were exposed to high temperatures of 28.5°C during a natural heatwave in the course of the experiment, 80% of the colonies at pH 7.1 died, and 50% at pH 7.5, compared to only 30% at pH 8. *Stylophora pistillata* demonstrated a similar response in the study of (*Reynaud et al.*, 2003), whereby the calcification rates at 25°C and 450 μatm or 734 μatm were the same (~0.4% d^{-1}), but increasing the temperature to 28°C and the pCO_2 to 798 μatm induced at 50% decline in calcification (~0.2% d^{-1}).

The combined effects of OA and ocean warming are believed to be responsible for a 14.2% calcification decline in Great Barrier Reef corals since 1990 – a decline "unprecedented in the last 400 years" (*De'ath et al.*, 2009). In a culturing experiment, *Reynaud et al.*, (2003) found that coral calcification at ambient temperature is not always

affected by increasing pCO_2, but when temperature and pCO_2 were increased simultaneously, the calcification rate declined. These field and culture results are evidence that assessing the effects of ocean warming and ocean acidification cannot be treated separately, because the response of corals are different when their habitat is impacted by these stressors simultaneously. Nevertheless, it is anticipated that the synergistic effects of ocean acidification and ocean warming will have decreased coral calcification by 80% by the time atmospheric CO_2 concentrations have climbed to a business as usual estimate of 560 ppm by approximately 2055 (*Hoegh-Guldberg et al.*, 2007; *Silverman et al.*, 2009). After this point, $CaCO_3$ erosion rates will exceed accretion rates and some coral reefs will become systems of Net Ecosystem Dissolution (NED; *Cantin et al.*, 2010).

1.2 Local anthropogenic stressors

Although coral reefs are experiencing the effects of anthropogenic climate change on a global scale, many reefs are also damaged by local stressors, such as marine and land-based pollution and over-fishing.

1.2.1 Land-based activities

Land-based pollution threatens at least 22% of coral reefs through the introduction of freshwater, toxic chemicals, sewage and sediment which can encourage large algal blooms, decrease rates of symbiont photosynthesis and inhibit recruitment (*Fabricius*, 2005). Up to 50% of coral reefs offshore from countries with widespread land clearing are vulnerable to terrestrial runoff (*Bourke et al.*, 2002). This problem is growing as populations increase, driving the demand for forested land to be cleared to make way for building development or agricultural land, which also increases fertiliser use (*Vitousek et al.*, 1997; *Tilman et al.*, 2001; *Zak et al.*, 2004). Further consequences of these changes include a reduction in absorption of water into soil; and a lack of vegetation causing uninterrupted flow, combined with new municipal areas having smoother (concrete) surfaces, which increase the rate at which sediment can reach the offshore reef.

The direct impacts of sedimentation include smothering and increasing water turbidity which reduces the amount of light available for photosynthesis. Corals also suffer indirectly through the input of dissolved inorganic nutrients which can trigger turf- and macrolalgae growth, which ultimately outcompetes coral (e.g. *Fabricius et al.*, 2005; *Restrepo et al.*,

2006), partly as a result of lower larvae settlement and recruitment (e.g. *Hodgson*, 1990; *Wittenberg and Hunte*, 1992; *Shimoda et al.*, 1998; *Restrepo et al.*, 2006). Sedimentation and nutrification are also associated with increasing macroalgae cover, which can influence increases in bioerosion by grazers and borers because there is more algae on the coral for them to consume (e.g. *Chazottes et al.*, 2002).

Much coastally-derived pollution is sewage, which is a significant problem because coral reefs often inhabit the coasts of developing countries where tertiary sewage treatment (which includes removal of inorganic compounds such as the nitrogen and phosphorus) is rare. Sewage transports vast quantities of inorganic nutrients that are utilised by fleshy macroalgae (Figure 1-12; *Fabricius et al*., 2005) or increase the prevalence of diseases such as white pox (*Patterson et al.*, 2002; *Sutherland et al.*, 2010; *Vega Thurber et al.*, 2014). Sewage also contains suspended particles which smother corals and decrease symbiont photosynthesis (e.g. *Fabricius*, 2005); heavy metals which decrease fertilisation (*Reichelt-Brushett and Harrison*, 1999); toxins in lethal and sub-lethal doses (e.g. *van Dam et al.*, 2011); and endocrine disrupters which decrease reproductive success (*Tarrant et al.*, 2004).

Figure 1-12. a) Sewage outfall directly adjacent to a Caribbean coral reef. b) The resulting ecosystem shift to macroalgae dominance. Image credits: Steve Spring of Photobank.

Although increasing the concentration of nutrients such a phosphate, nitrate and ammonia can have fatal consequences on coral colonies alone, the ratio of these concentrations has also been found to be critical and can be described by the nutrients effects model of *Weidenmann et al*., (2012). The nutrient effects model describes how the lipid composition of algal membranes becomes altered as the *Symbiodinium* experience a shift from nutrient limiting conditions to nutrient starved conditions (*D'Angelo and Weidenmann*, 2014). In ideal circumstances, coral symbiont growth is determined by the availability of nutrients, of which there is an optimal ratio of dissolved inorganic nitrogen to phosphate. However, under elevated nitrate conditions the nutrient levels are inbalanced, allowing the

photoshymbiont population to rapidly increase and cause part of the algal population to become phosphate starved, significantly reducing photosynthetic efficiency.

There is evidence that communities exposed to the persistent presence of dissolved inorganic nitrogen, coupled with limited phosphate availability have lower thermal tolerances, making them less resilient to ocean warming and are therefore more likely to become bleached (*Wooldridge*, 2009; *Wiedenmann et al.*, 2013; *Vega Thurber et al.*, 2014). For example, the upper thermal bleaching threshold of inshore coral reefs in high run-off areas in the Great Barrier Reef is up to 1.5°C lower than corals in low run-off areas (Figure 1-13, *Wooldridge*, 2009).

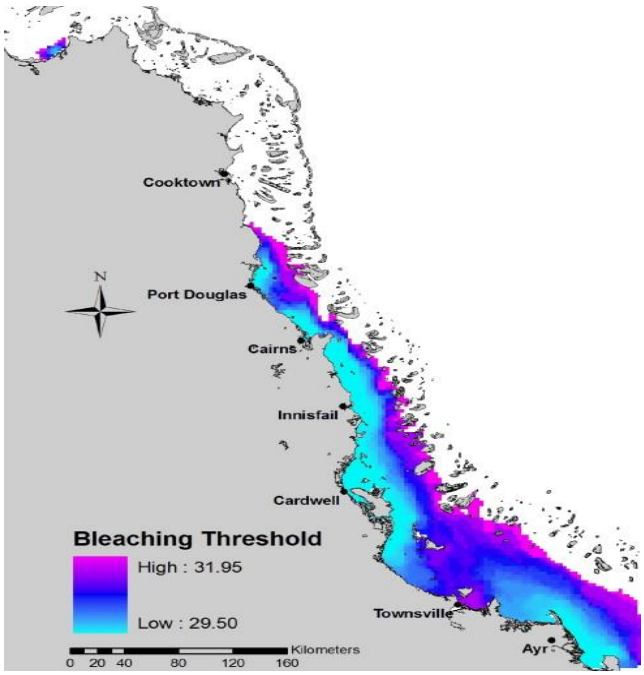

Figure 1-13. Corals exposed to high levels of dissolved nutrient run off (blue areas) have lower bleaching thresholds than offshore corals that are less exposed to nutrient inputs. Figure from *Wooldridge*, (2009).

1.2.2 Over-fishing

Herbivorous fish are important inhabitants of coral reefs, as they graze on algae that covers coral, reducing the competition between coral and macroalgae for light and nutrients, or space for larval settlement (e.g. *McCook et al.*, 2001). Therefore removing herbivorous fish can alter the ecological state of a coral reef by increasing the amount of fleshy macroalgae which can smother coral (*McClanahan et al.*, 1999). On one hand, it is beneficial to the reef

to remove parrot fish, because the process of corallivory (grazing algae from the surface of the coral) causes damage by removing parts of the tissue layer and even the skeleton (*Bruggemann et al.,* 1994, *Bruckner et al.,* 2000). Such bioerosion makes the coral more susceptible to disease and boring organisms. On the other hand, excessive removal of parrotfish can have detrimental impacts on the reef as a result of fewer herbivorous fish removing macroalgae, potentially causing an ecosystem shift from hard coral to macroalgae (*Mumby*, 2009). It was concluded by *Mumby* (2009) that overall, parrotfish have a positive impact on coral reefs, owed to the enhancement of coral recruitment by the removal of macroalgae. Decreases in grazer population have been associated with increasing macroalgae cover in the southern section of the Belize barrier reef and Cayos Cochinos, but this is not the case in northern Belize (Figure 1-14; *Suchley et al.*, 2016). It is estimated that 55% of reefs are directly impacted by overfishing (*Burke et al.*, 2011), and some fishing techniques, particularly blastfishing and cyanide use (*McManus et al.*, 1997; *Cesar et al.*, 2003), are physically damaging to coral reefs. Fishing mitigation is improving by founding no-take zones, and defining seasons to catch certain species. For example, the population of Nassau groupers in Belize decreased from 15,000 to <3,000 over 25 years (*Sala et al.*, 2001), and it is now illegal to fish grazers between 1st December and 31st March (Statutory Instrument No. 49 of 2009, Belize Fisheries). Although grazer population has not been fully assessed since the ban, a genetic study on fish fillets sold in Belize markets showed that only 5-7% is now parrotfish, suggesting that the ban is largely being enforced and population should be in the process of recovering (*Cox et al.*, 2013). Following a similar ban, the black grouper population in Florida has increased by 36% (*NMFS*, 2006).

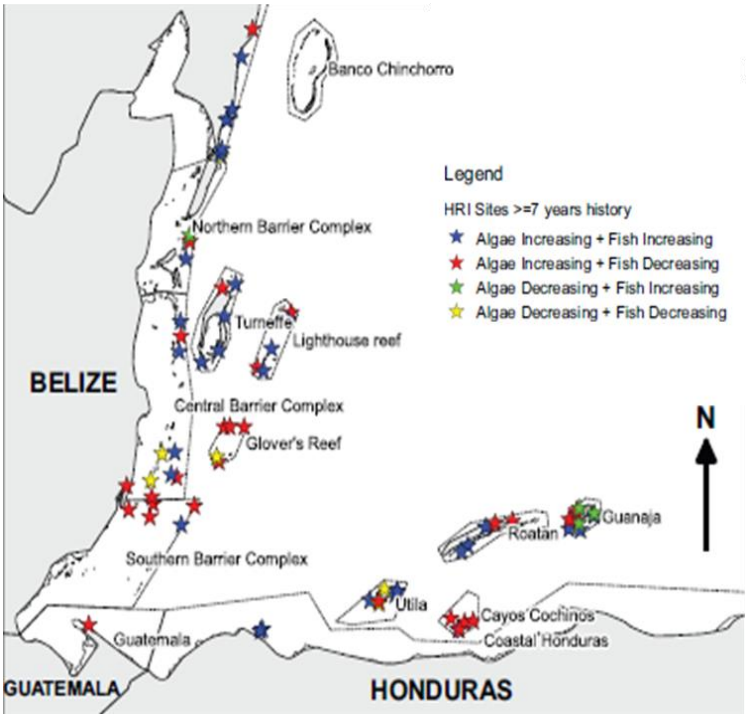

Figure 1-14. Cumulative 7 year relationship between changes in herbivorous fish biomass and fleshy macroalgal cover (2005/2006 to 2013/2014). Blue stars depict sites where macroalgae cover has increased alongside an increase in herbivorous fish. Red stars depict sites where algal cover is increasing and herbivorous fish populations are decreasing. Green stars depict sites where macroalgal cover is decreasing and herbivorous fish are increasing. Yellow stars depict sites where macroalgae cover is decreasing alongside decreases in herbivorous fish populations. Figure adapted from *Suchley et al.*, (2016), data from *Kramer et al.*, (2015).

1.2.3 Recreational activities

Coral reefs are attractive places for tourists to visit, and millions of people visit coral reefs either on a cruise, or to go snorkelling and scuba diving; for example more than 2 million people visit the GBR each year (www.australia.gov.au). Corals are broken by anchors, and anchorage is estimated to account for an average 7.1% of annual coral cover damaged at frequently visited reef sites (*Saphier and Hoffmann*, 2005; *Davenport and Davenport*, 2006). With greater than 300,000 visitors per year to a total reef area of 2 km^2 in Koh Tao, Thailand (*Larpnun et al.*, 2011; *Weterings*, 2011), or <250,000 divers per year to 4 km^2 of reef area in Eliat, Red Sea (*Zakai and Chadwick-Furman*, 2002), it is easy to see that a huge number of coral collisions, breakages, and sediment resuspension (*Tratalos and Austin*, 2001; *Zakai and Chadwick-Furman*, 2002; *Davenport and Davenport*, 2006) goes unreported and unmonitored. Divers are also believed to be accountable for a three times higher prevalence of coral disease at popular dive sites in comparison to less frequently visited sites nearby,

particularly eroding band disease after coral is made vulnerable from injury, and white syndromes (e.g. white band disease), which are linked with sediment accumulation on coral tissue (*Lamb et al.*, 2014). Sediment accumulation on coral tissue can result in coral mortality as a result of microbial respiration during breakdown of the organic matter in sediment, creating a low pH anoxic layer on the tissue. Following this, the coral tissue is decomposed by bacteria, producing toxic hydrogen sulphide that can diffuse across the tissue layer, resulting in colony mortality (*Weber et al.*, 2012).

1.3 Palaeoproxies

It is clear from the discussion above that corals face a multitude of stressors on a global scale (ocean warming and acidification) and a local scale (e.g. terrestrial runoff, fishing, tourism). One way to build an understanding of how these multi-stressors will affect future coral growth is to look back in time at how corals have responded thus far. However, monitoring of SST, pH, nutrient and sediment inputs has a poor coverage both spatially and temporally. Observations of SST are the most mature, but even these records are relatively short and sparse. However, palaeoproxies can be used to fill in spatial gaps and extend the observed record through SST reconstructions. It is vital for us to uncover what climate conditions carbonate organisms have been exposed to in the past and understand their response to those conditions in order to make better predictions about how they will respond to future projections of ocean warming and ocean acidification. A more thorough understanding of the resulting impacts and responses of coral can be considered when developing new climate change policies, ensuring that future emission targets allow marine organisms enough flexibility to survive.

1.3.1 History of sea surface temperature observations

Sea surface temperature records are essential for understanding climate change and predicting future changes and impacts on marine ecosystems. SSTs have been sporadically measured for centuries using a multitude of monitoring techniques such as: buckets, shipboard sensors, floating buoys and satellites (e.g. *Folland and Parker*, 1995; *Stephens et al.*, 1995; *Gould et al.*, 2004; *Morice et al.*, 2012). Measuring temperature using such a variety of instruments has resulted in records of SST measurements with differing accuracy, precision, and sampling depths. Both the mix of instruments and the overall sampling

patterns have changed temporally and spatially (*Boyer et al.*, 2009), complicating efforts to determine and interpret long-term change since the lack of homogeneity makes the records not directly comparable.

The International Comprehensive Ocean-Atmosphere Data Set (ICOADS) holds surface marine data spanning the past three centuries, combining huge variations in temporal and spatial datasets and collection methods, including data from as early as 1662 to state-of-the-art worldwide floating buoy systems (http://icoads.noaa.gov/). Observations from 1662-2007 are made up of 261 million individual marine reports, however, historical SST data is still considered to be sparse. Such ranges in data collection methods mean that anomalies between each data set need to be corrected (e.g. differences between shipboard sensors and monitoring buoys; Figure 1-15). Such biases can be as large as the anticipated change in climate signal, so studies such as *Smith et al.*, (2008) and *Kennedy et al.*, (2011) are working to resolve these uncertainties. Particular challenges are associated with the very early temperature data, for example, converting delayed mode archives (e.g. paper logbooks) to the same format as global telecommunications systems in the International Maritime Meteorological Archive (*Woodruff et al.*, 2011).

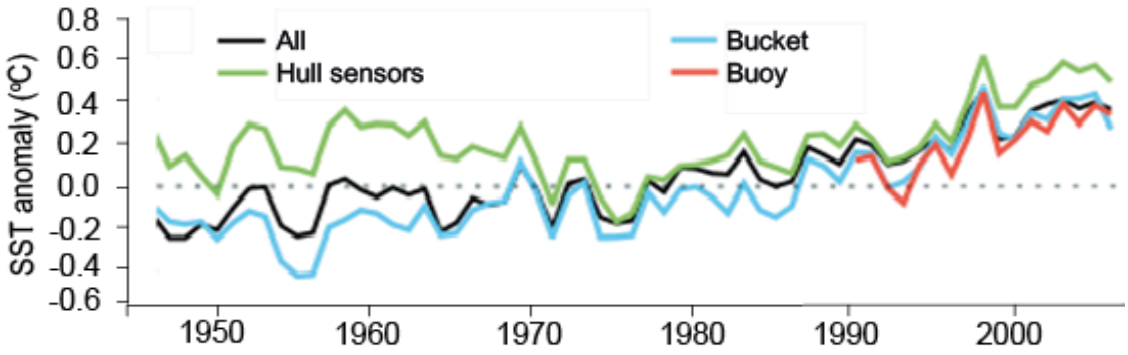

Figure 1-15. Global annual average sea surface temperature (SST) anomalies relative to 1961-1990 based on a range of *in situ* data collectors: Energy room intake and hull contact sensor (green), bucket (blue), buoy (red), total average (black). (Adapted from *Jones et al.*, 2007).

Despite the difficulties associated with combining records, there are multiple combined SST datasets that provide a single time-series of SST. A popular example is the Hadley Centre's HadISST-gridded SST product, which is an interpolated observational dataset from satellites and ship-based measurements from ICOADS (*Rayner et al.*, 2003). HadISST data spans from 1870 to the present day and depicts a warming trend throughout

the entire record (Figure 1-16a). Aside from the importance of observing changes in SST over time, historic SST measurements form the backbone of reanalysis models (e.g. ERA-Interim), which are constrained by observational data. Reanalysis models are simulations that assimilate multiple observations such as SST data from bucket records, satellite observations so that climate model outputs can be shifted towards measured observations. Reanalyses provide climate scientists with long-term global gridded datasets. Historic SSTs are also necessary to verify coupled global climate models (GCMs) which are used to make future climate projections (*Rayner et al.*, 2005). Climate reconstructions using geochemical techniques can serve as a more consistent alternative, eliminating biases attributed to changes in measurement techniques across a time-series. An example of a geochemical record includes the Western Atlantic SST anomaly (relative to 1961-1990) records reconstructed from coral Sr/Ca ratios and $\delta^{18}O$ analyses in Figure 1-16b (*Tierney et al.*, 2015). The main advantage of reconstructed temperature records is that they can be used to obtain SST estimates that pre-date measured observations, and this method has recently identified that SSTs began to increase as a results of anthropogenic climate change earlier (mid-nineteenth century) than previously considered (*Abram et al.*, 2016).

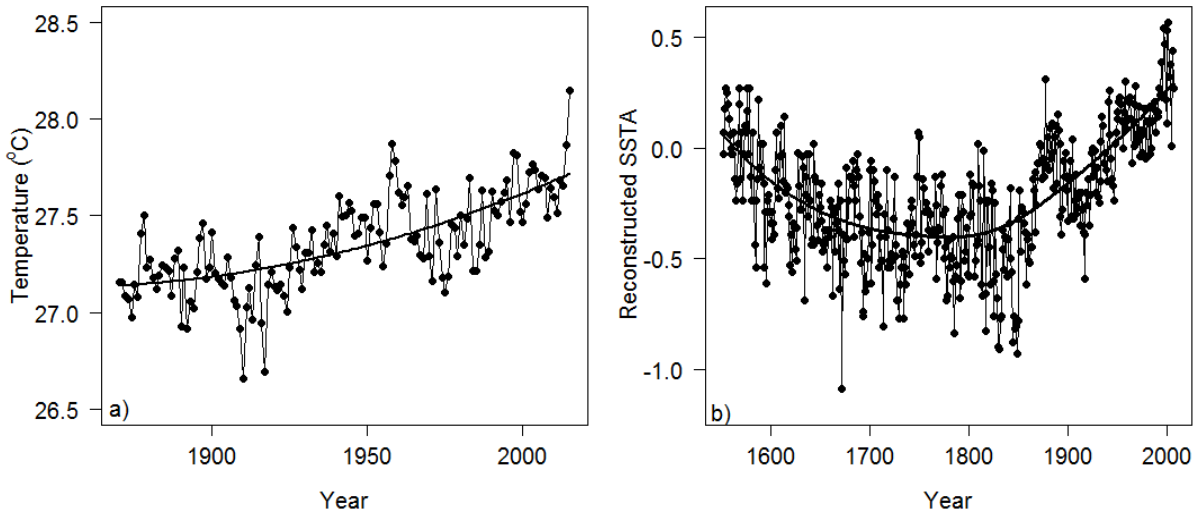

Figure 1-16. a) HadISST record for the Caribbean between 1870 and 2015 (*Rayner et al.*, 2003; Data downloaded from http://climexp.knmi.nl). b) Reconstructed sea surface temperature anomaly from coral Sr/Ca and $\delta^{18}O$ records (*Tierney et al.*, 2015; *Abram et al.*, 2016). Note the different scales, since the reconstructed record (1552 to 2007) is longer than the HadISST record.

1.3.2 History of seawater pH records

Despite its growing importance, seawater pH was not consistently or accurately measured prior to the late 1980s, despite the pH scale being invented in 1909 by S.P.L. Sørenson of the Carlsberg Laboratory's Chemical Department. In order to monitor the seawater CO_2 system, a minimum of two inorganic carbon parameters must be measured, typically dissolved inorganic carbon (DIC) and total alkalinity (A_T), as well as temperature and salinity to calculate pH, and the aragonite ($CaCO_3$) saturation state (Ω_{arag}). Seawater pH can be measured using a variety of pH sensor systems: spectrophotometric (e.g. *Rérolle et al.*, 2013), potentiometric, and most recently, ion sensitive field effect transistors (ISFET), which can be deployed in the field for up to 18 months (e.g. *Hofmann et al.*, 2011). Where pH measurements have been unavailable, it has been calculated from other parameters of the carbon system, particularly DIC, which reached higher levels of measurement precision earlier than pH.

Open ocean surface pH has been monitored for up to 30 years using shipboard measurements, including the Bermuda Atlantic Time-Series (BATS), the Hawaii Ocean Time-Series (HOT), Iceland Sea, Irminger Sea, CArbon Retention In A Colored Ocean sites in the North Atlantic (CARIACO), Munida (New Zealand, Pacific Ocean) and the European Station for Time-series in the Ocean (ESTOC; *Bates et al.*, 2014). These locations have each generated a pH time-series calculated from measured DIC and A_T, and each station exhibits a different rate of change (becoming more acidic; Figure 1-17) in the range -0.0013 to -0.0026 pH units per year (Table 1-1).

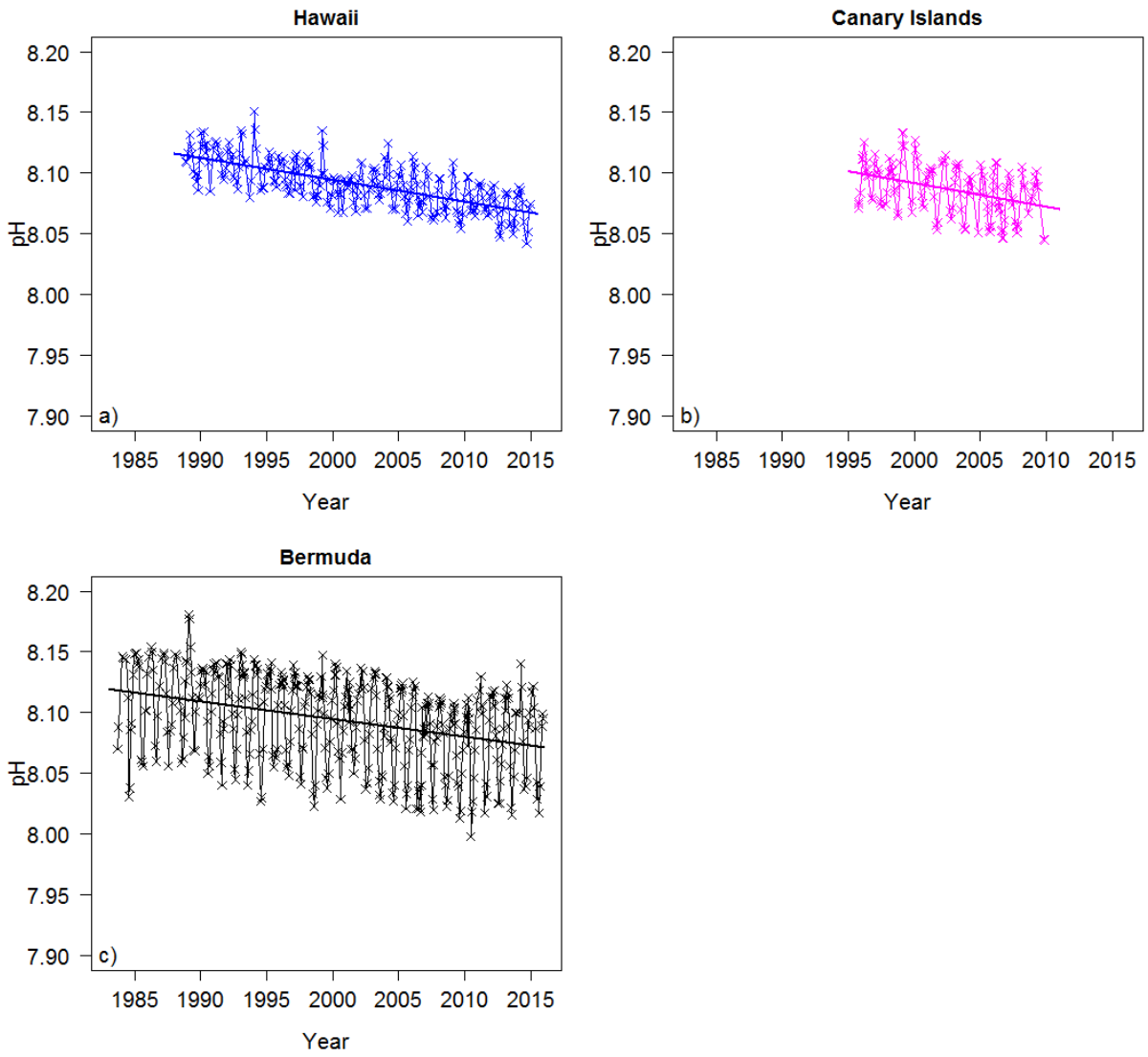

Figure 1-17. pH time-series spanning up to 30 years from (a) Hawaii (b) Canary Islands (c) Bermuda. Data freely available from the Environment Protection Agency's Climate Change Indicators in the United States (www.epa.gov/climate-indicators).

Table 1-1. Multiple time-series of surface seawater pH. Regions are listed in order of decreasing latitude. Sampling frequency per year is listed and the rate of change per year is given for both pH and aragonite saturation state ($\Omega_{aragonite}$). Table adapted from *Bates et al.*, (2014).

Time-series site	Region	Start year	Frequency (y^{-1})	pH	$\Omega_{aragonite}$
Iceland	Iceland Sea	1983	3-4	-0.0014	-0.0018
Irminger	Irminger Sea	1983	3-4	-0.0026	-0.008
BATS	Sargasso Sea	1983	14-16	-0.0017	-0.0095
ESTOC	Canary Islands	1995	4-6	-0.0018	-0.0115
HOT	North Pacific	1988	10	-0.0016	-0.0084
CARIACO	Cariaco Basin	1995	12	-0.0025	-0.0066
Munida	South Pacific	1998	4-6	-0.0013	-0.0085

The pH of seawater bathing coral reefs have recently been measured using a variety of techniques including potentiometric pH sensors (e.g. *Gattuso et al.*, 1999; *Yates and Halley*, 2006; *Santos et al.*, 2011), autonomous pCO_2 systems (e.g. *Bates et al.*, 2001; *Kayanne et al.*, 2005), and spectrophotometric sensors such as SAMI-pH (Submersible Autonomous Moored Instrument for pH) (*Martz et al.*, 2003; *Seidel et al.*, 2008; *Gray et al.*, 2011). ISFET pH sensors can be attached to reef beds, and are capable of collecting high frequency data - as often as every few seconds (*Rivest and Gouhier*, 2015). As a result of these measurements, there is a growing recognition that the carbonate system on coral reefs is not necessarily representative of open ocean pH (e.g. *Bates et al.*, 2010; *Gray et al.*, 2012a; *Georgiou et al.*, 2015). To demonstrate this, two examples are presented here. Firstly, reef water CO_2 is measured in Kaneohe Bay, Hawaii, as part of the Coral Reef Instrumented Monitoring Program, and Figure 1-18a shows calculated seasonal pH (from DIC and alkalinity using the seacarb package in R; *Lavigne and Gattuso*, 2010) between 2009 and 2011. Kaneohe Bay reef water has a larger seasonal variation (<0.25 pH units) than the open water (~0.03 pH units), and the average pH is ~0.1 pH units higher than the HOT record over the same time-period. The HOT record shows a decrease of 0.036 pH units between 1988 and 2014, which is less than the ~0.15 pH unit decrease in Kaneohe Bay across 3 years (Figure 1-18a). Secondly, there are similar differences between the open water BATS record and the Hog Reef in Bermuda (*Bates et al.*, 2010), whereby the pH of Hog Reef is ~0.15 pH units higher than the open ocean (Figure 1-18b, Figure 1-17c). Additionally, there is a greater seasonal range (~0.15 pH units) in Hog Reef than in the open ocean (~0.12 pH units).

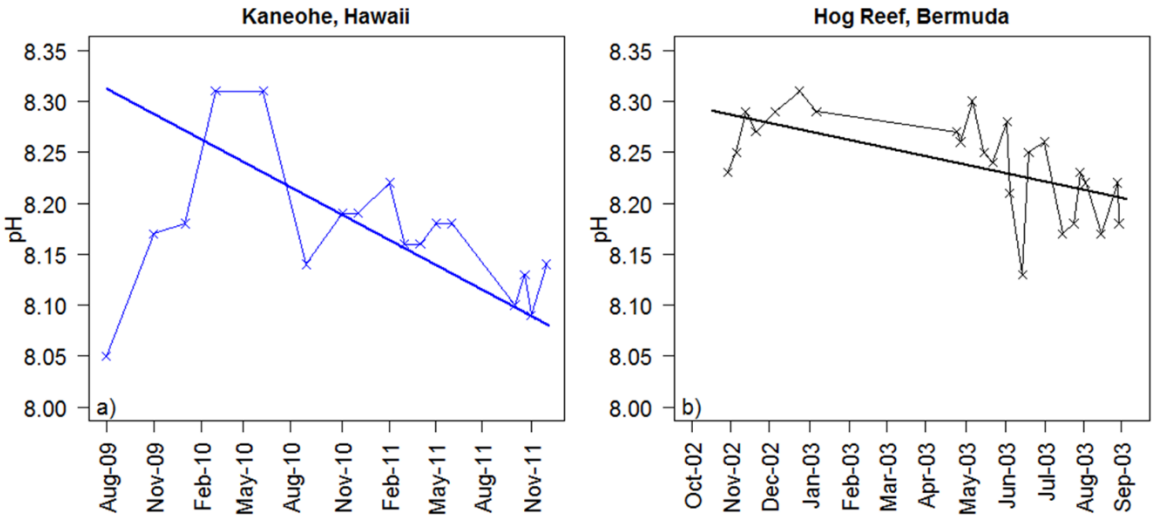

Figure 1-18. Coral reef based pH time-series calculated from dissolved inorganic carbon and alkalinity at a) Kaneohe Bay, Hawaii, and b) Hog Reef, Bermuda.

There are numerous potential drivers of seasonal pH variability, both on coral reefs and in the open ocean; for example, changes in the carbonate system (e.g. $[CO_3^{2-}]$, total alkalinity, Ω_{arag}), temperature, upwelling or salinity (*Wootton and Pfister*., 2012). Additionally, the driver of open ocean pH variability is not uniform across all oceans (e.g. *Flecha et al*., 2015, *Hofmann*, 2016, *Fabry et al*., 2009). Broadly speaking, *Hagens and Middleburg* (2016) calculated that in tropical and sub-tropical regions, pH seasonality is primarily a response to temperature variability, whereas in high-latitude regions, it is mostly driven by changes in dissolved inorganic carbon (DIC). It has been proposed by *Bates et al.*, (2010) that a "Carbonate Chemistry Coral Reef Ecosystem Feedback" (CREF hypothesis) exists. This works in a similar way to the diurnal CO_2 variability described in section 1.1.2 in that there is a feedback between hard coral and macroalgae growth, given that carbonate ion saturation states either stimulate or surpress coral calcification rates on a seasonal scale. The carbonate system of coral reefs is therefore dominated by net ecosystem calcification (NEC) and net ecosystem production (NEP).

Reef water pH fluctuates even on a diurnal cycle, as observed from CO_2 measurements at the Coral Reef Instrumented Monitoring Platform (CRIMP2) at Kaneohe Bay, Hawaii (Figure 1-19). In the daytime, CO_2 concentrations are higher (lower pH) following the removal of carbonate ions (alkalinity) during calcification that has been stimulated by photosynthesis (positive net photosynthesis). At nighttime, respiration exceeds photosynthesis (negative net photosynthesis), therefore calcification is minimal and a build-up of carbonate ions results in lower CO_2 concentrations (higher pH). This trend in diurnal CO_2 variability has also been shown to be similar to variations in total alkalinity

(*Shamberger et al.*, 2011). It has previously been calculated that reef calcification emits 0.6 moles of CO_2 to the surrounding reef water for each mole of $CaCO_3$ precipitated (*Bates* 2010 and references therein). Consequently, during periods of positive net calcification, the fixation of inorganic carbon by the newly formed coral skeleton decreases DIC to total alkalinity, resulting in a net production of CO_2 and therefore a decrease in pH (*Bates*, 2010).

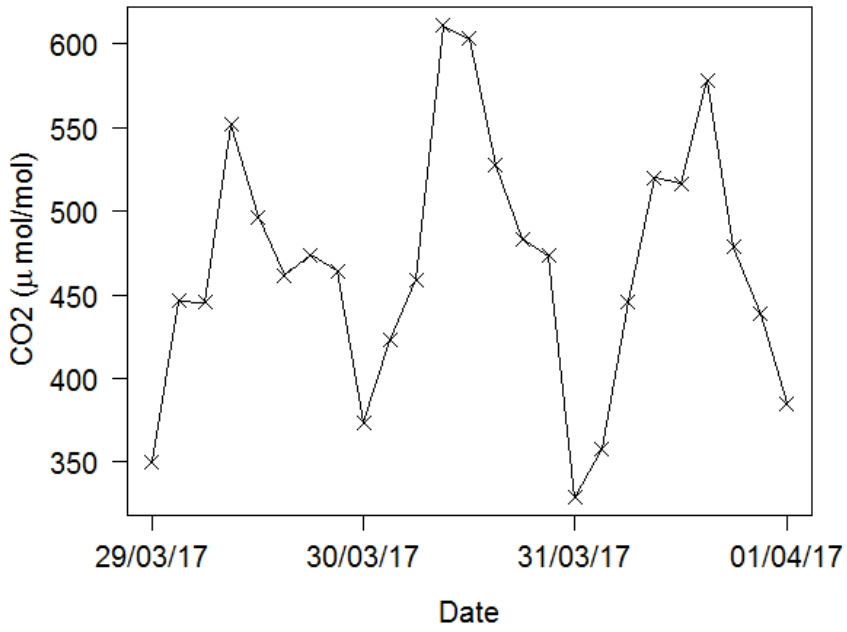

Figure 1-19. Dirunal variation in coral reef seawater CO_2 at Kaneohe Bay, Hawaii indicates higher CO_2 concentration in the daytime (lower pH) and lower CO_2 at nighttime (higher pH). Preliminary CO_2 data measured by the Coral Reef Instrumented Monitoring Platform, accessed from https://www.pmel.noaa.gov/co2/story/CRIMP2 on 4/4/2017.

1.3.3 Palaeoproxies – a suitable alternative to observational data?

The fact that *in situ* records of globally important SSTs, pH and pollution are both sparse and potentially biased, geochemical proxies provide a vital lifeline by using the same method to generate records of these parameters. Not only this, but SST and pH palaeoproxies can be applied to ecologically sensitive areas, where there may not be a large number of ship records, or for example, in coastal regions where satellite data is less reliable due to interference. Geochemical proxy reconstructions therefore provide an attractive "retrospective" alternative to the patchy *in situ* monitoring data sets as well as providing a long-term perspective. Although geochemical proxy SST estimates have been derived from a number of biogenic substrates such as alkenones (*Brassell et al.*, 1986), marine Crenarchaeota (*Schouten et al.*, 2002), sclerosponges (*Rosenheim et al.*, 2004) and

planktonic and benthic foraminifera (*Izuka*, 1988)), and corals (arguably the most popular choice in tropical regions). Living tropical corals are used as historical SST archives because their relatively fast growth rate and lifespan that can exceed 100 years, thus building a skeleton that can consistently provide the fine-scale temporal sampling (annual/seasonal) necessary to resolve SST changes over the last 300 years at an inter-annual resolution (e.g. *de Villiers et al.*, 1994; *Alibert and McCulloch*, 1997; *Swart et al.*, 2002; *Reynaud et al.*, 2007; *Maupin et al.*, 2008; *Mitsuguchi et al.*, 2008; *Nurhati et al.*, 2009; *DeLong et al.*, 2014). Fossilised tropical corals have been used to reconstruct SST records prior to the twentieth century (*Beck et al.*, 1992; *Gagan et al.*, 1998; *Quinn et al.*, 1998; *McCulloch et al.*, 1999), although these archives can be modified by diagenesis (*McGregor and Gagan*, 2003; *Quinn and Taylor*, 2006; *Sayani et al.*, 2011). Cold-water corals have also been explored as archives of intermediate-depth seawater temperatures, but at lower resolutions than tropical corals (*Smith et al.*, 2000; *Cohen et al.*, 2006; *Rüggeberg et al.*, 2008).

1.3.4 Biomineralisation in scleractinian corals

Scleractinian corals are hard, reef-building corals found in tropical regions supplied by oligotrophic seawater. As described earlier, corals depend on a symbiotic relationship with *Symbiodinium sp.* – a dinoflagellate which inhabits coral polyps and photosynthesises, producing up to 95% of the coral host's energy requirements (*Muscatine*, 1990) for numerous functions, including biomineralisation (*Iwasaki et al.*, 2016). Coral biomineralisation can be separated into two predominant mechanisms: the synthesis of the organic matrix, and the transport of ions to the calcifying centre. Scleractinian corals build extracellular calcium carbonate ($CaCO_3$) aragonite skeletons by primarily precipitating the dissolved calcium (Ca^{2+}) and carbonate (CO_3^{2-}) ions from seawater. Ca^{2+} ions are actively transported by the ATPase protein pump to the extracellular calcifying fluid (ECF) where they directly precipitate with CO_3^{2-} ions, which have been transported to the ECF through diffusion, to form the $CaCO_3$ skeleton (Figure 1-20). The principal reaction during biomineralisation is:

$$Ca^{2+} + CO_3^{2-} \rightarrow CaCO_3 \qquad \text{Equation 1-2}$$

$CaCO_3$ can also be precipitated from the bicarbonate ion (HCO_3^-) following the hydrogenation of carbon dioxide (Equation 1-3).

$$H_2O + CO_2 + Ca^{2+} \rightarrow HCO_3^- + H^+ + Ca^+ \rightarrow CaCO_3 + 2H^+$$ Equation 1-3

This reaction however, produces hydrogen ions (H^+) in the calcifying fluid, which decreases the pH, making the conditions for precipitation less favourable. Biological control of the pH in the ECF is dominated by Ca-ATPase as this transport protein removes H^+ ions generated by $CaCO_3$ precipitation and deposits them at the site of photosynthesis in the coelentron in the tissue layer (Figure 1-20). Proton removal from the ECF elevates the pH (*Cohen et al.,* 2009b; *Allemand et al.,* 2011) in a process known as "pH up-regulation" (*Venn et al.,* 2011; *McCulloch et al.,* 2012a); consequently, the Ω_{arag} of the calcifying fluid is also increased, enhancing the precipitation at the site of calcification (*Al-Horani et al.,* 2003; *Cohen and Holcomb*, 2009). The increased pH promotes the equilibrium reaction $Ca^{2+} + CO_3^{2-} \rightarrow CaCO_3$, favouring the presence of CO_3^{2-} relative to HCO_3^- in dissolved organic carbon. This process only has an energy cost <1% of that generated from photosynthesis in return for the combined benefits of higher pH and saturation states (*McCulloch et al.,* 2012a). *Venn et al.,* (2013) showed that the pH of the ECF (pH_{cf}) can range from 7.2 to 8.8 and areas of higher pH generally indicate more favourable growing conditions. The calcifying epithelium has the lowest pH because it is in closer proximity to the external seawater in contrast to the aragonite crystals that are generally surrounded by the most elevated pH fluid under the calicoblastic epithelium (*Venn et al*., 2011; Figure 1-21).

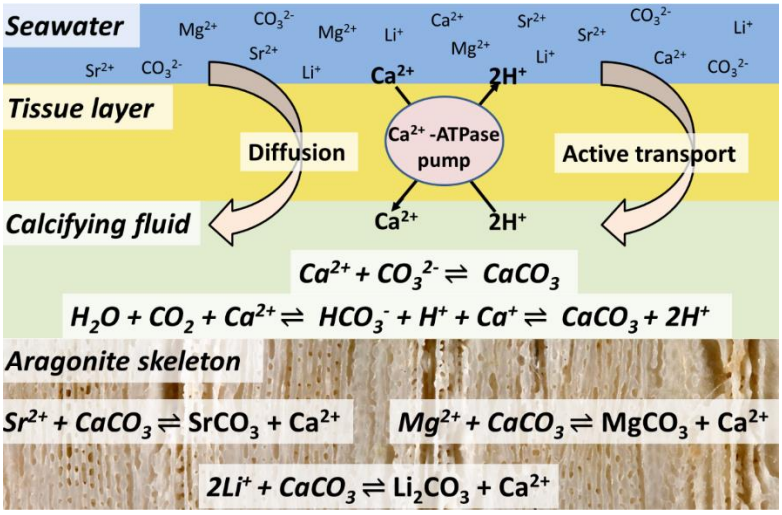

Figure 1-20. Schematic diagram of coral biomineralisation. Dissolved cations and anions are transported from the seawater, through the organic tissue layers and into the extracellular calcifying fluid by diffusion and active transport. Calcium ions (Ca^{2+}) are actively transported by the ATPase protein pump to the ECF where they directly precipitate with carbonate ions (CO_3^{2-}) to form the calcium carbonate skeleton ($CaCO_3$). Calcium carbonate can also be precipitated from the bicarbonate ion (HCO_3^-) following the hydrogenation of carbon dioxide (CO_2). This forms excess hydrogen ions (H^+) which are actively removed from the ECF by the ATPase pump (*Zoccola et al.*, 2004; *Sinclair and Risk*, 2006). Li^+, Sr^{2+} and Mg^{2+} can also substitute for Ca^{2+} in the aragonite skeleton. Figure based on *Allemand et al.*, (2004) and *McCulloch et al.*, (2012a).

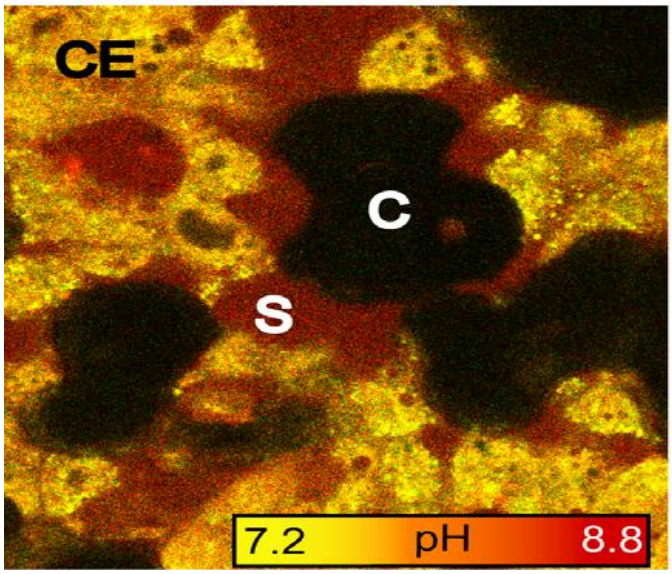

Figure 1-21. Distribution of pH in the calicoblastic epithelium of *S. pistillata*. Samples were stained with pH-sensitive indicator dye and imaged using inverted confocal microscopy. C = crystal. S = fluid-filled space under the calicoblastic epithelium. CE = calicoblastic epithelium. Figure from *Venn et al.*, (2011).

1.3.5 Corals as palaeothermometers

1.3.5.1 Temperature dependent elemental partitioning

Trace elements are incorporated in the growing $CaCO_3$ during biomineralisation in addition to Ca^{2+} and CO_3^{2-} ions (Figure 1-20). Corals are used as palaeothermometers because the partition coefficient (K_D) between seawater and coral aragonite of various cation contaminants (such as Li^+ (*Marriott et al.*, 2004a), Mg^{2+} (*Mitsuguchi et al.*, 1996) and Sr^{2+} (*Beck et al.*, 1992)) are temperature dependent and can be described by the equation:

$$K_{\mathrm{D}} = \left(\frac{\mathrm{X}}{\mathrm{Ca}}\right)_{\mathrm{coral}} / \left(\frac{\mathrm{X}}{\mathrm{Ca}}\right)_{\mathrm{sw}} \qquad \text{Equation 1-4}$$

Just like Ca^{2+} and CO_3^{2-} ions, these metal ions are transported from seawater to the semi-isolated ECF (*Sinclair and Risk*, 2006; *Gaetani et al.*, 2011; *Tambutté et al.*, 2011; *Gagnon et al.*, 2012) by direct diffusion or seawater leakage between cells (*Adkins et al.*, 2003; *Cohen et al.*, 2006; *Gaetani and Cohen*, 2006; *Gagnon et al.*, 2007; *Gagnon et al.*, 2012) or by active transport (Figure 1-19; *Ip and Lim*, 1991; *Ferrier-Pages et al.*, 2002). Sr^{2+} and Ca^{2+} ions are both doubly positive ions and similar in size (1.31 Å and 1.18 Å respectively; *Shannon*, 1976), enabling Ca^{2+} ions to be replaced by Sr^{2+} ions in the aragonite lattice [*Watson*, 1996; *Allison et al.*, 2005]. The incorporation pathway of smaller ions such as Li^+ and Mg^{2+} is less clear, and it is argued that their ionic radii (0.89 Å and 0.92 Å respectively; *Shannon*, 1976) are too small to directly substitute for Ca^{2+} (*Finch and Allison*, 2008; *Montagna et al.*, 2014). Despite this, the similarities between Mg^{2+} and Li^+ ionic sizes and partition coefficients (K_D <<1) indicate that similar processes govern their incorporation into coral aragonite (*Case et al.*, 2010; *Hathorne et al.*, 2013b; *Raddatz et al.*, 2013; *Montagna et al.*, 2014).

As more aragonite is precipitated, Ca^{2+} ions become depleted in the ECF, making cation contaminants relatively more abundant and increasingly more available to be incorporated. Sr is the second most abundant cation to Ca in aragonite (*Gagnon et al.*, 2012). The partition coefficient of Sr ($K_D^{Sr/Ca}$) in inorganic aragonite (*Gaetani and Cohen*, 2006) is:

$$K_D^{Sr/Ca} = \frac{D_{Sr}^{Aragonite-Seawater}}{D_{Ca}^{Aragonite-Seawater}} = 1.13 \; at \; 25\,^{\circ}C \qquad \text{Equation 1-5}$$

This causes Sr^{2+} ions to be preferentially incorporated into the coral skeleton because elements with a K_D >1 are preferentially incorporated, as opposed to elements that have a K_D <1; e.g. Li, which are not favoured (*Gaetani et al.*, 2011). The K_D of Sr/Ca and Li/Ca in aragonite all demonstrate an inverse relationship with temperature (*Marriott et al.*, 2004b; *Gaetani and Cohen*, 2006; *Montagna et al.*, 2014).

Coral thermometry therefore works on the assumption that aragonite is precipitated from a semi-isolated batch of calcifying fluid that can be replenished by flushed seawater, and that the variation in elemental ratios in the skeleton grown at any one time is a result of temperature dependent elemental partitioning. To interpret the environmental signal, the resulting skeletal elemental ratios are calibrated against a known SST record that can be from either *in situ* measurements (e.g. *Alibert and McCulloch*, 1997, *Hathorne et al*., 2013b) satellite measurements (e.g. *Cahyarini et al.*, 2014), a blended record of ship and satellite data (e.g. *Marshall and McCulloch*, 2002; *Linsley et al.*, 2004), or a collective record such as HadISST (e.g. *Grove et al*., 2013, *Maupin et al*., 2008). The resulting linear equation can then be applied to historic or fossilised coral samples in order to reconstruct temperature records that pre-date modern observations. The use of Sr/Ca ratios as an SST proxy in coral is discussed in section 1.3.5.3, and Li/Mg ratios in section 1.3.5.4.

1.3.5.2 Rayleigh fractionation

A complicating factor for element to calcium ratios in biogenic carbonates is Rayleigh fractionation: a process in which some elements are preferentially incorporated from the ECF into the precipitated aragonite skeleton relative to calcium. Rayleigh fractionation is largely driven by changes in the mass fraction of aragonite precipitated from each batch of calcifying fluid (*Gaetani and Cohen*, 2006; *Gagnon et al.*, 2007). As a consequence of the ECF being replenished by seawater diffusion, it is assumed that the initial composition of the ECF is similar to the composition of seawater. Using Sr/Ca as an example, like Equation 1-4, the partition coefficient (K_D) between the ECF and precipitated aragonite skeleton (arag) can be defined as:

$$K_{D_{Sr}}^{arag} = \left(\frac{Sr}{Ca}\right)_{arag} / \left(\frac{Sr}{Ca}\right)_{ECF} \qquad \text{Equation 1-6}$$

As $CaCO_3$ is precipitated from the ECF, the Ca^{2+} availability in the fluid decreases, so other ions such as Sr^{2+} become more preferentially incorporated. Rayleigh fractionation occurs if the K_D of an element is not equal to 1 and as the concentration of Ca in the calcifying fluid

decreases, the concentration of other elements will increase or decrease (depending on their K_D). Assuming a constant partition coefficient throughout precipitation, Rayleigh fractionation can be used to predict the Sr/Ca ratio in the composition of the precipitated aragonite skeleton from the initial ECF composition:

$$\left(\frac{Sr}{Ca}\right)_{ECF} = \left(\frac{Sr}{Ca}\right)_{SW} F^{(K_D^{Sr/Ca}-1)} \qquad \text{Equation 1-7}$$

where F is the fraction of Ca remaining in initial solution (i.e. represents the extent of precipitation from the ECF), which itself is defined as:

$$F = \frac{[Ca]_{ECF}}{[Ca]_{SW}} \qquad \text{Equation 1-8}$$

When F is equal to 1, no Ca^{2+} ions have been precipitated from the ECF, and when F is equal to 0, all of the Ca^{2+} ions have been precipitated. The Sr/Ca ratio of aragonite ($(Sr/Ca)_{arag}$) precipitated from an isolated batch of calcifying fluid can therefore be given by the equation:

$$\left(\frac{Sr}{Ca}\right)_{arag} = K_D^{Sr/Ca}\left(\frac{Sr}{Ca}\right)_{ECF} F^{(K_D^{Sr/Ca}-1)} \qquad \text{Equation 1-9}$$

Using Equation 1-9, the influence of Rayleigh fractionation on a number of element to calcium ratios in the calcifying fluid during aragonite precipitation were calculated from the starting composition of the ECF (seawater) and the calculated partition coefficient of each ratio. As expected, the Sr/Ca ratio decreases as more aragonite is precipitated because its high K_D (>1) means that more Sr will be removed from the ECF as more $CaCO_3$ is precipitated. The Li/Ca and Mg/Ca ratios both increase in the ECF relative the number of remaining Ca^{2+} ions because a low K_D (<<1) makes Li^+ and Mg^{2+} ions less likely to be precipitated. The apparent lack of Rayleigh fractionation influence on the Li/Mg ratio is discussed in more detail in section 1.3.5.4.

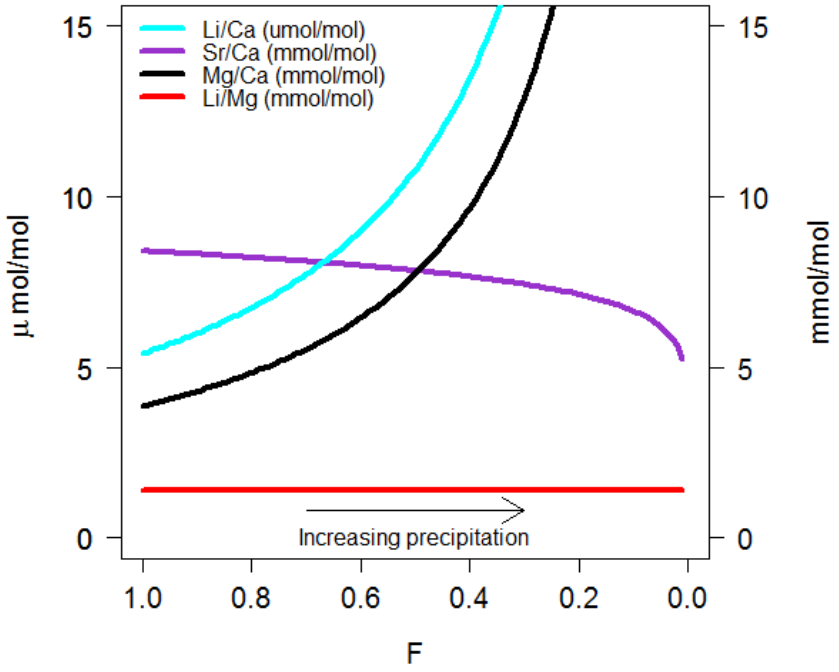

Figure 1-22. Changes in calcifying fluid elemental ratios during the precipitation of calcium. The Sr/Ca ratio (purple) of the calcifying fluid decreases as more aragonite is precipitated because the K_D>1. The Li/Ca and Mg/Ca ratios of the calcifying fluid increase due to Rayleigh fractionation because they become more available relative to calcium because their K_D<1. The effect on the Li/Mg ratio is negligible. Note that this model assumes a completely closed system and that the calcifying fluid is not replenished with flushed Ca, resulting in an extreme depiction of elemental ratio evolution with precipitation.

The elemental composition of coral aragonite in terms of element to calcium ratios is therefore determined by the K_D of each element, its relationship with temperature, and the amount of Ca precipitated from each batch of calcifying fluid (*Cohen et al.*, 2006; *Gaetani and Cohen*, 2006; *Gagnon et al.*, 2007; *Montagna et al.*, 2014).

1.3.5.3 Sr/Ca-SST proxy

The Sr/Ca ratio is by far the most commonly used geochemical temperature proxy in coral substrates (*Weber*, 1973; *de Villiers et al.*, 1994; *McCulloch et al.*, 1994; *Alibert and McCulloch*, 1997; *Cohen et al.*, 2001; *Cohen et al.*, 2002; *Ferrier-Pages et al.*, 2002; *Swart et al.*, 2002; *Fallon et al.*, 2003; *Gagnon et al.*, 2007; *Reynaud et al.*, 2007; *Mitsuguchi et al.*, 2008; *Caroselli et al.*, 2012; *Gagan et al.*, 2012; *Gagnon et al.*, 2013; *Raddatz et al.*, 2013; *DeLong et al.*, 2014), however, the reliability of this proxy has recently been called into question for a number of reasons.

Variations in the Sr/Ca composition of corals skeletons can occur as a result of "vital effects": biological processes that cause a constant isotopic/elemental composition offset with respect to inorganic precipitates, overriding environmental signals recorded in biominerals (*Urey et al.*, 1951; *Weber*, 1973). This is demonstrated by the depleted Sr/Ca in coral aragonite compared to abiogenically precipitated aragonite (i.e. in comparison to seawater Sr/Ca), in addition to coral Sr/Ca ratios being twice as sensitive to changes in SST than Sr/Ca ratios in abiogenic aragonite (*Gaetani and Cohen*, 2006).

In corals, the kinetic response of Sr/Ca is particularly evident in the lower ratios from skeleton precipitated in the day, and night precipitation being higher and more closely matching abiogenic precipitation trends (*Cohen et al.*, 2001). Additionally, the Sr/Ca of daytime precipitation is greater than four times more sensitive to temperature than nighttime precipitation (*Cohen et al.*, 2001).. Corals possess a gene which responds to changes in light (STPCA gene), and during the nighttime it produces double the amount of enzyme in the calcifying fluid which converts CO_2 to HCO_3^- ions than it does during the daytime. It has been suggested that this increased nighttime activity is required to buffer against H^+ ions (which decrease pH), because they are no longer removed during daytime photosynthesis. Therefore such differences in daytime and nighttime Sr/Ca ratios are a result of differing precipitation mecahnisms at these times, and may be response to a variation in calcifying fluid pH (*Moya et al*., 2008).

The most prominent demonstration of secondary influences on the Sr/Ca-SST proxy is the observation that different colonies of the same species for different locations or within different individuals belonging to the same colony produces a wide range of Sr/Ca-SST slope and intercept values. This can be illustrated by applying Sr/Ca-SST regressions generated from 37 studies of *Porites* coral to a Sr/Ca ratio of 9.035 mmol/mol (the Sr/Ca predicted at 25ºC for the mean of the compilation; *Corrège*, 2006). Most reconstructed temperatures fall within 2ºC of the 25ºC value, although extreme values of 19ºC and 32ºC are obtained (Figure 1-23; *Gaetani et al*., 2011). Similar differences in the SST-Sr/Ca calibration are also evident within individual studies (*Saenger et al.*, 2008). The observed variation in Sr/Ca between corals of the same colony could at least be partly explained by the possibility of each coral precipitating a different amount of aragonite per batch of calcifying fluid. The lesson from these observations is that the Sr/Ca-SST proxy is not robust enough to apply a single calibration to all tropical coral samples.

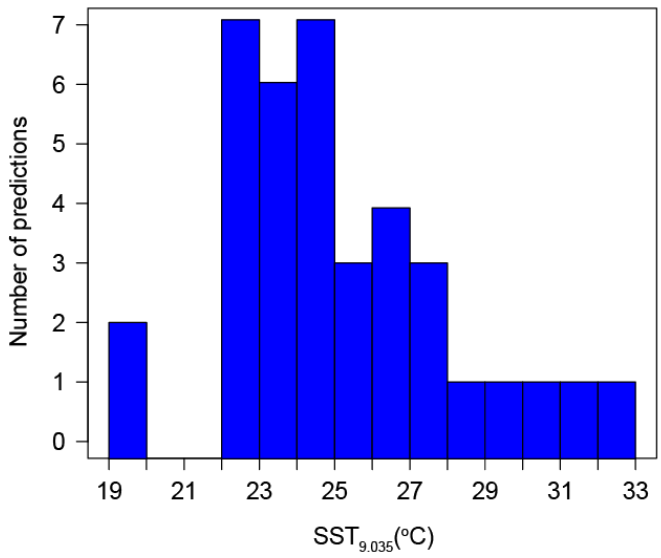

Figure 1-23. Bar chart showing the range of temperatures that would be generated from assuming a Sr/Ca ratio of 9.035 mmol/mol in 37 different calibrations of the *Porites* species. Adapted from *Gaetani et al.*, (2011).

Macro- and microstructural variations in the skeleton, and the rate at which the skeleton is deposited can also impact Sr/Ca ratios. For example, Sr/Ca is affected by the density of $CaCO_3$ which has alternating high (8.2 mmol/mol) and low density (8.9 mmol/mol; Figure 1-24a) bands between summer and winter growth (*Alibert and McCulloch*, 1997; *Cohen et al.*, 2001), bearing in mind that calcification rates can be stimulated by higher temperatures. Some faster growing corals have lower Sr/Ca ratios than slow growing corals (*de Villiers et al.*, 1994). The centres of calcification (COC) between the columella and theca wall (Figure 1-24b) experience more extreme vital effects such as calcification, resulting in significantly higher ratios of Sr/Ca in the COC (*Cohen et al.*, 2001; *Meibom et al.*, 2006; *Raddatz et al.*, 2013). An additional temperature influence is also given by the mass of aragonite precipitated from the isolated batch of seawater which is thought to increase with rising temperature (*Gaetani et al.*, 2011). For example, as temperature increases from 5°C to 30°C the $K_D^{Sr/Ca}$ decreases by 14% (*Gaetani et al.*, 2011), resulting in fewer Sr ions being incorporated into the aragonite.

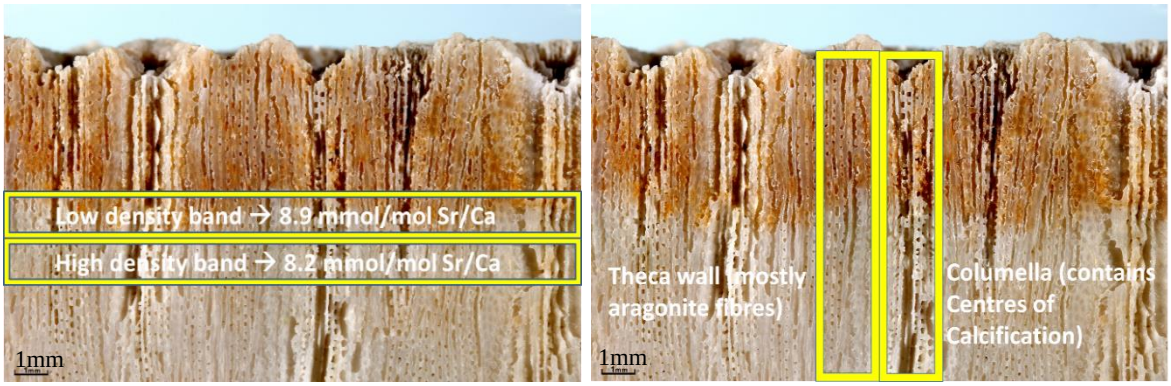

Figure 1-24. Macrostructure (left) and microstructure (right) variations in coral skeletons introduces deviations in Sr/Ca ratios. Sr/Ca ratios are higher in low density bands (winter) and lower in high density (summer) bands. The septa and theca wall also possess varying element/Ca ratios, with more variable conditions occurring in the centre of calcification, resulting in significantly higher ratios of Sr/Ca. Brown layer is the tissue layer where calcification occurs.

1.3.5.4 Li/Mg-SST proxy

The Li/Mg ratios of corals are inversely correlated to temperature, and have recently been explored as an alternative to Sr/Ca ratios based on the view that Li/Mg ratios are not significantly impacted by vital effects. The advantages of Li/Mg ratios are that Ca is not used to normalise, the similar K_D of Li/Ca and Mg/Ca (<<1), and the opposing effect of temperature on Li/Ca (positive relationship) and Mg/Ca (negative relationship) means precipitation progress does not have a significant influence on the Li/Mg ratio of the fluid (*Montagna et al.*, 2014), i.e. because the K_D Li/Ca and Mg/Ca are both extremely low, almost all of the available Ca ions in the ECF must be removed before the Li/Mg ratio of the ECF of the coral is altered. This is demonstrated by the Rayleigh fractionation model output in Figure 1-22, whereby the Li/Ca and Mg/Ca ratios of the ECF increase significantly during the precipitation of aragonite, in contrast to the Li/Mg ratio which does not appear to change as a function of the mass of aragonite precipitated (F). The positive relationship between measured Li/Ca and Mg/Ca in multiple coral species across a range of temperatures (0 to 28°C) shows that the values of these slopes (i.e. the sensitivity of one ratio to a change in the other), is dominated by temperature (*Montagna et al.*, 2014). It was further shown that the evolution of the $K_D^{Li/Mg}$ with temperature produced an exponential relationship that matched the sensitivity of the Li/Mg ratios to temperature (5% decrease per 1°C) and thus the incorporation of Li/Mg into aragonite is controlled by the $K_D^{Li/Ca}$ being more sensitive to temperature relative to $K_D^{Mg/Ca}$.

1.3.6 Boron isotope systematics

Boron is present in seawater as the two stable isotopes ^{10}B and ^{11}B and the ratio of these isotopes denotes the boron isotopic composition, which in marine carbonates such as coral can be used as a proxy for palaeo seawater pH (e.g. *Foster and Rae*, 2016, and references therein). The boron isotopic composition is reported using delta notation ($\delta^{11}B$; Equation 1-10), based on the measurement of a sample against the National Institute of Standards and Technology (NIST) Standard Reference Material (SRM) 951 boric acid (*Catanzaro*, 1970).

$$\delta^{11}B(‰) = \left[\left(\frac{^{11}B/\ ^{10}B_{sample}}{^{11}B/\ ^{10}B_{NIST951}}\right) - 1\right] \times 1000 \qquad \text{Equation 1-10}$$

This proxy is dependent on the observation that dissolved boron exists as boric acid ($B(OH)_3$; trigonal coordination) and the borate ion ($B(OH)_4^-$; tetrahedral coordination). The equilibration of these two species is described by the reaction:

$$B(OH)_3 + H_2O \rightleftharpoons B(OH)_4^- + H^+ \qquad \text{Equation 1-11}$$

The pH at which the proportions of these two species in a solution are equal is called the boron dissociation constant (pK_B^*), and in addition to pH, it can be influenced by temperature and salinity (Dickson, 1990). Boron isotopes are also fractionated by ~27‰ between aqueous $B(OH)_3$ and $B(OH)_4^-$ species (Figure 1-24; *Urey*, 1947; *Klochko et al.*, 2006) and the isotopic exchange is described by the reaction:

$$^{10}B(OH)_3 + {}^{11}B(OH)_4^- \rightleftharpoons {}^{11}B(OH)_3 + {}^{10}B(OH)_4^- \qquad \text{Equation 1-12}$$

This isotopic fractionation between the dissolved boron species, and their pH dependent abundance means that the boron isotopic composition of the species is also pH dependent (Figure 1-25b). The result is that at low pH, boric acid is the dominant species, and at high pH the dominant species is the borate ion (Figure 1-25a; *Hemming and Hanson*, 1992). The impact of changing seawater pH on $\delta^{11}B$ is demonstrated in Figure 1-25b, where it is evident that the $\delta^{11}B$ of borate as well as the abundance has a positive relationship with pH_{sw} and therefore increases with increasing pH_{sw}.

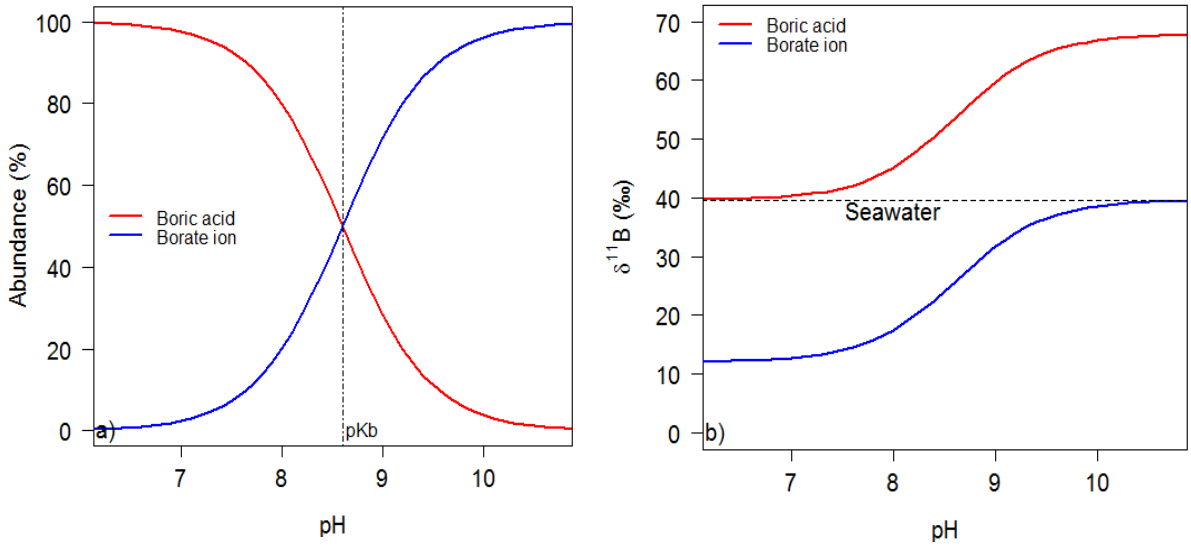

Figure 1-25. a) Changes in the proportion of borate ion $B(OH)_4^-$ and boric acid $B(OH)_3$ with evolving pH shows that the borate ion is dominant at high pH (T=25°C, S=35 psu). b) The boron isotopic composition ($\delta^{11}B$) increases with increasing seawater pH.

The boron isotopic composition of carbonates is ultimately calculated using the pK_B^*, the $\delta^{11}B$ of seawater (39.61‰; *Foster et al.*, 2010), the measured $\delta^{11}B$ of the carbonate sample, and the fractionation factor between boric acid and the borate ion ($\alpha_{B3\text{-}B4}$) using the equation of *Hemming and Hanson*, (1992):

$$pH = pK_B^* - log\left(-\frac{\delta^{11}B_{SW} - \delta^{11}B_{coral}}{\delta^{11}B_{SW} - (\alpha_{B3-B4} \times \delta^{11}B_{coral}) - 1000 \times (\alpha_{B3-B4} - 1)}\right)$$

Equation 1-13

1.3.6.1 $\delta^{11}B$-pH proxy in corals and the impact of pH up-regulation

The boron isotope pH-proxy is becoming a well-established method of indirectly measuring pH_{cf} in corals (*Sanyal et al.*, 1996; *Hönisch et al.*, 2004; *Reynaud et al.*, 2004; *Krief et al.*, 2010; *Trotter et al.*, 2011; *McCulloch et al.*, 2012b). Skeletal $\delta^{11}B$ has been measured by thermal ionization mass-spectrometry (*Hönisch et al.*, 2004; *Reynaud et al.*, 2004; *Trotter et al.*, 2011; *McCulloch et al.*, 2012b) multi-collector inductively-coupled plasma mass-spectrometry (*Krief et al.*, 2010), and ion microprobe (*Rollion-Bard et al.*, 2011), and results show that corals predominantly incorporate the borate ion species (*Hemming and Hanson*, 1992). Regardless of analytical approach, the majority of studies to date show broadly similar trends between $\delta^{11}B$ and pH (Figure 1-26a).

Early studies of boron isotope systematics in coral (*Sanyal et al.*, 1996; *Sanyal et al.*, 2001; *Hönisch et al.*, 2004; *Reynaud et al.*, 2004) proposed there was no significant offset from the borate curve and therefore no pH up-regulation. However, this is entirely due to the incorrect calculation of the borate curve through the use of an isotopic fractionation factor of 1.0194 derived by *Kakihana et al.*, (1977), which was later shown to be incorrect by *Rustad et al.*, (2010). The pH up-regulation mechanism was not recognised until the isotopic fractionation factor of 1.0272, derived by *Klochko et al.*, (2006) was employed (*Krief et al.*, 2010; *Trotter et al.*, 2011), but it is now widely acknowledged that this biological process impacts the δ^{11}B-pH proxy in coral as a direct result of increased pH_{cf} (*McCulloch et al.*, 2012a; *McCulloch et al.*, 2012b; *Holcomb et al.*, 2014).

The process of pH-upregulation means that the δ^{11}B of corals is a record of their internal pH, and not external seawater pH (pH_{sw}). This extent of internal pH elevation is species-specific and is the reason why coral δ^{11}B data do not lie on the borate ion curve in Figure 1-26a. This offset can be corrected for however after the relationship between external seawater pH and internal pH_{cf} has been calibrated in the field or laboratory. For example, Equation 1-14 is the calibration for the species *Stylophora pistillata* (*Krief et al.*, 2010), but a range of existing calibrations are shown in Figure 1-26.

$$pH_{SW} = \frac{\left(pH_{cf} - 6.06\right)}{0.70} \qquad \text{Equation 1-14}$$

Observations of the δ^{11}B of both tropical and cold-water coral aragonitic species demonstrate a greater offset from the borate ion curve at lower pH_{sw}, and that the pH buffering capacity is species-specific (Figure 1-26b). Cold-water and deep sea corals differ from tropical corals in that they are azooxanthellate and can be found in undersaturated or low saturation state waters in terms Ω_{arag} and carbonate ions (*Thresher et al.*, 2011). This opens up the question of whether such species have evolved a different biomineralisation mechanism than tropical coral species, to account for the effects of low carbonate saturation states and low temperatures. Cold-water and deep sea corals can be challenging archives to use, given the lack of pH and carbon chemistry measurements. However, such coral species hold an advantage over tropical corals, in that they are more uniformly distributed geographically, making it possible to reconstruct pH uniformly from δ^{11}B across the globe. The combination of a limited understanding of calcification mechanisms, narrowly constrained historic seawater composition and restricted observational data mean that

fossilised specimens are less suitable than sampling living coral colonies, restricting the time scale of historic climate reconstructions.

The heavier $\delta^{11}B$ compositions of cold-water coral indicates that corals from environments of lower pH and Ω_{arag} (even <1 Ω_{arag}) increase their internal pH 0.2 pH units higher than tropical corals relative to their respective ambient seawater pH (Figure 1-26; *Anagnostou et al.*, 2012; *McCulloch et al.*, 2012b; *Martin et al.*, 2016). According to the boron isotope based model derived by *McCulloch et al.*, (2012b), pH_{cf} increases in tropical corals can range from 0.3 – 1.2 units (Figure 1-26).

Through the comparison of six different tropical coral species, *Trotter et al.*, (2011) identified a linear relationship between the pH_{cf} and the pH_{sw}, with the biologically driven offset inversely proportional to the pH_{sw} (Figure 1-26), which is also present in cold-water corals (*Anagnostou et al.*, 2012; *McCulloch et al.*, 2012b; *Martin et al.*, 2016). However, the ability to change internal pH has been observed to decrease with decreasing pH_{sw} (*Cohen and Holcomb*, 2009; *Ries*, 2011; *McCulloch et al.*, 2012a; *Venn et al.*, 2013). This reduction was investigated by *Holcomb et al*., (2014) by culturing the tropical coral *Stylophora pistillata* at a range between 7.17 and 7.94 pH units. Growth rates and pH_{cf} measurements were taken from the apical growth region (vertical) and lateral growth region using a pH sensitive indicator dye and confocal microscopy, or boron isotopes. Lateral growth rates had a negative linear correlation with pH, and similar to the study of *Venn et al.*, (2013), the pH indicator dye showed that pH_{cf} also decreased with decreasing pH. The pH calculated from the skeletal $\delta^{11}B$ also reflected this trend, but importantly, both of these methods showed a similar rate of decrease in pH_{cf} with external pH (~0.2 pH unit decrease in internal pH corresponding to a 0.8 pH unit decrease in seawater pH).

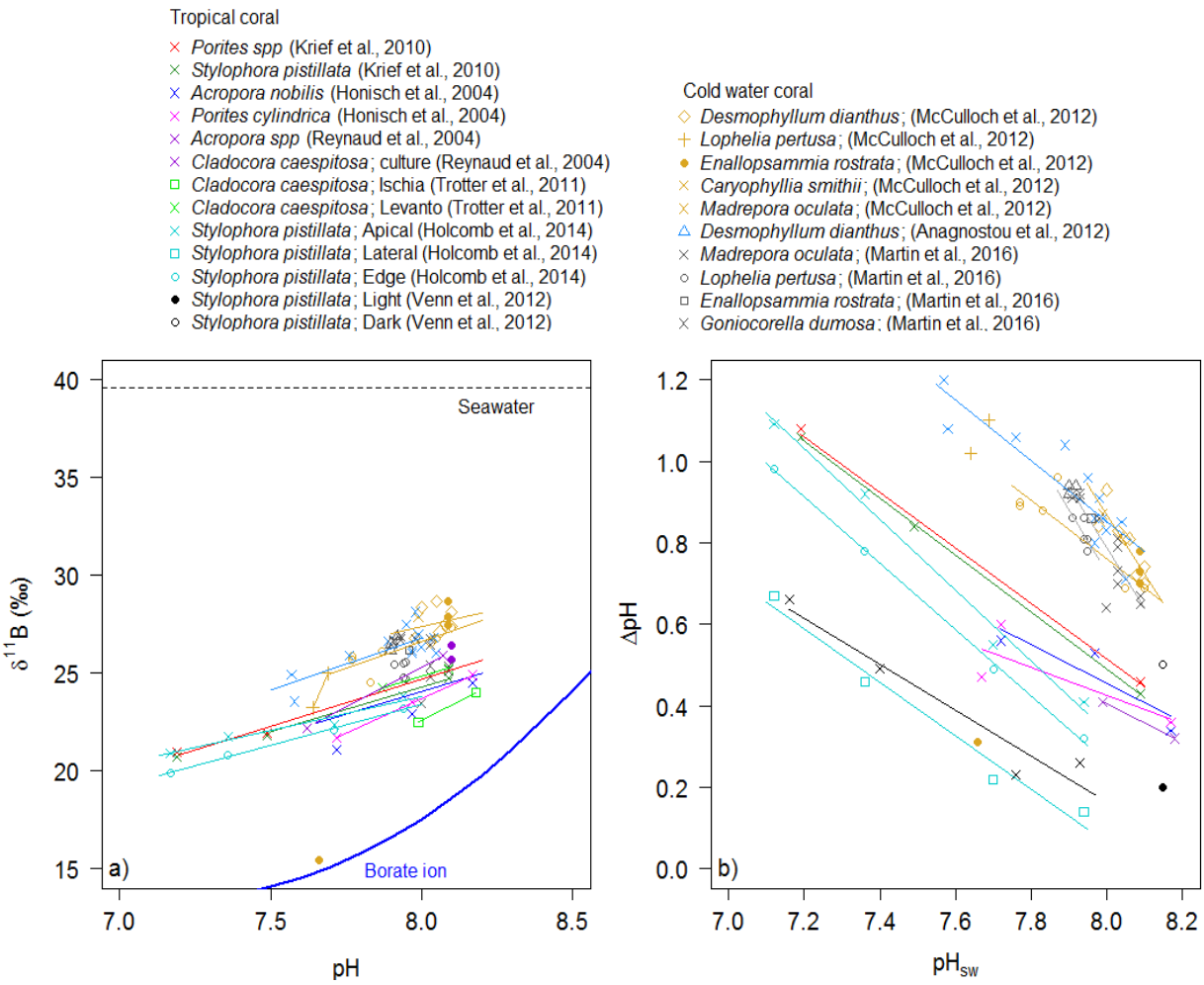

Figure 1-26. a) The $\delta^{11}B$ of corals are offset from the borate ion curve, and the cold water corals of *Anagnostou et al.*, (2012), *McCulloch et al.*, (2012b) and *Martin et al.*, (2016) are more offset than tropical corals (*Hönisch et al.*, 2004; *Reynaud et al.*, 2004; *Krief et al.*, 2010; *Venn et al.*, 2011; *Holcomb et al.*, 2014). The calcitic coral *C. smithii* almost sits on the borate curve (*McCulloch et al.*, 2012b). b) Existing relationships between seawater pH and the pH of calcifying fluid (ΔpH) imparted during calcification in the tropical coral species *Porites*, *Acropora*, and *Stylophora*. ΔpH is calculated as the difference between pH_{cf}, calculated directly from skeletal $\delta^{11}B$, using the fractionation factor (α=1.0272) of (*Klochko et al.*, 2006), and measured pH_{sw}. These linear regressions represent the species pH calibrations.

A novel study by *Georgiou et al.*, (2015) investigated the potential impacts of OA on pH_{cf} by exposing the coral *Porites cylindrica* to seawater pH between 7.73 (anticipated beyond 2100, *Gattuso and Lavigne*, 2009) and 8.23 using free ocean carbon enrichment facilities (FOCE). This involved transplanting nubbins of coral into FOCE chambers that allow natural seawater to flow through, whilst simultaneously adjusting the pH within the chamber by injecting CO_2, allowing natural reef variations to be assessed in the context of a more acidic environment. Using boron isotope analysis, the authors found that unlike laboratory-based cultures, these colonies maintained relatively consistent elevated pH_{cf} (8.4

to 8.6), regardless of increased CO_2 or seasonality, and with no apparent compromise in extension rates. However, the authors were unable to make any predictions for how much longer such pH homeostasis will be possible given the predicted declines in seawater pH.

1.4 Key research aims

Coral reefs are exposed to multiple anthropogenic stressors, and one way to study how they have been impacted over the last century is to use palaeoproxies in the coral *Siderastrea siderea*; one of the most prevalent reef-building and robust species in the Caribbean. In light of this, here an emerging SST proxy is explored and the boron isotope proxy is applied to meet the following aims:

Aim 1: Reconstruct the pH of the Belizean forereef and backreef between 1912 and 2008 (Chapter 3).

Despite holding part of the second largest barrier reef system in the world, Belize is poorly monitored in terms of the carbonate system. The first aim is therefore to reconstruct the pH of two areas of the Mesoamerican Barrier Reef using the boron isotopic skeletal composition of *S. siderea*. The first area is the forereef, located on the ocean-side of the reef crest; the second area is the backreef, located on the landward side of the reef crest. Have the forereef and backreef corals recorded the same changes in pH? What is the cause of any divergence? Can the evolution of open ocean pH be reconstructed by coral $\delta^{11}B$ in this region?

Aim 2: Testing the applicability of the Li/Mg-SST proxy in the Caribbean coral *Siderastrea siderea* (Chapter 4)

It is well documented that the traditional method of using Sr/Ca ratios to generate SST reconstructions can be inaccurate due to a large number of secondary effects that can influence these ratios. The Li/Mg-SST proxy has been recently developed in *Hathorne et al*., (2013b) and *Montagna et al*., (2014) but has not previously been examined in the tropical coral *S. siderea* - a resilient species that is common in the Caribbean. By meeting this aim, the following questions will be addressed: Can the Li/Mg-SST proxy be applied to *S. siderea*? If so, how do the Li/Mg derived SST reconstructions compare to Sr/Ca derived

SSTs? Do corals from different reef zones bring about spatial differences in Li/Mg-SSTs? And finally, if the Li/Mg and Sr/Ca ratios are combined in a multi-proxy approach, do the SST reconstructions improve?

Aim 3: Generate the first sub-annual, multi-year $\delta^{11}B$ record in *S. siderea* (Chapter 5)

Although the use of the $\delta^{11}B$-pH proxy in corals has grown in popularity over recent years, the majority of pH reconstructions generated are on an annual resolution. Is it possible to generate monthly to seasonal $\delta^{11}B$-pH records from *S. siderea*? If so, what do these reconstructions reveal aboutthe seasonal dynamics of the forereef and backreef zones? Is pH controlled by the same factor across different areas of the reef?

Aim 4: Determine how the Li/Mg-SST proxy can be impacted by secondary influences (Chapter 5).

Secondary impacts on traditional SST-proxies such as Sr/Ca and $\delta^{18}O$ have been widely investigated. However, the Li/Mg-SST proxy is still a novel technique and any secondary impacts have not yet been thoroughly investigated, particularly since the initial results have been so positive. The final questions of this thesis include asking, is there a secondary parameter affecting the Li/Mg-SST? Is this demonstrated equally in cultured and field coral samples?

1.5 Thesis outline

1.5.1 Chapter 2: Methodology

Chapter 2 describes in depth the techniques and processes involved in collecting coral samples from the field, subsampling, laboratory and analytical methods. The long-term analytical reproducibility is explored. The methods are also summarised in each chapter in a more relevant context.

1.5.2 Chapter 3: Declining coral calcification in Belize decoupled from ocean acidification

Chapter 3 explores the extent of ocean acidification in the forereef and backreef zones in Belize by analysing the boron isotopic composition of coral skeletons. The $\delta^{11}B$ records show that there has been a 0.15 pH unit decline in backreef water between 1915 and 2008, whereas no acidification trend was evident in the forereef, despite the corals here having a significant decline in extension rate over the same period. The influence of sedimentation and changes in primary production/macroalgae cover is considered to be the cause of these observations.

1.5.3 Chapter 4: Intra-reef variations in Li/Mg and Sr/Ca sea surface temperature proxies in the Caribbean reef-building coral *Siderastrea siderea*

This chapter is published in *Paleoceanography* (*Fowell et al*., 2016), and compares the Sr/Ca and Li/Mg-SST proxies in the coral *Siderastrea siderea*. Sr/Ca, a more traditional SST proxy, and Li/Mg, a novel SST proxy, are both applied at monthly resolution coral samples from the forereef and backreef environments of Belize. This enables both an investigation into the spatial variability in the Li/Mg and Sr/Ca SST calibrations and a comparison to be made between resulting SST reconstructions and the historic HadISST record. While the forereef temperature reconstructions are similar to the HadISST record, a secondary influence on Li/Mg prevented an accurate reconstruction to be made using backreef coral. However, applying a multi-elemental proxy to the backreef samples appeared to remove the impacts of this secondary parameter and allowed accurate reconstructions to be produced.

1.5.4 Chapter 5: Examining the effect of pH on the Li/Mg- and Sr/Ca-SST proxies: insights from culture and sub-annual boron isotope data

The data presented in Chapter 4 implied that there are unknown secondary influences on the Li/Mg-SST proxy. In Chapter 5 the role of pH in driving the discrepancies between forereef and backreef Li/Mg-SST reconstructions is explored. Monthly to seasonal resolution coral skeletal boron isotopic compositions were used to reconstruct pH, revealing that forereef and backreef pH cycles are controlled by different environmental parameters. The relationships

between cultured coral elemental ratios and field elemental ratios with both pH and SST were all negatively correlated. The pH effect on the Li/Mg and Sr/Ca ratios of field corals was removed using the relationship observed in the cultured samples, and in doing so, the Li/Mg- and Sr/Ca-SST relationships in forereef and backreef coral became more similar to each other, and in some instances, more similar to the relationship with SST in cultured samples. However, even by combing the SST and pH influence on these ratios in a multivariable model it failed to explain all of the variation in these ratios.

1.5.5 Chapter 6: Summary

The final chapter summarises the major findings of this thesis. The major findings include: corals in different environments have already demonstrated differing responses to the threats of climate change, and that each of these environments is also experiencing changes at different rates, and that these changes can interfere with the geochemical proxies used to reconstruct historic seawater parameters. Therefore, future directions are suggested to further develop our understanding of how corals may respond to future climate change, how we can monitor this in terms of local biogeochemistry, and how to limit the effects of different anthropogenic stressors on geochemical proxies. Preliminary geochemical data from corals from Bermuda, where a plethora of *in situ* monitoring data is available to help to further constrain proxy calibrations, is also presented in brief.

Chapter 2: Methods

The samples examined in this thesis come from two principal locations in the Mesoamerican Barrier Reef System: the forereef and backreef environments of the Sapodilla Cayes. This chapter opens by discussing the sample location and sampling methods, and is followed by a thorough discussion of the analytical techniques used during the sample analyses.

Figure 2-1 Aerial photograph of part of the Mesoamerican Barrier Reef System forereef. It is possible to see that the reef is not a continuous solid structure because there are channels through the barrier reef. Credit: Michelle Jasinska (Tobacco Caye Marine Station).

2.1 Field and sampling techniques

2.1.1 Coral coring

In February 2009, Professor Justin Ries (Northeastern University, Boston, US) and Dr Karl Castillo (University of North Carolina, Chapel Hill, US) collected thirteen *Siderastrea siderea* cores from individual colonies across the Southern Belize portion of the Mesoamerican Barrier Reef System (MBRS). Three cores were collected from the near shore reef zone in Port Honduras Marine Reserve, three from the backreef and seven from the forereef in the Sapodilla Cayes (*Castillo et al.*, 2011). Cores up to 1 m long were collected using a 2 horse power hand held pneumatic air drill with a custom hollow extension rod and wet diamond core bit (Figure 2-2; further details can be found in *Castillo et al.*, 2011). For this study, the forereef cores FR-02 and FR-12, and the backreef core BR-06 were selected (Figure 2-3). Given that it was not possible to analyse multiple cores from each reef zone during the time scale of this project, it is assumed that the cores discussed throughout this thesis are representative of their reef zone in terms of their skeletal composition and resulting climate reconstructions, but this cannot be guaranteed.

Figure 2-2. Dr Karl Castillo coring a *Siderastrea siderea* colony using a pneumatic air drill with a hollow extension rod and wet diamond core bit. Credit: Dr Karl Castillo.

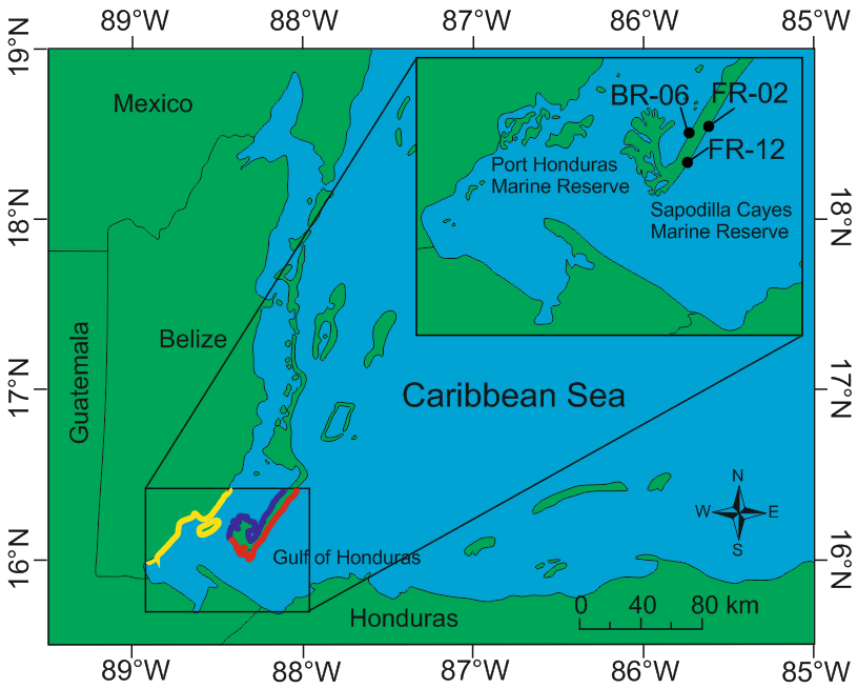

Figure 2-3. Sampling location map of *Siderastrea siderea* in Belize. Coral cores used in this study were taken from the forereef (red) and backreef (blue) zones in the Sapodilla Cayes. The yellow area outlines the nearshore reef zone which was also sampled but not used as part of this study.

2.1.2 Coral culturing

In July 2011, eighteen young *Siderastrea siderea* colonies (20-30 years old) were removed from the forereef, backreef and nearshore reef zones using a hammer and chisel (see *Castillo et al.*, 2014, for detailed sample locations) and flown to the Aquarium Research Center at the University of North Carolina at Chapel Hill, USA (Figure 2-4a). Eighteen sections were taken from each colony (Figure 2-5) and glued to microscope slides, which were then left to acclimatise for 30 days in recirculating artificial seawater tanks maintained at 35 psu and 28ºC. The aim of the culturing was to determine if the calcification rate would be affected by variable temperatures (25°C, 28°C and 32°C) or variable pCO_2 conditions (324 ppm, 604 ppm and 2553 ppm). After the initial acclimatisation period, the pCO_2 and temperature of the relevant tanks were incrementally changed to the experimental conditions over the course of 15 days (*Castillo et al.*, 2014; Figure 2-5). Intracolonial replicates allow the response of an individual to be tested. With intercolonial replicates, it is possible to investigate if individuals from the same reef zone exhibit the same response to the experimental conditions or if the response is more isolated to a particular individual (intercolonial replicates).

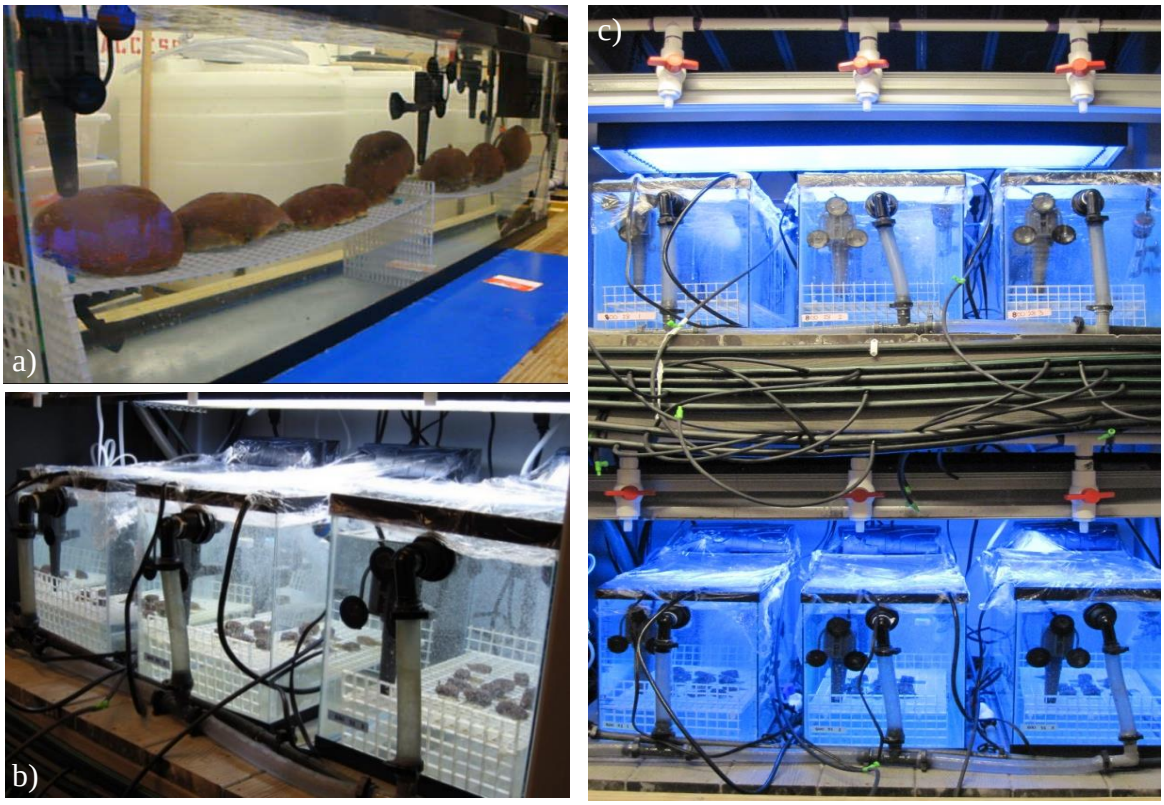

Figure 2-4. Culturing tanks at the University of North Carolina, Chapel Hill. a) Transport of live colonies from Belize. b) Tanks showing 3 replicate nubbins of forereef, backreef and nearshore reef colonies. c) Array of experimental tanks demonstrating the corals were kept under constant light and CO_2 conditions. Images courtesy of Professor Justin Ries.

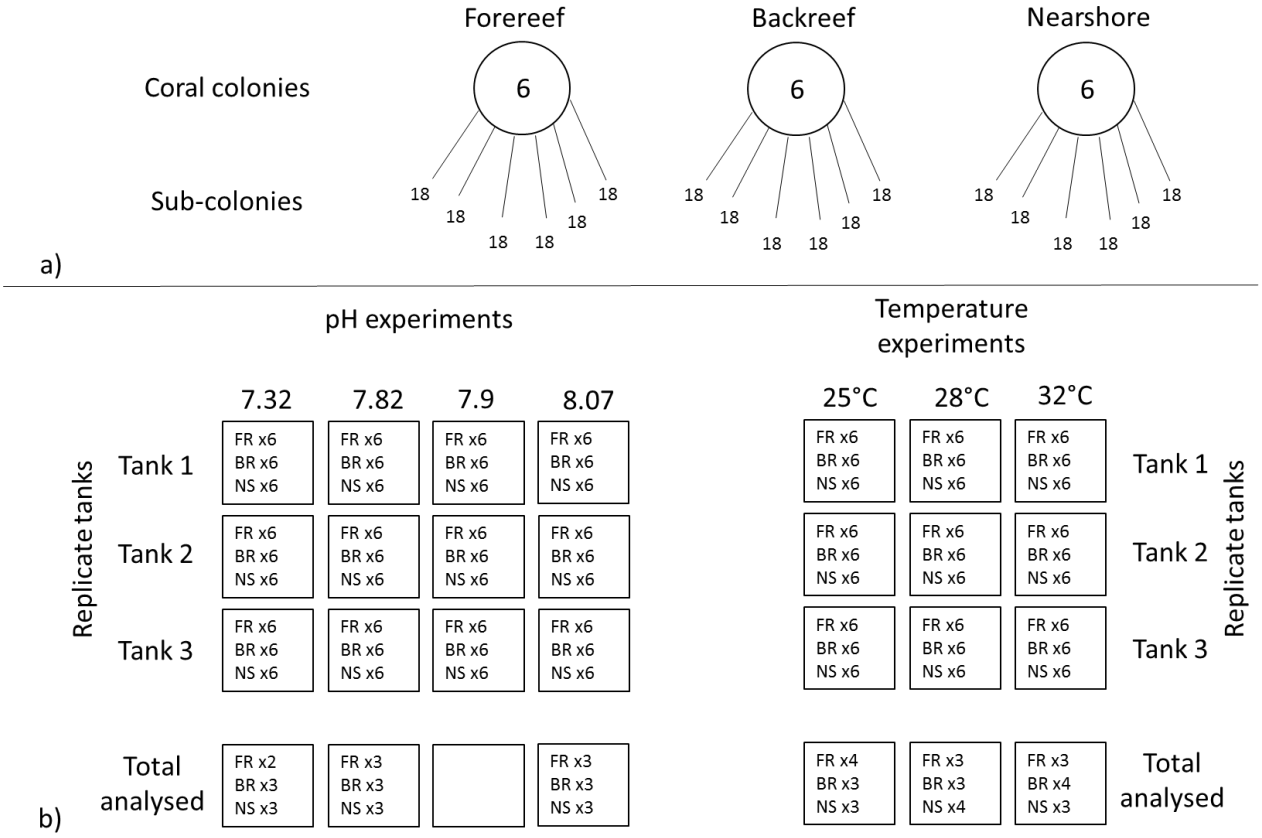

Figure 2-5. Coral cultures. a) 18 live coral colonies were collected from Southern Belize, 6 from the forereef, 6 from the backreef, 6 from the nearshore reef. Each live colony was sectioned into 18 replicate sub-colonies. b) The sub-colonies were used in the pH and temperature experiments. For each different experimental condition, there were three replicate tanks, each containing 18 sub-colonies. Generally, the elemental composition of one sub-colony from each reef zone from each tank was analysed.

All aquaria contained recirculating artificial seawater (*Instant Ocean Sea Salt;* Table 2-1) at 35.13 ± 0.13 psu. For two of the three temperature experiments, temperatures of 28.16°C ± 0.24, and 32.01°C ± 0.17 were maintained with 50 watt heaters, and for the remaining experiment a temperature of 25.01°C ± 0.14 was maintained using a 1 hp aquarium cooler. Temperatures were measured on alternate days with a NIST-calibrated 170 partial-immersion organic-filled glass thermometer. Three replicate samples from each reef zone were maintained in three replicate experiment tanks with an average pCO_2 concentration of 488 ppm (pH 7.94 ± 0.12). For the CO_2-induced acidification experiment, four pCO_2 partial pressures (±1σ standard deviation) of 324 ppm ± 89, 604 ppm ± 107 and 2553 ppm ± 506 (pH 8.07 ± 0.12, 7.82 ± 0.13 and 7.32 ± 0.14 respectively) were applied and each concentration was replicated in 3 tanks at an average temperature of 28.01°C ± 0.28. The pCO_2 concentrations were manipulated by altering the amount of compressed CO_2 gas bubbled into the aquaria controlled with mass flow controllers. Further details of the culture experiments can be found in (*Castillo et al.*, 2014). Here, in order to adjust for

variations between natural and artificial seawater elemental ratios, the culture media was sampled every week (total of 14 samples per tank), and a representative 6 samples were measured from each tank (total of 108 samples) using the X-Series ICP-MS. Any samples used from these experiments will be referred to as the "cultured samples" throughout this thesis.

Table 2-1. Composition of *Instant Ocean Sea Salt*.

	mmol/kg	mg/g
Na	462	10.62
Mg	52	1.26
Ca	9.40	0.38
Sr	0.19	0.02
Cl	521	18.47
Li	0.05	0.0004
Ba	0.0009	0.0001

2.1.3 Coral core structure statistics and annual resolution sampling

The skeletal age, extension rate, density and calcification rate of the corals was determined by Dr Karl Castillo. To do this, the cores were cut into 8 mm thick slabs using a diamond-tipped tile saw and X-rayed (Figure 2-6). The software Coral X-radiograph Densitometry System (Coral*XDS*) is used to trace the annual banding evident on the X-ray images allowing the chronology to be calculated by labelling the first high density band (deposited the same winter as the collection), and counting each subsequent high density band backwards in time (*Castillo et al.*, 2011). The individual bands were cut from the slabs using a diamond-tipped band saw (Inland Hobby DFS-100 ReefKeeper Saw) and ultrasonicated for 10 minutes, rinsed using 100% pure ethanol and then air-dried for >12 hours. Half of each section was finely crushed in 30 second intervals, with 1 minute breaks to avoid heat build-up, to talcum powder consistency. These samples were prepared and provided by Professor Justin Ries, and further details can be found in (*Castillo et al.*, 2012). From here-on in, these samples will be referred to as the "annual samples" and will be discussed in more detail in Chapter 3.

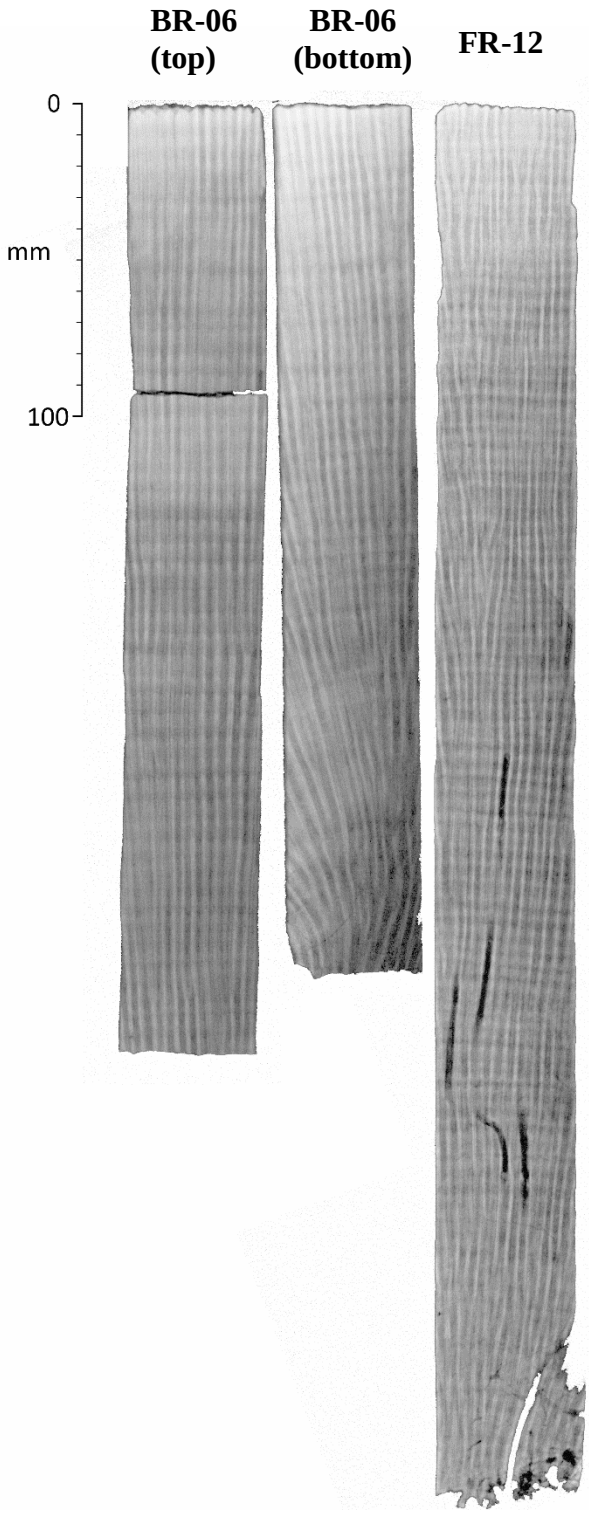

Figure 2-6. Example of X-ray images of the coral slabs. a) Backreef core BR-06. b) Forereef core FR-12.

2.1.4 High-resolution sampling

Monthly resolution samples (for elemental ratio analysis) were obtained from the field samples by micromilling coral slabs (Figure 2-7a) cut from the cores using a New Wave Research Micromill (Figure 2-7b). To prepare the coral for the micromill, the surfaces of the slab were polished using a diamond plate grinder, followed by silicon carbide grinding paper. Loose grains and debris were removed by ultrasonicating the coral in MilliQ water for 6 x 30 seconds and left to dry before being mounted on a glass slide. The glass slides were fixed to the moving platform of the micromill using double sided sticky tape to hold the slide completely firm whilst the milling was underway (Figure 2-7).

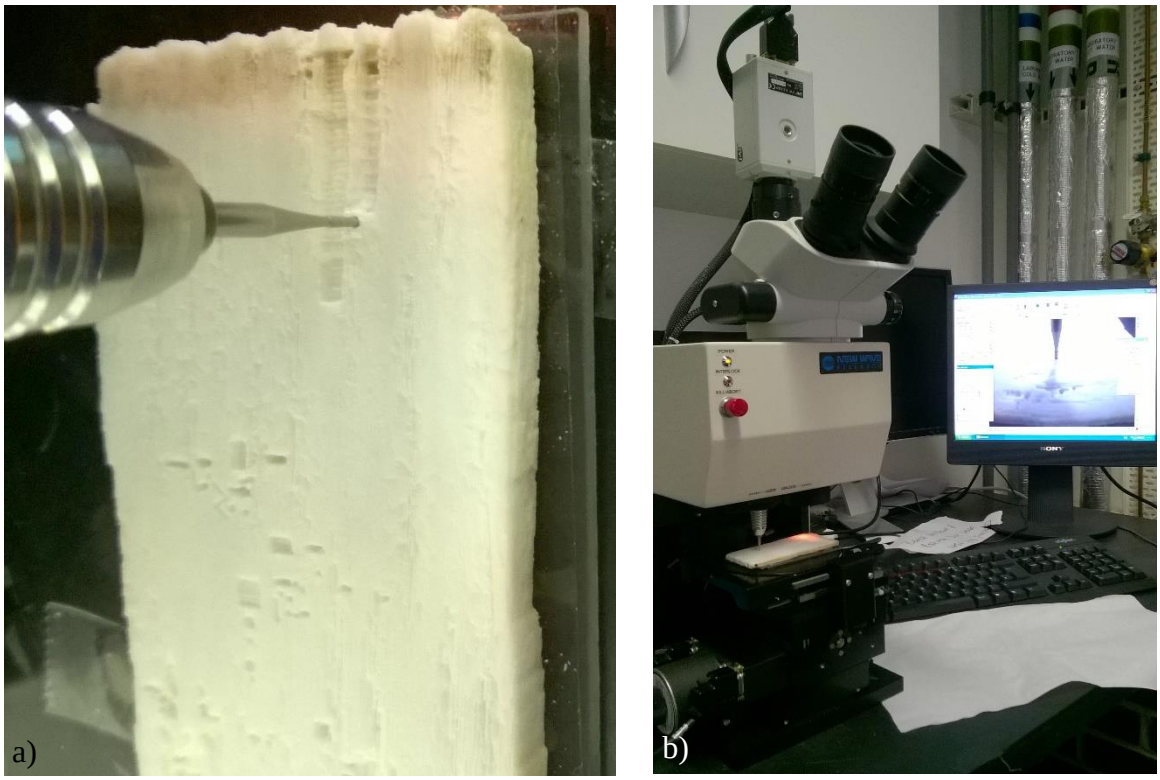

Figure 2-7. a) Micromilling in action: 500 µm diamond drill bit milling the theca wall of this coral slab to produce a fine powder, equivalent to approximately one month of coral growth. b) Micromill set up and the microscope video image on the computer screen.

The micromill was calibrated by determining the X, Y and Z offsets of the drill bit position, and regularly defining the tilted surface of the sample. The drill speed was set to 15%, the scan speed to 50 µm s^{-1} and the downward speed was set to 50 µm s^{-1}, which was found to give a precise entry and limit the amount of material lost. A diamond drill bit with a 500 µm diameter was used to drill ~1 mm wide trenches to a depth of 1 mm in the theca wall of *S. siderea* (Figure 2-6a), similar to *DeLong et al.*, (2011). The trenches were milled

in two passes to be confident all of the available material had been milled. A variable sample recovery of 0.3-1 mg was achieved by scooping up the milled powder with a paintbrush and transferred into an acid cleaned centrifuge tube. Any visible flakes from the columella were removed. Between samples, the coral slab and paintbrush were thoroughly cleaned with compressed air to prevent contamination between adjacent samples. A second theca wall of the same coral slabs were milled at a bimonthly resolution (e.g. yellow rectangle in Figure 2-8), to be used for boron isotope analysis where sample size requirements are relatively large. To do this a raster was drilled, giving a trench size equivalent to two single lines.

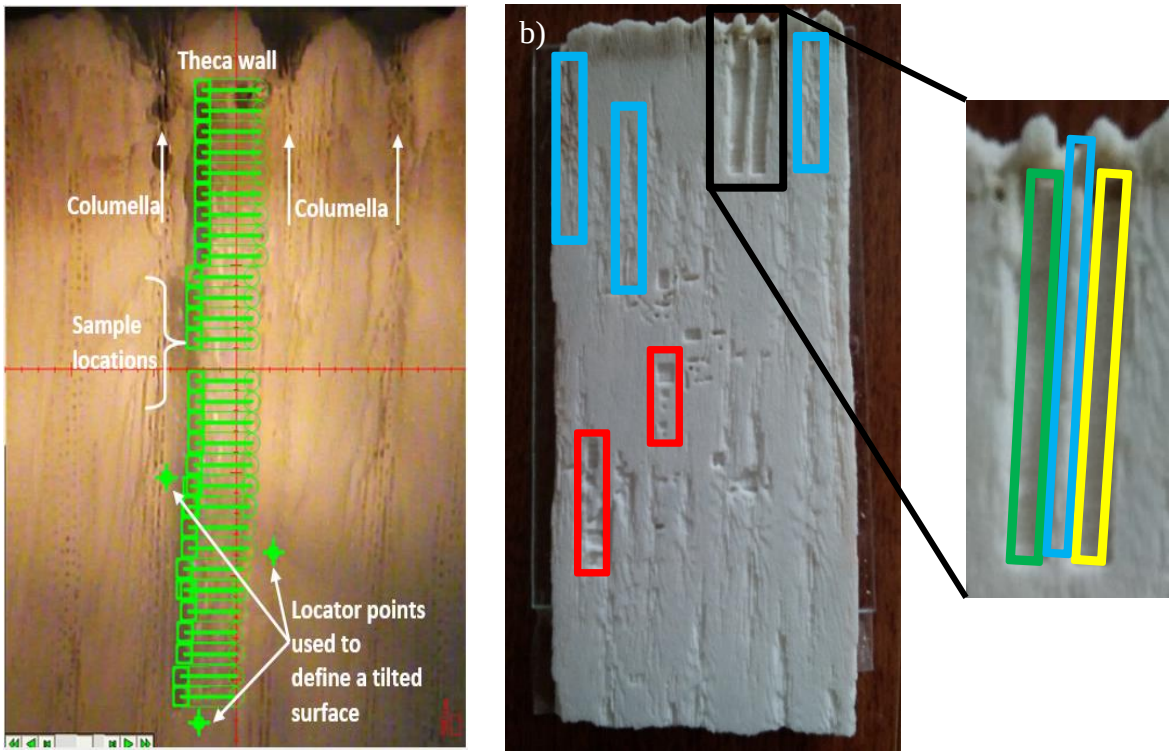

Figure 2-8. a) Microscope image of the BR-06 slab. The green lines (~0.75-1mm in length, 500µm in diameter) down the theca wall indicate each individual microdrilling sample location. The columellas are avoided during microdrilling. b) Photograph of the BR-06 slab. The red boxes indicate where test drills were performed during the calibration of the micromill. The blue boxes indicate examples of the columella, which needed to be avoided. In the magnified image, the yellow box represents the theca wall sampled at a bimonthly resolution, and the green box represents the theca wall sampled at a monthly resolution.

2.2 Laboratory techniques

2.2.1 Laboratory set up

The boron content of the samples analysed here for their isotopic composition is relatively low (<50 ppm), and sample sizes are typically small (<2 mg) so it is important that boron contamination from sample handling and chemical purification are kept at a minimum. To minimise contamination of the samples from external sources of boron, we must adhere to strict user protocols and limit the introduction of boron into the lab from air-borne particles by performing the majority of the chemical treatment of samples within the class 100 laboratories of the Geochemistry Group at the University of Southampton. Boron free High-Efficiency Particulate Air (HEPA) filters are fitted throughout the laboratories, and in addition, all boron chemistry (including sample dissolution) is performed in an overpressured fume box, both of which decrease the risk of air-borne contamination to the reagents or samples (e.g. *Rosner et al.*, 2005). All of the reagents required are of analytical grade, and contain <0.03 ppb B, and the 14.2 M HNO_3 is Teflon distilled using a Savillex DST-1000 sub boiling still (http://www.savillex.com/CategoryDetail.aspx?CategoryName=DST-1000-Sub-Boiling-Stills) before it is used to make more dilute nitric acids (5 M, 0.5 M and 0.0005 M HNO_3). The MilliQ (MQ) water is treated with an EMD Millipore© pack, and the MQ unit itself is fitted with a Q-guard to remove boric acid. All surfaces in the lab are thoroughly cleaned with MQ on a weekly basis, and the overpressure boxes are wiped down with 10% HNO_3 and MQ before each use.

2.2.2 Plastic and Teflon cleaning

To successfully maintain low levels of boron concentrations, effective vial cleaning protocols of all laboratory ware used in the chemical purification and dissolution process must be undertaken.

Pipette tips

Unused pipette tips were initially handled in the extraction only fume hood using Teflon tweezers. Small Teflon jars were 1/3 filled with ultra-pure 18.2 MΩ MQ and the pipette tips were filled with MQ (using a squeezy bottle, ensuring there were no bubbles inside the tip) and stacked upright in the jar.

Centrifuge tubes

Unused centrifuge tubes and lids were also handled in the extraction hood with Teflon tweezers, and they were filled with MQ and submerged into 1 L Teflon jars, also containing MQ. The beaker was then acidified with 9 M HCl, which was diluted to a molarity of 3 M and left on the hotplate at 90°C for <24 hours. Once the jar was removed from the hotplate it was wiped with MQ dampened white roll (to prevent the introduction of dust to the overpressure box) and the waste was removed in an overpressure box, and the beaker was then filled and drained of MQ a further two times. The acid cleaned pipette tips remain stored in the beaker in the overpressure box, and the centrifuge tubes were stored in a sealed plastic container. Immediately before use, both the pipette tips and centrifuge tubes were handled using Teflon tweezers and subjected to an additional two rinses with 10% Teflon-distilled HNO_3 followed by two MQ rinses (inside and out). All plastic ware is single use only.

Teflon beakers

Screw top 5 ml and 7 ml Teflon vials, and push-cap 2 ml auto-sampler vials (both from Savillex) were used for boron isotope analysis and underwent a more rigorous cleaning protocol than simple plastic ware. Firstly, ink labels were removed using acetone, and the vial immediately deposited into a beaker filled with MQ and then rinsed three times with MQ. Secondly, the inside of the beakers were wiped with acetone and rinsed three times with MQ to ensure any residual organics from the previous sample were removed. Thirdly, each vial was ~2/3 filled with 7 M HNO_3, closed, and left on the hotplate at 140°C for a minimum of 2 hours. The vials were then emptied and rinsed three times in MQ, before being stacked with the aid of Teflon tweezers into a 1 L jar of 7 M HNO_3. Once filled, this jar was heated on a hotplate at 140°C for a minimum of 24 hours. The jar was then emptied of its acid in the fume cupboard while the acid was still warm, the contents were rinsed twice in MQ and replaced upright in the Teflon jar, and subjected to an additional 24-hour reflux in 2% HNO_3. Finally, the Teflon beakers were rinsed three times with MQ in an overpressure hood, tapped dry and stored (capped) in a sealed box. Before these vials were used to store samples they were filled with 10% Teflon-distilled HNO_3 and heated at 140°C for at least 30 minutes, and then rinsed twice with MQ.

2.3 Coral cleaning

In order to ensure only elements from within the coral skeleton are measured, an extensive cleaning protocol is aimed at removing organic and other contaminant phases following *Barker et al.*, (2003). Initial $CaCO_3$ powders, weighing between 0.3-2 mg, were transferred to 2 ml plastic centrifuge tubes for cleaning. To minimise loss, samples were centrifuged (45 seconds, 13 rpm) between each stage of cleaning. Cleaning began by oxidatively cleaning samples in 250-500 µl (depending on sample size) of 1% H_2O_2 in 0.1 M NH_4OH at 80°C to remove any organic content. The use of 0.1 M NH_4OH ensures that the pH of the H_2O_2 remains >7 and no $CaCO_3$ dissolution occurs. Samples and oxidative mixture were heated in the water bath for 5 minutes and then ultrasonicated for 15 seconds, and this process was repeated a minimum of three times until the oxidative reaction stopped. The vials were then filled with MQ, centrifuged, and then the supernatant was extracted; a process which was repeated three times. After rinsing, the samples were transferred to a second clean plastic centrifuge tube before a 30 second weak acid (0.0005 M HNO_3) leach was performed using a volume of 250-500 µl (depending on sample size). This last step aimed to remove any oxidised contaminants that adsorbed onto the $CaCO_3$ during the cleaning process. Samples were then rinsed a further 3 times with MQ before being dissolved in 0.5 M HNO_3. Dissolution volumes between 100-175 µl were added incrementally until the sample was dissolved to ensure a minimum of excess H^+ ions. Sample losses ranged anywhere between 0.2% and 92%, but averaged around 30% for annual samples and 67% for high resolution (monthly and bimonthly) samples. To minimise sample losses, particularly from micromilled samples, the protocol was adapted so that the pipette tip used to transfer the sample was rinsed with MQ (inside and out) into the second centrifuge tube to increase the amount of carbonate material transferred for subsequent cleaning.

The dissolved samples were centrifuged for 3-5 minutes to remove any potentially remaining undissolved solids. For the annual and cultured samples, the dissolved sample minus the bottom 20 µl was transferred into a clean centrifuge vial. For the annual and high-resolution $\delta^{11}B$ samples, an aliquot of 20 µl was taken and added to 120 µl 0.5 M HNO_3 ("Element cut"), and an isotope cut of 73 µl was stored in a 5 ml Teflon beaker. The high resolution trace element samples were not diluted, and were stored as the total dissolved sample.

With each batch of coral samples, a sample of JCp coral reference material was also cleaned and dissolved simultaneously. By repeatedly subjecting independent JCp samples to the same processes as the coral samples, this represents an opportunity to monitor long-term

reproducibility of elemental ratios in a matrix similar to what we expect in the *S. siderea* samples (section 2.5.2.3).

2.4 Column chromatography

In simple terms, column chromatography is a method used to isolate a particular chemical compound from a solution containing multiple compounds; here, it was used to purify boron from a mixture of trace elements and calcium of a dissolved carbonate. At the University of Southampton, columns are hand made by heat-shrinking Teflon Shrinktek around a cylindrical stainless steel mould to produce a column with an ~1 cm x ~2 cm reservoir and an ~3.8 mm column at the end, allowing the column to retain ~1.5 ml of liquid. A polyethylene frit (10-30 µm pore size) is cut using a belt-hole cutter with a 3.8 mm diameter, and is inserted into the end of the column using pipette tips, ensuring that the shiny side is facing down. These columns are flushed with MQ and acetone to remove air bubbles from within the frit, and to ensure that the column is dripping. If it isn't dripping at this stage, the frit is either reinserted, or a new frit is used. Columns which successfully drip are then cleaned overnight at 140°C in 7 M HNO_3, followed by 2% HNO_3, then 10% Teflon distilled HNO_3. After the cleaning process, the columns are loaded with ~20 µl of ground Amberlite 743 resin (sieved to 63-120 µm and thoroughly rinsed; *Kiss*, 1988).

At this point, the structural stability of the columns were tested by passing a number of MQ elutions to identify if any grains of resin are leaking by checking the collected waste or looking directly at the droplets passing through. Columns that leaked resin were discarded because if any resin was introduced into the MC-ICP-MS during the analysis stage (section 2.5.2.4), the nebuliser could become blocked or the plasma could become unstable. It was also important to note how long it takes for a column to drain its ~1.5 ml load: if the column dripped too slowly, it would take too long to purify future samples, but if it dripped too quickly, there was a possibility that all of the B in the sample would not completely bind to the resin and result in fractionation (*Lemarchand et al.*, 2002). The 20% success rate of the columns produced during this study was typical within the B-Team (20-30% success rate).

Before the new columns can be used, the resin needs to be cleaned by passing a total of 15 ml of 0.5 M HNO_3 through the column prior to characterising the elution profile (*Lemarchand et al.*, 2002). The elution profile is determined by passing 27.5 ng National Institute of Standards and Technology Standard Reference Material (NIST SRM) 951

standard (*Catanzaro*, 1970) though each column and collecting 10 rinses of 110 µl (volume was based on the elution profile of the existing working columns). 99% of the B must be washed off within ~500 µl, and this is evident in Figure 2-9, where 99.9% of B was washed off within 550 µl. This is important because ^{11}B is enriched in the first elutions, and between the beginning and the end of B recovery an isotopic fractionation equivalent to 100‰ is possible, and a loss of only 1% of B at the end of the elution will cause a shift of 0.2‰ in recovered B (*Lemarchand et al.*, 2002). To avoid these potential sources of fractionation, it is imperative that B is completely recovered. The final test before the columns can be used for coral samples is to pass standards; generally a 27.5 ng SRM 951 sample and a 16 ng JCp sample and ensure that there is no fractionation detectable (SRM 951 = 0 ‰, JCp = 24.25 ‰). The method of purifying samples and standards through ion exchange is discussed below, accompanied by a schematic diagram (Figure 2-10).

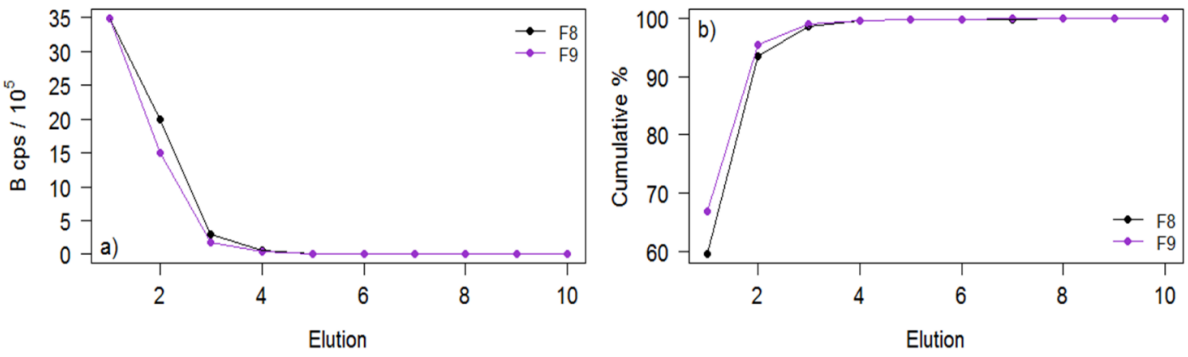

Figure 2-9. Elution curves from columns F8 and F9 demonstrating that 99.9% of boron is washed off with 550 µl 0.5 M HNO_3. a) B counts per second decrease with each elution. b) Cumulative percent of boron washed off the columns reaches 99.9% within 550 µl 0.5 M HNO_3.

The boron columns facilitate the purification and extraction of boron from the $CaCO_3$ matrix through the boron specific ion-exchange Amberlite resin, which absorbs boron in the $B(OH)_4^-$ form. Prior to sample loading, the columns are cleaned and conditioned by passing 2 x 1.5 ml of 0.5 M HNO_3 and 2 x 1.5 ml of MQ. Aliquots of the dissolved coral sample (4 ng to 35 ng B) are mixed with a 2 M Na acetate-0.5 M acetic acid buffer (sample:buffer ratio is 1:2). Buffering the acidic sample increases the pH to ~5.5, which allows boron to bind to the resin. Once the buffered solution has been loaded directly onto the pre-cleaned resin, 10 x 160 µl MQ are passed through the column to wash off the sample and buffer matrix (the first five washes are pipetted as droplets around the rim of the column). This step is key to prevent sample matrix influencing the ionisation of the sample during isotopic measurement

using MC-ICP-MS (e.g. *Guerrot et al.*, 2011). Resin-bound boron is eluted by five additions of 110 µl 0.5 M HNO_3 (leaving 5 minutes between each elution) which decreases the pH to <1 and releases the boron from the resin (*Lemarchand et al.*, 2002). Multiple additions enhance the reaction time between the resin, acid and sample whilst also avoiding the resin to become resuspended. Samples were collected in screw top Teflon beakers that have been freshly leached in 10% HNO_3 at 140°C for a minimum of 2 hours. A sixth elution was collected separately, and measured to monitor the efficiency of the column. Less than 0.2% of the total B concentration should be present in this "tail" sample. If the percentage were greater, it would be likely that sample fractionation has occurred, or the resin had begun to degrade.

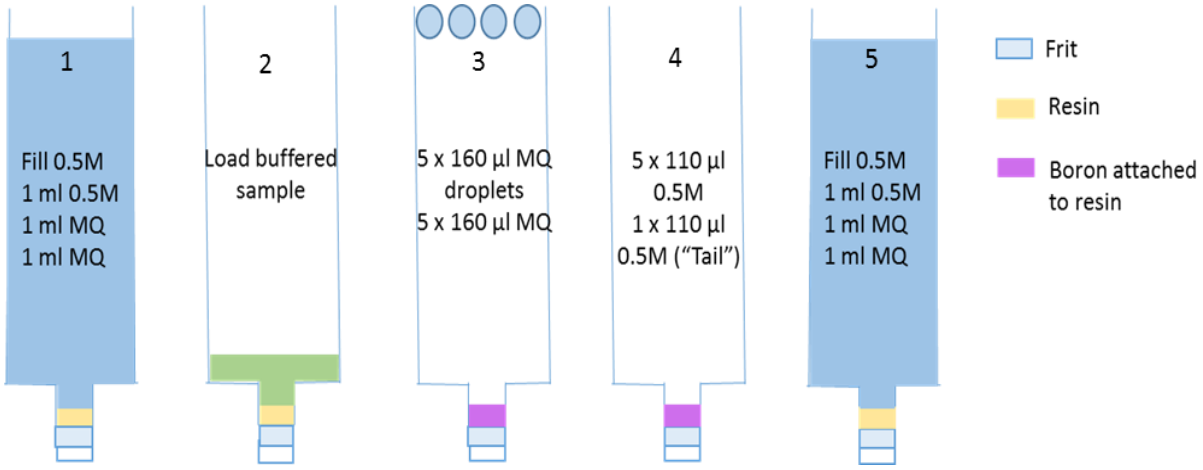

Figure 2-10 Schematic diagram of the ion exchange process: (1) The column is cleaned and preconditioned using Milli-Q water (MQ) and 0.5 M HNO_3. (2) The dissolved coral aliquot (buffered with 2 M Na acetate-0.5 M acetic acid buffer) is loaded onto the resin. (3) The matrix is washed off the column using MQ. (4) The sample is collected from 5 x 0.5 M HNO_3 elutions. (5) The column is cleaned by passing 0.5 M HNO_3 and MQ through the column.

Through the duration of this study samples were processed in batches of ten. Alongside every batch of samples, a minimum of one aliquot of JCp-1 with a concentration similar to that expected from the batch of samples, was also passed through a column. JCp-1 is a coral reference material made from homogenised *Porites* (*Okai et al.*, 2002), and functions as a consistency standard because we know what the $\delta^{11}B$ should be through repeat measurements within the B-Team or via comparisons with other laboratories (24.2-24.4‰; (*Wang et al.*, 2010; *Dissard et al.*, 2012; *Liu et al.*, 2014; *McCulloch et al.*, 2014)). Measuring JCp serves two purposes: 1) Because JCp is rotated around the set of columns, it can monitor the performance of the column; the column is deemed questionable and subject

to further testing if the $\delta^{11}B$ of JCp deviates from the long-term mean. 2) To constrain long-term precision of samples that can only be measured once. Additionally, a total procedural blank (TPB) is prepared (50 µl 0.5 M HNO_3, 100 µl buffer) and passed through a column, allowing for a monitor of how much boron was introduced into the samples during the purification process as a result of potential contamination of reagents and through handling. The boron concentration and isotopic composition of the TPB was measured and used to apply a correction to the samples if the TPB is >80 pg B, but this did not occur.

2.5 Analytical methods

In order to maximise the accuracy and precision of trace (e.g. Li) and major element (e.g. Ca) compositions, and the boron isotopic compositions of the samples, three types of inductively coupled plasma mass spectrometer (ICP-MS) instruments were used during this study: quadrupole ICP-MS, sector field ICP-MS and multi-collector ICP-MS. This section starts by briefly describing the principal theory of mass spectrometry before describing the methods employed for each individual ICP-MS instrument.

2.5.1 Brief introduction to ICP-MS

Mass spectrometry is used to detect ionised particles of different mass. This process can be broken down into four main sections: 1) Sample introduction. 2) Ionisation. 3) Mass analyser. 4) Ion detection.

Samples are aspirated through a nebuliser into a spray chamber as a wet aerosol mixed with argon sample gas. The spray chamber serves as a means to filter droplet sizes, which is necessary to maintain plasma stability. These droplets are then introduced into the quartz injector inside the torch with the sample gas.

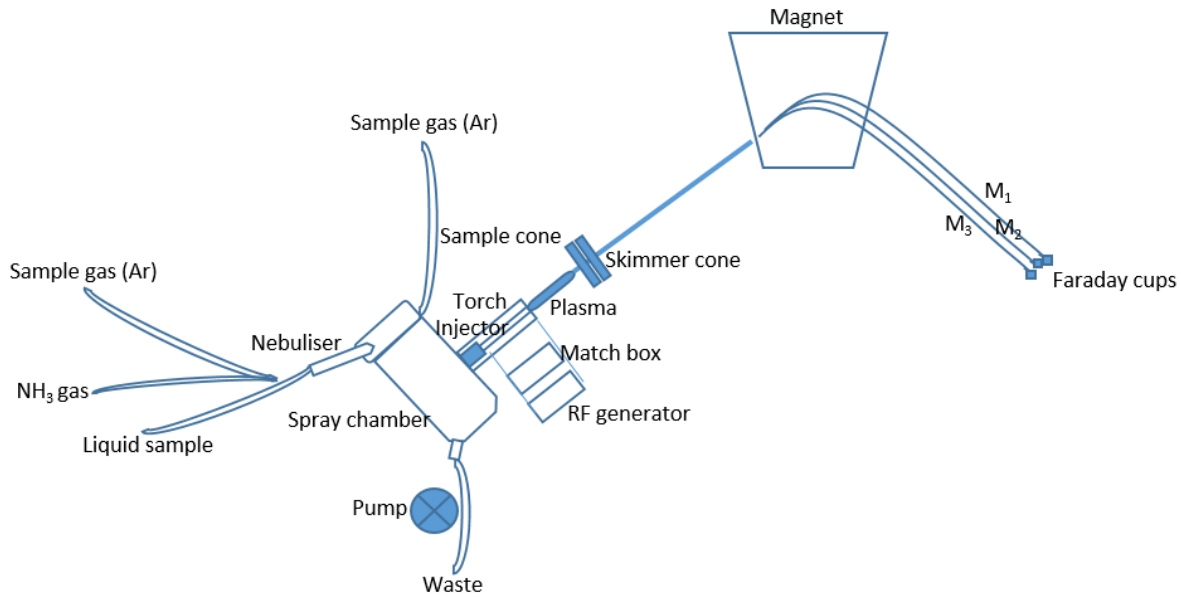

Figure 2-11. Schematic diagram of the multi-collector inductively coupled plasma mass spectrometer. The introduction system is comprised of the sample gas, ammonia, and liquid sample lines directed into the Teflon spray chamber. The injector inside the torch introduces droplets into the plasma where they become ionised. The beam of ions passes through the sample and skimmer cones to the magnet, where the ions are deflected. The focussing of these ions is mass dependant and the ions of different isotopes are collected and counted by the Faraday cups.

The principal component of an ICP-MS is the argon plasma ion source. Plasma is a cloud of partially ionised gas, typically 8000-10000 K, which vaporises and ionises the sample. Extracted ions are accelerated and projected through a sample cone and a skimmer cone, shaping the ion beam before it is accelerated into the analyser. The role of the mass analyser is to separate ions by their mass to charge ratio (*m/z*) using electromagnets. Ions of various *m/z* cannot pass through the mass analyser simultaneously, so a range of voltages and radio frequencies are passed through a quadrupole allowing some ions to remain stable whilst others travel to the detector. Changes in frequency are rapid, enabling the mass analyser to move across the full range of *m/z* (*ICP-MS Technical guide*).

Ions hit the dynode of an electron multiplier (detector), initiating a cascade of electrons, which are amplified and measured. The ion detection system varies between machines with the principal difference being whether single ion counting (secondary electron multiplier(s)), or multiple ion detection (Faraday collectors) is performed. The advantage of a multi-collector over a single ion detector is that intensity variations that may occur when measuring two (or more) ion beams is common to each detector and therefore effectively cancels out, allowing for precise measurements of isotope ratios.

Mass dependent isotope fractionation occurs in all ICP-MS instruments. Generally, this is referred to as 'mass bias' and needs to be corrected for in order to calculate the "true" isotopic composition of the target samples. Mass bias can be caused by space charge effects which cause the lighter isotopes (those with smaller inertia) to be pushed away from the central beam of the plasma, allowing heavier isotopes to become enriched (Figure 2-12). This is problematic because the sample and skimmer cones preferentially sample the centre of the plasma, so if lighter isotopes become displaced, they will not be fully transmitted to the extraction area and the measured isotope ratio will be light. The extent of mass bias depends on the mass of the analyte isotope and is ~1% per amu at high mass (e.g. >200) but can be as much as 16% at light isotopes (e.g. at mass 10 and 11). There are a number of ways to correct for mass bias: 1) Internal correction (e.g. *Barbaste et al.*, 2002). 2) Element doping (e.g. *Archer and Vance*, 2004). 3) Double spiking (e.g. *Galer*, 1999). 4) Sample-standard bracketing (e.g. *Foster*, 2008).

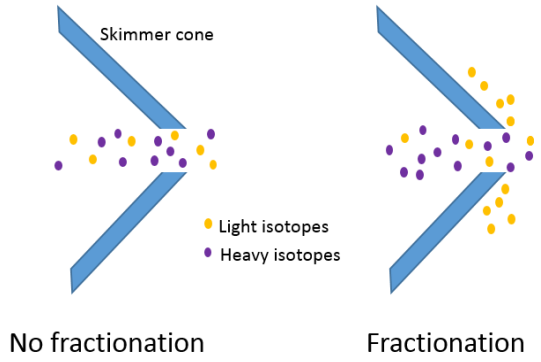

Figure 2-12. Isotopic mass fractionation around the skimmer cone.

2.5.2 ICP-MS analyses

2.5.2.1 Uncertainty in ICP-MS analyses

Before undertaking any sample analyses, it is important to understand sources of measurement uncertainty, and how this can be minimised and monitored from the beginning of the sampling stage to the final data processing stage, since uncertainty can be introduced at all stages of measurement. It is vital to be able to monitor and quantify the degree of uncertainty associated with each analytical measurement, not just so we can gain an accurate elemental or isotopic value for each sample, but also so we can incorporate such errors into the environmental reconstructions focused on here. Reproducibility comes in a number of forms: internal, intermediate, and external.

Internal reproducibility is the uncertainty associated with making a measurement made using mass spectrometry. The size of this uncertainty is largely dependent on the concentration of the desired analytes in solution, introduction system set-up, stability, tuning quality, and length of analysis (*John and Adkins*, 2010). Internal uncertainty can also refer to the uncertainty on an isotope ratio following error propagation through mass bias and blank correction. Intermediate reproducibility describes the repeatability of a single sample measurement (in multiple cycles) when measured multiple times (using different sub-samples) during different analytical sessions. It is larger than internal uncertainty and can vary widely between analytical sessions due to short-term variations in mass bias. External reproducibility is the variability in measured values of identical samples (e.g. JCp) that have been subjected to the same preparations (cleaning methods, column chemistry etc) and analysed multiple times. Uncertainty can be introduced here from the same sources as internal reproducibility in addition to variations in cleaning efficiency, sample heterogeneity and purification techniques.

This framework is used here to describe reproducibility on the X-Series, Element and Neptune are discussed in their relevant sections below.

2.5.2.2 X-Series ICP-MS

The X-Series quadrupole ICP-MS (Thermo Scientific X-Series) is fitted with a concentric spray chamber, into which samples are introduced via a nebuliser. Tuning is optimised using a solution of In, U, Fe, Li, Sr (all 1 ppb) in 3% HNO_3 spiked with 5 ppb In, 5 ppb Re and 20 ppb Be (3% InReBe HNO_3) and aims to maximise sensitivity whilst maintaining low oxides.

Before the multielemental analysis of coral samples can be performed on the Element ICP-MS, it is required that the Ca concentration ([Ca]) of the dissolved coral samples is known. This makes it possible to matrix match the samples and standards by diluting all of the solutions to the same [Ca]. If there is a discrepancy between the sample and standard concentrations, a matrix effect caused by high concentrations of ions from the major element (Ca) can affect analyte signal intensities, ionisation, and mass bias behaviour of other abundant elements in the plasma (*Tan and Horlick*, 1987; *Rosenthal et al.*, 1999). To this end, the X-Series was used to determine the calcium concentration within the samples, providing information needed to prepare the Element samples and standards to a uniform [Ca].

A multielement standard stock solution was made using high concentration (~10,000 ppm) single element (B, Mg, Al, Sr, Ca) solutions and was then diluted to make four

gravimetric standards with differing Ca concentrations (Table 2-2) that were used to generate calibration lines for each element (Figure 2-13). Aliquots of the annual sample dissolutions were diluted to have Ca concentrations of ~5 ppm (calculations based on estimated sample loss during cleaning) in a total of 5 ml 3% InReBe HNO_3. For the high-resolution samples, 20 µl of the aliquot for multielemental analysis (section 2.3) was added to 1.68 mls of 3% InReBe HNO_3, allowing three runs of each sample to be made.

Table 2-2. Concentrations of elements found in the multielement stock solution and standards 1-4 used during coral analysis.

	Standard stock solution	**STD1**	**STD2**	**STD3**	**STD4**
Element	**ppm**	**ppb**	**ppb**	**ppb**	**ppb**
Ca	30	270	540	1500	3000
Mg	0.05	0.5	1	3	6
Na	0.25	2.5	5	15	30
Sr	0.8	8	16	45	90
B	0.005	0.05	0.1	0.3	0.6
Al	0.005	0.05	0.1	0.3	0.6

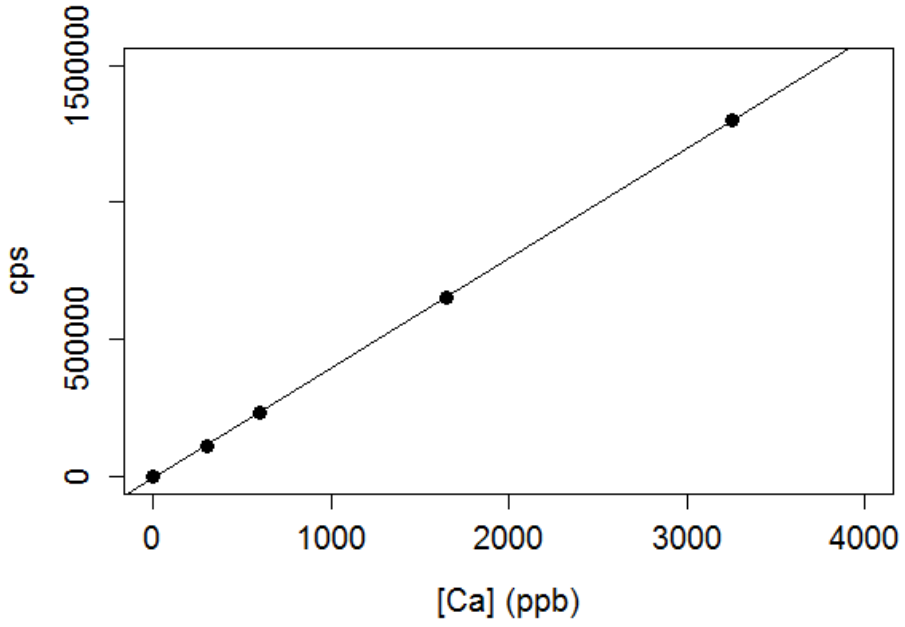

Figure 2-13. Example of a calcium calibration from the gravimetric standards on the Thermo Scientific X-Series.

Calcium concentration determinations on the X-Series ICP-MS began with five alternating 10% HNO_3 and blank (3% HNO_3 InReBe spiked) rinses in order to lower the background counts of the machine. Consistency standards of 1 ppm, 3 ppm and 7 ppm Ca CS2 and CS3 (*Ni*, 2006) were analysed four times at the beginning and end of each run to check the accuracy of the measurements and detect any drift. When combining the results for CS2 and CS3, the average value was 0.93 ± 0.01 ppm (n=64, 1σ) for 1ppm Ca, 2.91 ± 0.14 ppm (n=453, 1σ) for 3 ppm Ca, and 6.85 ± 0.31 ppm (n=409, 1σ) for 7 ppm Ca. Based on these analyses the intermediate precision at 1σ is estimated to be 1.01% for 1 ppm Ca, 4.91% for 3 ppm Ca and 4.94% for 7 ppm Ca. Internal (machine) reproducibility is monitored by repeat measurements of the In, Re, Be peaks giving the relative standard deviation.

Samples of the artificial seawater from the coral culturing tanks were also measured using the X-Series. Samples underwent a 200x dilution, resulting in 300 µl of artificial seawater being added to 5.97 ml 3% InReBe HNO_3 to dilute the Na concentration enough to prevent the Na from affecting the plasma or from overloading the detector. A concentrated multielement stock solution for seawater analysis standards was made in 3% InReBe HNO_3 and diluted to make four gravimetric standards (STD1-4) of different concentrations (Table 2-3). A separate Na standard (1800 ppm Na) in 3% InReBe HNO_3 was added to each standard so they had equal Na concentrations of 54 ppm, equivalent to 35 psu (Table 2-3), minimising any matrix effects between the samples and standards.

The gravimetric standards (STD1-4) were measured at the beginning and end of each analytical session. The bracketing blank (3% InReBe HNO_3) had a Na concentration equal to the samples and standards of 54 ppm to reduce matrix effects. The seawater standard for trace metals NASS-5 was also measured at 200x dilution in order to determine the deviation of *Instant Ocean* (section 2.1.2; Table 2-4) elemental composition from standard seawater.

Table 2-3. Concentrations of elements measured in the multielement stock solution and standards STD1-4 used during seawater analysis.

	Standard stock solution	STD1	STD2	STD3	STD4
Element	**ppm**	**ppb**	**ppb**	**ppb**	**ppb**
Na	0	54×10^{3}	54×10^{3}	54×10^{3}	54×10^{3}
Ca	100	1.03	2.06	4.12	8.25
Mg	320	3.30	6.60	13.2	26.39
Sr	2	0.020	0.040	0.080	0.160
B	1.1	0.011	0.023	0.045	0.091
U	0.002	2.1×10^{-5}	4.1×10^{-5}	8.3×10^{-5}	1.6×10^{-4}
Li	0.045	5.0×10^{-4}	9.0×10^{-4}	18.0×10^{-4}	37.0×10^{-4}
Ba	3.7×10^{-3}	3.8×10^{-5}	7.6×10^{-5}	1.5×10^{-4}	3.1×10^{-4}

Table 2-4. Summary of average elemental ratios of interest measured in *Instant Ocean* artificial seawater and NASS-5 seawater standard.

	Li/Ca µmol/mol	**Mg/Ca mmol/mol**	**Sr/Ca mmol/mol**	**Li/Mg mmol/mol**
Instant Ocean	5375.38	5571.57	8.90	0.95
NASS-5	2522.60	5489.00	7.60	0.50

2.5.2.3 Element ICP-MS

A sector field inductively coupled plasma mass spectrometer (SF-ICP-MS; Thermo Scientific Element XR; herein referred to as "the Element") was used to measure the multielemental composition of all coral dissolutions. A suite of element intensity (counts per second) ratios were measured (Table 2-5) to examine both the changing elemental composition of the coral skeleton and also the effectiveness of the cleaning protocol. Samples throughout this study had Ca concentrations ranging from 1 mM to 4 mM in 310-320 µl 0.5 M HNO_3.

Samples were introduced into a Teflon barrel spray chamber using a fused ESI Ltd. PFA 90 µl min^{-1} Teflon nebuliser. The sample gas and ammonia additional gas were introduced into the spray chamber through the nebuliser at rates of 0.7 L min^{-1} and ~0.4 L min^{-1} respectively (Table 2-6).

.

Tuning was carried out ~30 minutes after switching the Element on to allow sufficient time for the machine to 'warm up'. Tuning was optimised to increase the sensitivity for In and U measured in the tuning solution (0.1 ppb In, 0.1ppb U; typically gives 120,000 cps and 140,000 cps respectively) by adjusting torch position, additional gas flow rate, and lens position without increasing uranium oxide formation above 6%. Higher gas flows and torch positions closer to the interface tend to increase oxides. A typical set of parameters can be found in Table 2-6.

Table 2-5. List of isotopes measured during ICP-MS analysis of dissolved coral. All isotopes are measured in low resolution, with the exception of Fe, which is measured in medium resolution.

^{7}Li	^{11}B	^{23}Na	^{24}Mg	^{25}Mg	^{27}Al	^{43}Ca	$^{87}Sr^{++}$	^{48}Ca
^{55}Mn	^{86}Sr	^{87}Sr	^{111}Cd	^{138}Ba	^{146}Nd	^{238}U	^{56}Fe	

Table 2-6. Typical operating and tuning parameters for the Thermo Scientific Element ICP-MS.

Torch Positions		**Gas Flows (L min^{-1})**		**Tuning (cps in 1 ppb)**	
X	~6	Cooling	16	^{115}In	80000
Y	~2	Aux	0.9	^{238}U	120000
Z	~2.5	Sample	0.7	UO	5-6%
		Add 1	0.38		
		Add 2	0.07		

In order to reduce boron wash-out an additional ammonia gas (NH_3) was introduced into the spray chamber at a flow rate of 0.07 ml min^{-1} simultaneously with the sample gas. This made the internal environment of the spray chamber basic, despite samples, standards and blanks being introduced as 0.5 M HNO_3. Because boric acid is volatile, this method has been shown to reduce the amount of boron build up in the spray chamber four-fold, and completely removing any boron memory effect after 2 minutes of wash-out (*Al-Ammar et al.*, 2000).

Although the NH_3 additional gas improves the quality of B concentration (and B/Ca ratio) determinations it does lead to some isobaric interferences. For instance, when using NH_3, ^{7}Li has an isobaric interference by $^{14}N^{++}$ (Figure 2-14). This was resolved by minimising the background signal at ^{7}Li in low resolution. This was possible by identifying

that a 0.1 ppb Li (~7.015 amu) solution generally gave ~20,000 cps, and determining the mass range at which the $^{14}N^{++}$ interference (~90,000 cps) is present. The mass offsets were then adjusted so the peak centre was at a mass which demonstrates ~20,000 cps in the 0.1 ppb Li solution and also allows for some drift before part of the interference peak is measured (typically ~7.015; Figure 2-14). This method of determining mass offsets to avoid the interfering $^{14}N^{++}$ peak was considered successful given the average external reproducibility (2σ) of a range of Li/Ca ratios (12.48 to 41.52 µmol/mol) measured in low resolution is 2.5%.

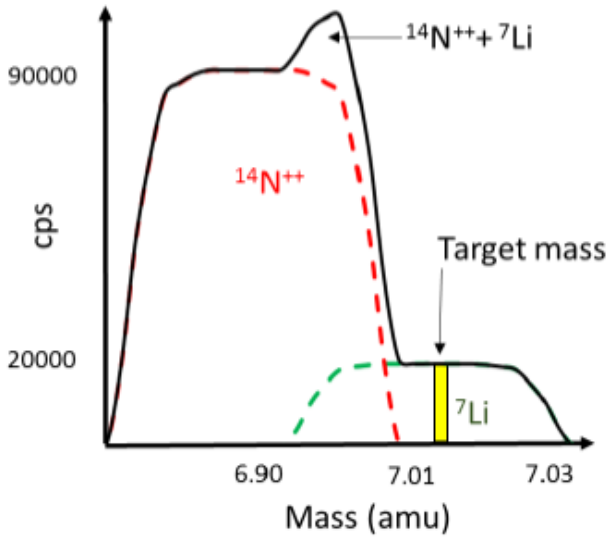

Figure 2-14. Isobaric interference on ^{7}Li from $^{14}N^{++}$. A typical ^{7}Li peak (green dotted curve) has ~20,000cps (0.1 ppb) when ^{115}In and ^{138}U sensitivity is 200 x 10^3 cps per 0.1 ppb. The red dotted curve reveals the $^{14}N^{++}$ isobaric interference located at the left (lower mass) of the ^{7}Li peak with an intensity of ~90,000 cps for the same tuning conditions as above, when additional gas (NH_3) is set to 0.070 ml min^{-1}. The area where these overlap causes a $^{7}Li^{+}$ $^{14}N^{++}$ spike. Note that the ^{7}Li blank is insignificant compared to the signal (typically ~200 cps or 1 ppt).

All samples and standards in the analysis were blank corrected enabled by a "blank" dissolution matrix (0.5 M HNO_3) being measured between every sample/standard (*Rosenthal et al.*, 1999). Samples were bracketed by in-house multi-elemental gravimetric standards (BSGS; (*Ni*, 2006), or MCS, supplied by Cardiff University), all of which were diluted to have equal Ca concentrations (based on prior X-Series ICP-MS analysis). Groups of three samples were measured between bracketing standard pairs so that the mass bias factor can be calculated for each elemental ratio of the samples. The mass bias factor is the ratio between the known elemental ratio in the gravimetric standard and the measured ratio of a pair of isotopes in the sample.

As an initial check on the machine's performance, a "standard run" of three consistency standards (CS1, CS2 and CS3; (*Ni*, 2006), or SECS1, SECS2 and SECS3; *Fowell et al., submitted*), each with a 2 mM Ca concentration but a different elemental ratio, was made prior to the sample run to ensure that the elemental ratios expected from the gravimetric ratios are met within 5% (2σ). If coral samples were 2 mM [Ca] or less, a run of the external standard (MCS) with variable [Ca] (0.5 mM, 1 mM, 1.5 mM) was added to the standard run to examine the influence of sample matrix on the accuracy of the mass bias correction which was found to be more significant at lower [Ca] (Figure 2-15).

During sample runs, coral samples were sequenced from the lowest to highest Ca concentration to minimise the impact of build-up in the blank. Additionally, consistency standards were measured at least at the beginning, and end of the runs to monitor reproducibility alongside a JCp, which provides a measure of external reproducibility (discussed below).

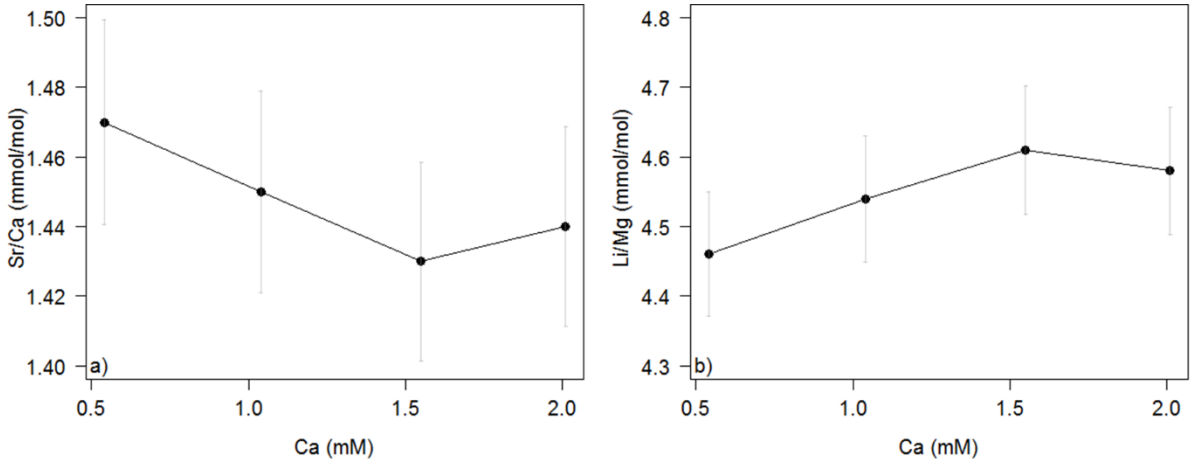

Figure 2-15. a) Sr/Ca and b) Li/Mg ratios of the external bracketing standard MCS at a range of calcium concentrations between 0.5 mM and 2 mM. Errors bars represent 2% of the measured value, demonstrating that although there is a greater influence from the matrix at lower concentrations, the difference is generally small.

Long-term reproducibility on the Element was monitored through intermediate and external precision of the final multielement analyses. Intermediate precision was determined by measuring the three consistency standards which have varying elemental ratios; either CS1-3 (original consistency standards), or SECS1-3 (current University of Southampton consistency standards) and act as internal standards to monitor accuracy and thus efficiency of correcting for mass bias effects and instrumental drift. Using the bracketing standards

method, precise values of repeat measurements were obtained for these standards. SECS3 is the most similar in composition to the coral samples, and yielded average measured values (2σ) for Sr/Ca of 1.97 ± 0.04 mmol/mol, and Li/Mg of 5.51 ± 0.09 mmol/mol compared to 2 mmol/mol and 5.73 mmol/mol respectively determined gravimetrically. Both the expected and measured ratios for these standards (as determined gravimetrically) are shown in Table 2-7 (CS) and Table 2-8 (SECS).

Table 2-7. Various elemental ratios for CS1, CS2 and CS3 consistency standards as determined gravimetrically and average measured ratios against the MCS bracketing standard.

	CS1		**CS2**		**CS3**	
	Gravimetric	**Average measured**	**Gravimetric**	**Average measured**	**Gravimetric**	**Average measured**
Li/Ca (µmol/mol)	12.51	12.44	26.59	28.43	41.52	39.43
n		8		9		12
2σ		0.31		0.51		0.96
%RSD (2σ)		2.49		1.79		2.43
Mg/Ca (mmol/mol)	1.28	1.29	3.29	3.31	7.57	7.48
n		11		9		15
2σ		0.03		0.07		0.16
%RSD (2σ)		2.33		2.04		2.09
Sr/Ca (mmol/mol)	0.46	0.47	0.91	0.91	2.06	1.85
n		11		9		15
2σ		0.01		0.01		0.02
%RSD (2σ)		1.91		1.18		1.23
Li/Mg (mmol/mol)	9.79	9.69	8.09	8.60	5.48	5.26
n		8		9		12
2σ		0.27		0.21		0.17
%RSD (2σ)		2.77		2.49		3.15

Table 2-8. Various elemental ratios for SECS1, SECS2, SECS3 consistency standards as determined gravimetrically and average measured ratios against the MCS bracketing standard.

	SECS1		SECS2		SECS3	
	Gravimetric	Average measured	Gravimetric	Average measured	Gravimetric	Average measured
Li/Ca (µmol/mol)	12.48	11.82	23.98	23.68	40.02	37.47
n		11		20		16
2σ		0.39		0.67		0.83
%RSD (2σ)		3.30		2.83		2.22
Mg/Ca (mmol/mol)	1.00	1.03	3.00	2.97	6.99	6.80
n		13		21		16
2σ		0.03		0.10		0.12
%RSD (2σ)		2.91		3.37		1.76
Sr/Ca (mmol/mol)	0.50	0.50	1.00	0.99	2.00	1.97
n		13		22		16
2σ		0.02		0.03		0.04
%RSD (2σ)		4.00		3.03		2.03
Li/Mg (mmol/mol)	12.48	11.50	7.99	7.96	5.73	5.51
n		11		19		16
2σ		0.47		0.19		0.09
%RSD (2σ)		4.09		2.39		1.63

External reproducibility is determined through repeat measurements of the *Porites* coral reference material JCp-1 (Geological Survey of Japan; *Okai et al*., 2002). The long-term external reproducibility of key elemental ratios can be found in Table 2-9. While Li/Mg measurements of JCp-1 for this study are comparable to those of other laboratories, our mean Sr/Ca value is at the low end of the range of values in the *Hathorne et al.* (2013a) interlaboratory study. This difference between the mean value and precision of JCp-1 Sr/Ca measurements of the University of Southampton and the interlaboratory study is not likely to be a product of the more extensive cleaning procedure at the University of Southampton because no difference between the Sr/Ca of cleaned and uncleaned JCp samples was observed (Figure 2-16d). In contrast, a 25% decrease was observed in Li/Ca and Mg/Ca ratios after cleaning, but these equal reductions meant that the Li/Mg ratio was not impacted by cleaning. Similar changes in Mg/Ca ratios have previously been identified in foraminiferal calcite cleaning by (*Barker et al.*, 2003). These results demonstrate that Li and Mg form part of the organic material which is removed as part of the standard cleaning protocol at the University of Southampton.

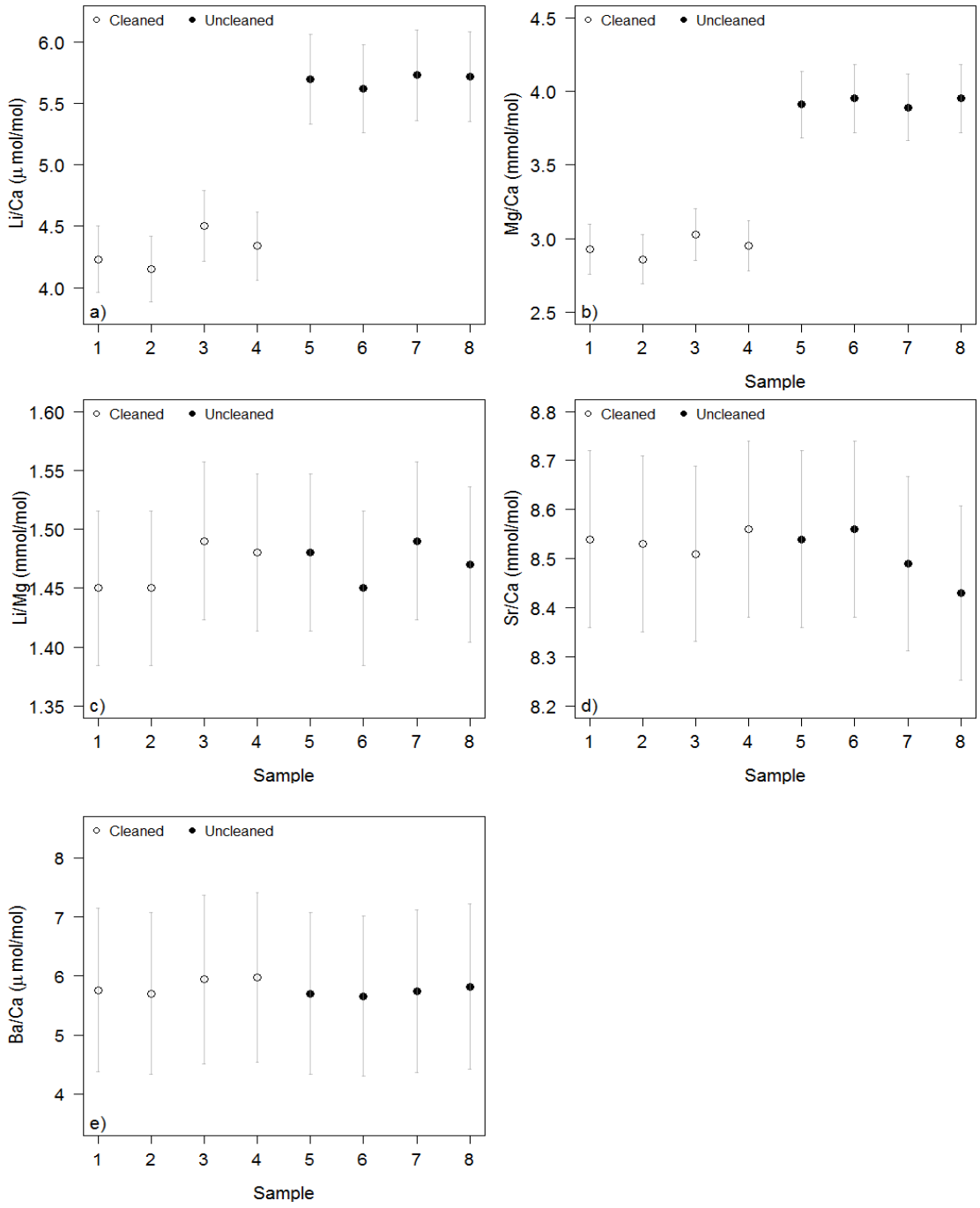

Figure 2-16. Results of JCp-1 elemental analysis after samples were either cleaned (open circles) or directly dissolved in 0.5 M HNO_3 without being cleaned. (a) Li/Ca and (b) Mg/Ca ratios are lower in cleaned samples, in contrast to (c) Li/Mg and (d) Sr/Ca ratios which are unaffected by the cleaning process. e) Ba/Ca ratios are within error between the cleaned and uncleaned samples (24% external error). Error bars represent the 2σ external precision based on long term measurements of JCp-1 bracketed against the Cardiff University multi-element standard MCS.

Table 2-9. Comparison of elemental ratios from JCp-1 from this study (measured against Cardiff University MCS) and ratios from the interlaboratory comparison (*Hathorne et al.*, 2013a). The interlaboratory standard deviation and external precision are calculated from robust statistics, and *n* is the number of laboratories that measured the relevant elemental ratio. The external precision of the elemental ratios for this study are based on repeat measurements of JCp-1, where *n* in this study equals the number of individual measurements and *n* in the Interlab comparison equals the number of independent laboratories.

	This study	**Interlab comparison**
Li/Ca µmol/mol average	4.58	6.19
	(*n* =16)	(*n* =5)
Standard deviation	0.15	0.11
External precision (%)*	6.44	3.46
Mg/Ca mmol/mol average	3.06	4.2
	(*n* =20)	(*n* =19)
Standard deviation	0.09	0.07
External precision (%)*	5.78	3.10
Sr/Ca mmol/mol average	8.66	8.84
	(*n* =20)	(*n* =21)
Standard deviation	0.10	0.04
External precision (%)*	2.21	0.95
Li/Mg mmol/mol average	1.51	1.48
	(*n* =16)	(*n* =5)
Standard deviation	0.03	0.06
External precision (%)*	4.45	7.43

* External precision reported as 2 relative standard deviations.

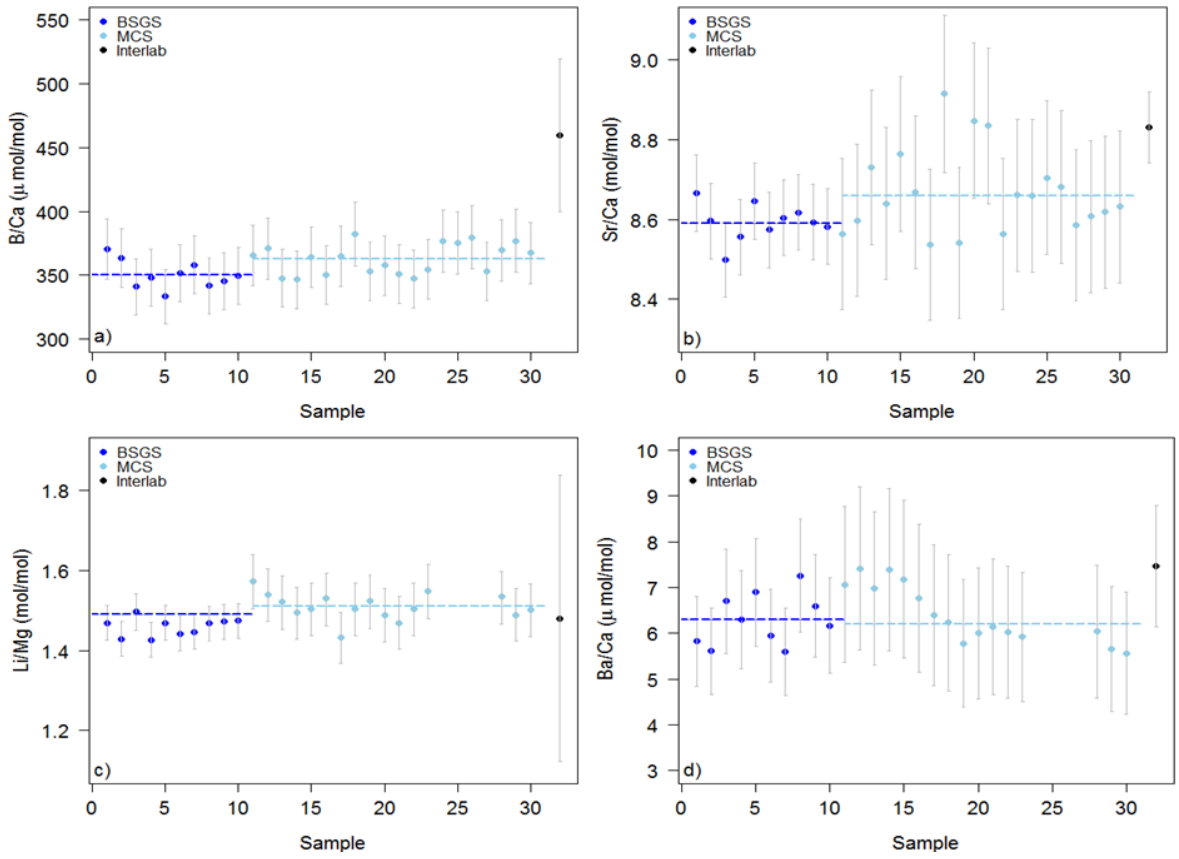

Figure 2-17. Repeat measurements of JCp elemental ratios. a) B/Ca. b) Sr/Ca. c) Li/Mg. Dark blue points represent JCp samples bracketed against BSGS, light blue points represent those bracketed against MCS. The error bars represent 2 relative standard deviations (external precision) against the bracketing standard specific for that sample. The dashed line is the mean value of the measurements. Average measurements (±1σ) for JCp (when bracketed against MCS) are 362.82 ± 11.87 µmol/mol B/Ca, 8.66 ± 0.10 mmol/mol Sr/Ca, and 1.51 ± 0.03 mmol/mol Li/Mg. Black points indicate the mean value from the interlaboratory experiment, where the error bars represent the expanded uncertainty (*U*) at the 95% confidence level, which combines the median of the within laboratory standard deviation with the robust interlaboratory standard deviation and expanded by a coverage factor of 2 (see *Hathorne et al.*, 2013a for more details).

2.5.2.4 Neptune MC-ICP-MS

The ThermoScientific Neptune multi-collector inductively coupled plasma mass spectrometer (MC-ICP-MS) is used to measure the boron isotopic composition of samples at the University of Southampton, closely following the methods outlined in *Foster*, (2008) and *Foster et al.*, (2013). The Neptune MC-ICP-MS is highly sensitive for low mass elements such as B; allows simultaneous measurements of ^{10}B and ^{11}B, and fully resolves the isobaric interference of $^{10}Ar^{4+}$ on $^{10}B^{+}$ (*Foster*, 2008).

Samples were introduced into a Teflon barrel spray chamber using a fused ESI Ltd. PFA 75 µl min^{-1} Teflon nebuliser. The sample gas was introduced into the spray chamber from two separate ports: ~0.955 L min^{-1} are introduced through the nebuliser, and

~0.02 L min^{-1} is directly introduced into the spray chamber. Two nebulisers were used during this study: one with a low uptake of 65 µl min^{-1} for low concentration samples, and one with an uptake of 125 µl min^{-1} for samples with high B content. As with the Element, ammonia gas was also added into the spray chamber at a rate of ~0.3 ml min^{-1} to make the spray chamber environment more basic, reducing the possible build-up of boron (*Al-Ammar et al.*, 2000). Sensitivity was maximised through tuning with the NIST SRM 951 standard (*Catanzaro*, 1970) and was typically 0.6 to 0.7 V for a 50 ppb solution. Maximum signal was achieved through manipulating torch position (X, Y and Z dimensions), sample gas volume, additional gas (NH_3) volume, and source lens positions. Washout was judged acceptable when less than 3% of the 951 B signal (mV) remains after a 2 minute wash out. The sample gas was then tuned to optimise stability (*Foster*, 2008), aided through performing a "sample gas test" where the $^{10}B/^{11}B$ ratio of SRM 951 was determined at a range of sample gas flow rates, allowing a stability plateau to be identified whereby the ratio was minimally impacted by changes in sample gas flow rate (Figure 2-19). The sample gas volume that resulted in the best stability was used during the run to minimise the effect of variation in instrumental mass fractionation on measured $^{11}B/^{10}B$. A peak shape with a flat top (Figure 2-18) is also necessary in aiding good reproducibility, and was achieved by adjusting the focus quad and shape lens.

Table 2-10. Example of tuning parameters for the Thermo Neptune MC-ICP-MS at the University of Southampton for boron isotope analysis. Gas fluxes are in L min^{-1}. There is variability amongst these settings between independent analytical sessions, with the exception of RF power, cool and aux gas, rotation and dispersion quad.

Inlet system		**Lenses**	
X	2.35	X	2.75
Y	4.09	Y	-4.3
Z	0.78	Focus	-651
Aux gas	0.9	Shape	196
Cool gas	15.5	Focus quad	5
Sample gas	0.955	Rotation quad	0
Additional gas 1	0.02	Dispersion quad	0
Additional gas 2	0.23		
RF power	1350		

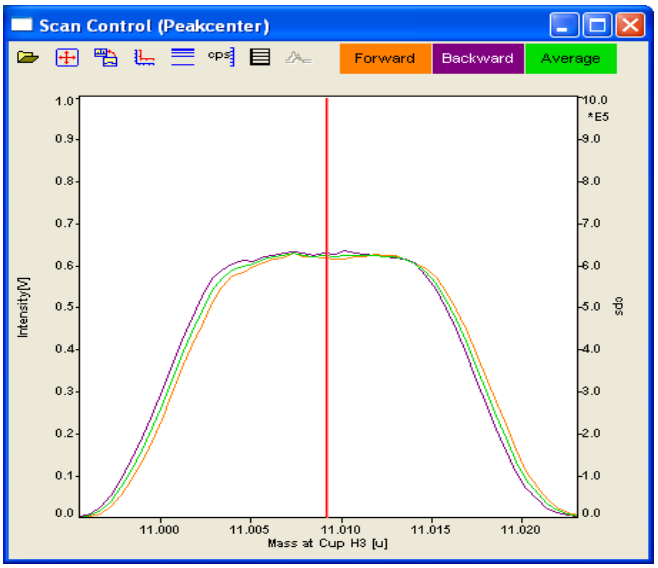

Figure 2-18. Example of a good peak shape and peak centre for ^{11}B. The important features to attain for a good peak shape are a flat top, high intensity, absence of round shoulders, and small tails.

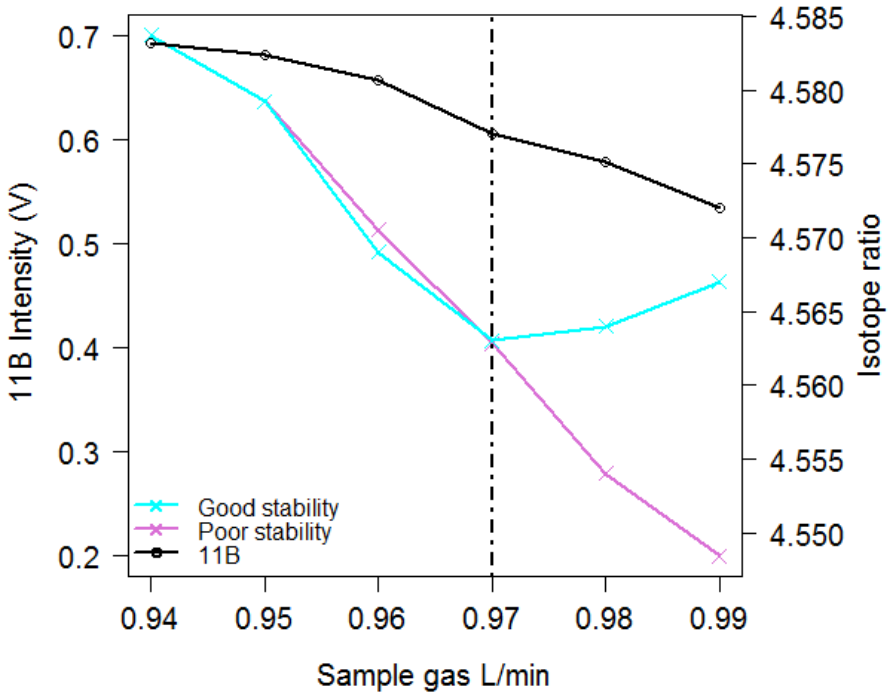

Figure 2-19. Example of a good (blue) and poor (purple) sample gas test. Increasing the sample gas volume decreases the overall intensity and $^{11}B/^{10}B$ ratio. The final sample gas volume is selected from the point at which a change in intensity has the smallest impact on the isotope ratio (stability plateau; dashed line).

For coral samples, the B intensity of the purified samples in a diluted aliquot (20 µl sample + 100 µl HNO_3) was first measured to ensure that a suitable B concentration of SRM

951 (25 ppb, 35 ppb or 50 ppb) was used as a bracketing standard in the $\delta^{11}B$ run to avoid potential offsets in the SRM 951 (*Guerrot et al.*, 2011). These measurements also allow the samples to be sequenced from lowest to highest concentration to minimise the impact of possibly increasing the B blank in the instrument. Furthermore, Na intensity is a proxy for general matrix contamination as high levels of Na are indicative of inefficient boron separation and generate anomalous sample results through an altered mass fractionation in adjacent bracketing SRM 951 standards (*Guerrot et al.*, 2011). If a sample was found to have a high Na concentration, it was transferred to a different autosampler vial and analysed at the end of the run to avoid any matrix influence on neighbouring samples. Samples should be rejected if neighbouring 951s are significantly affected (Figure 2-20). Following the sample intensity measurements, the [B] (pg) and $\delta^{11}B$ of the TPB were measured. Long-term analysis by the B-Team (n=62) gives a median TPB $\delta^{11}B$ of -7.27‰. This is used to make corrections on samples <7.5 ng (or <0.07 V) or samples purified when TPB >80 pg B.

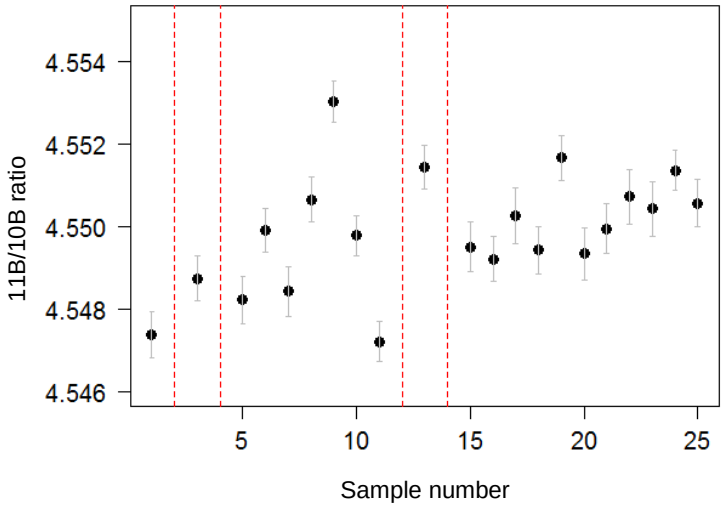

Figure 2-20. Impact of samples with high sodium concentrations on subsequent 951 boric acid standards. Black circles indicate the $^{11}B/^{10}B$ ratio of boric acid standards with 2 standard error bars. Red lines indicate the position in the sequence where a high sodium sample was measured.

In order to check machine stability prior to sample analysis, a batch of NIST SRM 951 boric acid standards at B concentrations of 35 ppb and 50 ppb were analysed. Instability is characterised by large jumps between adjacent standards (Figure 2-21a), and mass stability was deemed suitable if the isotopic ratio of the standards are within 2 standard errors of each other (Figure 2-21b).

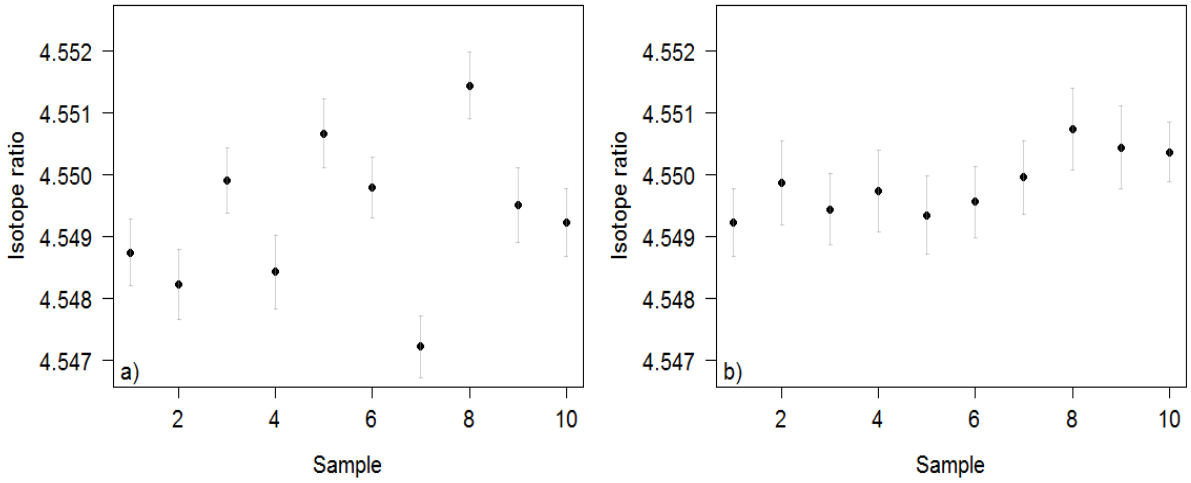

Figure 2-21. NIST SRM 951 boric acid standard was analysed prior to sample analyses to determine if the machine was (a) unstable or (b) stable. The error bars represent 2 standard errors on the $^{11}B/^{10}B$ isotopic ratio.

Sample volumes were increased from the 550 µl HNO_3 collected after purification to combat the problem of evaporation, allowing a sufficient volume of solution for two measurements. A typical block of analysis sequence can be found in Table 2-11. Samples were bracketed by 951 boric acid standards (25 ppb, 35 ppb, or 50 ppb depending on sample B concentration) and normalised to the average value of these bracketing standards, correcting for any instrumental mass fractionation. The ratio of ^{11}B to ^{10}B is typically measured and reported in delta notation relative to NIST SRM 951 boric acid standard, which has an $^{11}B/^{10}B$ of 4.04367 (*Catanzaro*, 1970). Through standard bracketing, we get the mass bias corrected boron isotope ratio as $\delta^{11}B$ notation (Equation 1-10, Chapter 1).

A "blank" (same volume 0.5 M HNO_3 as samples) was measured every three samples to monitor and correct for B fall-in. The full sequence of samples was run twice as two separate blocks in order to make the replicates fully independent. The average $\delta^{11}B$ of these two measurements was used to determine the final isotopic composition of the sample. Between the sample blocks, a block of NIST 951 standards were measured as an analytical reproducibility check, making sure that the machine was still stable. In-house boric acid

standards were also measured during each run to check long-term accuracy and reproducibility.

Table 2-11. Typical example of the opening two blocks for an analytical sequence on the MC-ICP-MS. The solutions have equal volumes, with the exception of the 951-35 ppb. Sequences open with a block of standard solutions of known isotopic composition (BIG-D, BIG-E, +20) before measuring samples in blocks of 3, bracketed by 951 boric acid standard.

Solution	Name	[B] (ppb)	$\delta^{11}B$ (‰)
Blank 0.5 M HNO_3	Blank	0	0
Standard	951	50	0
Standard	BIG-D	50	14.6
Standard	951	50	0
Standard	BIG-E	50	25.2
Standard	951	50	0
Standard	+20	50	19.6
Standard	951	50	0
Blank 0.5 M HNO_3	Blank	0	0
Standard	951	50	0
Sample	Sample 1	50	~24
Standard	951	50	0
Sample	Sample 2	50	~24
Standard	951	50	0
Sample	Sample 3	50	~24
Standard	951	50	0
Blank 0.5 M HNO_3	Blank	0	0

Long-term intermediate precision and long-term external reproducibility for $\delta^{11}B$ are well described at NOCS. In-house boric acid standards (BIG-D, BIG-E and +20‰) of various, known, isotopic composition (14.6‰, 25.2‰, 19.6‰ respectively) are measured during every analytical session as a means of determining long-term intermediate precision Figure 2-22). The carbonate reference material JCp (*Okai et al.*, 2002) is measured to monitor long-term external reproducibility, and these measurements are also used to calculate a reproducibility curve (Figure 2-23). This curve shows that the error and the $\delta^{11}B$ increases with decreasing B concentration. The relationship between signal size and uncertainty is controlled by Johnson noise (electrical noise on the detectors) and shot noise (counting statistics; ability of the detectors to detect ion arrival events; *Rae*, (2011)).The uncertainty of the sample $\delta^{11}B$ is therefore determined by an empirical relationship of the external reproducibility of the long-term measurements of JCp using 10^{12} resistors ($\delta^{11}B$ = 24.31 ± 0.42‰ (2σ), n = 62, [B] = 14 ng), giving us the equation:

$$2\sigma = 12960 \times exp^{-212[11B]} + 0.3385 \times exp^{-1.544[11B]}$$ Equation 2-1

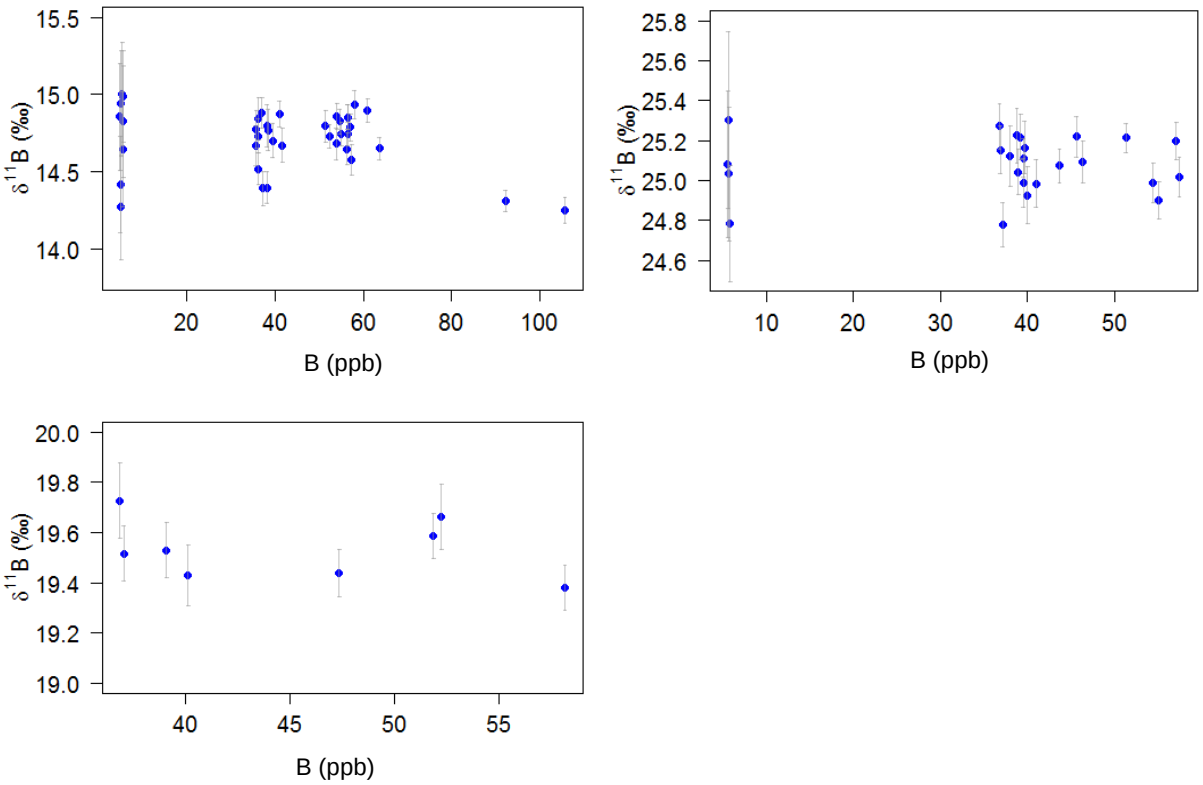

Figure 2-22. Boron isotopic composition ($\delta^{11}B$) of in-house boric acid standards (a) BIG-D, (b) BIG-E and (c) +20‰. The error bars represent the standard error of each individual measurement. In BIG-D and BIG-E measurements, a much greater error is associated with measuring samples at concentrations below 10 ppb. The solid line represents the average measured value, and the dashed lines represent 2 standard deviations of the average.

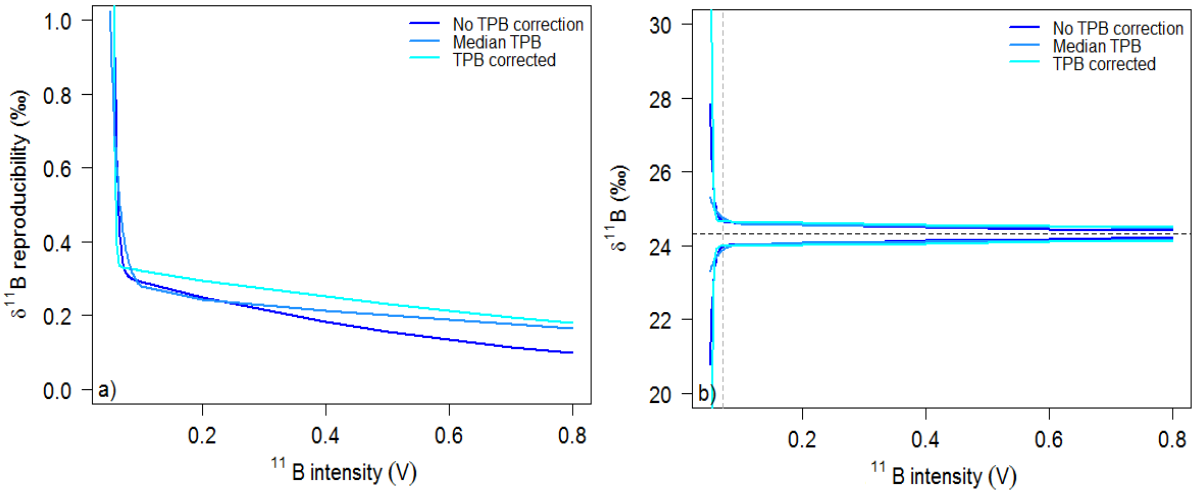

Figure 2-23. a) External reproducibility based on repeat measurements of JCp-1 across an intensity range of samples from all analysts at the University of Southampton measured using 10^{12} Ω resistors. b) Effect of uncertainty on JCp values calculated from the reproducibility curve from Equation 2-1. Dashed line represents mean JCp value (24.31‰). Blue lines show the uncertainty on the JCp value at each 11B intensity. Dark blue line shows the value not corrected for the total procedural blank (TPB), pale blue line shows the value when the median TPB is applied to correct JCp, and the cyan line shows the value based on each TPB correction. The boron isotopic composition of JCp ($\delta^{11}B$) is less reproducible and more uncertain at lower ^{11}B intensities.

Chapter 3: Declining coral extension in Belize decoupled from ocean acidification

This chapter is written in the style of a research article with the intention of future submission for publication. The contributions of co-authors to this work are detailed below.

Sara Fowell: Concept, data analysis and interpretation, manuscript writing
Elwyn de la Vega: Sample analysis, manuscript editing
Toby Tyrrell: Manuscript editing
Karl Castillo: Sample collection and skeletal extension analysis
Justin Ries: Concept, sample collection and $\delta^{13}C$ analysis
Hannah Donald: Sample analysis
Gavin Foster: Concept, data interpretation and manuscript drafting

Abstract

The health of coral reefs are threatened by a number of simultaneous anthropogenic impacts, including ocean acidification (OA), ocean warming, elevated nutrients and sedimentation. These processes, either individually or collectively, have been shown to reduce the ability of corals to calcify and thrive, although there are considerable spatial variations in the nature and magnitude of the responses (e.g. *Rogers*, 1990; *Marubini and Davies*, 1996; *Lough and Barnes*, 2000; *Hughes et al.*, 2003; *De'ath et al.*, 2009; *Cantin et al.*, 2010; *Castillo et al.*, 2012; *Castillo et al.*, 2014). In common with many places worldwide, the Caribbean has seen a rapid decline in coral cover by ~80% since the mid-1970's (*Gardner et al.*, 2003) accompanied by a significant expansion of fleshy algae (*Hughes*, 1994; *McClanahan et al.*, 1999). The role of ocean acidification in the decline in coral in the Mesoamerican Barrier Reef System (MBRS) is currently unknown due to the lack of historic *in situ* pH data. Here, using the boron isotope palaeo-pH proxy, we show that between 1919 and 2008, seawater in the backreef of the MBRS suffered a rapid decline of ~0.15 pH units, at rates similar to that observed for the open ocean (*Bates et al.*, 2014). However, this acidification occurred with no associated negative impact on *Siderastrea siderea* extension rates, in agreement with laboratory experiments on a range of coral species that indicates a resistance to relatively minor OA (e.g. *Marubini et al.*, 2001; *Ries et al.*, 2010; *Castillo et al.*, 2014). In contrast, the forereef zone extension rates of *S. siderea* declined markedly from 1923 to 2008, yet we

see no significant long term pH trend, although it exhibits large interannual variability (up to 0.2 pH units). A consideration of the carbon isotope gradient between the two reef zones indicates that the lack of a significant decline in pH in the forereef is likely driven by a shift away from net community calcification toward net primary production, perhaps driven by the expansion of fleshy algae and the decline in overall coral calcification (e.g. *Hughes*, 1994; *Gardner et al.*, 2003). Proxies for sediment input (e.g. Ba/Ca), and modern observations of water quality (*Andréfouët et al.*, 2002) reveal the forereef region receives more sediment than the backreef, and that this situation was reversed between the 1920s and 2000s. Over this time, there has been a significant increase in forereef Ba/Ca ratios ($p<<0.001$), we thus support the view (e.g. *Prouty et al.*, 2008) that increases in riverine nutrient and sediment input from Honduras may have played an important role in the decline of coral on the MBRS. Therefore, ocean acidification is not implicated in the declining extension rates of *S. siderea* in the MBRS.

3.1 Introduction

A number of local and global stressors currently threaten 75% of the world's coral reefs, and, if their protection is not increased, it is estimated that >90% will be vulnerable by 2030 with almost all reefs negatively impacted by 2050 (*Burke et al.*, 2011). In recent decades, these stressors have led to global declines in coral cover, decreased the ability of corals to calcify, and reduced biodiversity and fish abundance. The Great Barrier Reef (GBR) in particular has been particularly negatively impacted over the last 20 years, with calcification rates decreasing by 20% (*Kline et al.*, 2012). In the GBR, the bleaching event of 1998 caused 42% of reefs to bleach, followed by 54% in 2002 (*Berkelmans et al.*, 2004), and finally followed by the current bleaching event of 2016 which, exacerbated by a strong El Niño, has affected 93% of corals, and it is estimated that 35% died within 3 months (Hughes, *in progress*). Elsewhere, the calcification rate of *Diploria labyrinthiformis* in Bermuda has also decreased by >50% compared to pre-industrial rates (*Bates et al.*, 2010), and the 1998 bleaching event caused a 30% decline in calcification in *Diploastrea heliopora* in the Red Sea (*Cantin et al.*, 2010). In addition, a 60% decline in coral cover in a Papua New Guinea marine reserve occurred in just 8 years, resulting in a 75% decline in fish species, and the population levels of around half of those species has declined by at least 50% (*Jones et al.*, 2004).

The causes of these chronic declines are debated and are not the same amongst coral reefs worldwide. Instead, multiple stressors frequently work simultaneously with the most important anthropogenic stressors including, but not limited to, ocean warming (e.g. (*Aronson et al.*, 2000; *Carpenter et al.*, 2008), ocean acidification (e.g. *Kleypas*, 1999; *Hoegh-Guldberg et al.*, 2007), sediment loading (e.g. *Fabricius*, 2005), nutrient enrichment (e.g. *Szmant*, 2002), pollution (e.g. *Lewis et al.*, 2009; *Brodie et al.*, 2012), tourism (e.g. *Johnson*, 2002; *Barker and Roberts*, 2004), overfishing (e.g. *Hawkins and Roberts*, 2004), and microplastic pollution (*Hall et al.*, 2015). If corals are exposed to local chronic stressors such as sedimentation and nutrification, they can become more susceptible to temperature and light induced coral bleaching (*Wooldridge*, 2009; *Carilli et al.*, 2010; *Wiedenmann et al.*, 2013).

The Mesoamerican Barrier Reef System (MBRS) stretches for more than 1000 km along the coast of Mexico, Belize, Guatemala and Honduras, making it the largest coral reef system in the northern hemisphere (*Ezer et al.*, 2005), comprising of barrier reefs, shelf reefs, fringing reefs and atolls (*Soto et al.*, 2009). The MBRS consists of three individual zones along an inshore-offshore gradient which display different characteristics and experience different environmental regimes. The nearshore reef is characterised by patch reefs within 10 km of the coastline; the backreef consists of colonies on the landward side of the reef crest which experience limited water circulation; and finally the forereef is composed of colonies on the seaward side of the reef crest and therefore experience high wave activity in a stenothermal environment (*Lugo-Fernández et al.*, 1998; *Castillo and Helmuth*, 2005; *Castillo et al.*, 2011).

The entire Caribbean basin saw hard coral communities decline by as much as 80% over the last 30 years of the twentieth century (*Gardner et al.*, 2003). The bleaching event of 1998 impacted every reef zone along the MBRS, and the lettuce coral *Agaricia tenuifolia* was almost completely eradicated, making the coral reef vulnerable to encrusting sponge cover (*Aronson et al.*, 2002). As a result of low coral cover, increased nutrient input, and reductions in herbivorous fish and sea urchins, it is thought the MBRS in Belize has become increasingly dominated by fleshy macroalgae since the 1980s (e.g. *Hughes*, 1994; *McClanahan and Muthiga*, 1998; *McClanahan et al.*, 1999), including remote reefs such as Glovers Reef which suffered an almost complete loss of *Acropora palmata* and *A. cervicornis*, and a 300% increase in the abundance of fleshy algae which increased from <20% to ~80% coral cover (*McClanahan et al.*, 1999). *Castillo et al.*, (2011) reported that, accompanying these major changes in assemblage composition, extension rates of the more resilient coral *S. siderea* in the forereef zone of the MBRS significantly declined from, on

average, 5.5 mm y^{-1} to 3.5 mm y^{-1} between 1935 and 2008. This however was not the case for *S. Siderea* from the backreef or nearshore colonies, arguably as a result of forereef corals being less genetically predisposed to adapting to rapidly changing environmental conditions (*Castillo et al.*, 2011).

Ocean acidification (OA) is a global phenomenon that has already caused a decrease of 0.1 pH units in open ocean surface water since the Industrial Revolution (*Doney et al.*, 2009), and it is widely anticipated that an increase in ocean acidification over the course of this century (0.3-0.6 pH unit decrease by 2100; *Caldeira and Wickett*, 2003; *Orr et al*., 2005) will cause further declines in coral calcification. OA is linked to coral calcification as a result of increasing acidity decreasing the availability of carbonate ions (CO_3^{2-}) (*Kleypas*, 1999; *Hoegh-Guldberg et al.*, 2007), which in turn decreases the aragonite saturation state (Ω_{arag}) of seawater ($\Omega_{arag} = [Ca^{2+}][CO_3^{2-}]/K_{sp}^*$, where K_{sp}^* is the solubility product of aragonite). Coral reefs are generally found in areas where Ω_{arag} is supersaturated (Ω>3.3), but calcification is possible where Ω>1, however, dissolution becomes dominant at Ω=1 and below, because the seawater is undersaturated in terms of CO_3^{2-} ions (*Kleypas et al.*, 2005; *Krief et al.*, 2010). Mesocosm experiments have been a valuable tool in providing an insight into future OA scenarios; for example, *Andersson et al.*, (2009) exposed a community dominated by *Montipora capitata* to a daily average pCO_2 of ~1,147 µatm (Ω = 1.4), resulting in a 24% decrease in calcification and a 138% increase in dissolution. Numerous studies have shown the ability of corals to calcify is reduced under low pH conditions, and different species of corals have different thresholds at which they become unable to calcify (e.g. *Schneider and Erez*, 2006; *Anthony et al.*, 2008b; *Marubini et al.*, 2008). For instance, the laboratory based culturing experiment of *Castillo et al.*, (2014) showed the calcification rate of *S. siderea* colonies to exhibit a parabolic response to ocean acidification, and the calcification rate at 2553 µatm (Ω = 1.1) was approximately the same as at 324 µatm (Ω = 2.8). In addition, the combination of warmer, more acidic oceans over the next century are expected to decrease the calcification rate of *S. siderea* while simultaneously modifying the skeletal morphology (*Horvath et al.*, 2016).

A potentially valuable, but currently underexplored, way to investigate the impact of ocean acidification (and potentially other stressors) on coral is to compare how corals have responded naturally to historic acidification. This approach has the advantage that, rather than examining simply the response of an individual to the anthropogenic stressor, information is gained on an ecosystem level. The complication of course is the lack of available records of environmental change at the local level. For instance, there is currently

only limited pH data from the MBRS available to analyse the response of *S. siderea* to ocean acidification.

The $\delta^{11}B$ of coral skeletons has been used widely as a proxy for historic surface seawater pH (*Hemming et al.*, 1998; *Hönisch et al.*, 2004; *Liu et al.*, 2009; *Pandolfi et al.*, 2011; *Shinjo et al.*, 2013; *D'Olivo et al.*, 2015; *Wei et al.*, 2015), and therefore offers a means to reconstruct the pH a particular coral experienced, potentially revealing the importance of pH change at an individual level. The proxy is based principally on the observation that dissolved boron in seawater exists as boric acid ($B(OH)_3$) and the borate ion ($B(OH)_4^-$) with the relative proportions of the dissolved species strongly dependent on pH_{sw} (*Hemming and Hanson*, 1992). The relationship between pH_{sw} and the concentration of $B(OH)_4^-$ in seawater is well-described by *Dickson*, (1990). The basis of the $\delta^{11}B$-pH proxy is that an isotopic fractionation of ~27‰ exists between the borate ion and boric acid, with the former relatively depleted in ^{11}B (*Klochko et al.*, 2006). Because the abundance of the two species is pH dependent, as pH changes so does the isotopic composition of each species (Figure 3-1). Existing isotopic evidence strongly suggests it is predominantly $B(OH)_4^-$ that is incorporated into biogenic carbonate, and therefore the boron isotopic composition of such carbonate is pH dependent (*Vengosh et al.*, 1991; *Hemming and Hanson*, 1992).

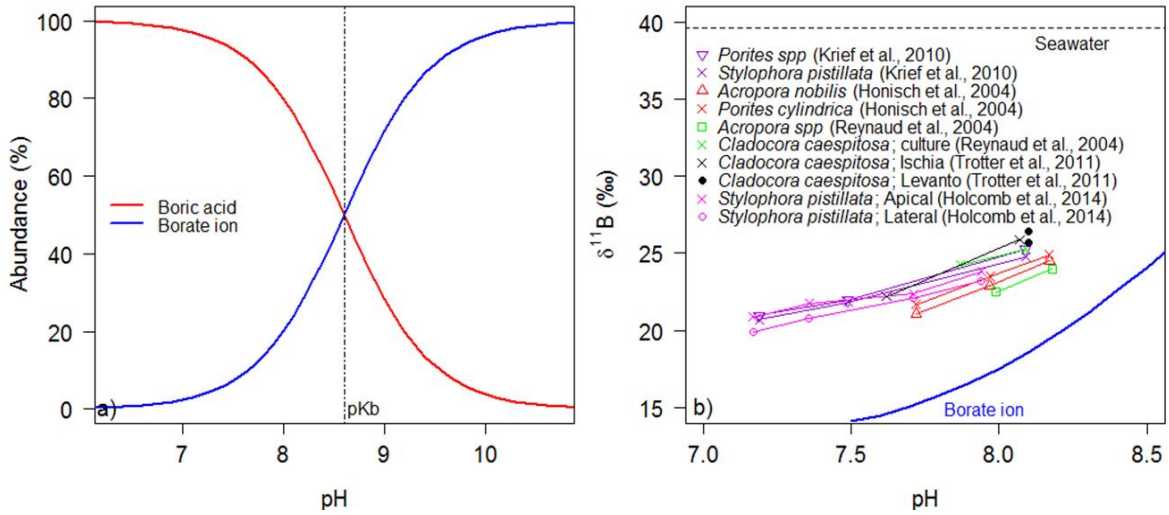

Figure 3-1. a) The relative abundances and isotopic compositions of the two most abundant boron species in seawater, at 25°C and a salinity of 35 psu. Boric acid, $B(OH)_3$, is marked in red, while borate ion, $B(OH)_4^-$, is marked in blue. b) The $\delta^{11}B$ of corals are offset from the borate isotope curve of *Klochko et al.*, (2006). The dashed line follows the boron isotopic composition of seawater (39.61‰; *Foster et al.*, 2010).

The $\delta^{11}B$ of corals tends to respond to pH change with less sensitivity than the borate ion and both tropical and cold-water corals are positively offset from the borate isotope curve of

Klochko et al., (2006) (Figure 3-1b; *Krief et al.,* 2010; *Trotter et al.,* 2011; *Anagnostou et al.,* 2012; *McCulloch et al.,* 2012a). This offset is thought to be related to a number of biological processes mediated by the coral, collectively known as "vital effects" (*Trotter et al.,* 2011). It is believed that the most influential vital effect is pH-upregulation, a process in which corals increase the pH of their internal calcifying fluid by 0.3-1.1 pH units (Figure 3-2) to facilitate biomineralisation (*Venn et al.,* 2011; *McCulloch et al.,* 2012a). In this case, the $\delta^{11}B$ of the coral skeleton ($\delta^{11}B_{coral}$) is representative of internal pH (pH_{cf}) as opposed to external seawater pH (pH_{sw}; *McCulloch et al.,* 2012a; *McCulloch et al.,* 2012b; *Holcomb et al.,* 2014). The offset between external and internal pH ($\Delta pH = pH_{cf} - pH_{sw}$) has been quantified in a small range of species based on culture studies using $\delta^{11}B$ (*Krief et al.,* 2010; *Holcomb et al.,* 2014) and by using pH sensitive dyes (*Venn et al.,* 2011; *Venn et al.,* 2013; *Holcomb et al.,* 2014). Although there are subtle differences between the species so far studied with regard to the amount of up-regulation at any given pH, the relationship between ΔpH and external seawater is similar regardless of species studied (Figure 3-2; *Hönisch et al.,* 2004; *Reynaud et al.,* 2004; *Krief et al.,* 2010; *Trotter et al.,* 2011; *D'Olivo et al.,* 2015). Despite the ΔpH being a species-specific biological control (*Trotter et al.,* 2011; *Anagnostou et al.,* 2012; *McCulloch et al.,* 2012a), boron within the aragonite matrix is understood to come directly from seawater (*Hemming and Hanson,* 1992), which has a known $\delta^{11}B$ composition (*Foster et al.,* 2010). Using a thermodynamic equation, pH_{cf} can be directly calculated from skeletal $\delta^{11}B$ (*Zeebe and Wolf-Gladrow,* 2001), and because pH_{cf} is related to pH_{sw} (*Venn et al.,* 2013) and hence the $\delta^{11}B_{coral}$, using boron isotopes via the ΔpH calibrations is a justifiable method of reconstructing pH_{sw}, and not simply a monitor of the magnitude of internal vital effects. There is currently no evidence to suggest that the relationship between pH_{cf} and pH_{sw} is affected by factors such as food supply, temperature or light.

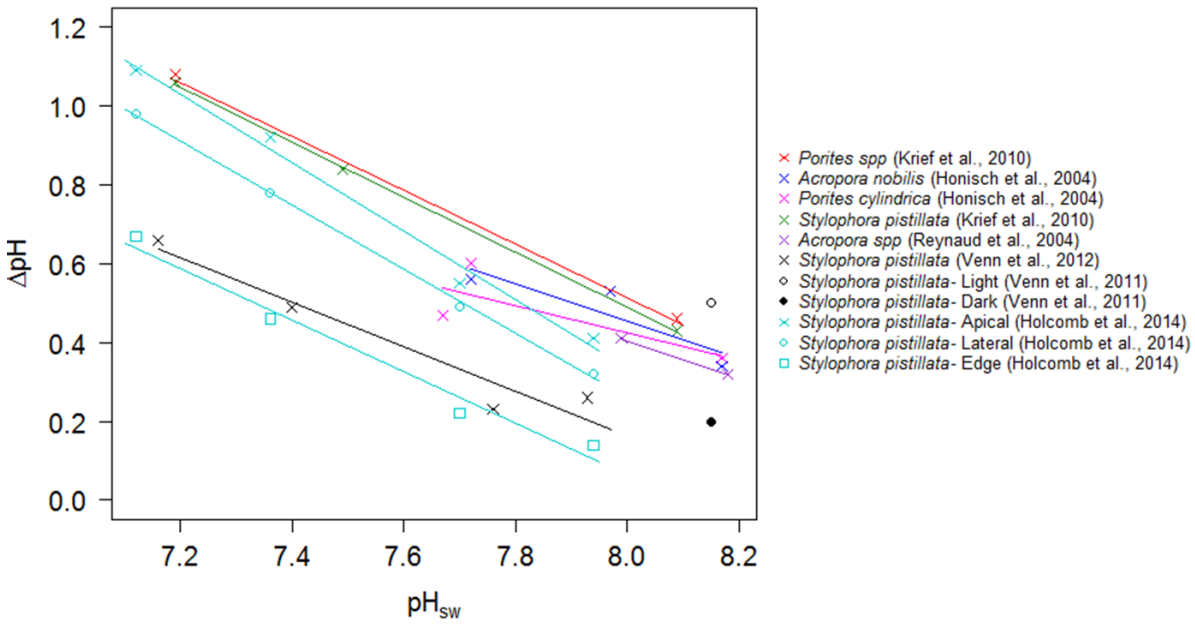

Figure 3-2. Existing relationships between seawater pH (total scale) and the pH of calcifying fluid (ΔpH) imparted during calcification in the tropical coral species *Porites*, *Acropora*, and *Stylophora* (*Hönisch et al.*, 2004; *Reynaud et al.*, 2004; *Krief et al.*, 2010). The *S. pistillata* samples of *Venn et al.*, (2011) are measurements of the subcalicoblastic medium using pH sensitive dye and have been converted to the pH total scale). ΔpH is calculated as the difference between pH_{cf}, calculated directly from skeletal $\delta^{11}B$, using the fractionation factor (α=1.0272) of *Klochko et al.*, (2006), and measured pH_{sw}.

Terrestrial influences on coral, such as sediment loading and nutrient enrichment (e.g. *Szmant*, 2002; *Fabricius*, 2005), are largely driven by precipitation patterns across the watershed and subsequent riverine transport and deposition of terrestrial run-off. Precipitation patterns across the Caribbean are influenced by multiple large-scale spatial and temporal anomalies that influence the variability of atmospheric circulation, and are known as teleconnections. These include: (i) the Atlantic Multidecadal Oscillation (AMO), which is characterised by 50 and 20 year temperature anomalies (*Schlesinger and Ramankutty*, 1994) with phases of positive anomalies that increase Caribbean precipitation (*Taylor et al.*, 2002). A positive AMO index also increases the likelihood of tropical storms turning into hurricanes as a result of high sea surface temperatures (SSTs; *Taylor et al.*, 2002). (ii) The Pacific Decadal Oscillation (PDO), which exhibits 20 to 30 year period oscillations between warm and dry (positive PDO index) phases, and cold and wet (negative PDO index) phases (*Hastenrath*, 1976; *Mantua and Hare*, 2002). It is thought that tropical Pacific SST anomalies have a smaller influence on Central American precipitation than tropical Atlantic SST anomalies (*Enfield and Alfaro*, 1999). (iii) El Niño Southern Oscillation Index (ENSO); a 2 to 7 year cycle of fluctuating SST and air pressure, where a high El Niño phase corresponds to higher SSTs and air pressure, resulting in warmer weather (*Giannini et al.*,

2000). (iv) the Intertropical Convergence Zone (ITCZ), a global band of tropical precipitation controlled by meridional temperature gradients that control convergence (*Waliser and Gautier*, 1993). Such temperature gradients are also partly established by the AMO and PDO.

In this study we explore a suite of proxies within the skeletons of *S. siderea*, including the δ^{11}B-pH proxy, and Ba/Ca ratios as a riverine freshwater flux proxy, to examine the causes of coral calcification decline in the MBRS, with a particular focus on the effects of ocean acidification and terrigenous inputs.

3.2 Methods

3.2.1 Sample collection and preparation

Cores of *S. siderea* were drilled from a total of three nearshore colonies, three backreef colonies, and seven forereef colonies in the southern region of the MBRS (see *Castillo et al., 2011* for more details). These cores were collected in December 2009 using the techniques described in Chapter 2. We focus here on cores from two *S. siderea* colonies from the forereef (FR-02; 16.13715^{o}N, 88.252883^{o}W, and FR-12; 16.10004^{o}N. 82.26669^{o}W) and backreef (BR-06; 16.14045^{o}N, 88.26015^{o}W) zones in the Sapodilla Cayes region of the MBRS (Figure 3-3). Sub-sampling of coral cores to separate annual growth bands, X-ray and dating techniques are described in *Castillo et al.*, (2011) and Chapter 2. Briefly, to prepare the annual resolution samples for boron isotope analysis (FR-02, BR-06), cores were cut into 8 mm slabs using a diamond-tipped tile saw. Annual banding was then traced onto a scale computer and cut into individual bands, before cutting vertically in half using a diamond-tipped band saw (Inland Hobby DFS-100 ReefKeeper Saw). These sections were ultrasonicated for 10 minutes, rinsed using 100% pure ethanol and air-dried for >12 hours and half of each section was finely crushed. Monthly resolution samples were obtained from the top (2006-2008) and bottom (1921-1926) of coral cores FR-12 and BR-06 for Ba/Ca analysis by micromilling (New Wave Research micromill) ~1 mm wide trenches to a depth of 1 mm in the theca wall with a 500 µm diameter diamond drill bit.

In the class-100 boron-free clean lab at the University of Southampton, organic matter was removed from the coral samples using 3% H_2O_2 (buffered in 0.1 M NH_4OH_4) and ultrasonicating at 80°C for 3 rounds of 5 minutes prior to a 30 second weak acid leach (0.0005 M HNO_3) to remove any contaminants that may have been adsorbed during the

cleaning process (Chapter 2, section 2.3). Samples were finally dissolved in <200 µl 0.5 M HNO_3 and centrifuged for 3 to 5 minutes (13,000 rpm) to separate the supernatant from any remaining non-carbonate solids. The dissolved solution was separated into two aliquots; 20 µl of the dissolution was added to 120 µl 0.5 M HNO_3 in a clean vial (for Ba/Ca analysis), and the remainder was stored in a 5 ml 10% HNO_3 leached Teflon beaker (for $\delta^{11}B$ analysis). The boron content of the dissolved samples (average = 27 ng B) was separated from the $CaCO_3$ matrix by passing them through Amberlite Resin ion-exchange columns following an established protocol (*Foster*, 2008).

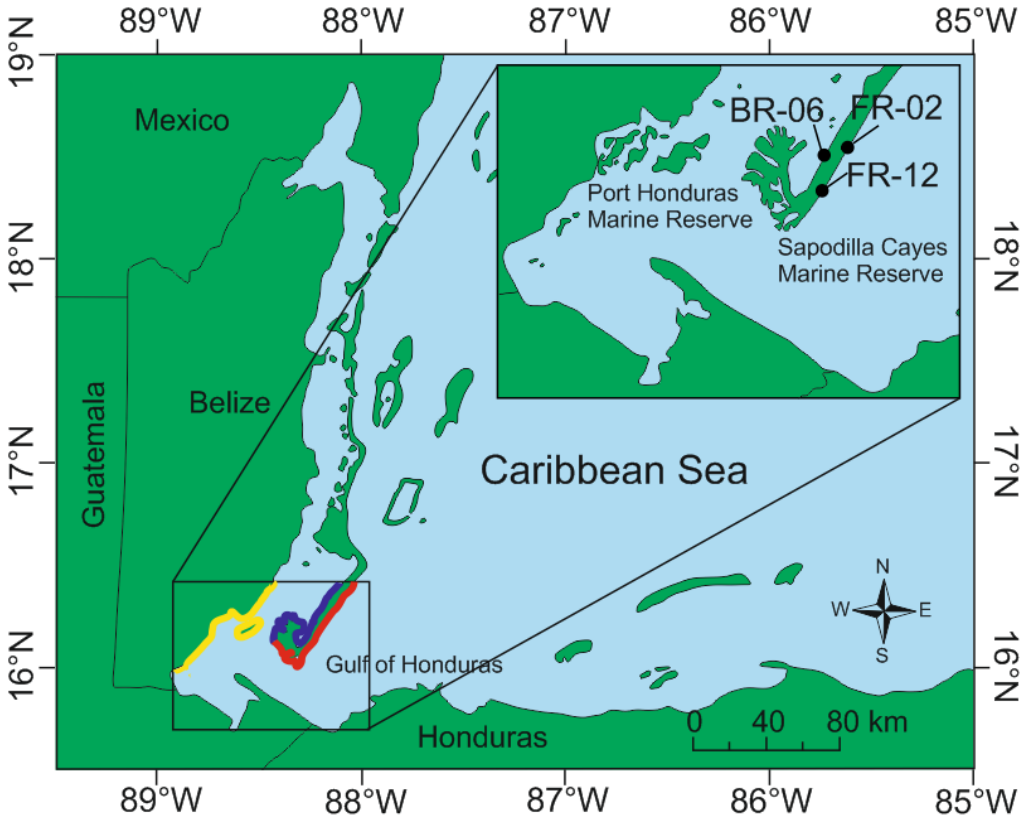

Figure 3-3. Map of forereef and backreef coral coring locations in the Sapodilla Cayes. In the Southern portion of the Belize Barrier Reef, the red zone indicates the forereef, the blue zone indicates the backreef, and the yellow zone indicates the nearshore reef.

3.2.2 Analytical techniques

An Element XR (Thermo Scientific) sector field ICP-MS was used to determine the elemental ratios of the coral dissolutions. Briefly, samples are analysed at Ca concentrations between 1 mM and 3 mM and every group of 3 samples were bracketed by an in-house matrix matched gravimetric standard which allowed us to correct for drift and mass bias.

Additionally, three gravimetric consistency standards (either CS1, CS2 and CS3, or SECS1, SECS2 and SECS3), each with different gravimetrically determined elemental ratios, were analysed to monitor measurement accuracy (*Ni*, 2006; *Ni et al.*, 2007). Samples were blank corrected with a 0.5 M HNO_3 acid blank measured between every sample (*Rosenthal et al.*, 1999). In order to provide an assessment of external reproducibility, the international coral reference material JCp-1 (made from homogenised *Porites* by the Japanese Geological Survey; *Okai et al.*, 2002) underwent the same sample cleaning and analytical protocols simultaneously with the coral samples. A thorough description of the analytical method is found in Chapter 2 section 2.5.2, including the results of the external reproducibility as determined by multiple analyses of JCp-1. The mean measured Ba/Ca ratio of JCp (±2σ) was 6.41 ± 1.26 µmol/mol, which falls in the range of values reported from an interlaboratory study, where the mean Ba/Ca ratio was 7.47 ± 1.31 µmol/mol (*Hathorne et al.*, 2013a).

3.2.2.1 Boron isotope analysis and pH reconstructions

The boron isotopic composition was measured on a Thermo Neptune multi-collector inductively couple plasma mass-spectrometer (MC-ICP-MS) at the University of Southampton using the standard bracketing technique of (*Foster*, 2008) (also described in Chapter 2). Boron isotopic ratios are expressed in delta notation ($\delta^{11}B$) relative to the NIST SRM951 (National Institute of Standards and Technology Standard Reference Material) boric acid standard (Equation 3-1):

$$\delta^{11}\text{B}\ (‰) = \left(\left(\frac{^{11}B_{standard}/\,^{10}B_{sample}}{^{11}B_{standard}/^{10}B_{sample}}\right) - 1\right) \times 1000 \qquad \text{Equation 3-1}$$

Through repeat analyses of the JCp-1 coral reference material ($\delta^{11}B = 24.33‰$), the external reproducibility at the University of Southampton can be described by:

$$2\sigma = 129600(exp^{-212\times 11B}) + 0.3385(exp^{-1.544\times 11B}) \qquad \text{Equation 3-2}$$

where ^{11}B is the intensity of ^{11}B in volts. The $\delta^{11}B$ compositions of the forereef and backreef corals were used to calculate the pH_{cf} using the equation:

$$pH_{cf} = pK_B^* - log\left(-\frac{\delta^{11}B_{SW} - \delta^{11}B_{coral}}{\delta^{11}B_{SW} - (\alpha_{B3-B4} \times \delta^{11}B_{coral}) - 1000 \times (\alpha_{B3-B4} - 1)}\right)$$

Equation 3-3

where the $\delta^{11}B_{sw}$ is the B isotopic composition of seawater (39.61‰; *Foster et al.*, (2010)), and $\alpha_{B3\text{-}B4}$ is the B fractionation factor (1.0272; *Klochko et al.*, 2006). The B dissociation constant (pK_B^*) was determined for each sample based on the sea surface temperature from the HadISST1 dataset (*Rayner et al.*, 2003) and the assumption that salinity was constant at 36.5 psu (using the *R* package "seacarb"; *Lavigne and Gattuso*, 2010) based on the limited salinity measurements from satellites (Figure A-1). Salinity has only a minor effect on δ^{11}B-derived pH (*Foster and Rae*, 2016), for instance, a salinity range of 35 psu to 37 psu changes reconstructed pH by 0.01 pH units.

Currently, there is no δ^{11}B-pH calibration for *S. siderea*, and therefore to estimate the pH_{sw} from the pH_{cf}, the equations of *Trotter et al.*, (2011), *McCulloch et al.*, (2012a) and *Liu et al.*, (2014) for *Porites cylindrica* are applied here to convert pH_{cf} into pH_{sw} (Equation 3-4). This particular equation reconstructs pH values closest to what is expected to open ocean values when using forereef coral boron isotopic compositions.

$$pH_{SW} = \frac{(pH_{cf} - 4.72)}{0.466}$$

Equation 3-4

As noted above, the choice of calibration determines the absolute pH but has little influence on relative pH change which we focus on here (Figure 3-2). In order to isolate the long-term trends in the time-series (1912-2008), reconstructed pH_{sw} values are fitted with LOESS smoothers with 2 standard error confidence intervals with the degree of smoothing determined by general cross-validation. A LOESS smoother is a non-parametric smoother that estimates the fitted points and associated standard errors with respect to the whole curve rather than for each individual data point. Cross-validation optimises model predictions without overfitting the data trend. To do this, each data point is removed in turn and the model is fit using a range of smoothing parameters to predict the response of the missing data point. The smoothing parameter that achieves the lowest prediction error on the model for the entire timeseries is the optimal value (*Chandler and Scott*, 2011).

3.2.3 Climate cycles

To determine any influence of global climate cycles on sediment deposition on the MBRS, the Ba/Ca data from both coral coretops (BR-06 = 2 mm to 19 mm, FR-12 = 2 mm to 14 mm) are compared here to the AMO and PDO indices, which are detrended and smoothed for each month. The bimonthly resolved Multivariate El Niño Southern Oscillation Index (MEI) data is based on observations of six tropical Pacific variables: sea-level pressure, zonal and meridional components of the surface wind, SST, surface air temperature, and total cloudiness (*Wolter and Timlin*, 1998). These data were obtained before annual averages were calculated to allow direct comparison with reconstructed pH data. The Caribbean Index sea surface temperature anomaly forecast (CAR) data is a monthly time-series of averaged SST anomalies from the Comprehensive Ocean-Atmosphere Data Set and the National Centers for Environmental Predictions (*Penland and Matrosova*, 1998); here, the data were averaged to give annual anomalies that could be directly compared with the pH reconstructions. All data were freely downloaded from the Earth System Research Laboratory of the National Oceanic and Atmospheric Administration (esrl.noaa.gov).

3.3 Results

3.3.1 $\delta^{11}B$ time-series

To a first order, the $\delta^{11}B$ data alone (Figure 3-4a) describe an increase in the pH gradient between the reef zones from approximately 0.07 to 0.2 pH units (Figure 3-4a,b; given the known relationship between $\delta^{11}B$ and pH; Figure 3-2). Using Equation 4-4 and the methodology above, the $\delta^{11}B$ can be used to calculate absolute pH_{sw}. Following this, the backreef $\delta^{11}B$ values describe a pH decrease over ~90 years from 8.05 to 7.87 pH units, with an average rate of -0.02 units per decade, similar to the recorded -0.015 units from the Bermuda Atlantic Time-series (1983-2012; *Bates et al.*, 2014).

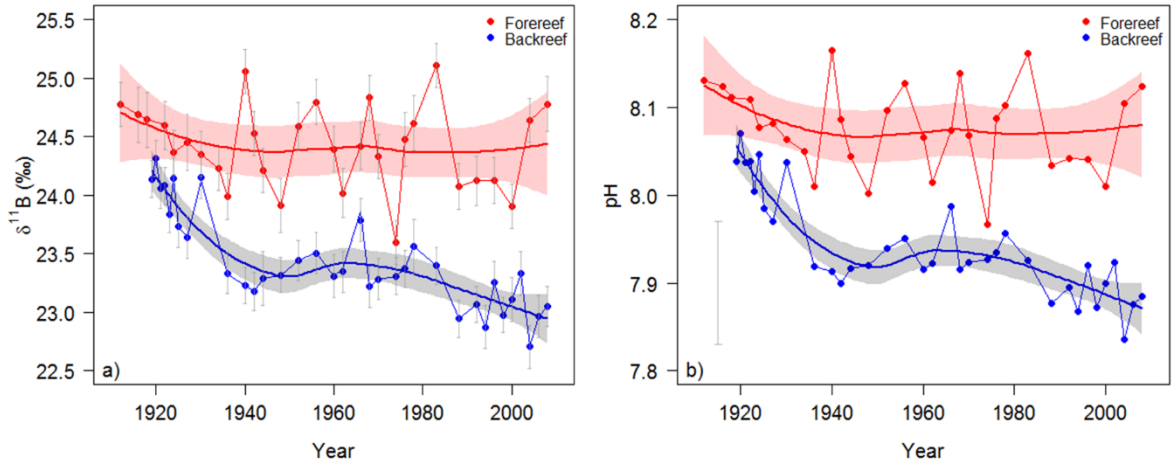

Figure 3-4. a) Boron isotopic composition ($\delta^{11}B$) of forereef coral FR-02 (red) and backreef coral BR-06. The $\delta^{11}B$ of FR-02 is higher, and more variable than the $\delta^{11}B$ of BR-06 and importantly, the $\delta^{11}B$ of FR-02 has remained relatively unchanged over the time-series whereas there has been a decline of ~1‰ in the backreef coral. Error bars represent the 2 standard error based on long-term measurements of JCp-1. b) Forereef and backreef pH reconstructions based on the boron isotopic composition of the FR-02 (red) and BR-06 (blue) corals. The data are fitted with a LOESS smoother and the borders represent the 2σ error of the LOESS smoother.

At the start of the time-series, the $\delta^{11}B$ of both reef zones were similar (p=0.07) (Figure 3-4), however, by 1941 to 1950 the difference in mean $\delta^{11}B$ of the forereef (24.22‰) and backreef (23.26‰) corals had become significantly different (p=0.02). Through the rest of the time-series this difference increases (Figure 3-4); because the decadal average of the forereef coral $\delta^{11}B$ remains approximately constant over time, this trend is driven principally by a decline in the $\delta^{11}B$ of the backreef, which significantly decreases from 24.01‰ in the first decade to 23.02‰ in the last decade (p=0.001; Figure 3-4b). The variability of $\delta^{11}B$ in the forereef is two times greater than in the backreef, up to 0.46‰, even within decadal groups (Figure 3-5c,d), and the variance in the decadal groups of forereef $\delta^{11}B$ data ranges from 0.004 to 0.54, but the variance does not increase linearly over the course of the time-series.

An autocorrelation function of a detrended and interpolated $\delta^{11}B$ time-series (Figure 3-6) showed a significant 8 to 22 year cycle in the forereef and a 5 to 16 year cycle in the backreef. However, despite these cycles mimicking those of some global climate cycles, the pH variability in the forereef was not found to be correlated with either the MEI, CAR, PDO or AMO indices. On the other hand, the backreef pH is significantly correlated to both the AMO and CAR (p=0.001 and p=0.04 respectively).

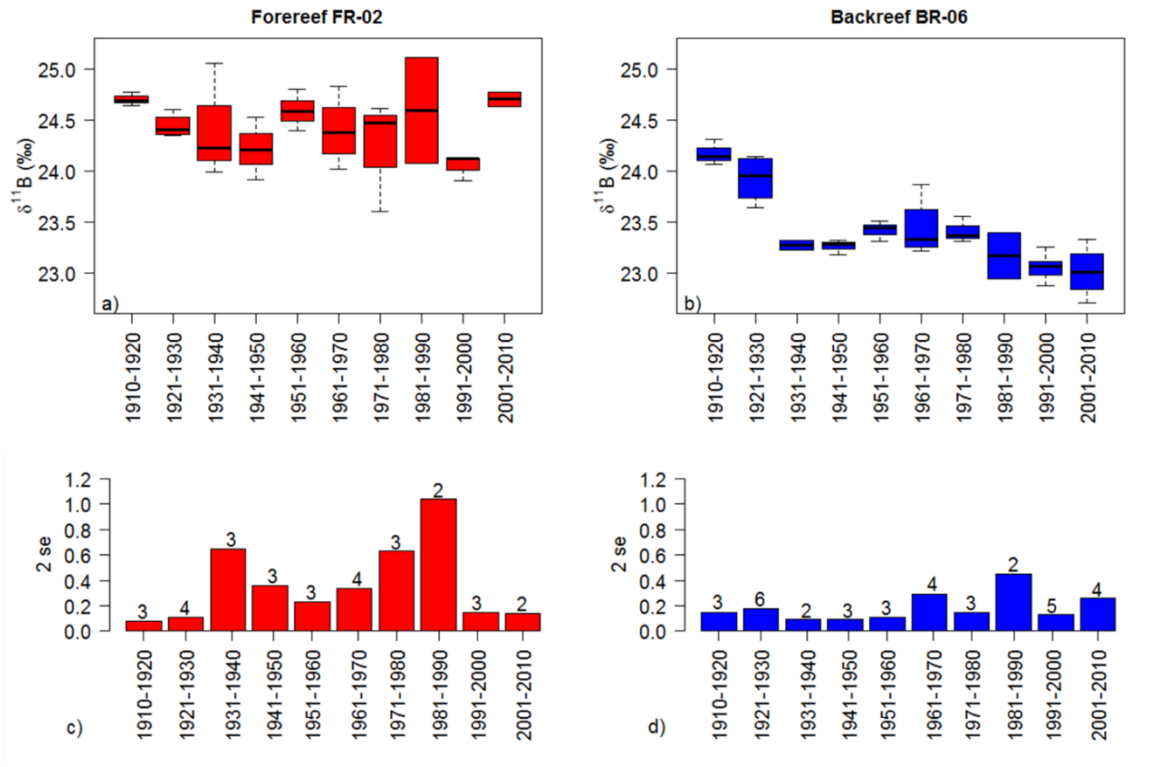

Figure 3-5. Boxplots of decadal groups of $\delta^{11}B$ data for the (a) forereef FR-02 coral and (b) the backreef BR-06 coral. Coloured boxes show the interquartile range of the data within each group, the black line denotes the median $\delta^{11}B$ value of the group and the whiskers show the minimum and maximum values. Bar plots represent the 2 standard error of the mean in each decadal group in the (c) forereef and (d) backreef. The numbers above each bar is the number of samples included in in each group.

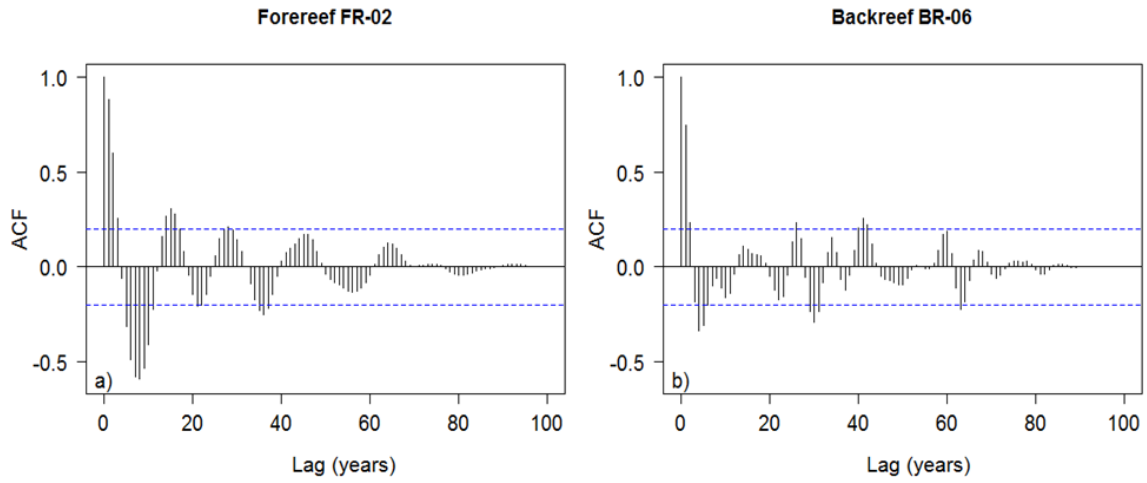

Figure 3-6. Autocorrelation function (ACF) of detrended and interpolated $\delta^{11}B$ values, where each time lag represents 1 year. a) The forereef and (b) backreef corals demonstrate cycling trends of $\delta^{11}B$ over the time-series. Blue lines indicate the boundary of statistical significance (5%).

It has previously been documented that the overall linear extension of forereef *S. siderea* colonies significantly declined over the last century, as opposed to the backreef colony extension remaining relatively constant (*Castillo et al.*, 2011). The extension rates of core FR-02 are respresentative of the forereef zone since the range of annual extension rates (~2 to 8 mm y^{-1}) over the 90 year time-series and the extension trend corresponds closest to the population average reported in *Castillo et al.*, (2011). Of the three backreef colonies sampled, BR-06 exhibits the fastest extension rate, at ~2 mm y^{-1} faster than the population average, making it have the most similar range to the forereef colonies. Here, we show that the linear extension rates of the two reef zones have opposing trends between $\delta^{11}B$ and pH (Figure 3-7), where the backreef coral BR-06 has a significant negative correlation with pH (r^2=0.42, p<0.001), in contrast to the insignificant positive correlation between forereef extension and pH (r^2=0.04, p=0.32). The extension rates from neither reef zone are correlated with any of the climate indices. The extension rates of both core FR-02 and BR-06 are within a normal extension range for this species (4.63 mm y^{-1} and 4.31 mm y^{-1}, *DeLong et al.*, 2011, 2.06 mm y^{-1} to 4.06 mm y^{-1} *DeLong et al.*, 2014), therefore no unusual growth effects are anticipated to have made an impact on the boron isotopic composition.

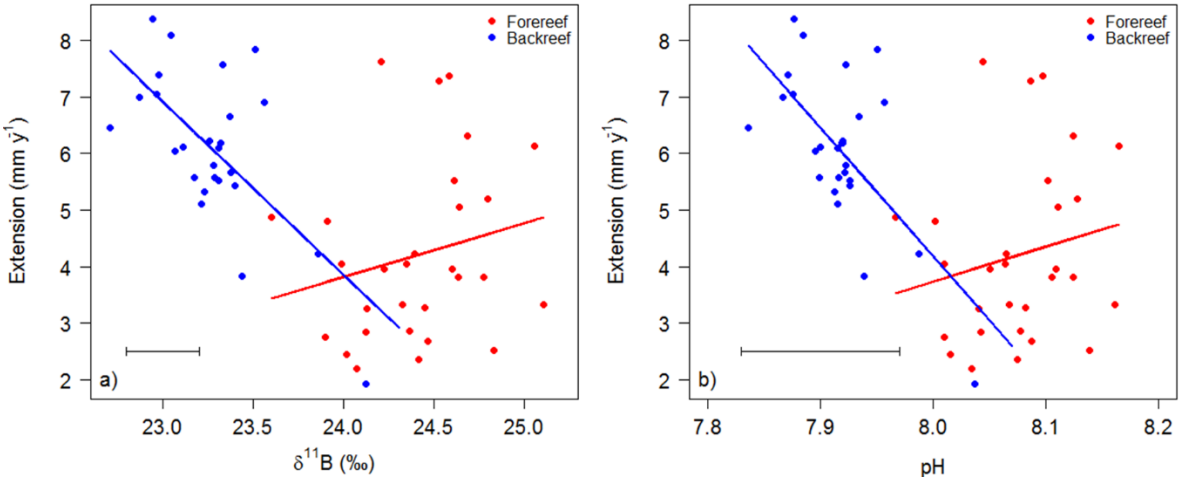

Figure 3-7. Linear relationships between forereef (red) and backreef (blue) skeletal extension rate with (a) $\delta^{11}B$, where the error bar represents a 0.2‰ 2 standard error on the mean $\delta^{11}B$; and (b) pH, where the error bar represents a 0.07 pH unit error on the reconstruction, based on the 2 standard error of the $\delta^{11}B$.

The carbon isotopic composition ($\delta^{13}C$) of the coral cores at annual resolution shows a strong decline from -0.66‰ to -1.40‰ in the forereef coral (1912 to 2008) and -1.04‰ to -2.42‰ in the backreef coral (1919 to 2008; Figure 3-8a; J. Ries, unpublished). During the first decade in both records, $\delta^{13}C$ signatures are significantly heavier than during the final decade (forereef: p<0.001, backreef: p<0.001). Throughout each time series, $\delta^{13}C$ is

significantly lighter in the backreef coral (mean = -1.47‰, $p<0.001$). Between 1970 and 2008, the decline in skeletal $\delta^{13}C$ is similar between both reef zones (backreef = -0.014‰ per year, forereef = -0.010‰ per year). However, between 1990 and 2008 the rate of decline increases by 2.8 times in the backreef to -0.040‰ per year.

Opposing relationships are demonstrated between $\delta^{13}C$ and extension rate, with forereef skeletal $\delta^{13}C$ being positively correlated to extension, and backreef skeletal $\delta^{13}C$ being negatively correlated (Figure 3-8e). $\delta^{13}C$ and $\delta^{18}O$ are significantly positively correlated in the backreef ($p<0.001$) but no relationship was found in the forereef coral (Figure 3-8c). Skeletal $\delta^{13}C$ was also found to be significantly correlated to $\delta^{11}B$ in both the forereef and backreef coral ($p<0.01$ and $p<0.001$ respectively; Figure 3-8d), and as the pH difference between the two reef zones increases for a given year (Figure 3-4b), the difference between the $\delta^{13}C$ also increases (Figure 3-8a).

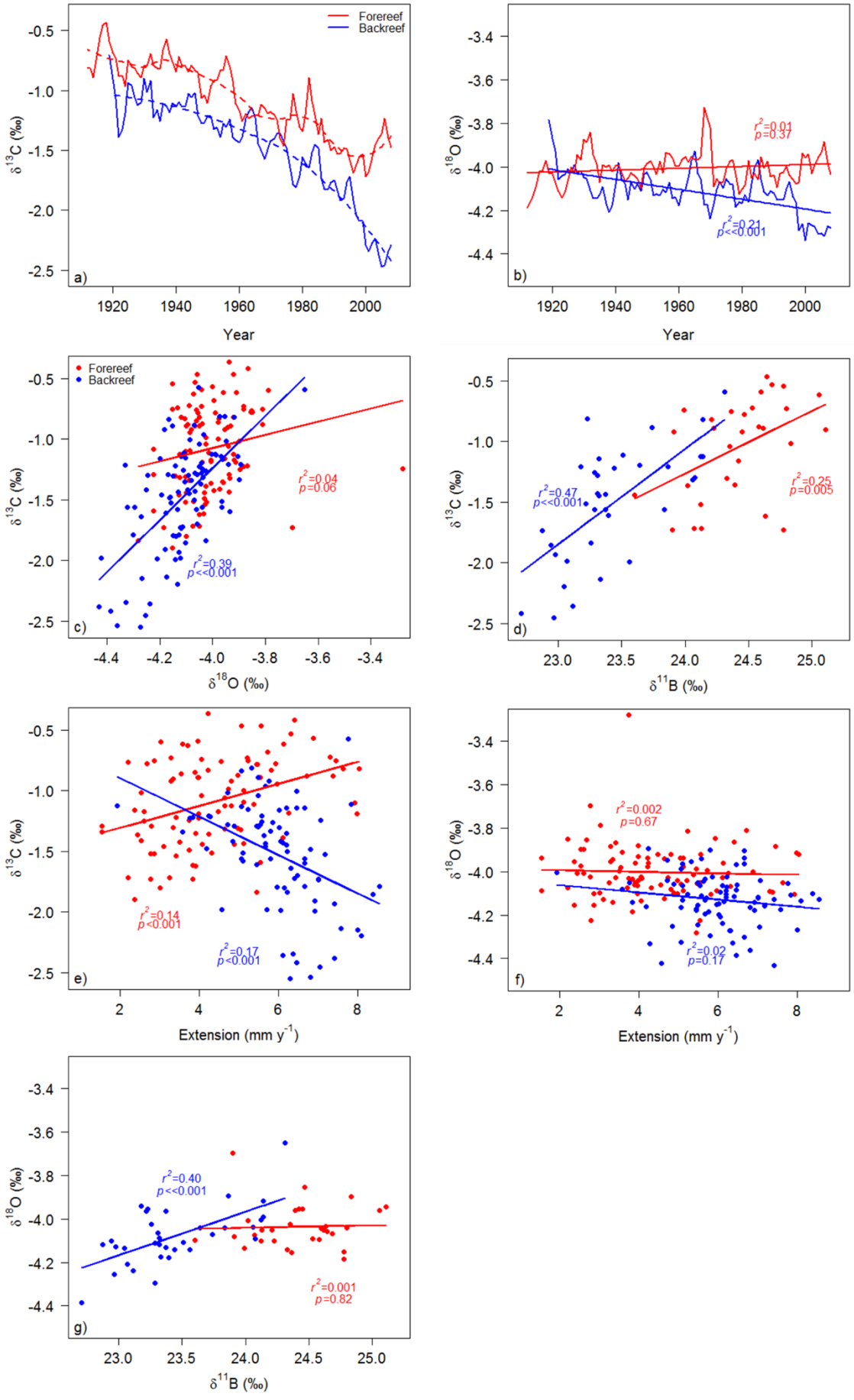
Forereef
Backreef
a)
δ13C (‰)
Year
b)
δ18O (‰)
r2=0.01
p=0.37
r2=0.21
p<<0.001
c)
r2=0.04
p=0.06
r2=0.39
p<<0.001
δ18O (‰)
d)
r2=0.47
p<<0.001
r2=0.25
p=0.005
δ11B (‰)
e)
r2=0.14
p<0.001
r2=0.17
p<0.001
Extension (mm y-1)
f)
r2=0.002
p=0.67
r2=0.02
p=0.17
Extension (mm y-1)
g)
r2=0.40
p<<0.001
r2=0.001
p=0.82
δ11B (‰)

Figure 3-8. Correlations between $\delta^{13}C$, $\delta^{18}O$, $\delta^{11}B$, and linear extension rate. Red points indicate data from the forereef FR-02 coral, and blue points indicate data from the backreef BR-06 coral. a) Three year running mean annual $\delta^{13}C$ time-series fitted with a LOESS smoother. b) Three year running mean annual $\delta^{18}O$ time-series. c) Positive correlations between $\delta^{13}C$ and $\delta^{18}O$. d) Positive correlations between $\delta^{13}C$ and $\delta^{11}B$. e) Positive correlation between forereef $\delta^{13}C$ and linear extension rate; negative correlation in the backreef coral. f) Correlations are not evident between $\delta^{18}O$ and linear extension. g) Positive correlations between $\delta^{11}B$ and $\delta^{18}O$ (not significant in the forereef).

3.3.2 Ba/Ca ratios

Seasonal cycles are evident in the monthly Ba/Ca ratios of both reef zones, but the peaks in these cycles occur at different times of the year in each zone (Figure 3-9), with peak Ba/Ca in the backreef corresponding to the late rainy season of Honduras (Oct-Jan) compared to the summertime in the forereef (~Aug). Low Sr/Ca ratios are further indicative of summertime, and high Sr/Ca ratios are indicative of wintertime (Figure 3-9). Welch's unequal variance t-tests were used to reveal that in the downcore samples (1922-1926), the backreef BR-06 coral had a significantly higher Ba/Ca ratio (mean=11.23 µmol/mol) than the forereef FR-12 coral (mean=7.37 µmol/mol, $p<<0.001$). In the modern record (2006-2008), the patterns of Ba/Ca change are reversed, with the forereef demonstrating greater Ba/Ca ratios than the backreef. One particularly notable feature is the peak in Ba/Ca (beginning after September 2007, based on the age model presented in *Fowell et al.*, 2016) when the forereef Ba/Ca ratios increased ~10 times, and backreef coral ~8 times, coinciding with when Hurricane Felix made landfall in Nicaragua, Honduras and Belize in September 2007. Even if this post-September 2007 data is excluded, a doubling of Ba/Ca ratios between downcore and recent forereef coral Ba/Ca ratios ($p<<0.001$) is still evident, and for the most recent samples the forereef coral ratios are on average ~4 µmol/mol greater than in the backreef coral ($p<0.001$). In contrast to this increase in the forereef, no significant difference was found between the 1922 to 1926 and 2006 to 2008 backreef coral Ba/Ca ratios ($p>0.5$).

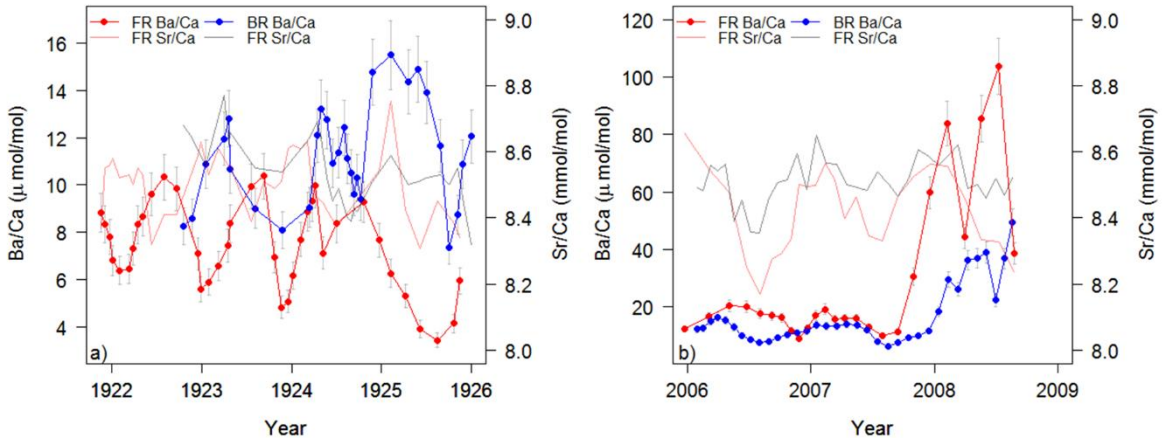

Figure 3-9. a) Forereef (red) and backreef (blue) Ba/Ca ratios between 1922 and 1926. Ratios from both reef zones have seasonal oscillations, but ratios in the backreef are higher. b) Ba/Ca ratios between 2006 and 2009 are lower in the backreef than the forereef. Forereef ratios also increase up to five times following Hurricane Felix in September 2007. Error bars represent 1σ external precision. Sr/Ca ratios are also plotted to indicate winter (high Sr/Ca) and summer (low Sr/Ca) seasons.

3.4 Discussion

3.4.1 Ocean acidification and extension rates

In the absence of calcification rate data (currently the subject of an ongoing study at the University of North Carolina, Chapel Hill), linear extension rates are cautiously used here as a proxy for calcification rate, given the strong positive correlation between these two metrics demonstrated by *Carricart-Ganivet et al.*, (2013) in *Siderastrea siderea* colonies (r^2=0.92, p<0.0001).

The backreef coral BR-06 has a significantly higher mean annual extension rate (6 mm y^{-1}) than the forereef FR-02 coral (4.4 mm y^{-1}; p<0.001; Figure 3-10a). Not only is the mean extension rate of BR-06 greater than FR-02, but the extension rate has actually increased between 1919 and 2008 by 2.1 mm y^{-1} (p<<0.001), simultaneously with decreasing pH (Figure 3-4b), whereas the forereef *S. siderea* has suffered a significant reduction in extension rate between 1912 and 2008 (1.6 mm y^{-1}, p=0.003), despite recording no decline in pH (Figure 3-4b). Within the long-term extension rates, there is a significant 18 year cycle, as demonstrated by the autocorrelation function (Figure 3-10b). This cycle is likely to have influenced the calculated rate of extension decrease, given that the beginning of our record is near a peak in extension rates, as opposed to the end of the record which is coming out of a trough. Conversely, there is no significant pattern to the extension rate in the BR-06 coral

(Figure 3-10c). The faster extension rates in backreef corals may have also had an influence on causing the more negative $\delta^{13}C$ and $\delta^{18}O$ compositions of the backreef particularly since the faster rates of decline in the 1990s coincides with the faster rate of extension at this time (Figure 3-10; *McConnaughy*, 1989).

The implications of these observations are twofold: firstly, pH is unlikely to be the dominant control of calcification rate in *S. siderea* since the observed relationship between extension (calcification) and pH are negligible (forereef) or opposite to what is expected (backreef); secondly, this provides evidence that the evolution of pH on coral reefs, even areas which are in relatively direct contact with the open ocean, are not necessarily equal to open ocean surface water pH, in agreement with observational studies (*Suzuki and Kawahata*, 2003; *Anthony et al.*, 2011; *Kleypas et al.*, 2011; *Andersson et al.*, 2014)..

The decadal groups of extension rate (Figure 3-10 b,c) demonstrate that there is greater variability in FR-02 extension rate than in BR-06. It is worth noting that these inter-decadal variations, which can reach 2.8 mm in FR-02 and 4.5 mm in BR-06 are double the long-term changes described above.

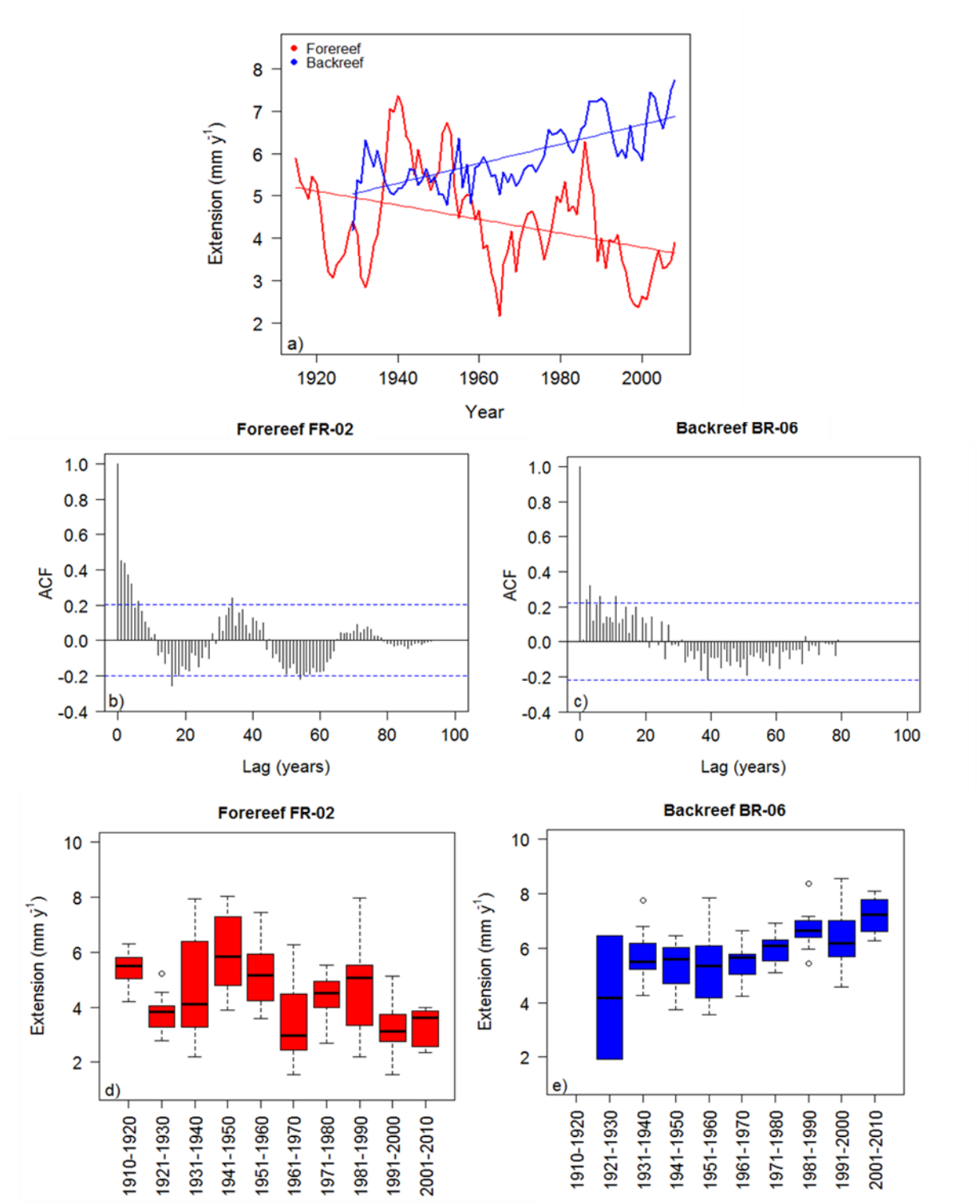

Figure 3-10. a) 3 year running means and linear lines of best fit for the forereef coral FR-02 (red) and the backreef coral BR-06 (blue) extension rates. Data from *Castillo et al.*, (2011). b) Autocorrelation function of linear extension rate in the forereef FR-02 coral. c)Autocorrelation function of linear extension rate in the backreef BR-06 coral. Blue lines indicate the boundary of statistical significance (5%). d) Boxplot of decadal variations in FR-02 extension rates. e) Boxplot of decadal variations in BR-06 extension rates.

The calcification rates of *S. siderea* have been shown to increase from pH 7.32 to 7.82 and decrease from pH 7.82 to 8.07 in the culturing experiment of *Castillo et al.*, (2014),

hence, the opposing relationships between forereef and backreef extension were expected, given the pH range of the forereef is 7.97 to 8.16 and the pH range of the backreef is 7.8 to 8.1. The lack of relationship between forereef pH and extension rate may suggest that the calcification rates are buffered for pH ≥8. As with the increase in cultured samples calcification rates, the increased extension rates of the backreef coral may be a response to increased temperatures and pCO_2 simultaneously aiding the photosynthetic ability of their dinoflagellate endosymbionts and thus providing more energy for calcification (*Holcomb et al.*, 2010). Whatever the cause of the difference between the extension rates of the two reef zones (also observed in additional coral cores published in *Castillo et al*., 2011), *S. siderea* in the Sapodilla Cayes do not appear to be strongly negatively impacted by declining seawater pH.

3.4.2 Sediment loading and global climate cycles

Ba/Ca ratios in the skeletons of scleractinian corals have been identified as a way to monitor the Ba content of water, which can be derived from either upwelling (*Montaggioni et al.*, 2006) or suspended sediments (*Ogden and Ogden*, 1998). Upwelling can cause high Ba/Ca ratios in coral (*Lea et al.*, 1989) due to the higher concentration of Ba in intermediate depth waters from decaying organic matter remineralisation (*Alibert and Kinsley*, 2008). However, there is no evidence of upwelling within the Gulf of Honduras and therefore the inter-annual Ba/Ca cycle (Figure 3-12) is unlikely to be the product of variable periods of upwelling (*Mann and Lazier*, 1996; *Prouty et al.*, 2008). The primary source of Ba to the Gulf of Honduras is Ba released from organic material transported from watershed run-off (*Ogden and Ogden*, 1998). The southern section of the MBRS is affected by the Belizean rivers Monkey, Rio Grande and Deep River in addition to the Honduran River Ulua (*Soto et al.*, 2009). It is estimated that 80% of the sediment, and 50% of the nutrients originate from Honduras, 16% of all sediment and 25% of nitrogen and phosphorous from Guatemala and only 10-15% of the nutrients from Belize and 5% from Mexico (*Burke and Sugg*, 2006; *Chérubin et al.*, 2008). The Ulua watershed has one of the largest soil erosivity factors, and is the largest contributor of both sediment, nitrogen and phosphorous to the MBRS (Figure 3-11; *Burke and Sugg*, 2006). The plume from the Ulua River interacts with the southern section of the MBRS 61% of the time, based on a 9-year time-series of SeaWIFS satellite ocean colour images (*Soto et al.*, 2009). Physical sedimentation and the high concentrations of nutrients adhered to the sediment act as a coupled stressor to coral reefs since sediment can smother coral and decrease light-levels (e.g. *Rogers*, 1979), and

nutrification can increase the dominance of macroalgae (e.g. *Hughes*, 1994); a prevalent factor in declining coral health (e.g. *Rogers*, 1990; *Fabricius*, 2005).

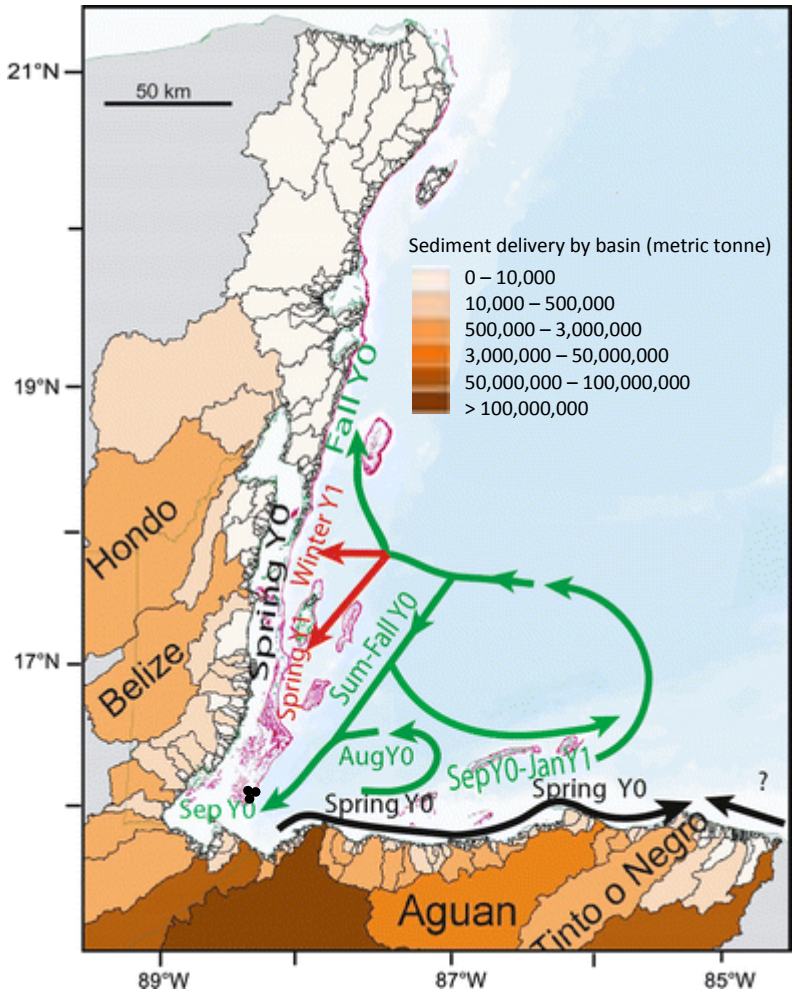

Figure 3-11. Annual sediment delivery from Mesoamerican Barrier Reef watersheds. The Ulua and Motagua watersheds provide the largest sediment delivery in close proximity to the Sapodilla Cayes. Pink sections outline the coral reefs, and the black circles mark the location of the sampling in the Sapodilla Cayes. Seasonal variation in terrestrial run-off dispersion patters are also outlined; black arrows show the coastal transport, which can flow in a northerly or southerly direction between Belize and the barrier reef, and then easterly across the northern Honduras coastline; green arrows show the offshore circulation patterns within the Gulf of Honduras, featuring two cyclonic eddies; red arrows show the remaining dispersion of sediment from the previous year. Figure adapted from *Burke and Sugg*, (2006) by *Cherubin et al*., (2008).

Temporal variation in the amount of Ba transported to coral reefs is affected by two main factors. Firstly, land clearance induced soil erosion as a result of increasing populations has been shown to increase the Ba content of fluvial plumes in other parts of the world including the Great Barrier Reef (*Alibert et al.*, 2003; *McCulloch et al.*, 2003; *Sinclair and*

McCulloch, 2004; *Lewis et al.*, 2009; *D'Olivo et al.*, 2015), Hawaii (*Lewis et al.*, 2009), Mexico (*Carriquiry and Horta-Puga*, 2010) and Kenya (*Fleitmann et al.*, 2007). In the Veracruz Reef System, Mexico, there was a 14% increase in Ba concentrations between pre-industrial and post-industrial times following a quadrupling of population (*Carriquiry and Horta-Puga*, 2010); and Great Barrier Reef coral Ba/Ca ratios indicated a 5 to 10-fold increase in sediment fluxes following European settlement between 1870 and 1998 (*McCulloch et al.*, 2003). Secondly, the volume of river water may itself be influenced by the position of the ITCZ, the seasonal variation of which causes the rainy season of Southern Belize to be between June and October, or March and October in Honduras (*Soto et al.*, 2009). When the AMO is in an anomalously warm phase, the ITCZ moves further north from between the two atmospheric Hadley Cells that meet at the Equator to the Caribbean, causing seasonal and decadal oscillations in Caribbean rainfall. It is well established that a negative PDO index results in a wetter Caribbean (*Hastenrath*, 1976) and also increases rainfall and the likelihood of tropical storms turning into hurricanes as a result of high sea surface temperatures (SSTs; *Taylor et al.*, 2002). At times of a positive AMO index, a weakening of easterly winds from the Caribbean Low-Level Jet brings greater volumes of rain and an increased probability of hurricane formation (*Knaff*, 1997).

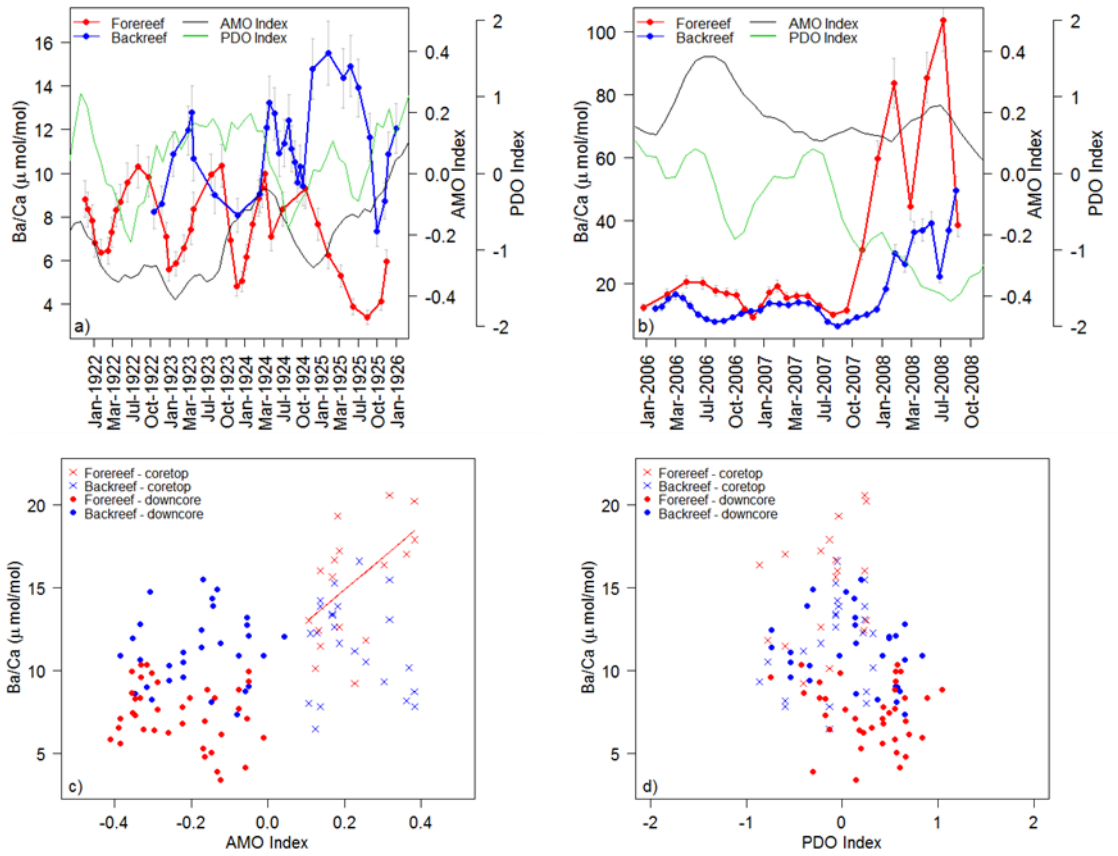

Figure 3-12. Forereef FR-12 (red) and backreef BR-06 (blue) coral Ba/Ca ratios at a monthly resolution are also compared with 4 month running mean indices of the Atlantic Multidecadal Oscillation (AMO; black line) and the Pacific Decadal Oscillation (PDO; green line). a) Downcore samples from 1922-1926. b) Recent samples from 2006-2009. Seasonal cycles are evident in both reef zones. Note the larger Ba/Ca scale in the modern record snapshot to account for the five-fold increase in forereef Ba/Ca influxes after September 2007. All error bars represent the 1σ external precision of the ICP-MS measurement. c) Downcore (circles) and coretop (pre-Hurricane Felix; crosses) correlations between sub-annual skeletal Ba/Ca ratios and running mean AMO index. d) Downcore (circles) and coretop (pre-Hurricane Felix; crosses) correlations between sub-annual skeletal Ba/Ca ratios and running mean PDO index.

Between the 1920s and 2000s, the AMO switched from being in the negative phase in the 1920s, to a positive phase in the 2000s, coupled with the PDO switching from a weak positive phase to a negative phase (Figure 3-12), while the Caribbean Index SST anomalies (CAR) increased. It was expected that these changes would have resulted in stronger winds and more precipitation in the Caribbean, increasing the amount of sediment, or desorbed Ba in seawater (*Hanor and Chan*, 1977), transported to the corals which would have recorded higher Ba/Ca ratios, but there is no evidence that precipitation across the Honduras and Belize watersheds increased between the 1920s and 2000s (Figure 3-13). The caveat of these conclusions is that there are only three years of Ba/Ca data which is being compared with the decadal index of AMO, so the full correlation may not be recognised.

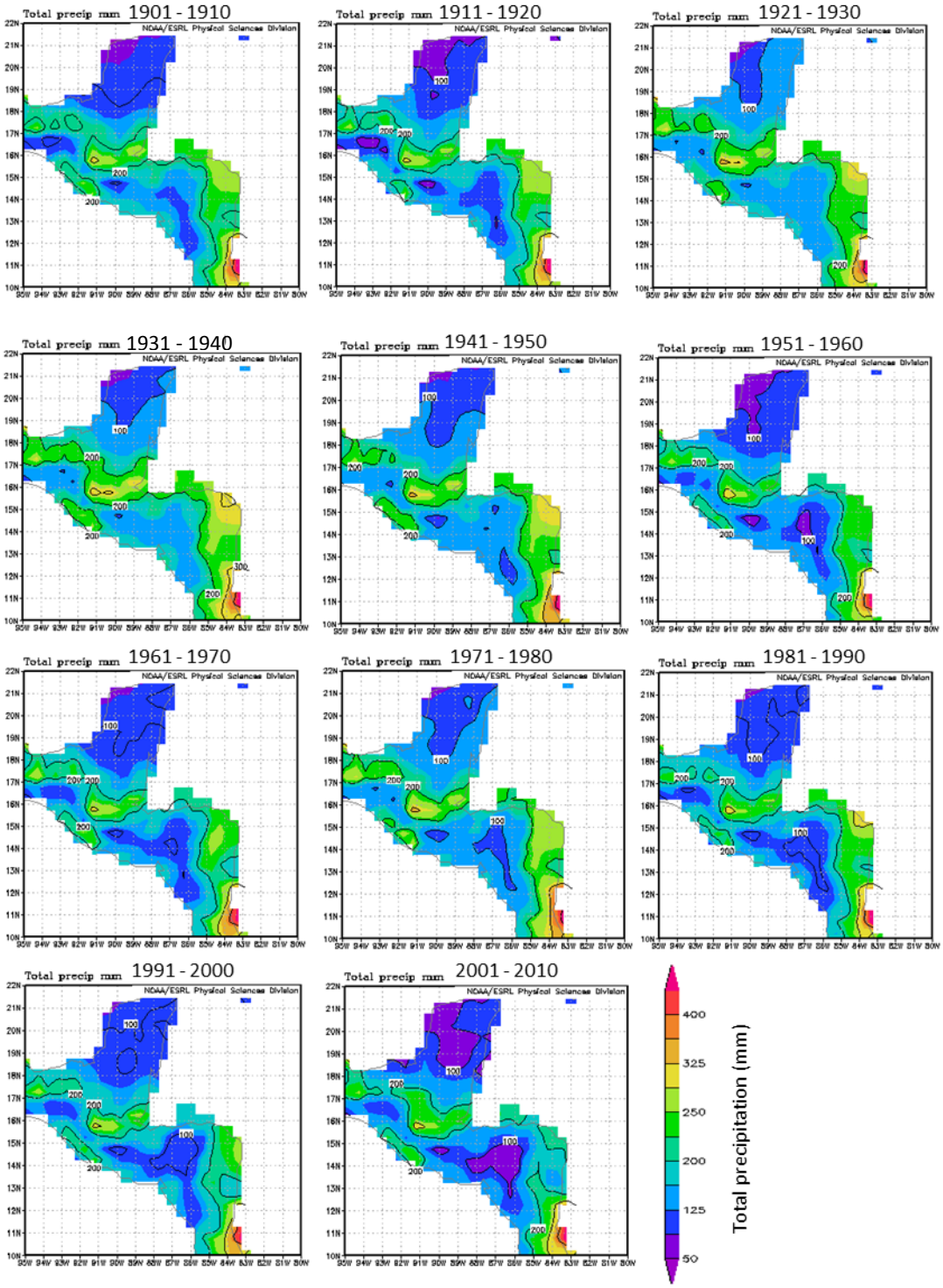

Figure 3-13. Total precipitation over Honduras and Belize for the months of March to October. Each panel represents a decade of precipitation. Panels made using the Global Precipitation Climatology Center website (http://www.esrl.noaa.gov/psd/data/gridded/data.gpcc.html).

In support of our hypothesis, the backreef coral recorded precipitation-driven sediment deposition, demonstrated by the significant correlation between both the monthly modern (pre-hurricane) and historic Ba/Ca ratios with CAR (Table 3-1). However, in the modern forereef samples (pre-hurricane), a significant relationship is found between Ba/Ca ratios and the AMO (Table 3-1). These findings support the hypothesis that the skeletal compositions of corals in the MBRS are impacted by terrestrial run-off and large scale climate cycles that influence precipitation patterns. Despite the lack of increased precipitation (Figure 3-13), the Ba/Ca ratios of the forereef doubled between the historic and modern samples ($p<<0.001$; Figure 3-12). Over this time, sediment delivery has increased by a factor of 20, nitrogen by a factor of 3, and phosphorous by a factor of 7 (*Burke and Sugg*, 2006), suggesting that terrestrial run-off as a function of increased population and changes in land use is the main driver of the Ba/Ca composition of the coral.

Table 3-1. Table of correlations between forereef and backreef Ba/Ca ratios and the AMO, PDO, CAR and MEI climate indices. The Pearson's product correlation coefficient (Cor) and *p*-value are given for each relationship. Correlations in the coretop are separated into pre-hurricane data only and the full coretop.

	Cor	***p***		**Cor**	***p***
Coretop forereef			*Pre-hurricane*		
CAR	**-0.50**	**0.011**	CAR	-0.39	0.11
AMO	-0.18	0.39	**AMO**	**0.53**	**0.022**
PDO	**0.73**	**<<0.001**	PDO	0.33	0.18
Coretop backreef			*Pre-hurricane*		
CAR	**-0.72**	**<<0.001**	**CAR**	**-0.80**	**<<0.001**
AMO	-0.23	0.18	AMO	-0.21	0.35
PDO	**0.71**	**<<0.001**	PDO	0.34	0.11
Downcore forereef					
AMO	-0.23	0.17			
PDO	-0.14	0.41			
MEI	**-0.34**	**0.03**			
Downcore backreef					
AMO	-0.11	0.57			
PDO	-0.24	0.19			
MEI	-0.17	0.38			

Our results also agree with those of *Prouty et al.*, (2008), who sampled *Montastrea faveolta* colonies (skeletal growth dating from 2000-2006) from the Sapodilla Cayes, Turneffe Atoll, Cayos Cochinos and Utila (Figure 3-14). Their study found no variation in Ba/Ca ratios at a colony scale within the region of the Sapodilla Cayes, which contradicts

the significant difference between our forereef and backreef samples (1920s: $p<<0.001$, 2000s: $p=0.001$, Welch unequal variance two sample t-tests), both collected within the Sapodilla Cayes Marine Reserve. However, regional effects were found and colony location was responsible for 73% of Ba/Ca variance, with Turneffe Atoll having the lowest Ba/Ca ratios (5.4 µmol/mol), followed by Utila and Cayos Cochinos (5.9 µmol/mol and 6.2 µmol/mol respectively), and the Sapodilla Cayes having the highest ratios at 6.4 µmol/mol (similar to the minimum values in our historical forereef Ba/Ca ratios). Finding the highest Ba/Ca ratios in corals from the Sapodilla Cayes, and the lowest ratios in Turneffe Atoll is further evidencethat skeletal Ba/Ca ratios are responding to the local water quality since the Sapodilla Cayes are in closer proximity to the plumes from the major watersheds (Figure 3-11). The largest differences between our *S. siderea* results and those of *Prouty et al.*, are that the *M. faveolta* corals have lower Ba/Ca ratios (<10 µmol/mol) than our modern *S. siderea* corals. Furthermore, the Ba/Ca ratios of *M. faveolta* are more consistent with each other, even across the different reef sites.

Similarly to *S. siderea*, data from the coral *Porites lobata* in Moloka'i, Hawai'i (*Prouty et al*., 2010) reveals an interannual variation in skeletal Ba/Ca ratios. Additionally, the Ba/Ca ratio in *P. lobata* is lower at sites farthest away from the watershed (4.74 µmol/mol) and highest at the site closest to the estuary (6.28 µmol/mol), coupled with a lower extension rate. An additional similarity to the observations in our forereef coral, *Prouty et al*., (2010) reported a significant increase in coral Ba/Ca ratios (up to five times) across their time-series (maximum 1921 to 2006), and attributed this to changes in land use.

If salinity and seawater Ba/Ca data were available, it would have been possible to calculate the Ba Effective River End-Member (EREM) concentration, which would quantify the concentration of dissolved Ba and desorbed Ba from riverine sediments (*Prouty et al*., 2010). Ideally, a basline measurement of reef and river EREM would be established and then compared to analyses of samples from the rainy seasons of Belize and Honduras, or following hurricane events. This would provide a clearer interpretation of how much terrigenous Ba reaches the forereef and backreef; how much this increases following high volumes of precipitation and run-off, including how much more Ba arrives in the forereef than the backreef, if this indeed is the case; and potentially whether the Ba in the forereef and backreef originate from the same watershed. However, given that a 1:1 ratio was not observed between coral Ba/Ca ratios and water discharge in the *P. lobata* samples of *Prouty et al.*, (2010), we must also assume a secondary parameter, such as sediment resuspension, influences the Ba/Ca transport in seawater and subsequent incorportation into coral skeletons.

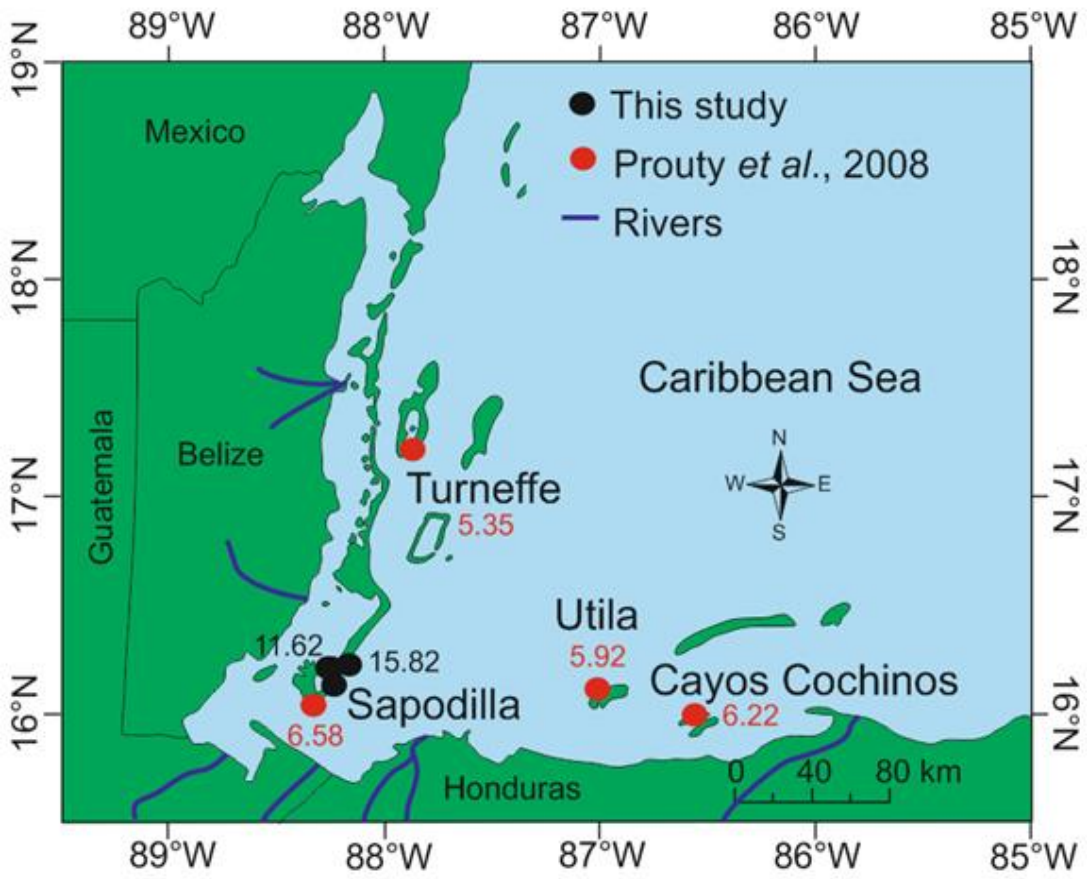

Figure 3-14. Map of coral coring locations around the Mesoamerican Barrier Reef System (Sapodilla Cayes, Turneffe Atoll and the Bay Islands) for the purpose of Ba/Ca analysis. Red markers indicate the regions sampled by *Prouty et al.*, (2008) and the associated average 2000-2006 Ba/Ca ratios in µmol/mol. Black markers indicate the sampling locations of this study and the associated average Ba/Ca ratio for the year 2000. Blue lines indicate the approximate locations of rivers likely to impact the sampled corals.

The dominant circulation of coastal water is a north-westerly current from the south-east of Honduras to Mexico (*Ezer et al.*, 2005; *Tang et al.*, 2006; *Chérubin et al.*, 2008), transporting terrestrial run-off to Belizean reefs in the time scale of a few days to a few weeks (*Sheng et al.*, 2007; *Soto et al.*, 2009). However, there are more complex seasonal patterns of circulation within the Gulf of Honduras, including a southerly current (7 months of the year) in the straits between the Belizean mainland and the barrier reef that generally turns eastward at the southernmost extremity of the barrier reef (Figure 3-11, *Chérubin et al.*, 2008, *Ezer et al.*, 2011, *Ezer et al.*, 2012). There are also two prevalent cyclonic eddies that circulate terrestrial run-off offshore, circulating Honduran river plume run-off from Honduras to Belize to Mexico (which can flow to the west), and additionally the presence of mesoscale eddies turns the southwestern corner of the Gulf of Honduras into a retention area for buoyant matter (*Chérubin et al.*, 2008). On a local scale, reef water of the Sapodilla Cayes receive terrestrial run-off from 6 Belizean rivers, and 8 Guatemalan/Honduran rivers (*Paris*

and Chérubin, 2008), but the Belizean rivers only impact inshore reefs as the barrier reef limits the circulation of mesoscale flow in coastal waters (*Chérubin et al.*, 2008). Therefore, the stipulated direction of advection, coupled with a smaller sediment load from mainland Belize compared to nothern Honduras (Figure 3-11) implies that the forereef receives more turbid water masses from Honduras, whereas the backreef receives less turbid water masses from Belize. This is demonstrated in the Ba/Ca ratios in the modern record (Figure 3-9b) whereby there are higher Ba/Ca ratios in the forereef coral than in the backreef coral (p=0.001), showing that a more sediment and nutrient rich water mass reaches the forereef.

Although terrestrial run-off onto the reefs around the MBRS is always connected due to seawater circulation, hurricane events can highlight run-off circulation patterns because a large volume of terrestrial run-off is deposited over a short time-scale, making the higher concentrations of organic compounds or sediment easier to trace. After Hurricane Mitch in 1998, *Andréfouët et al.*, (2002) derived a water quality index using SeaWIFS chlorophyll-a, coloured dissolved organic matter, and suspended matter data. This water quality index was used as a tracer to show that after hurricanes in this region, the coastal waters of Honduras become extremely turbid and this low salinity water mass is loaded with nutrients, dissolved organic matter and particulate organic matter and circulates northwards across the MBRS (*Andréfouët et al.*, 2002; *Sheng et al.*, 2007). Hurricane Mitch reportedly caused 50% of the average annual sediment to be transported to the MBRS (*Burke and Sugg*, 2006), and after such events, the water around Honduras can remain turbid for up to a month afterwards (*Andréfouët et al.*, 2002). The coral Ba/Ca data indicates that the effects of this last for at least 12 months, given that the Ba/Ca ratios in the forereef remain elevated for at least 12 months following the hurricane. The likely explanation for this observation is that damage to vegetation on mainland Honduras causes a higher sediment load to be washed into the riverine systems for an extended period. An alternative might be an accumulation of Ba in the tissue layer (the most modern samples of the record), which has previously been observed in other elements such as Sr (*Gagan et al.*, 2012). The fact that the Ba/Ca influx to the forereef is twice as high as the backreef following Hurricane Felix in September 2007 provides observational evidence that the forereef receives a greater amount of sedimentary deposits than the backreef (Figure 3-12b), and the lag between forereef and backreef peak Ba/Ca ratios is either evidence of a westerly circulation after a hurricane, or a result of the slower run-off expulsion from Belize suggested by *Chérubin et al.*, (2008).

To summarise, large-scale climate cycles drive precipitation in the Caribbean, but the driver of Ba/Ca cycles in coral is riverine inputs of nutrient-rich terrestrial-derived sediment, which have changed not as a result of a new precipitation regime, but increased land-use

change and soil erosion. Therefore, the Ba/Ca ratios of the corals are correlated with climate indices because the Ba is transported here following climate cycle led processes. The impact of nutrification on reef water pH is addressed in the following section.

Given that riverine inputs are driven by climate cycles, we might expect to see further changes in the future, more than likely in the form of an increase in precipitation. For example, the ITCZ has been shown to be expanding northwards towards the Caribbean (*Bronnimann et al.*, 2015) so increases in precipitation may yet be to come, but it is also argued that predicted decreases in anthropogenic aerosols may limit this expansion (*Allen*, 2015). Purely as a result of further land clearance, the input of sediments and nutrients are anticipated to increase by >10% by 2025 relative to the beginning of the 21st century, so further declines in forereef extension rates are predicted (*Burke and Sugg*, 2006).

Although it is commonplace for coral Ba/Ca ratios to reflect riverine discharge, anomalies in this pattern have also been reported, including peaks in Ba/Ca not associated with high volumes of discharge, or correlated with SST, and also corals from the same region as each other displaying deviations in Ba behaviour (*Tudhope et al*., 1996, *Hart et al*., 1997, *Esslemont et al*., 2004, *Sinclair*, 2005b). Although there are no anomalous peaks in either forereef or backreef Ba/Ca ratios (with the exception of those we have attributed to Hurricane Felix), the fact that the cycle of peaks and troughs between these corals do not align (Figure 3-9) is not yet fully resolved. Alternative hypotheses for anomalous Ba behaviour have included: response to phytoplankton blooms; *Trichodesmium* blooms (which concentrate Ba); physiological processes such as reproduction; and mass coral spawning (*Sinclair*, 2005b). However, no significant or reproducible correlations were found between these factors and anomalous Ba behaviour, and is not explored further here.

3.4.3 Spatial differences in pH

As noted above, the pH time-series of the forereef contrasts with that of the backreef, with the forereef demonstrating no decline in pH and the backreef recording a 0.15 pH unit decline over 90 years (Figure 3-4b). The decrease in pH_{sw} from backreef corals is equivalent to ~ -0.017 pH units per decade; greater than the ~ -0.011 pH unit per decade observed in Guam corals (NW Pacific; *Shinjo et al.*, 2013), but the same as those observed using the boron isotope pH proxy in inner- and mid-shelf corals (−0.017 and −0.018 respectively) in the Great Barrier Reef (GBR; Pandora Reef and Rib Reef respectively; 1960-2010), and therefore also consistent with recent (1984-2011) global estimates of 0.017-0.019 pH unit

decrease per decade of surface seawater globally (*Bates et al.*, 2012; *Bates et al.*, 2014). These estimates are less than the -0.041 pH units per decade observed in Arlington Reef mid-reef corals (GBR; 1940-2004; *Wei et al.*, 2009); however, this rate of decline is similar to the steep decline observed in the backreef samples between 1910 and 1940, with a rate of ~0.053 pH units per decade. The lack of long term OA signal in the forereef resembles the findings of (*Pelejero et al.*, 2005), whose outer-shelf corals from Flinders Reef (GBR) lacked a long term OA trend (1708-1988), but large variability (0.3 pH units) over 50 year cycles.

The pH regime of a coral reef is controlled by the balance between Net Ecosystem Calcification (NEC = gross calcification – gross dissolution) and Net Primary Production (NPP) and in order for coral reefs to keep growing, NEC must exceed Net Ecosystem Dissolution (NED = gross dissolution – gross calcification; (*Bates et al.*, 2010; *Andersson and Gledhill*, 2013; *Andersson et al.*, 2014)). Calcification removes HCO_3^- ions from seawater and releases CO_2 into the surrounding water and is ultimately controlled by the concentration of CO_3^{2-} ions ($[CO_3^{2-}]$) and Ω_{arag}, both of which decrease with decreasing pH.

$$Ca^{2+} + 2HCO_3^- \rightarrow CaCO_3 + CO_2 + H_2O \qquad \text{Equation 3-5}$$

In contrast to calcification, primary production removes CO_2 and HCO_3^-, which drives Equation 3-6 to the left, reducing the number of available H^+ ions, thus increasing the pH (*Prins and Elzenga*, 1989):

$$CO_2 + H_2O \rightleftharpoons H_2CO_3 \rightleftharpoons HCO_3^- + H^+ \rightleftharpoons CO_3^{2-} + 2H^+ \qquad \text{Equation 3-6}$$

That reef pH is controlled by these processes and is not a simple function of open ocean pH is evident in multiple existing boron isotope time-series from a number of different countries and reef zones (Figure 3-15), as well as various observational and modelling studies mentioned previously (*Suzuki and Kawahata*, 2003; *Anthony et al.*, 2011; *Kleypas et al.*, 2011; *Andersson et al.*, 2014). For instance, *Suzuki and Kawahata* (2003) observed lower pCO_2 concentrations in lagoonal reefs than offshore reefs, which is a comparable pattern to backreef $\delta^{11}B$ being lower than forereef $\delta^{11}B$. Benthic carbon fluxes have no significant impact on oceanic variations in pH, pCO_2 and Ω_{arag}, yet modelled simulation show that in reefs with long residence times such fluxes can buffer the impacts of ocean acidification (*Anthony et al.*, 2011). On shallow reefs, a net increase in Ω_{arag}, can be stimulated by photosynthesis DIC utilisation and coral calcification exceeding the draw down of total

alkalinity (A_T), and therefore changes in benthic community structure and changes in the ratio of calcification to photosynthesis can alter the local carbon chemistry, helping to buffer against OA (*Kleypas et al.*, 2011).

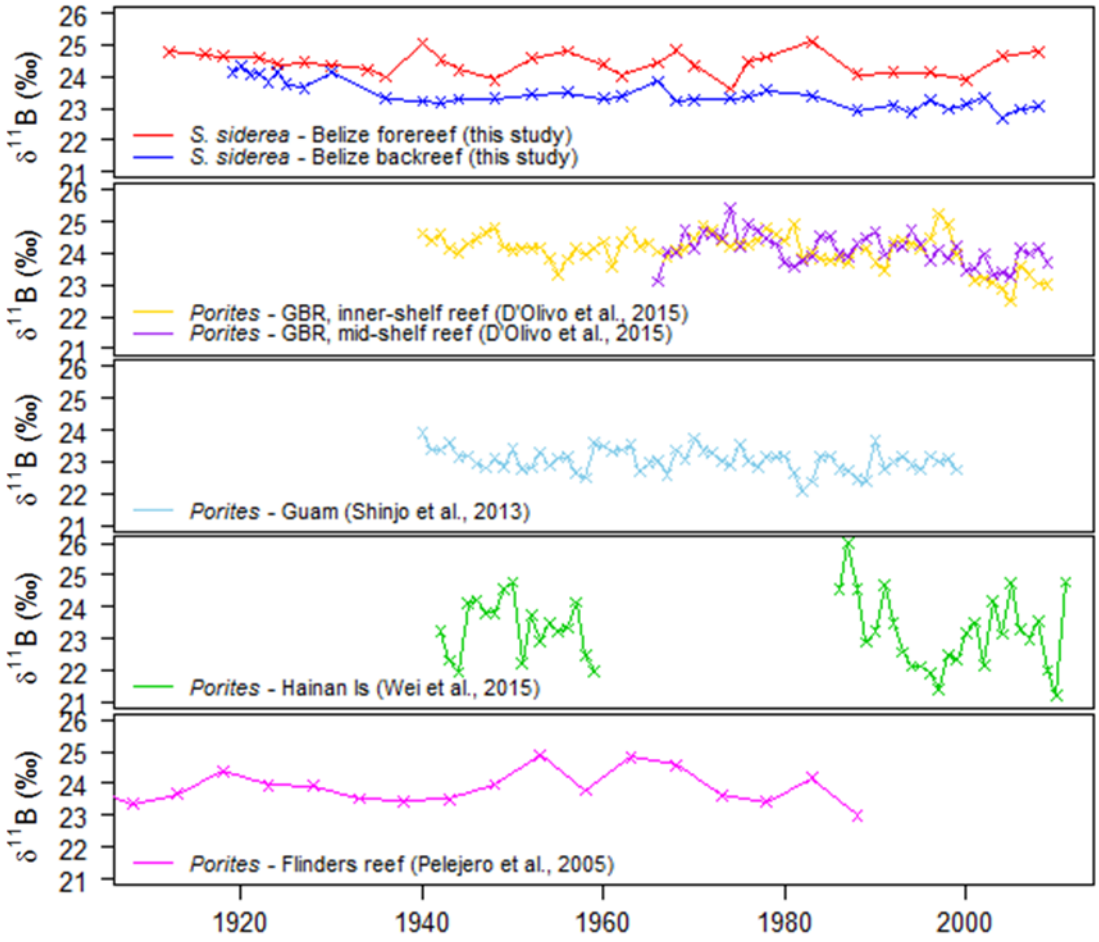

Figure 3-15. $\delta^{11}B$ records from 1910-2010 from various studies using *Porites* from Guam (*Shinjo et al.*, 2013), Hainan Island (*Wei et al.*, 2015), Flinders Reef (*Pelejero et al.*, 2005), and two reef zones in the Great Barrier Reef (inner-shelf and outer-shelf; *D'Olivo et al.*, 2015). Both the forereef and backreef reconstructions using *Siderastrea siderea* in this study fit within the range demonstrated by previous studies.

$\delta^{13}C$ in coral skeletons is used as a proxy for inorganic carbon utilisation (*Swart*, 1983) and therefore a potential tracer of NPP in the reef. As mentioned previously, its interpretation is complicated by vital effects such as growth rate (e.g. *Rodrigues and Grottoli*, 2006), photosynthesis and respiration rate (e.g. *Swart*, 1983; *McConnaughy*, 1989; *Muscatine et al.*, 1989) and the Suess Effect (*Swart et al.*, 2010), which is related to the uptake of isotopically light carbon from fossil fuel use. The observed decrease in mean $\delta^{13}C$ in the ~100 year record for the forereef (-0.010‰ y^{-1}) is only half of that observed in tropical atmospheric $\delta^{13}C$ (-0.02‰ y^{-1}; *Keeling et al.*, 2005), while the -0.014‰ y^{-1} decrease observed in the backreef

is closer to the atmospheric decrease and nearby *Montastraea faveolata* coral records from Puerto Rico (-0.018‰ y^{-1}; *Moyer and Grottoli*, 2011). The significant positive relationship between detrended $\delta^{13}C$ and reconstructed pH in the forereef (Figure 3-16) is expected, given the same observation in other coral species (*Martin et al.*, 2016), despite an insignificant variation in $\delta^{13}C$ at seawater pH (<0.2‰ between 7.5 and 9 pH units; *Zeebe*, 1999).

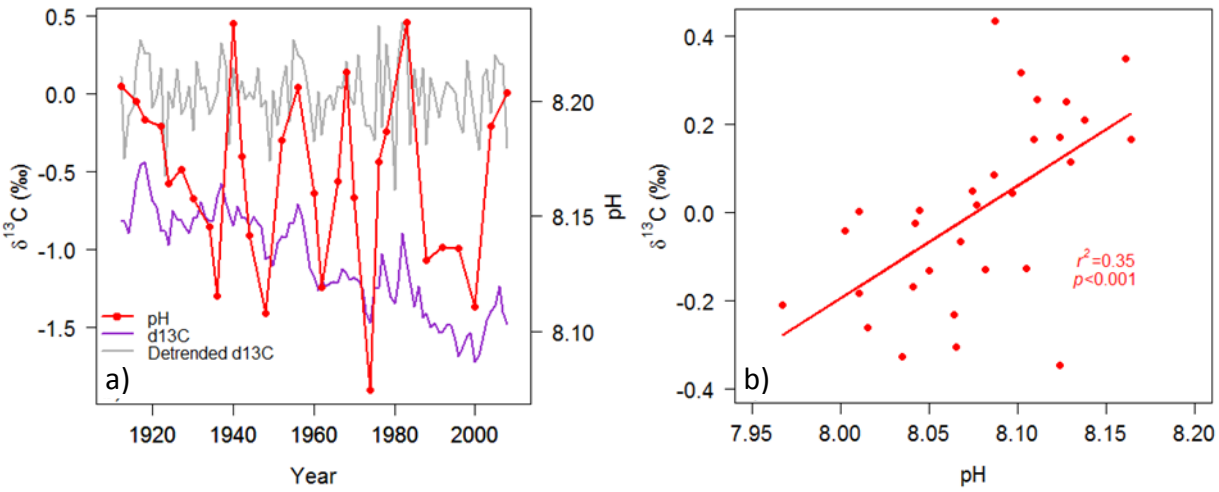

Figure 3-16. a) Comparing the forereef pH time-series (red) with the $\delta^{13}C$ time-series (purple) highlights the positive relationship between pH and $\delta^{13}C$ through the matching high peaks approximately every 20 years. b) Significant anti-correlation between detrended $\delta^{13}C$ and forereef pH.

At the base of the coral cores the $\delta^{13}C$ values for the forereef and backreef are comparable but become increasingly divergent over time (Figure 3-8a), similar to the divergence we see between the pH of the reef zones (Figure 3-4b). Despite the difficulties associated with interpreting $\delta^{13}C_{coral}$, the higher $\delta^{13}C$ values in the forereef (in both the raw and detrended data; Figure 3-16a) are likely indicative of higher degrees of nutrient utilisation, with NPP having a preference for the light isotope of carbon.

Taking the difference between the $\delta^{13}C$ as a proxy for the difference in carbon utilisation in the two reef zones, we find a good correlation between differences in forereef and backreef pH differences and $\delta^{13}C$ differences (Figure 3-17). This correlation suggests that the lack of ocean acidification signal in the forereef may be a response to an increase in carbon utilisation by macroalgae ($\delta^{13}C_{organic}$ = -30 to -10‰) through the last 100 years as a result of increased nutrient supply (see section 3.4.2) which stimulates NPP causing both the $\delta^{13}C$ and pH to increase relative to the backreef. If the decline in forereef extension rate is representative of a decline in NCC in general, this reduction in calcification in the forereef will play a role in increasing the $[CO_3^{2-}]$ in the local reef water, further buffering the local pH

against open ocean acidification. We can simulate this effect by removing increasing amounts of dissolved inorganic carbon ($\delta^{13}C_{organic}$ = -22‰) from a parcel of water with a starting $\delta^{13}C$ of dissolved inorganic carbon (DIC) of 0‰. This produces an evolution of $\delta^{13}C$ and pH that matches the observed differences well, strongly suggesting that both the changes in pH and $\delta^{13}C$ are driven by increased NPP:NCC ratio in the forereef, relative to the backreef (Figure 3-17).

The positive relationship modelled between the difference in reef zone pH and $\delta^{13}C$ supports our findings in the field samples because when more nutrient-rich sediment is transported to the reef, more nutrients are available, stimulating NPP which removes the CO_2 and HCO_3^- components of DIC, making the $\delta^{13}C$ less negative which increases the difference between the two reef zones. Our findings are also supported by the results of other studies, for instance, the recent study by *Diaz-Pulido et al.*, (2016) demonstrated that reef zones with large terrestrial influences have a lower coral cover and higher macroalgae cover than areas further away from terrestrial inputs. Here, this would indicate that the forereef zone of the Sapodilla Cayes is indeed more populated by macroalgae than the backreef, which utilise both HCO_3^- and CO_2 during photosynthesis, and therefore increasing the pH of the seawater (e.g. *Anthony et al.*, 2013) and the $\delta^{13}C$ of the coral. This hypothesis will soon be tested by analysing video transects and reef survey data collected across the MBRS in 2010-2011 by Tobacco Caye Marine Station.

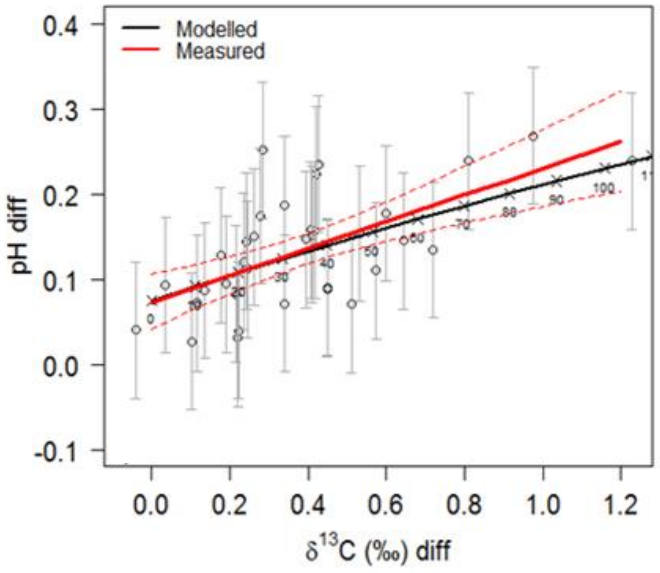

Figure 3-17. The difference in pH between the forereef and backreef shows a positive relationship with the difference in $\delta^{13}C$ between the two reef zones. The black line represents the modelled evolution curve of dissolved inorganic carbon (DIC) $\delta^{13}C$ and pH with increasing DIC removal and the numbered labels represent the total µM of DIC removed.

Despite the correlation between the modelled and observed data, the model is only a simplistic representation of the reef processes in this region. The limitations of this model include assuming the chemistry of the forereef and backreef water masses are the same at the beginning of the record and also it does not account for the fact that there will be seawater exchange, or reef-modified seawater exchange between the forereef and backreef through wave action and currents through breaks in the barrier reef. A final key point that has not been considered in the model is the potential difference in residence time between the two reef zones. There are no published estimates of reef water residence time in this area, but in order for coral reefs to be able to modify their surrounding seawater, the seawater cannot be completely flushed with each turn of the tide.

3.4.4 Impact of additional stressors on skeletal extension rate

It is evident that short-lived natural 'disasters' decrease extension rate, demonstrated by the lowest forereef extension (0.154 cm y^{-1}), corresponding to the time at which Belizean corals were impacted by a bleaching event (e.g. *Goreau et al.*, 2000; *Aronson et al.*, 2002) and Hurricane Mitch (*Aronson et al.*, 2000) in 1998. In the long term, despite a >1°C increase in SST in the forereef since 1922 (based on the HadISST record; *Rayner et al.*, 2003), ocean warming is not likely to be responsible for the decline in forereef linear extension because the average temperature of both reef zones is still only 28.3°C, which has been shown to be conducive to calcification in cultured *S. siderea* (*Castillo et al.*, 2014). However, if forereef corals have been subjected to more intense local chronic stressors, such as sedimentation (from riverine inputs or mangrove removal) and nutrient enrichment (from riverine input or excessive guano from local bird populations) as we have demonstrated in this study, they may have a reduced thermal tolerance (*Carilli et al.*, 2010), making them more susceptible to negative impacts from relatively minor temperature increases.

3.5 Conclusions

In the first long-term, continuous application of the δ^{11}B-pH proxy with the coral species *S. siderea*, we have demonstrated a spatial variability in a century-long time-series of reconstructed seawater pH in the Caribbean (Sapodilla Cayes, Belize). The backreef coral, which does not exhibit a decline in skeletal extension, recorded an ~0.15 pH unit decline in stark contrast to the forereef coral which indicated that the forereef environment has not

experienced ocean acidification, despite a significant reduction in skeletal extension rates. Combining these pH estimates with $\delta^{13}C$, we propose that the ocean acidification signal in the forereef has been masked by both an increase in Net Primary Productivity (NPP), which promotes DIC removal and drives pH up in the forereef, and the reduction in coral calcification (assuming that the decline in linear extension of forereef corals is indicative of the wider calcification response). Increasing NPP in the forereef has been enabled by increasing volumes of nutrient-rich sediment being transported to this region, mainly via Honduran rivers. This hypothesis is supported by a north-westerly circulation pattern, particularly highlighted following the passage of Hurricane Felix, whereby nutrient-rich riverine water reaches the forereef, before a dilute water mass circulates to the backreef. The Ba/Ca ratios demonstrate that the nutrient input to the forereef has significantly increased over the time-series ($p<<0.001$) as a result of a 10-fold increase in the population of Honduras increasing the demand for land clearance, agriculture and fertiliser application. We therefore conclude that not only do coral reefs not necessarily experience open ocean pH, but that pH is not the main influence of declining forereef extension rates in the Mesoamerican Barrier Reef System. Rather, our multi-proxy data suggests that this reduction is driven by increased nutrient availability, stimulating Net Primary Productivity at the expense of Net Community Calcification.

Chapter 4: Intra-reef variations in Li/Mg and Sr/Ca sea surface temperature proxies in the Caribbean reef-building coral *Siderastrea siderea*

This chapter is published in *Paleoceanography*, *31*(10), 1315-1329. The contributions of co-authors to this work are detailed below.

Sara Fowell: Concept, sample preparation, sample analysis, data analysis and interpretation, figure making, manuscript writing
Kate Sandford: Sample preparation, sample analysis
Joe Stewart: Clean laboratory and mass spectrometer training, sample analysis, manuscript editing
Karl Castillo: Sample collection and manuscript editing
Justin Ries: Concept, sample collection and manuscript editing
Gavin Foster: Concept, data interpretation, manuscript drafting

Abstract

Caribbean sea surface temperatures (SSTs) have increased at a rate of 0.2°C per decade since 1971; a rate double that of the mean global change. Recent investigations of the coral *Siderastrea siderea* on the Belize Mesoamerican Barrier Reef System (MBRS) have demonstrated that warming over the last 30 years has had a detrimental impact on calcification. Instrumental temperature records in this region are sparse, making it necessary to reconstruct longer SST records indirectly through geochemical temperature proxies. Here we investigate the skeletal Sr/Ca and Li/Mg ratios of *S. siderea* from two distinct reef zones (forereef and backreef) of the MBRS. Our field calibrations of *S. siderea* show that Li/Mg and Sr/Ca ratios are well-correlated with temperature, although both ratios are three times more sensitive to temperature change in the forereef than in the backreef. These differences suggest a secondary parameter also influences these SST proxies, highlighting the importance for site- and species-specific SST calibrations. Application of these paleothermometers to downcore samples reveals highly uncertain reconstructed temperatures in backreef coral, but well-matched reconstructed temperatures in forereef coral, both between Sr/Ca-SSTs and Li/Mg-SSTs, and in

comparison to the HadISST record. Reconstructions generated from a combined Sr/Ca and Li/Mg multi-proxy calibration improve the precision of these SST reconstructions. This result confirms that there are circumstances in which both Li/Mg and Sr/Ca are reliable as stand-alone and combined proxies of sea surface temperature. However, the results also highlight that high-precision, site-specific calibrations remain critical for reconstructing accurate SSTs from coral based elemental proxies.

4.1 Introduction

Global mean sea surface temperatures (SSTs) have been rising since the Industrial Revolution, primarily as a result of the change in the radiative forcing imposed by increasing anthropogenic greenhouse gas emissions (e.g., atmospheric pCO_2 change from 280 to 400 ppm; *Cubasch et al.*, 2013). The atmosphere carries only 2% of the heat content of the ocean-atmosphere system and in tandem with an increase in atmospheric temperature, the global average warming in the upper 75 m of the oceans has been 0.11°C per decade (between 1971 and 2010). This global SST increase is not geographically uniform and is amplified in areas such as the Caribbean Sea, where it has increased at a rate of more than 0.2°C per decade, resulting in a total change of ~0.8°C over the last 40 years (*Rhein et al.*, 2013; *Glenn et al.*, 2015).

Valuable insight into the impacts of future SST changes on areas of ecological importance, such as coral reefs, can be obtained from the response of ecosystems to past environmental change. Yet historical records of SST prior to the period of modern instrumentation (1970s), are based on relatively sporadic measurements acquired using a wide range of SST monitoring techniques including buckets, shipboard sensors, floating buoys and satellites. These techniques have differing accuracies, precisions, and sampling depths, leading to relatively large uncertainties and anomalies within the historical records (*Kennedy et al.*, 2011; *Smith et al.*, 2013). Geochemical proxy reconstructions of SSTs therefore provide an attractive alternative to the intermittent *in situ* monitoring data sets and a means to potentially extend SST records well beyond that of the instrumental monitoring period (*Tierney et al.*, 2015). To this end, a number of biogenic substrates have been utilized for geochemical proxy SST reconstruction including organic material such as alkenones (*Brassell et al.*, 1986) and membrane lipids of marine Crenarchaeota (*Schouten et al.*, 2002), as well as the calcium carbonate skeletons of marine organisms such as planktonic foraminifera (*Anand et al.*, 2003), sclerosponges (*Rosenheim et al.*,

2004), and tropical corals (*Beck et al.*, 1992; *de Villiers et al.*, 1994; *Alibert and McCulloch*, 1997; *Swart et al.*, 2002; *Reynaud et al.*, 2007; *Maupin et al.*, 2008; *Mitsuguchi et al.*, 2008; *DeLong et al.*, 2014). Of these possible archives for SST estimates, only the skeletons of tropical corals offer the fine-scale temporal resolution and long growth histories necessary to resolve SST changes over the last ~300 years at an inter-annual resolution (*Anderson et al.*, 2013).

Corals are used as paleothermometers because the partition coefficient between seawater and coral aragonite ($K_D = (X/Ca)_{coral}/(X/Ca)_{sw}$) of various auxiliary cations such as Li^+ (*Marriott et al.*, 2004a), Mg^{2+} (*Mitsuguchi et al.*, 1996), and Sr^{2+} (*Beck et al.*, 1992) are understood to be temperature dependent. These ions are transported from seawater to the semi-isolated extracellular calcifying fluid (ECF) (*Sinclair and Risk*, 2006; *Gaetani et al.*, 2011; *Tambutté et al.*, 2011; *Gagnon et al.*, 2012) by direct diffusion (*Cohen et al.*, 2006; *Gaetani and Cohen*, 2006; *Gagnon et al.*, 2007; *Gagnon et al.*, 2012) or by active transport (*Ip and Lim*, 1991; *Ferrier-Pagès et al.*, 2002). Sr^{2+} ions are thought to replace Ca^{2+} ions in the aragonite lattice due to their similar ionic radii (1.31 Å and 1.18 Å respectively; *Shannon*, 1976) (*Watson*, 1996; *Allison et al.*, 2005). However it is argued that the ionic radii of Mg^{2+} and Li^+ (0.89 Å and 0.92 Å respectively; *Shannon*, 1976) are too small to directly substitute for Ca^{2+} (*Finch and Allison*, 2008; *Montagna et al.*, 2014). Nonetheless, while the incorporation pathways remain debated, the similar ionic sizes and partition coefficients (K_D <<1) for both Mg^{2+} and Li^+, and the positive correlation between Mg/Ca and Li/Ca ratios in coral (*Montagna et al.*, 2014), provide evidence that similar processes govern their incorporation into coral aragonite (*Case et al.*, 2010; *Hathorne et al.*, 2013b; *Raddatz et al.*, 2013; *Montagna et al.*, 2014).

The Sr/Ca ratio is the most commonly used geochemical temperature proxy in coral archives (*Weber*, 1973; *Beck et al.*, 1992; *de Villiers et al.*, 1994; *McCulloch et al.*, 1994; *Alibert and McCulloch*, 1997; *Cohen et al.*, 2001; *Cohen et al.*, 2002; *Ferrier-Pages et al.*, 2002; *Swart et al.*, 2002; *Fallon et al.*, 2003; *Gagnon et al.*, 2007; *Reynaud et al.*, 2007; *Maupin et al.*, 2008; *Mitsuguchi et al.*, 2008; *Caroselli et al.*, 2012; *Gagan et al.*, 2012; *Gagnon et al.*, 2013; *Raddatz et al.*, 2013; *DeLong et al.*, 2014). However, the reliability of this proxy has been recently called into question. For instance, the sensitivity of Sr/Ca to temperature change differs amongst and between coral species, and relative to inorganically precipitated aragonite (e.g. *Cohen et al.*, 2006 and *Corrège*, 2006), suggesting that species- and even colony-specific calibrations are needed (e.g. *Alpert et al.*, 2016).

The lack of a robust universal Sr/Ca-SST calibration for a single species of coral, or even different individuals within the same colony, is well demonstrated (*Corrège*, 2006; *Saenger et al.*, 2008; *Gaetani et al.*, 2011). Such inter- and intra-colonial variations may arise from factors other than the temperature influence on the Sr/Ca ratio of coral skeletons. For example, some studies identify a mineralogical/microstructural control such as crystal shape and location within the skeletal microstructure (*Cohen et al.*, 2001; *Meibom et al.*, 2006; *Raddatz et al.*, 2013), and the influence of kinetic processes such as calcification rate (*Cohen et al.*, 2001; *Gaetani and Cohen*, 2006). An additional complicating factor for Sr/Ca and all element to calcium ratios in biogenic carbonates is Rayleigh fractionation that occurs during the precipitation of ions from a semi-isolated batch of calcifying fluid, which is only periodically replenished by the diffusion of ions from seawater (*Gaetani and Cohen*, 2006). The extent to which Rayleigh fractionation affects a particular elemental ratio depends on the partition coefficient (K_D) that is itself temperature dependent (*Gaetani and Cohen*, 2006). For example, as temperature increases from 5°C to 30°C, the $K_D^{Sr/Ca}$ for inorganic aragonite decreases by 14% (*Gaetani et al.*, 2011), resulting in fewer Sr ions becoming incorporated into the carbonate matrix. In aragonite, the K_D of Li/Ca and Mg/Ca also exhibits an inverse relationship with temperature (*Marriott et al.*, 2004b; *Gaetani et al.*, 2011). Rayleigh fractionation influences the composition of an isolated fluid undergoing partial crystallization when the K_D of the participating elements is not equal to 1. As $CaCO_3$ is precipitated, the concentration of Ca in the calcifying fluid decreases, causing the concentration of other elements with a K_D <1 to increase relative to Ca (and *vice versa*). The elemental composition of coral aragonite in terms of element-to-calcium ratio is therefore determined by the K_D of each element, its relationship with temperature, and the amount of Ca precipitated from each batch of calcifying fluid (*Cohen et al.*, 2006; *Gaetani and Cohen*, 2006; *Gagnon et al.*, 2007; *Montagna et al.*, 2014).

These complicating factors associated with coral Sr/Ca have prompted a search for alternative SST proxies, such as Li/Mg ratios (*Case et al.*, 2010; *Hathorne et al.*, 2013b; *Raddatz et al.*, 2013; *Montagna et al.*, 2014). The potential of the Li/Mg-SST proxy lies in the opposing temperature controls on Li/Ca and Mg/Ca in the coral skeleton, thereby amplifying the effect of temperature on Li/Mg, and the similar responses of these ratios to Rayleigh fractionation, meaning precipitation progress does not have a significant influence on the Li/Mg ratio of the calcifying fluid (*Montagna et al.*, 2014). Li and Mg incorporation into aragonite is therefore, in theory at least, simply reliant on the temperature dependent partition coefficients of Li and Mg, rather than on the extent

of Rayleigh fractionation. Several recent studies have confirmed a strong temperature dependence for Li/Mg ratios in corals, which appears to be relatively insensitive to the species used (*Montagna et al.*, 2014, and references therein). Use of the first multi-species Li/Mg-SST calibration permits reconstruction of SSTs with an uncertainty of ±1.8°C (at 95% confidence; *Montagna et al.*, 2014); an improvement on the uncertainties associated with the *Porites*-only Li/Mg-SST calibrations (*Hathorne et al.*, 2013b).

Here, we present new Li/Mg and Sr/Ca data from the previously unexamined coral species *Siderastrea siderea* sampled from the Caribbean Sea (Belize), which allow us to place this taxa in the broader context of other, tropical coral species utilized for SST-reconstruction, such as *Porites* (*Hathorne et al.*, 2013b). Additionally, we examine the use of multi-proxy calibrations to test whether combining elemental ratios with strong temperature dependencies improves the reliability of SST reconstructions. These detailed calibrations of SST proxies in the coral *S. siderea* allow us to assess the robustness of these proxies in characterizing the extent of ocean warming in the ecologically vulnerable region of the southern Mesoamerican Barrier Reef System.

4.2 Methodology

4.2.1 Sample collection

In February 2009, coral cores were collected from the forereef and backreef in the Sapodilla Cayes Marine Reserve (southern Belize; western Caribbean Sea). A full description of the core extraction and sectioning methods are available in *Castillo et al.* (2011). The cores analysed in this study were FR-12 (16.10004^{o}N, 88.26669^{o}W) and BR-06 (16.14045^{o}N, 88.26015^{o}W, Figure 4-1a).

4.2.2 Temperature data

High temporal resolution *in situ* temperature measurements from the study site were acquired from 2002 to 2008 using *Hobo* (Onset, Massachusetts) temperature loggers (Figure 4-1, Table B1; *Castillo and Lima,* 2010). These data were augmented by Reynolds SST data from paired 0.25° latitude/longitude sized grids (Figure 4-1, Table B1; http://www.nhc.noaa.gov/sst/) to account for incompleteness in the *in situ* logger records. Reynolds SSTs were found to be strongly correlated with the *in situ* SST measurements

and are therefore representative of the temperature regimes experienced by the investigated corals (*Reynolds et al.*, 2007; *Castillo and Lima*, 2010; *Castillo et al.*, 2012). No significant difference was found between the temperatures experienced in the two coral reef zones, either in the Reynolds dataset (p=0.86) or the temperature loggers (p=0.89) of *Castillo and Lima*, (2010).

The *in situ* temperature reconstructions were compared to the Hadley Centre's HadISST1 (*Rayner et al.*, 2003) historic temperature record for this location (16-17°N; 88-87°W). HadISST is a global SST product with 1° × 1° resolution grids and monthly temperature records from January 1870 to present (http://climexp.knmi.nl; Table B1). Grid points that are missing satellite data within the HadISST dataset were statistically interpolated from adjacent grids (*Rayner et al.*, 2006). Although the overall forereef and backreef Reynolds composites do not differ significantly from HadISST (p=0.26 and p=0.20 respectively), the summer temperatures are frequently lower in the HadISST record, with the Reynolds derived summer temperatures being on average 0.41°C higher for the forereef, and 0.44°C higher for the backreef (both with p<<0.01).

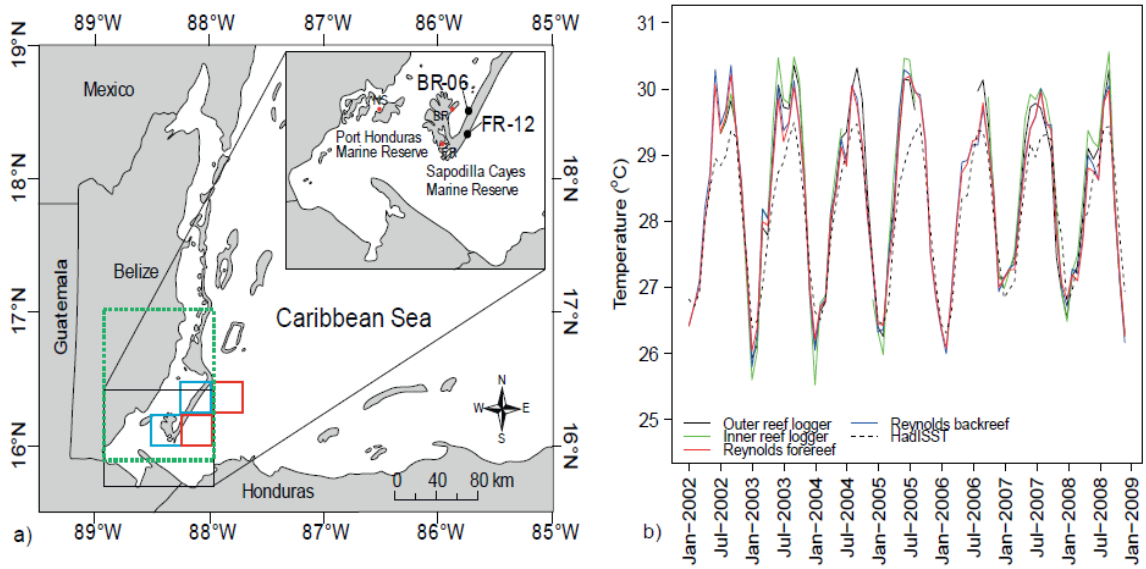

Figure 4-1. Coral core and temperature data locations in southern Belize. (a) The 0.25° × 0.25° grids represent the areas covered by the Reynolds forereef (red) and backreef (blue) temperature data. The red circles show the location of the temperature loggers, with the nearshore logger representing the inner reef, and the forereef and backreef representing the outer reef. The 1°×1° green dashed box represents the area covered by the HadISST satellite temperature data. BR-06 and FR-12 are the sampling locations of the forereef FR-12 and backreef BR-06 cores respectively, which were analysed in the present study. (b) Monthly resolved temperature data from the outer reef *in situ* logger (black), inner reef *in situ* logger (green), Reynolds forereef composite (red), Reynolds backreef composite (blue) and HadISST data (dashed).

4.2.3 Sample preparation and analysis

4.2.3.1 Monthly resolution sub-sampling

Coral slabs (70 × 45 × 5 mm) were X-rayed using a *Fuji FCR* radiography system at the UNC-Chapel Hill Campus Health Services Radiology Department, at 6 mA s^{-1} and 40 kV. These images were used to calculate an annual chronology by labelling the first high-density band (deposited the same winter as the collection), and counting each subsequent high-density band backwards in time.

Slabs from FR-12 and BR-06 were sampled at monthly to bimonthly resolution from the top (September 2008 to January 2006 and September 2008 to February 2006 respectively) and bottom (November 1921 to December 1925 and November 1922 to January 1926 respectively) of each coral slab (Figure 4-2). A New Wave Research micromill with a 500 µm diameter diamond drill bit was used to drill ~1 mm wide trenches to a depth of 1 mm in the thecal wall (Figure 4-2), using a protocol similar to that of *DeLong et al.* (2011). The widths of the thecal walls were identified under the microscope to minimize the chance of sampling the columella. Sample sizes ranged from 0.3 to 1.4 mg.

Final age models were built for the field calibrations following a standard approach (*Felis et al.*, 2004; *Maupin et al.*, 2008; *Felis et al.*, 2009). A preliminary age range was estimated by counting annual high-density bands (Figure 4-2a,c). Then, this annually-resolved age model, the coral age at collection, the skeletal location of the first monthly sample, and subsequent peaks and troughs in the Sr/Ca ratio were used to identify warm and cold intervals in the SST time-series, assuming the inverse relationship between Sr/Ca and SST seen in other studies (*Maupin et al.*, 2008; *DeLong et al.*, 2011; *DeLong et al.*, 2014). A polynomial curve was fit through 6 depth-age points allowing the age at each sample depth to be predicted. Instrumental SST was then interpolated on to this coral age-scale to permit direct comparison of temperature records.

Downcore samples from FR-12 (1921-1925) and BR-06 (1922-1926) were dated by counting the annual density bands on the X-ray images (Figure 4-2b,d). To determine exact months, a method similar to that of *Maupin et al.* (2008) was used whereby the summer and winter peaks from the reconstructed SSTs were tied to the monthly resolved Hadley Centre HadISST gridded temperature dataset for the corresponding year.

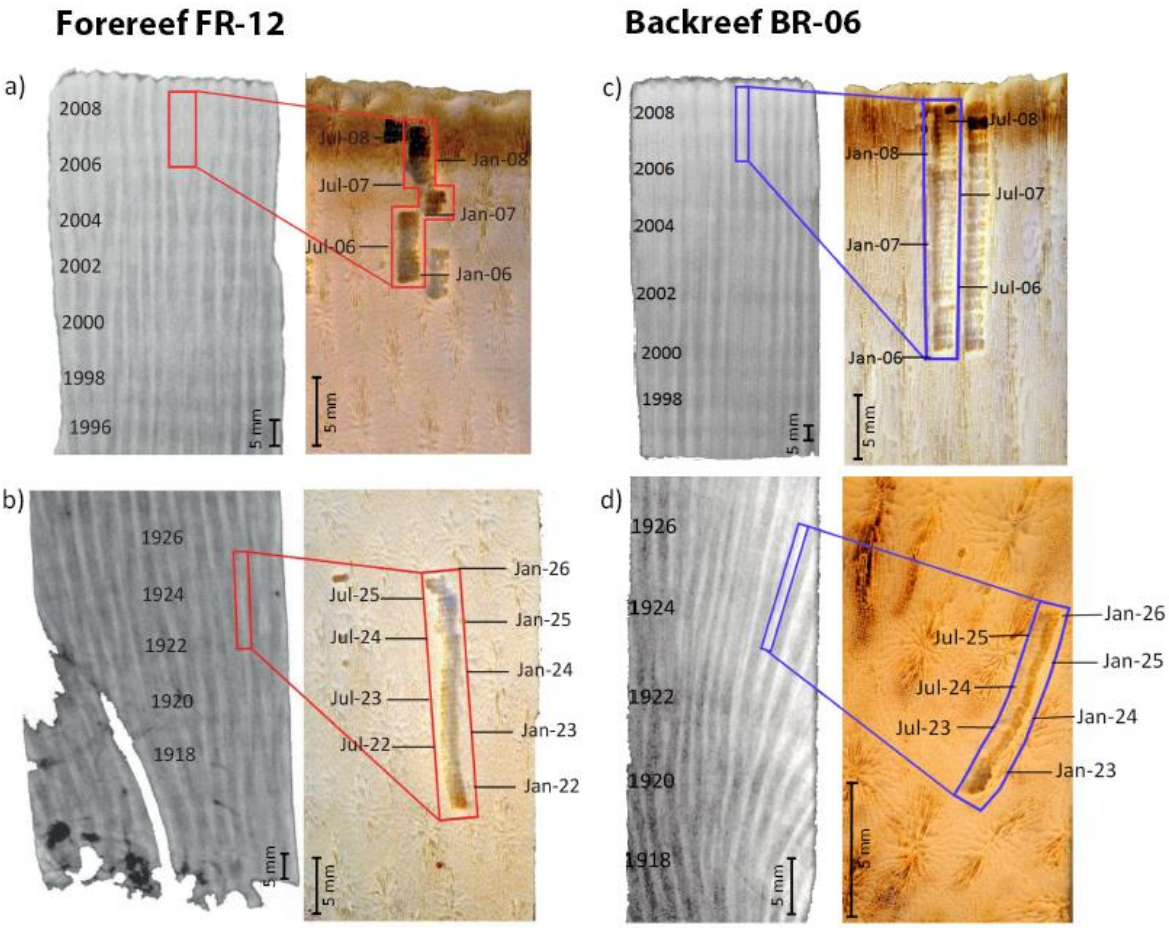

Figure 4-2. Coral slab X-rays with annual bands labelled. Rectangles indicate where the coral was subsampled along the high density theca wall (bright vertical bands). Optical images after subsampling are labelled with the position of the January and July samples. Theca walls are identified by a smoother, less porous appearance. a) Top of the forereef FR-12 coral. b) Downcore FR-12. c) Top of the backreef BR-06 coral. d) Downcore BR-06.

4.2.4 Cleaning procedure

Residual organic matter removal protocols are derived from foraminiferal calcite oxidative cleaning techniques and following the standard protocol of *Henehan et al.*, (2013), originally described by *Barker et al.*, (2003). Micromill extracted $CaCO_3$ powders were oxidatively cleaned in 250-500 µl of 1% H_2O_2 (buffered in 0.1 M NH_4OH_4) at 80°C for a total of 15 minutes with intermittent ultrasonication. The spent oxidative mixture was removed and samples were thoroughly rinsed using 18.2 MΩ Milli-Q water. Between each subsequent rinse step, the powdered samples were centrifuged for 2 minutes (13,000 rpm) to minimize sample loss. Samples were then transferred into acid-cleaned micro-centrifuge tubes before a weak acid (0.0005 M HNO_3) leach was performed to remove any ions readsorbed onto the sample surface. Samples were then dissolved in the

minimum volume of 0.5 M HNO_3. Dissolved sample solutions were finally centrifuged for 3 to 5 minutes (13,000 rpm) and transferred into clean vials to separate the supernatant from any remaining non-carbonate solids.

4.2.5 ICP-MS analysis

All analyses were carried out at the University of Southampton (UK). Calcium concentrations of the dissolved samples were first determined using quadrupole ICP-MS (Thermo Scientific X-Series) giving an estimate of the major elemental composition of the dissolved samples in order to accurately matrix match for subsequent quantitative multi-elemental analysis. X-Series standards and samples were made using 3% HNO_3 spiked with 5 ppb In, 5 ppb Re and 20 ppb Be which act as internal standards to monitor drift and correct for mass bias in the absence of bracketing standards. A multielement standard stock solution made using high concentration (10,000 ppm) single element (B, Mg, Al, Sr, Ca) solutions was diluted to make four gravimetric standards with differing Ca concentrations (0.2 to 3 ppm Ca). To monitor the accuracy and precision of the measurements, consistency standards of 1 ppm, 3 ppm and 7 ppm Ca CS2 and CS3 [*Ni*, 2006; *Ni et al.*, 2007] were analysed at the beginning and end of each analytical session. Based on these analyses the external precision at 1σ was estimated to be ±1.01% for 1 ppm Ca, ±4.91% for 3 ppm Ca and ±4.94% for 7 ppm Ca.

An Element XR (Thermo Scientific) sector field ICP-MS was used to determine the element to Ca ratios of the coral dissolutions. A suite of element intensity ratios (including Li/Ca, B/Ca, Mg/Ca and Sr/Ca) were measured to determine the skeletal elemental composition of the samples and also the efficacy of sample cleaning (e.g., Al/Ca <100 μmol/mol indicative of minimal clay mineral contamination). Further information regarding the measurement of Li can be found in the supporting information (Text A1 and Figure A1; *Al-Ammar et al.*, 2000; *Ni*, 2006). Samples were analysed in batches of equal Ca concentrations between 1 mM and 3 mM, and blank corrected with a 0.5 M HNO_3 "blank" measured between every sample/standard (*Rosenthal et al.*, 1999). Each block of three samples was bracketed against a matrix-matched (i.e., of equal Ca concentration to the samples; *Rosenthal et al.*, 1999), well characterized, gravimetric standard solution (prepared by Cardiff University). Sample ratios were calculated by calibrating to the standard solution, which had values of 11.38 μmol/mol, 2.44 mmol/mol and 1.43 mmol/mol for Li/Ca, Mg/Ca and Sr/Ca respectively, allowing samples to be corrected for instrumental and matrix induced mass bias.

Additionally, three consistency standards (SECS1, SECS2, SECS3, University of Southampton) of matching [Ca] but different gravimetrically prepared and cross-calibrated elemental ratios (Table B2) were used as internal standards to monitor accuracy and thus efficiency of correcting for mass bias effects and instrumental drift. Using the bracketing standards method, precise values of repeat measurements were obtained for these standards. SECS3 is the most similar in composition to the coral samples, and yielded average measured values (2σ) for Sr/Ca of 1.97 ± 0.04 mmol/mol, and Li/Mg of 5.51 ± 0.09 mmol/mol compared to 2 mmol/mol and 5.73 mmol/mol respectively determined gravimetrically (Table B2).

Alongside each batch of ~15 coral samples, a JCp-1 standard (international coral reference material made from homogenized *Porites; Okai et al.*, 2002) was analysed in the same manner as the coral samples in this study (1 to 2 mg JCp-1). Replicates of JCp-1 passed through the entire sample cleaning and analytical protocol provide a rigorous assessment of true external precision. The average JCp-1 values and standard deviation during the course of this study are shown in Table 4-1. While Li/Mg measurements of JCp-1 for this study are comparable to those of other laboratories, our mean Sr/Ca value is at the low end of the range of values in the *Hathorne et al.* (2013a) interlaboratory study (Table 4-1). By comparing analyses of cleaned and uncleaned samples of JCp-1, we found that both Li/Ca and Mg/Ca ratios decreased by 25% as a result of the removal of organic matter (Figure A2), a similar result to that observed in foraminferal calcite Mg/Ca following oxidative cleaning (*Barker et al.*, 2003). In contrast, both Sr/Ca and Li/Mg ratios are shown to be relatively unaffected by this sample cleaning procedure (Text A2 and Figure A2), the latter due to a precisely equal reduction in [Mg] and [Li]. Further details about the cleaning test can be found in the supporting information (*Ni*, 2006; *Ni et al.*, 2007).

Table 4-1. Comparison of JCp-1 elemental ratios measurements. Long term precision is determined by repeat JCp-1 measurements which are compared with the recent Li/Mg studies of *Hathorne et al.* (2013b) and *Montagna et al.* (2014) in addition to the international laboratory comparison (*Hathorne et al.*, 2013a).

	This study	**Interlab comparison**	**Hathorne et al., (2013b)**	**Montagna et al., (2014)**
Sr/Ca mmol/mol average	8.66	8.84		
	(*n* =20)	(*n* =179)		
Standard deviation	0.10	0.04		
External precision (%)[a]	2.21	0.95[b]		
Li/Mg mmol/mol average	1.51	1.48	1.51	1.43
	(*n* =16)	(*n* =5)	(*n* =25)	
Standard deviation	0.03	0.06	0.04	
External precision (%)[a]	4.45	7.43	5.30	3.20

[a] External precision reported as 2 relative standard deviations

[b] Median interlab external precision is 0.28%

4.2.6 Data handling

4.2.6.1 Statistical analysis

The statistical software package R Studio (*R Development Core Team*, 2013) was used for all data analysis and for constructing linear regression models on measured Li/Mg and Sr/Ca data. The uncertainty of the temperature estimates using the linear regression models was assessed using 95% prediction intervals. Welch unequal variance two sample t-tests (2-tailed) were also used to determine whether there were significant differences between mean summer or winter temperatures between reconstructed temperatures and the historic HadISST record.

4.2.6.2 Data compilations

A "multi-species" Li/Mg-T calibration of cold-water, temperate, and tropical coral species was developed using the data from this study and solution ICP-MS data from previous studies (*Case et al.*, 2010; *Hathorne et al.*, 2013b; *Raddatz et al.*, 2013; *Montagna et al.*, 2014). Based on a consideration of the long term average of JCp-1 at the

University of Southampton, Li/Mg results from *Montagna et al.* (2014) were increased by 5% to make them comparable with the results of the present study (Table 4-1).

4.3 Results

4.3.1 Monthly resolved Sr/Ca and Li/Mg ratios

Geochemical coral data (Table S3) are compared to composite observational temperature data (Table B1) in Figure 3. Both the Li/Mg and Sr/Ca ratios in the forereef coral FR-12 (Figure 4-3a, b) demonstrate a strong seasonal cycle in step with observed intra-annual temperature fluctuations. Similar, but smaller amplitude cycles, are also present in the backreef coral BR-06 (Figure 4-3c,d). In both corals, these elemental ratios are higher during colder months, demonstrating both Li/Mg and Sr/Ca ratios exhibit typical inverse relationships with temperature.

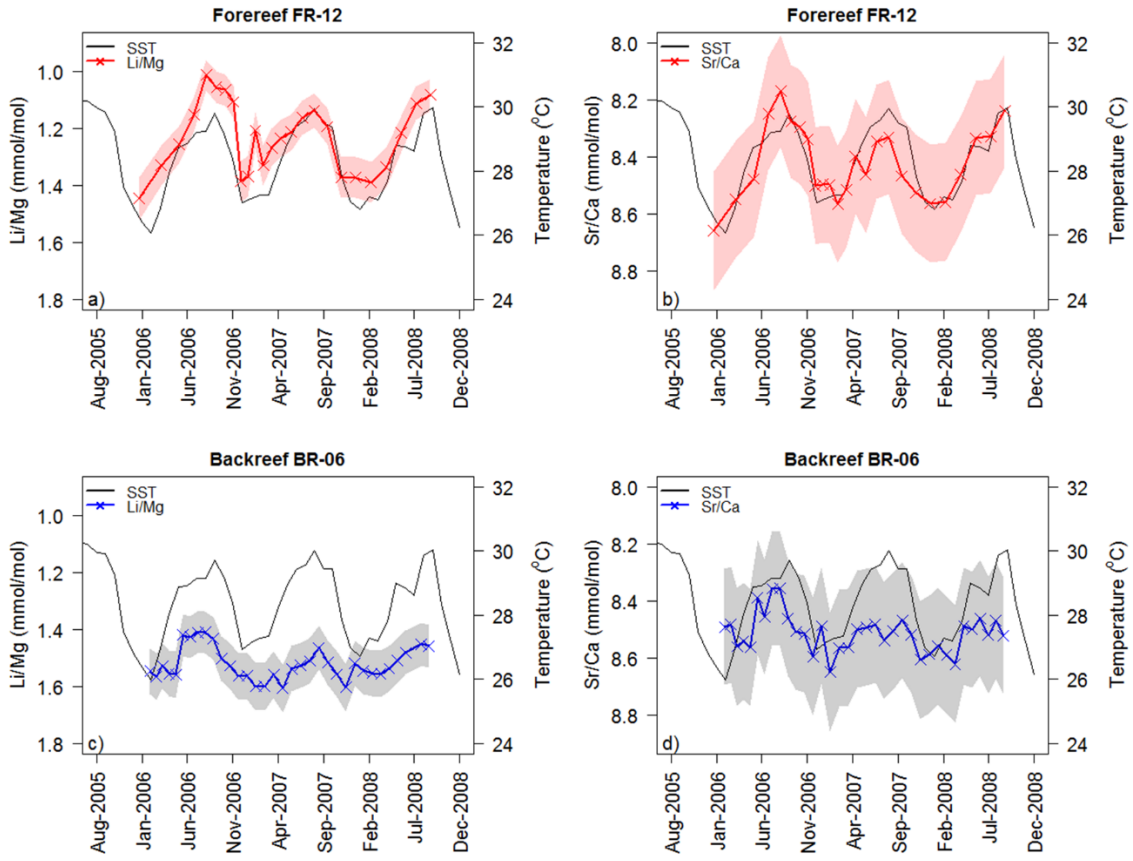

Figure 4-3. Monthly resolved Li/Mg and Sr/Ca ratios in forereef FR-12 (red) and backreef BR-06 (blue) samples. Crosses represent ICP-MS measured data with 2σ external reproducibility shown as a shaded band. Reynolds composite temperature records are shown in black for comparison.

4.3.2 Calibrations

Simple linear regressions reveal that the Li/Mg ratio of the forereef coral FR-12 has the best defined correlation with more than 70% of variation explained by temperature (r^2=0.71, p<<0.01, Figure 4-4a), as opposed to only 40% explained by temperature in the backreef coral BR-06 (r^2=0.40, p<<0.01, Figure 4-4c). The Sr/Ca ratio is also better correlated with temperature in the forereef coral FR-12 (r^2=0.69, p<<0.01, Figure 4-4b) than in the backreef BR-06 coral (r^2=0.26, p<<0.01, Figure 4-4d). These relationships between elemental ratios and temperature are also summarized in Table 4-2.

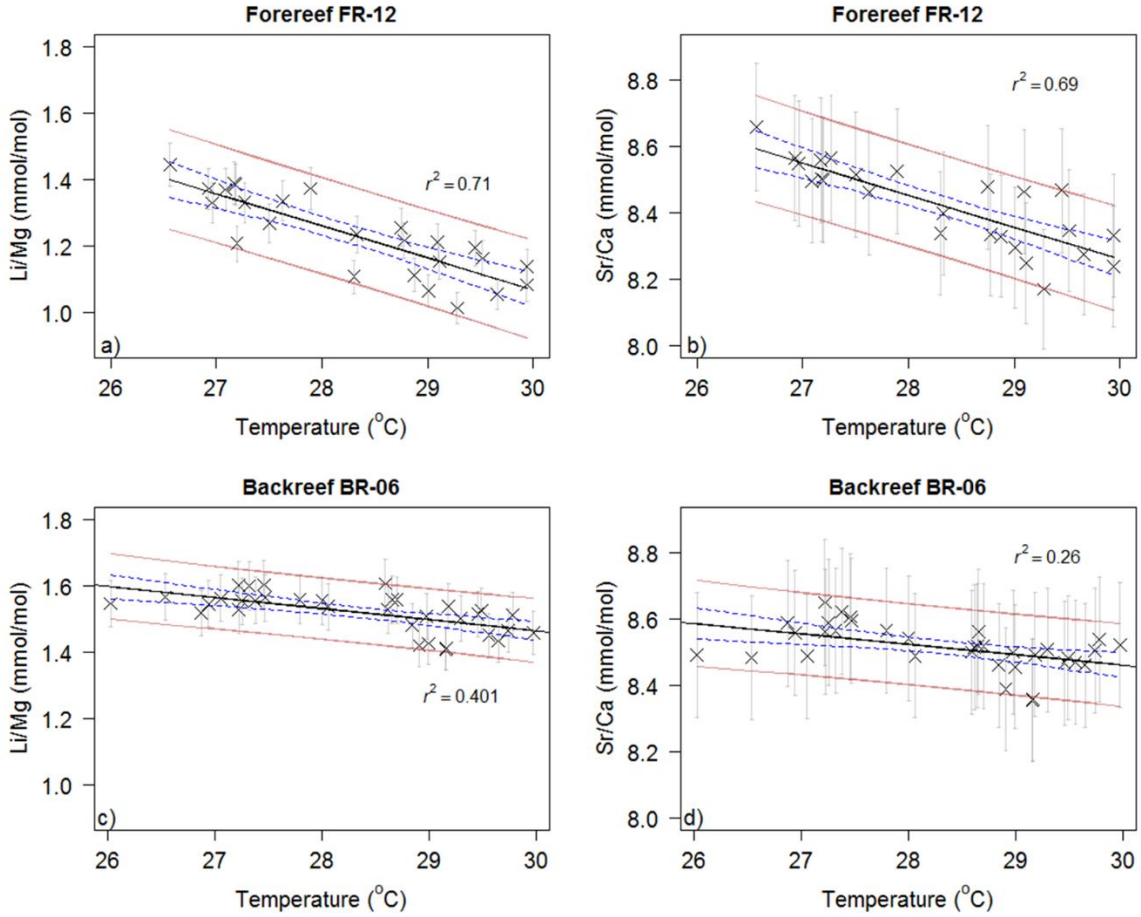

Figure 4-4. Forereef and backreef field-based calibrations of Sr/Ca and Li/Mg temperature proxies in *Siderastrea siderea*. Crosses indicate individual samples with 2σ external reproducibility errors. Blue and red dashed lines show the 95% confidence and prediction intervals respectively.

Stronger correlations the forereef calibrations result in more precise SST reconstructions than for the backreef calibrations and, independent of elemental ratios, lower reconstruction uncertainties are associated with the forereef samples (Table 4-2).

Two multiple linear regressions were also performed on the corals to generate multi-proxy-SST calibrations. The first multiple linear regression combined the Li/Mg and Sr/Ca ratios (hereafter referred to as "MLR1"). The second multiple linear regression combined Li/Ca, Sr/Ca and Mg/Ca ratios (hereafter referred to as "MLR2"). The regression coefficients for these multi-proxy calibrations are shown in Table 4-3.

Table 4-2. Regression statistics for the forereef and backreef calibrations. Calibrations in this study were fitted with a linear regression in the form Li/Mg = m × SST(°C) + c. Temperature precision estimates were derived from the prediction intervals.

Calibration	***c***	**± 2 se**	***m***	**± 2 se**	r^2	***p***	**95% precision at 28°C (°C)**
Forereef Li/Mg	3.962	± 0.730	-0.097	± 0.013	0.71	<<0.01	1.5
Backreef Li/Mg	2.458	± 0.406	-0.033	± 0.007	0.40	<<0.01	2.7
Forereef Sr/Ca	11.158	± 0.772	-0.097	± 0.014	0.69	<<0.01	1.6
Backreef Sr/Ca	9.406	± 0.536	-0.031	± 0.009	0.26	<0.01	4.0

Table 4-3. Multiple linear regression statistics for the multi-elemental forereef and backreef calibrations. MLR1 calibrations are in the form SST(°C) = c – (x_1 × Li/Mg) – (x_2 × Sr/Ca). MLR2 calibrations are in the form SST(°C) = c – (x_3 × Li/Ca) – (x_2 × Sr/Ca) + (x_4 × Mg/Ca). Temperature precision estimates were derived from the prediction intervals.

Calibration	***c***	x_1	x_2	x_3	x_4	r^2	**95% precision at 28°C (°C)**
Forereef MLR1	59.854	4.484	3.090	–	–	0.70	1.3
Forereef MLR2	33.177	–	1.205	0.657	2.066	0.75	1.2
Backreef MLR1	54.624	11.115	1.104	–	–	0.36	1.8
Backreef MLR2	38.153	–	0.490	3.466	3.722	0.38	1.8

The Li/Mg-SST calibrations were added to the existing combined-species calibration described in section 4.2.6.2 (Figure 4-5) to generate what will be referred to henceforth as the "multi-species calibration". The *S. siderea* samples broadly fit the trend of the multi-species calibration of *Montagna et al.* (2014) and extend the upper end of the temperature range by ~2°C. The backreef data are slightly offset from the curve fitted through the combined data (Figure 4-5). The resulting exponential equation of the multi-species calibration (r^2=0.95, p<<0.001) is:

$$Li/Mg = 5.405exp^{(-0.05(\pm0.001)\times T)} \quad \text{Equation 4-1}$$

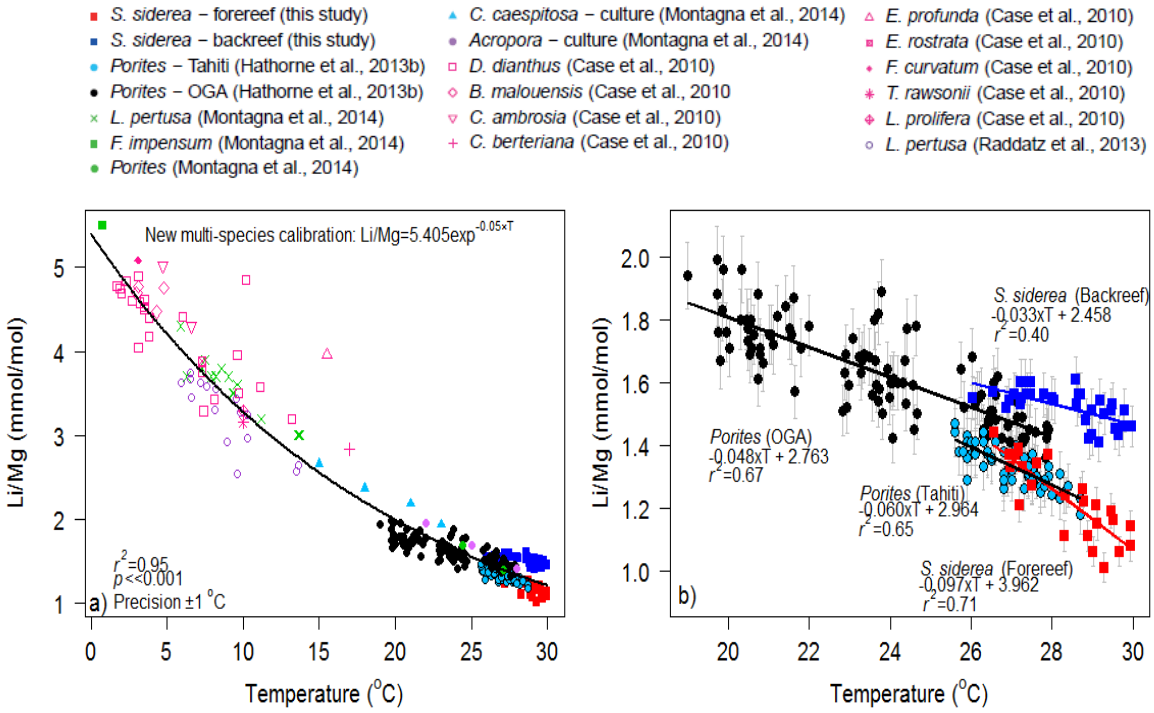

Figure 4-5. a) Combined Li/Mg-T calibration for a range of coral species at seawater temperatures between 0°C and 30°C. An exponential regression is used to form the new multi-species calibration. The forereef and backreef calibrations of *S. siderea* from this study are shown by the solid red and blue squares respectively. b) Comparison of the linear relationships of the Li/Mg ratios of the tropical species *Porites* (closed circles) and forereef and backreef *S. siderea* (closed squares). 2σ external precision error bars are shown.

4.3.3 Downcore samples and temperature reconstructions

Strong seasonal cycles in Li/Mg and Sr/Ca are evident in the forereef and backreef downcore samples (Figure 4-6, Table B4). The mean Li/Mg of the forereef coral (1.33 mmol/mol) is significantly lower than that of the backreef coral (1.50 mmol/mol; $p<<0.01$). The mean Sr/Ca ratios however, are not significantly different between reef zones (8.50 mmol/mol and 8.53 mmol/mol in the forereef and backreef respectively; $p=0.27$).

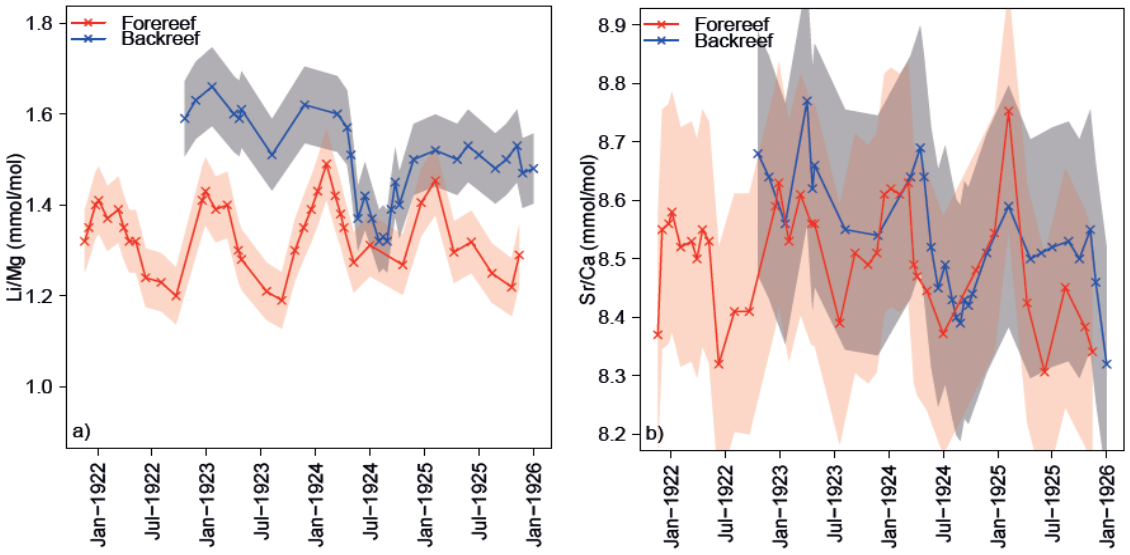

Figure 4-6. (a) Downcore Li/Mg ratios and (b) Sr/Ca ratios of FR-12 forereef (red) and BR-06 backreef (blue) *S. siderea* samples from years 1921 to 1926. Error envelopes (pink and grey) represent the 2σ external precision. HadISST data are shown in black for comparison (black line).

Forereef and backreef field-based *S. siderea* calibrations (Table 4-2) were applied to their respective downcore time-series to reconstruct monthly resolved SSTs between 1921 and 1926 (Table B4). In both reef zones the temperature reconstructions using single regressions of Li/Mg and Sr/Ca are within uncertainty (2σ) of each other, although this is largely a consequence of the propagation of the uncertainty in the backreef calibrations, which are up to ±12°C in some instances (Figure 4-7). Table 4-4 shows a comparison between the individual SST reconstructions and the HadISST dataset. In the forereef, the overall means of both the Li/Mg- and Sr/Ca-SSTs are within 0.3°C of HadISST, and within 0.7°C and 0.1°C in the summer and winter, respectively all within calibration

uncertainties (±1.5°C; Table 4-2). In the backreef, the overall means of the Li/Mg- and Sr/Ca-SSTs are both within 1.4°C of HadISST; however, summer Li/Mg-SSTs are 3.3°C greater than HadISST and winter Sr/Ca-SSTs are 1.9°C greater than HadISST (Table 4-2). In both of the reef zones, however, the root mean square error (RMSE) is within the uncertainties of the single proxy calibrations (Tables 4-2 and 4-4).

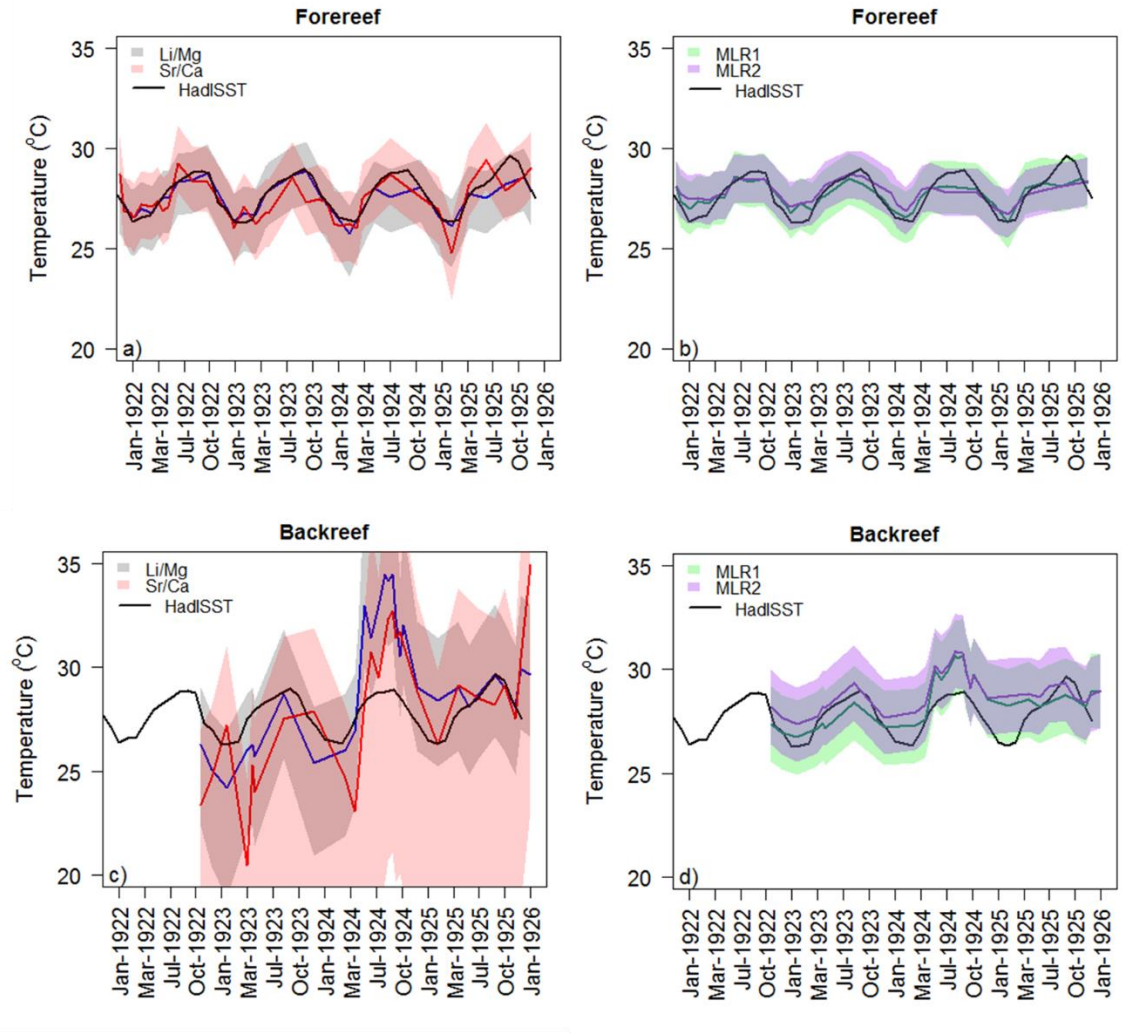

Figure 4-7. Sea surface temperature (SST) reconstructions from 1921-1926 using the site specific *S. siderea* Li/Mg and Sr/Ca-SST proxies and multi-proxy calibrations. The blue line shows the Li/Mg-SST; the red line shows the Sr/Ca-SST; the green line shows the combined Li/Mg-Sr/Ca-SST; and the purple line shows the combined Li/Ca-Sr/Ca-Mg/Ca-SST. Shaded regions show the precision estimates derived from the 95% prediction intervals of the linear regressions. HadISST data are also shown for comparison (black line).

Table 4-4. Mean summer, winter and overall sea surface temperatures based on the Li/Mg, Sr/Ca, and multi-proxy reconstructions for both the forereef and backreef. Errors are reported as 2 standard errors. The RMSE of the reconstructed mean against the mean HadISST is also shown.

Method	Mean SST (°C)	RMSE HadISST	Summer mean (°C)	RMSE HadISST	Winter mean (°C)	RMSE HadISST
HadISST	27.7 (±0.3)		28.9 (±0.2)		26.7 (±0.2)	
FR Li/Mg	27.4 (±0.3)	1.08	28.4 (±0.6)	0.76	26.8 (±0.3)	0.46
FR Sr/Ca	27.4 (±0.3)	1.27	28.2 (±0.6)	0.90	26.7 (±0.6)	0.96
FR MLR1	27.6 (±0.2)	0.97	28.3 (±0.2)	0.68	27.1 (±0.3)	0.68
FR MLR2	27.8 (±0.2)	0.96	28.4 (±0.4)	0.69	27.4 (±0.3)	0.86
BR Li/Mg	29.2 (±1.0)	3.03	32.2 (±2.3)	4.14	27.4 (±1.8)	2.40
BR Sr/Ca	28.1 (±1.2)	3.41	30.7 (±1.7)	2.76	28.6 (±2.5)	3.89
BR MLR1	28.6 (±0.4)	1.62	29.8 (±0.9)	1.44	27.9 (±0.7)	1.69
BR MLR2	29.0 (±0.4)	1.76	30.2 (±0.6)	1.52	28.2 (±0.5)	1.84

The multi-proxy calibrations yield temperature records similar to those predicted by the single proxy calibrations (Table 4-4). However, the multi-proxy calibrations have lower reconstruction uncertainties (Table 4-3), and therefore predict temperatures that match more closely between reef zones and between reconstructed SSTs and HadISST (Table 4-4), particularly with respect to the backreef reconstruction, albeit with a tendency to reconstruct lower amplitude seasonal variations (Figure 4-7b,d). The multi-proxy SSTs in the backreef reduce the differences from HadISST to ≤1.6°C (Table 4-4). As with the single proxy reconstructions, the RMSE of the multi-proxy based means are within the uncertainty of the calibration when comparing to the HadISST dataset.

4.4 Discussion

4.4.1 Li/Mg-, Sr/Ca- and multi-proxy-SST models in *S. siderea*

Both Sr/Ca and Li/Mg ratios exhibit a well correlated inverse relationship with temperature in both reef zones (Figures 4-3 and 4-4). Within the same reef zone, the slopes of both calibrations are within error of each other, suggesting that both proxies have similar temperature sensitivities. Both Li/Mg and Sr/Ca are also more strongly correlated with temperature in the forereef coral (Table 4-2). These differences arise even though both reef zones experienced similar temperature histories according to the

available observational data (Figure 4-1b), suggesting that at least one other factor must be influencing both SST-proxies.

Geographic differences in Sr/Ca-SST calibrations have been reported before. Several studies have ascribed such variability to the influence of other variables such as seawater pH (*Tanaka et al.*, 2015), seawater Sr/Ca composition (*de Villiers et al.*, 1994), extension rate (*de Villiers et al.*, 1994), and calcification rate (*Ferrier-Pagès et al.*, 2002; *Kuffner et al.*, 2012), which individually, or in combination, influence variation in the extent of Rayleigh fractionation and elemental incorporation in coral aragonite at a particular site. We confirm here that Li/Mg also exhibits a geographically dependent SST calibration and, because the K_D for Li/Mg is close to unity, we cannot ascribe this variation to Rayleigh fractionation. The influence of a non-SST driver on Li, Mg, and Sr uptake in the backreef coral may also be indicated by: (i) the generally poor agreement between Li/Mg-SST, Sr/Ca-SST and HadISST for the backreef in the years 1922-1926 (Figure 4-7c), which contrasts the good agreement found for the forereef reconstruction (Figure 4-7a); (ii) a lack of evidence for coral bleaching or mortality that would be expected to occur if SSTs were in excess of 32^{o}C as suggested by backreef SST reconstructions (Figure 4-7). Potential differences between seawater pH of the backreef and forereef may partly explain the spatial variability in SST-calibrations (*Tanaka et al.*, 2015). Furthermore, calibrating the SST proxies when extension rates of backreef corals were higher than forereef corals (since the 1990s; *Castillo et al.*, 2011) and applying them to samples from a time when the extension rates of forereef and backreef corals were more similar may also be at least partially responsible for the breakdown of the Li/Mg- and Sr/Ca-SST proxies. Our assessment of the importance of parameters such as these on Li/Mg and Sr/Ca ratios are the focus of a future study. Nonetheless, part of the degraded performance of both proxies in the backreef coral is also likely due to the size of the analytical uncertainty (Table 4-1) and the shallower relationship between the measured ratio and observed temperature (Table 4-2). Indeed, the RMSE between Li/Mg-SST and Sr/Ca-SST with HadISST in the backreef is similar to the calibration uncertainty suggesting that the predictive capabilities of these proxies would improve if the analytical uncertainties were reduced (Tables 4-2 and 4-4).

Applying the multi-proxy calibrations to the downcore data improved the precision of the reconstructions and reduced the extreme values recorded by the Li/Mg and Sr/Ca based SSTs in the backreef (Figure 4-7d). This improvement is likely, at least in part, a consequence of the increased precision resulting from using multiple variables (Table 4-3). Despite this advantage, the multi-proxy models still fail to predict the

expected wintertime temperatures in the backreef that are expected based upon the forereef reconstructions or the HadISST data (Table 4-4). This result suggests that although the multi-proxy calibrations offer some improvement over the single proxy models in the backreef (Table 4-4), combining the proxies does not completely eliminate the errors evident in the single proxy models (Figure 4-7d, section 4.3.2).

4.4.2 Assessment of tropical coral Li/Mg-SST calibrations

Previous studies have highlighted that Li/Mg ratios exhibit a similar inverse relationship with temperature across multiple coral species and over a temperature range of 0°C to 30°C (see references in Figure 4-5a). Although the forereef and backreef coral data generally agree with this overall trend (Figure 4-5a), detailed inspection reveals that both of the new Li/Mg-SST calibrations are slightly offset from the multi-species calibration, further highlighting the influence of a non-SST based parameter(s) in driving Li/Mg variability (Figure 4-5b). Similar, but more subtle variations are also evident in *Porites* (*Hathorne et al.*, 2013b). The slope of the backreef *S. siderea* (-0.033) is almost half that of both the Tahiti and OGA *Porites* data (-0.060 and -0.048 respectively; *Hathorne et al.*, 2013b), which are themselves almost half that of the forereef *S. siderea* (-0.097; Figure 4-5b). This suggests that although there is a clear overall relationship between temperature and coral Li/Mg, the divergence of tropical corals from a single calibration highlights that accurate reconstructions still require site- and species-specific calibrations.

To demonstrate the importance of these site and species-specific calibrations, the multi-species calibration (Figure 4-5a, Equation 4-1) was applied to the downcore Li/Mg ratios and reconstructed temperatures are compared to historic HadISST data (Figure 4-8). The forereef SSTs reconstructed using the multi-species calibration (Equation 4-1) are mostly within error of HadISST, with the exception of the 1922 and 1923 summertime SSTs, which are slightly overestimated. However, backreef SSTs reconstructed in the same manner are consistently lower than HadISST temperatures (Figure 4-8).

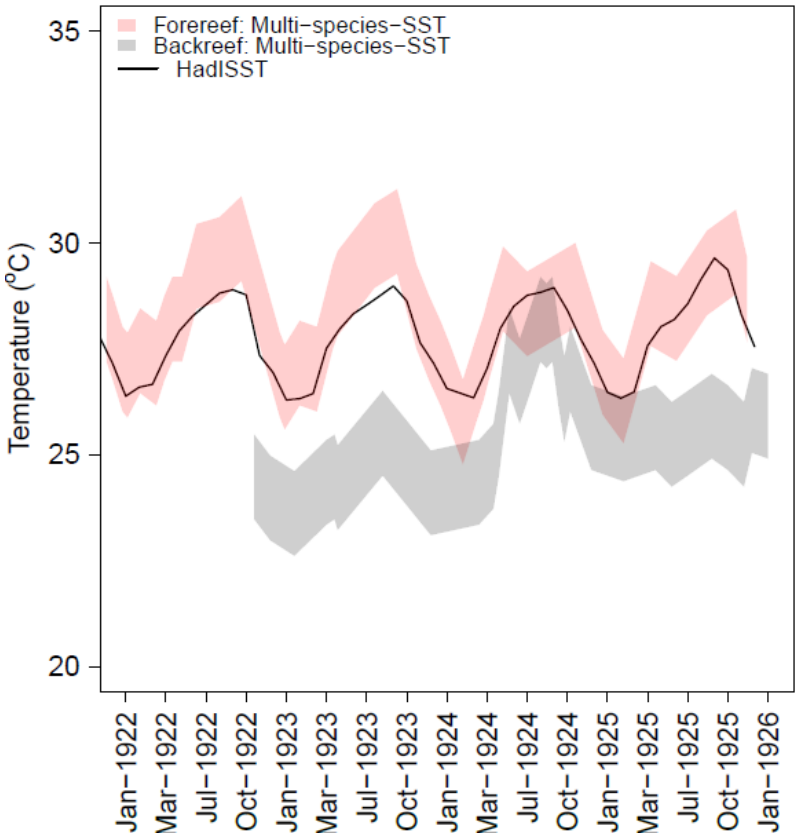

Figure 4-8. Sea surface temperature (SST) reconstructions from 1921 to 1926 using the updated multi-species Li/Mg-SST proxy. The error envelopes show the absolute SST precision estimates derived from the 2 standard error of the exponential calibration slope. Forereef SST reconstructions (red) and backreef SST reconstructions (grey) are compared against the HadISST data (solid black line).

4.5 Conclusions and recommendations

The sea surface temperature calibrations presented here demonstrate that the Li/Mg-SST proxy is equal to, and in some locations, more precise than the more commonly used Sr/Ca proxy for the species *S. siderea* (± 1.5°C vs. ± 1.6°C in forereef coral FR-12). By combining elemental ratios to form multi-proxy SST calibrations, the precision of the SST reconstructions are further improved. Both single elemental ratios (Sr/Ca, Li/Mg) in the backreef locality were found to be less sensitive to temperature, indicating that a secondary, non-SST variable impacts the uptake of these elements in the skeletal aragonite of *S. siderea* in these environments. As a test of reliability, reconstructed temperatures from 1921 to 1926 in both reef zones were compared to the HadISST record. Reconstructed forereef temperatures using the Li/Mg, Sr/Ca and the combined Li/Mg-

Sr/Ca and Li/Ca-Mg/Ca-Sr/Ca proxies were not significantly different from each other, and these SSTs were also found to be within error of the HadISST data. Reconstructed temperatures from the backreef were found to be substantially offset from forereef reconstructions and HadISST data, and recorded anomalously high temperatures approaching 35°C (presumably damaging or fatal to coral), confirming their inaccuracy.

These results demonstrate that in some regions, Li/Mg, when used in isolation or in combination with other elemental ratios as part of a multi-proxy approach, is a suitable addition to the temperature reconstruction tool-box of *Siderastrea siderea*. It remains unclear why our backreef reconstructions using Sr/Ca and/or Li/Mg are compromised, but this may be related to spatial variability in linear extension rates of *S. siderea* documented in this region, and for these samples in particular, by *Castillo et al.* (2011). Nonetheless, in light of the more precise SST reconstructions that result from the multi-proxy calibrations, we encourage their use over single elemental ratio proxies as a means of quantifying local surface ocean warming from elemental ratios within the coral *S. siderea*. While further investigation of the non-SST controls on SST-proxies, such as Li/Mg, is required, it is clear from our study that the most reliable coral-based reconstructions of sea surface temperatures are obtained through combining multi-proxy records that are calibrated in the same region to which they are applied.

Chapter 5: Examining the effect of pH on Li/Mg- and Sr/Ca-SST proxies: insights from culture and sub-annual boron isotope data

This chapter is written in the style of a research article with the intention of future submission for publication. The contributions of co-authors to this work are detailed below.

Sara Fowell: Concept, data analysis and interpretation, manuscript writing
Karl Castillo: Concept, sample collection, coral culturing
Justin Ries: Concept, sample collection, coral culturing
Gavin Foster: Concept, data interpretation and manuscript drafting

Abstract

It is widely recognised that the Sr/Ca composition of coral skeletons is not fully controlled by temperature, and recently, Li/Mg ratios have also been shown to be influenced by a secondary parameter. This study investigates the influence of pH using a combination of sub-annual boron isotopes ($\delta^{11}B$) from field samples of the coral *Siderastrea siderea* from the forereef and backreef of the Sapodilla Cayes Marine Reserve, Belize, and by analysing the elemental compositions of *S. siderea* samples cultured at a pH of 7.32, 7.82 or 8.07. The culture study showed both Sr/Ca, Li/Ca and Li/Mg ratios and partition coefficients (K_D) to be significantly inversely correlated with pH ($p<0.01$), while Mg/Ca ratios were significantly positively correlated ($p=0.05$). The backreef field samplesagree with the trends of the cultured samples, but the Li/Mg and Sr/Ca ratios of forereef coral exhibited a positive correlation with pH due to the different seasonal cycles in forereef and backreef pH. By removing the pH signal from the sea surface temperature (SST) calibrations using the $\delta^{11}B$-pH reconstructions, the slopes of the forereef, backreef and culture Li/Mg-SST calibrations fall within error of each other. A multivariable calibration combining the effects of SST and pH on elemental ratios explained as much as, or more, of the variation than the single variable regressions in both reef zones. However, the remaining scatter, and a difference in the absolute ratios of the pH corrected forereef and backreef Li/Mg ratios points to another controlling factor such as microskeletal variations or calcification rate. However,

calcification rate was not found to have a significant influence on Li/Mg, with the exception of one experimental condition. Microskeletal variations demonstrated the potential to impact Li/Mg ratios but these results are limited and inconclusive. Therefore, the application of a multivariable calibration may be the most accurate method to reconstruct historic climate.

5.1 Introduction

In order to determine how corals will respond to climate change over the course of this century, particularly in terms of ocean warming and coral bleaching events, it is vital to understand how they have already responded to anthropogenic changes since the Industrial Revolution. Given the incompleteness and heterogeneity of existing historic sea surface temperature (SST) records (*Kennedy et al.*, 2011), it has become popular to reconstruct SST using accepted geochemical proxies fixed within tropical coral skeletons (*Tierney et al.*, 2015). Corals are archives of historic SSTs (e.g. *Alibert and McCulloch*, 1997; *DeLong et al.*, 2007) because during biomineralisation, a range of elements (e.g. Li, Mg, Sr) become incorporated into the aragonite $CaCO_3$ matrix, the concentrations of which are dependent on temperature due to their partition coefficients (e.g. *Beck et al.*, 1992; *Hathorne et al.*, 2013b). While the response of coral calcification to increased temperature and acidification are widely reported in the literature (e.g. *Doney et al.*, 2009; *Kleypas and Yates*, 2009; *Ries et al.*, 2009; *Ries et al.*, 2010; *Castillo et al.*, 2014; *Pandolfi*, 2015), the effects these processes have on element incorporation other than Ca^{2+} or CO_3^{2-} are less prevalent.

It is already established that the Sr/Ca-SST proxy in coral can be impacted by a range of environmental parameters and biological processes (or "vital effects"; Sinclair, 2005), and is evident within numerous existing Sr/Ca-SST calibrations of *Porites* coral (Figure 5-1), where the large range of SST sensitivities can cause inaccuracies in reconstructed SST of up to 7°C (*Gaetani et al.*, 2011). There are a number of potential causes of these variations including differences in seawater pH (*Cohen et al.*, 2009a); gender (*Carricart-Ganivet et al.*, 2013); light (*Reynaud et al.*, 2004); microskeletal heterogeneity such as density (*de Villiers et al.*, 1994; *Alibert and McCulloch*, 1997) or presence of centres of calcification (*Cohen et al.*, 2001; *Meibom et al.*, 2006); nutrient availability (*Atkinson et al.*, 1995); and Rayleigh fractionation, which can also be exacerbated by different calcification rates (*Gaetani and Cohen*, 2006). Not only do such differences occur between corals of the same species from different coral reefs, but different Sr/Ca sensitivities to temperature have been observed in multiple colonies from the same reef (*Saenger et al.*, 2008; *Cahyarini et al.*, 2009; *Pfeiffer*

et al., 2009; *Alpert et al.*, 2016), potentially related to variations in tissue thickness (*Gagan et al*., 2012).It has been reported that, for example, one colony can show an increase in SST over time, whereas a neighbouring colony can record a decrease in SST (*Grove et al.*, 2013; *Alpert et al.*, 2016). Although Sr/Ca-SSTs do not always match satellite SSTs (e.g. *Carilli et al*., 2014), some of this variability may be a candid representation of differences across dynamic reef environments not captured in SST records (*Linsley et al.*, 2004; *Cahyarini et al.*, 2009).

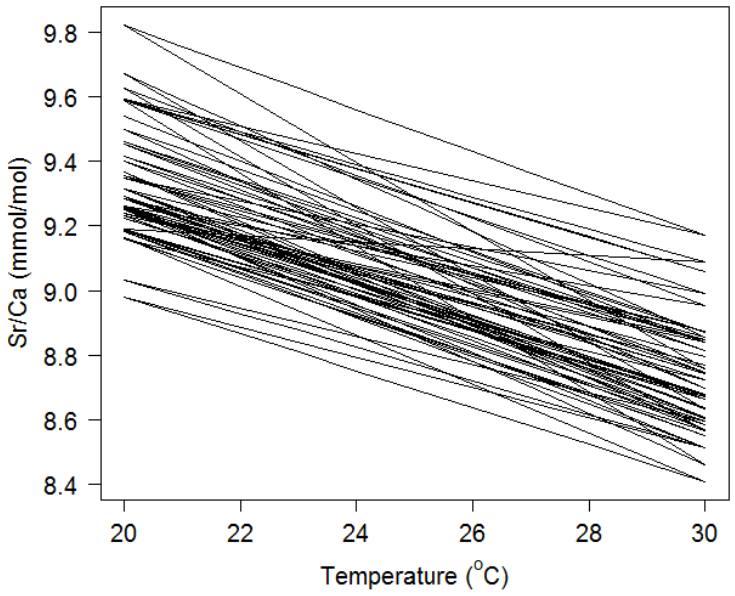

Figure 5-1. Numerous Sr/Ca-SST calibrations exist in the literature for various *Porites* species, but within these, a great range of SST sensitivity is evident. The calibrations and associated references are listed in Table 1 of *Corrège*, (2006).

The recently explored and promising Li/Mg-SST proxy in corals (*Hathorne et al.*, 2013b; *Montagna et al.*, 2014) has received limited research into potential impacts by parameters other than temperature, but the robustness of this proxy was investigated by *Montagna et al.*, (2014) following analyses of an extensive range of natural and cultured tropical, temperate and cold-water corals. It was concluded that Li/Mg is not affected by salinity or aragonite saturation state (in contrast to the more traditional thermometers, e.g. Sr/Ca and other ratios such as Li/Ca, Mg/Ca). Previous studies using deep-sea corals showed that Li/Mg can be used to reconstruct temperature to a precision of ±1.6°C (*Case et al.*, 2010). Using only *Porites* coral, SST reconstructions had extreme uncertainties up to ±3.8°C at 95% confidence (*Hathorne et al.*, 2013b). The novel multi-species calibration of

Montagna et al., (2014) however was able to reconstruct SSTs with an uncertainty of ±1.8°C (at 95% confidence).

However, in Chapter 4 it was discovered that the modern monthly resolved Li/Mg ratios of *Siderastrea siderea* coral from the backreef are less sensitive to changes in temperature than their counterparts in the forereef environment of the Sapodilla Cayes. This led to significant differences between downcore forereef and backreef Li/Mg based reconstructed SSTs (Li/Mg-SSTs), with the backreef coral producing noisy and implausible SST reconstructions up to 35°C. Additionally, the Li/Mg ratios of the backreef coral were offset from the general trend of the multi-species curve of *Montagna et al.*, (2014). This suggests that corals from the Sapodilla Cayes backreef were exposed to physical or biological processes not experienced by corals in the forereef, causing differences in the Li/Mg ratios. It was suggested that these differences may be a result of potential pH differences between the reef zones, or different rates of calcification and extension rate (Chapter 3). In addition, biological processes in tropical corals that change the starting composition of the extracellular calcifying fluid have the potential to impact the process of Li/Mg incorporation; this has already been demonstrated in calcitic organisms, whereby the concentration of Mg^{2+} is likely manipulated to aid calcification (*Zeebe and Sanyal*, 2002).

Open ocean pH has only been measured for approximately 30 years (*Bates et al.*, 2012), so in order to reconstruct historic seawater pH (pH_{sw}) prior to this time, or in areas where there has been no long-term pH monitoring, such as the Southern Mesoamerican Barrier Reef System (MBRS), it is possible to employ boron isotope systematics as a pH-proxy. This is achievable because boron has two stable isotopes, ^{10}B and ^{11}B, and dissolved boron exists as boric acid ($B(OH)_3$) and the borate ion ($B(OH)_4^-$); the relative proportions of which are strongly dependent on pH_{sw}. The borate ion is predominantly incorporated into coral skeletons, making the boron isotopic composition of coral pH dependent (Section 1.4.1.1; *Hemming and Hanson*, 1992). However, $\delta^{11}B_{coral}$ measurements are positively offset from the theoretical curve of *Klochko et al.*, (2006) for borate in seawater as a result of isotopic fractionation caused by corals to increase the pH of their internal calcifying fluid (pH_{cf}) to make conditions more favourable for the precipitation of $CaCO_3$, and thus results in measurements of $\delta^{11}B_{coral}$ reflecting pH_{cf} rather than pH_{sw} (*Krief et al.*, 2010; *Trotter et al.*, 2011; *McCulloch et al.*, 2012a).

The $\delta^{11}B_{coral}$ has previously been used to reconstruct pH at annual resolutions to study long term variation over the last three centuries (*Pelejero et al.*, 2005; *Wei et al.*, 2009; *Shinjo et al.*, 2013; *Wei et al.*, 2015). However, scleractinian corals such as *Porites* also offer the

opportunity to sample at sub-annual resolution, allowing seasonal cycles in coral reef pH to be reconstructed (*Hemming et al.*, 1998; *Pelejero et al.*, 2005; *D'Olivo et al.*, 2015).

Here, cultured samples of *S. siderea* and a short but highly resolved $\delta^{11}B$ time-series will be analysed in addition to examining spatial variation within coral skeletons. This will allow a further assessment of the species independent character of the Li/Mg temperature proxy recognised by *Montagna et al.*, (2014), and examine any secondary controls on the SST-proxy (based on calibrations against Reynolds SST data (*Reynolds et al.*, 2002) that has been demonstrated to be representative of logger data; *Castillo and Lima*, 2011; *Fowell et al.*, 2016 by investigating the importance of (i) pH_{sw} via culturing *S. siderea* at multiple pHs (7.33, 7.82, 8.07), and by using monthly to seasonal reconstructed pH data from boron isotopes; (ii) skeletal heterogeneity by analysing the elemental composition of multiple theca walls and columellas in an individual colony; (iii) coral calcification rate using cultured samples at multiple pHs and temperatures (25, 28, 32°C). In light of these new data, corrected SST calibrations are explored and a full critique of the controls on the emerging Li/Mg-SST proxy and well-established Sr/Ca-SST proxy are given.

5.2 Methods

5.2.1 Coral sampling

In February 2009, coral cores were collected from the forereef and backreef in the Sapodilla Cayes Marine Reserve. A full description of the core extraction and sectioning methods can be found in *Castillo et al.*, (2011). The cores analysed in this study were FR-12 (16.10004ºN, 88.26669ºW) and BR-06 (16.14045ºN, 88.26015ºW; Figure 5-2). The FR-12 slab was sampled at a monthly resolution, and the BR-06 slab (Figure 5-3) was sampled at an approximately bimonthly resolution from a single corallite from the top (November 2007 to July 2006 and August 2008 to January 2006 respectively) of each coral slab. A New Wave Research micromill with a 500 µm diameter diamond drill bit was used to drill ~1 mm wide trenches (2 trenches were combined to make a single backreef sample) to a depth of 1 mm in the theca wall for each sample. Throughout this chapter, any references to the monthly

subsampling and resulting trace elements first described in Chapter 4 are referred to as the "original" samples, or theca 1.

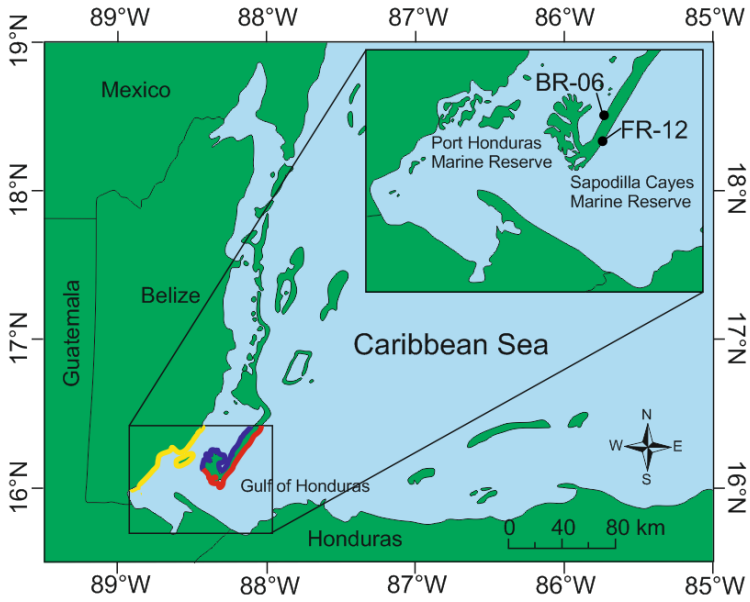

Figure 5-2. Map of sampling locations of the forereef (red zone) FR-12 coral, backreef (blue zone) BR-06 coral within the Sapodilla Cayes Marine Reserve, and nearshore reef (yellow zone) in the Port Honduras Marine Reserve. Live colonies were collected from each reef zone for the culturing experiment.

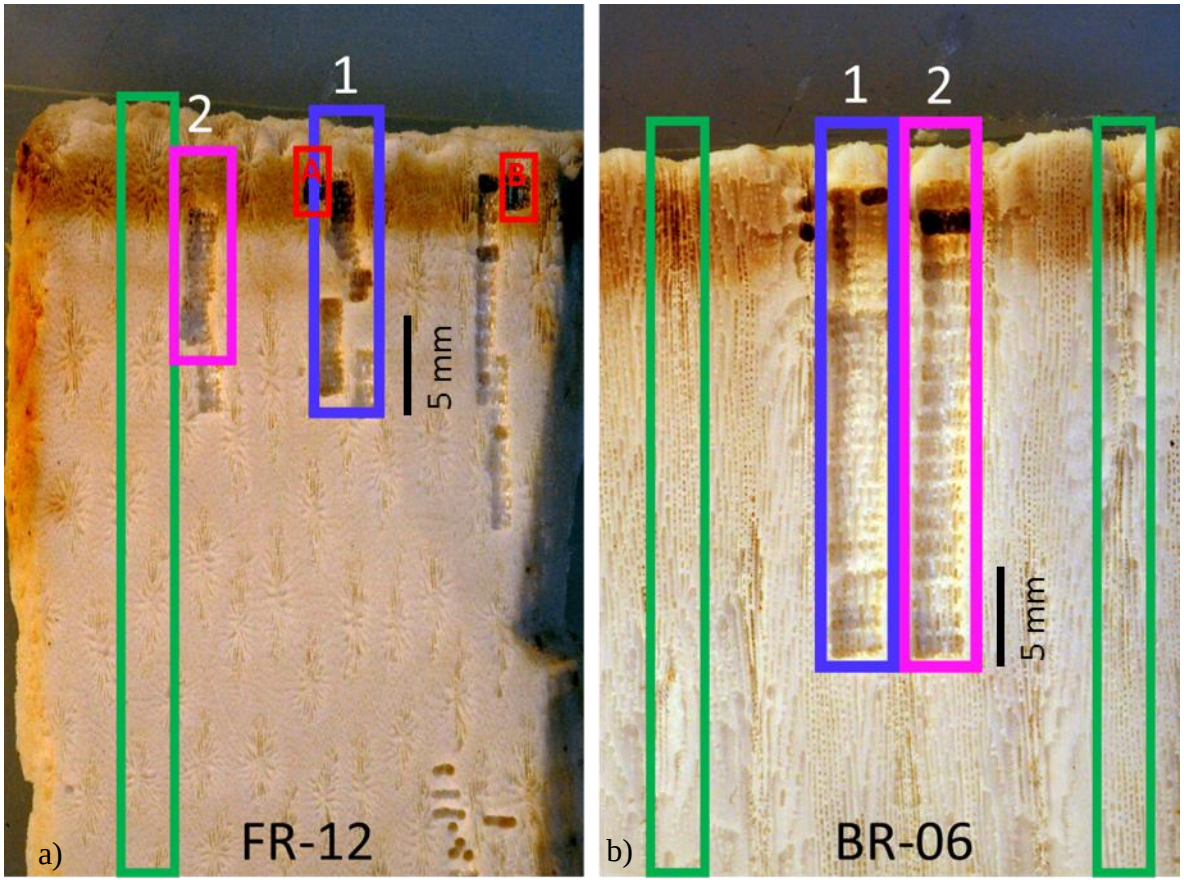

Figure 5-3. Micromilling paths of the (a) Forereef FR-12 core and (b) Backreef BR-06 coral after micromilling. The blue rectangle highlights "Theca 1", which was sub-sampled at a monthly resolution to generate trace element sea surface temperature calibrations in Chapter 3. The pink rectangle highlights "Theca 2", which was sub-sampled at a monthly resolution in FR-12 and a bimonthly resolution in BR-06 to obtain samples for boron isotope analysis. In BR-06 it is possible to see the size of the drilled spaces are twice as large on theca 2. The green rectangles highlight examples of columellas where centres of calcification can be found. They are characterised by being in the centre of the corallite, and the skeleton has a flaky and porous appearance. A columella also separates thecas 1 and 2 in BR-06. The dark hole near the top of BR-06 theca 2 indicates a position where the microdrill has gone all the way through the theca wall to the columella behind it. The red rectangles (A and B) indicate the sampling location of the centres of calcification. The tissue layer is identifiable by the brown band at the top of the slabs.

5.2.2 Coral culturing

S. siderea was cultured under variable temperatures or variable pCO_2 concentrations by *Castillo et al.*, (2014) at the Aquarium Research Center at the University of North Carolina at Chapel Hill, USA. All aquaria contained recirculating artificial seawater (*Instant Ocean Sea Salt*) at 35.13 ± 0.13 psu. For the temperature variation experiment, replicate samples from the forereef, backreef and nearshore reef zones were maintained in three replicate experiment tanks (Figure 2-5) with an average pCO_2 concentration of 488 ppm (pH 7.94 ±

0.12). Temperatures of 28.16 ± 0.24°C or 32.01 ± 0.17°C were maintained with 50 watt heaters and the final temperature of 25.01 ± 0.14°C was maintained using a 1 hp aquarium cooler. Temperatures were measured on alternate days with a NIST-calibrated 170 partial-immersion organic-filled glass thermometer. For the CO_2-induced acidification experiment, four pCO_2 partial pressures (±1σ standard deviation) of 324 ± 89 ppm, 604 ± 107 ppm and 2553 ± 506 ppm (pH 8.07 ± 0.12, 7.82 ± 0.13 and 7.32 ± 0.14) were applied and each concentration was replicated in 3 tanks at an average temperature of 28.01 ± 0.28°C (Figure 2-5). The pCO_2 concentrations were manipulated by altering the amount of compressed CO_2 gas bubbled into the aquaria controlled by mass flow controllers. Further details of the culture experiments can be found in *Castillo et al.*, (2014) and Chapter 2.

5.2.3 Sample cleaning and analytical techniques

All coral samples were oxidatively cleaned in 250-500 µl of 1% H_2O_2 (buffered in 0.1 M NH_4OH_4) at 80°C for a total of 15 minutes with intermittent ultrasonication. The spent oxidative mixture was removed and samples were thoroughly rinsed using 18.2 MΩ Milli-Q water. Between each subsequent rinse step, the powdered samples were centrifuged for 2 minutes (13,000 rpm) to minimise sample loss. Samples were then transferred into acid-cleaned micro-centrifuge tubes before a weak acid (0.0005 M HNO_3) leach was performed to remove any ions readsorbed onto the sample surface. Samples were then dissolved in incremental volumes of 0.5 M HNO_3 (typically ~125 µl) and centrifuged for 3 to 5 minutes (13,000 rpm) before 20 µl of the dissolution was added to 120 µl 0.5 M HNO_3 in a clean centrifuge tube and the remainder (with the exception of the last 20 µl) transferred into an acid leached (10% HNO_3, 30 mins, 140°C) 5 ml Teflon beaker (for $\delta^{11}B$ analysis).

A 20 µl aliquot from each diluted dissolution was added to 1.68 ml InReBe spiked 3% HNO_3 (5 ppb In, 5 ppb Re and 20 ppb Be) and analysed on the X-Series quadrupole ICP-MS to determine the calcium concentration ([Ca]) of each sample. A multielement standard stock solution made using high concentration (10,000 ppm) single element (B, Mg, Al, Sr, Ca) solutions was diluted to make four gravimetric standards with differing Ca concentrations (0.2 to 3 ppm Ca). Consistency standards of 1 ppm, 3 ppm and 7 ppm Ca CS2 and CS3 (*Ni*, 2006; *Ni et al.*, 2007) were analysed at the beginning and end of each analytical session to monitor the precision and accuracy. Based on these analyses the external precision at 1σ was estimated to be ±1.01% for 1 ppm Ca, ±4.91% for 3 ppm Ca and ±4.94% for 7 ppm Ca.

After the [Ca] of each sample had been determined, aliquots for elemental ratio analysis were diluted with 0.5 M HNO_3 to Ca concentrations of <2 mM in 320 µl allowing a suite of element intensity ratios (Li/Ca, B/Ca, Na/Ca, Mg/Ca, Al/Ca, Mn/Ca, Sr/Ca, Cd/Ca, Nd/Ca, Ba/Ca, U/Ca, Fe/Ca) to be measured on an Element XR (Thermo Scientific) sector field ICP-MS. Samples were analysed in batches of equal Ca concentrations, and blank corrected with a 0.5 M HNO_3 "blank" measured between every sample/standard (*Rosenthal et al.*, 1999). Each block of three samples was bracketed against a matrix-matched (i.e., of equal Ca concentration to the samples; *Rosenthal et al.*, 1999), gravimetric standard solution (prepared by Cardiff University). Three consistency standards (SECS1, SECS2, SECS3, University of Southampton) of matching [Ca] but gravimetrically prepared with different ratios were used as internal standards to monitor accuracy and thus efficiency of correcting for mass bias effects and instrumental drift. SECS3 is the most similar in composition to the coral samples, and returned average measured values (2σ) for Sr/Ca of 1.97 ± 0.04 mmol/mol, and Li/Mg of 5.51 ± 0.09 mmol/mol compared to 2 mmol/mol and 5.73 mmol/mol respectively determined gravimetrically.

Aliquots for the determination of skeletal $\delta^{11}B$ composition were buffered using 2 M Na acetate-0.5 M acetic acid buffer (sample:buffer ratio is 1:2) and the boron was separated from the $CaCO_3$ matrix using 20 µl-volume columns of Amberlite IRA743 boron-specific resin (*Kiss*, 1988) following *Foster et al.*, (2013), with typical boron yields of >99.9% in 550 µl 0.5 M HNO_3. The total analytical B blank was always <50 pg with a median $\delta^{11}B$ of approximately -7‰ and hence can be treated as being insignificant given our typical sample size (10 ng). The $\delta^{11}B$ of the samples were measured using a Thermo Scientific Neptune MC-ICP-MS using the standard bracketing technique described in *Foster*, (2008). A range of in-house boric acid standards and the Japanese Geological Survey *Porites* (JCp; *Okai et al.*, 2002) coral standard ($\delta^{11}B$ = 24.31 ± 0.42‰ (2σ), *n* = 62, [B] = 14 ng) were used to monitor reproducibility throughout the analyses. Uncertainty on the $\delta^{11}B_{coral}$ is calculated from the relationship between the intensity of the ^{11}B signal in volts and the $\delta^{11}B$ of JCp (Equation 5-1).

$$2\sigma = 12960 \times exp^{-212[11B]} + 0.3385 \times exp^{-1.544[11B]} \qquad \text{Equation 5-1}$$

5.2.4 Age model

Age models were built for the field samples by counting the annual skeletal bands, considering the coral age at collection, the distance down the skeleton of the first micromilled sample, and subsequent peaks and troughs in the Sr/Ca ratio were used to identify warm and cold intervals in the SST time-series, assuming the inverse relationship between Sr/Ca and SST seen in other studies (*Maupin et al.*, 2008; *DeLong et al.*, 2011; *DeLong et al.*, 2014). A polynomial curve was fit through 6 depth-age points allowing the age at each sample depth to be predicted. Instrumental SST was then interpolated on to this coral age-scale to permit direct comparison of temperature records.

Due to high Li blank issues on the Element during the analysis of the FR-12 monthly samples, the trace element ratios from the appropriate depths of the original micromilling path in Chapter 4 have been used as a substitute for these samples. These values should be representative of the theca wall from which was micromilled for the $\delta^{11}B$ samples as, Sr/Ca ratios at least, are reproducible along different theca walls of the same *S. siderea* core (*DeLong et al.*, 2014). Successful sampling and analysis of two independent theca walls of the same length (but different resolutions) from BR-06 will allow us to determine if the same is true for Li/Mg.

5.2.5 Analysis of artificial seawater

In order to adjust the elemental compositions of the cultured corals for variation between natural and artificial seawater elemental ratios, the culture media was sampled every week (total of 14 samples per tank), and a representative 6 samples from each tank were analysed (total of 108 samples) for Li/Ca, B/Ca, Mg/Ca, Sr/Ca and Ba/CaCulture media and the seawater standard for trace metals, NASS-5, were measured using the X-Series ICP-MS. Samples were diluted by 200 times in 3% InReBe HNO_3 and the calibrations of Li, B, Na, Mg, Ca, Sr and Ba were made using four gravimetric standards of different concentrations but equal elemental ratios. Each gravimetric standard was prepared with 1800 ppm Na to reduce matrix effects.

5.2.6 Reconstructing seawater pH

The sub-annually resolved $\delta^{11}B$ composition of the forereef and backreef was used to generate pH reconstructions between 2006 and 2008. To do this, the seacarb package in the

statistical software R Studio (*R Development Core Team*, 2013) was used (*Lavigne and Gattuso*, 2010); the $\delta^{11}B_{sw}$ was assigned a value of 39.61‰ (*Foster et al.*, 2010), and $\alpha_{B3\text{-}B4}$ 1.0272 (*Klochko et al.*, 2009). The dissociation constant of boric acid (K_B, mol/kg) was calculated with a salinity of 35 psu, a hydrostatic pressure of 0 bar, on the total pH scale, and the temperature associated with each sample from the Reynolds dataset (section 4.3.2, Chapter 4). The dissociation constant of boron (pK_B^*) was then calculated as $pK_B^* = -\log_{10}(K_B^*)$, allowing the pH_{cf} to be calculated (*Zeebe and Wolf-Gladrow*, 2001) using the following equation:

$$pH_{cf} = pK_B^* - log\left(-\frac{\delta^{11}B_{SW} - \delta^{11}B_{coral}}{\delta^{11}B_{SW} - (\alpha_{B3-B4} \times \delta^{11}B_{coral}) - 1000 \times (\alpha_{B3-B4} - 1)}\right)$$

Equation 5-2

The equation of *Trotter et al.*, (2011), *McCulloch et al.*, (2012a) and *Liu et al.*, (2014) was then applied to convert pH_{cf} into pH_{sw} on the total scale:

$$pH_{SW} = \frac{(pH_{cf} - 4.72)}{0.466}$$

Equation 5-3

This equation was applied because there is no existing calibration for the relationship between $\delta^{11}B_{coral}$ of *S. siderea* skeletons and pH_{sw}. However, calibrations exist for *Porites sp.*, *Cladocora caespitosa* and *Acropora* and *Stylophora* species (*Hönisch et al.*, 2004; *Krief et al.*, 2010; *Trotter et al.*, 2011) and similar slopes are found between pH_{sw} and measured $\delta^{11}B_{coral}$. It's important at this point to state that it is the relative change in pH over time, and the relative difference between the forereef and backreef pH that is important, rather than absolute pH values since no calibration currently exists for *S. siderea*, and the relative change in δ^{11}B-pH is largely independent of the calibration chosen (*Foster and Rae*, 2016).

5.3 Results

5.3.1 Seawater analysis

Before any calibrations could be made from the cultured coral, it was necessary to apply corrections to the elemental ratios of each sample using the average elemental compositions

of the artificial seawater (Table 5-1) from each tank group to account for differences between natural and artificial seawater compositions using Equation 5-4. The natural seawater ratios used were 2.51 mmol/mol Li/Ca, 42 mmol/mol B/Ca, 5.13 mol/mol Mg/Ca and 8.83 mmol/mol Sr/Ca. Elemental partition coefficients (K_D) were also calculated using the elemental ratios of the artificial seawater from the relevant tanks $K_D = (X/Ca)_{coral}/(X/Ca)_{sw}$). The seawater values used were 2.51 mmol/mol Li/Ca, 5126.21 mmol/mol Mg/Ca, 8.83 mmol/mol Sr/Ca, and 0.049 mmol/mol Li/Mg. Analysis of the seawater standard NASS-5 highlighted that the artificial seawater had approximately half the Li/Ca and Li/Mg ratios of natural seawater, but was broadly similar for Sr/Ca and Mg/Ca.

$$Corrected\ coral\ ratio = Measured\ coral\ ratio \times \left(\frac{Natural\ seawater}{Artificial\ seawater}\right)$$

Equation 5-4

Table 5-1. Average artificial seawater elemental ratios of each culture tank variation and the elemental ratios of the seawater standard NASS-5.

Temp °C	CO_2 ppm	Li/Ca µmol/mol	Mg/Ca mmol/mol	Sr/Ca mmol/mol	Li/Mg mmol/mol
25	400	5490.7	5342.9	8.4	1.0
28	280	5279.1	5723.3	9.5	0.9
28	400	5415.2	5634.9	9.0	1.0
28	700	5390.1	5804.7	8.9	0.9
28	2800	5344.9	5653.0	8.9	0.9
32	400	5332.3	5270.6	8.7	1.0
NASS-5 Seawater Standard					
		2522.6	5489.0	7.6	0.5

5.3.2 pH reconstructions

The $\delta^{11}B$ of the sub-annual samples were used to reconstruct seawater pH in the forereef and backreef between 2006 and 2008 by using Equations 5-2 and 5-3. An approximately one year long pH_{sw} reconstruction was made at monthly intervals from the forereef FR-12 coral, giving a mean pH_{sw} of 8.09. An approximately three years long pH record was recontructed at bimonthly to seasonal intervals from the backreef BR-06 coral, giving a lower mean pH_{sw} of 7.91 (Figure 5-4). Both corals demonstrate a seasonal cycle in seawater pH, but the forereef pH_{sw} has a larger variation over the seasonal cycle than the backreef overall, although this is not the case if the backreef pH in March 2007, which is outside of the error

band, is included (0.29 and 0.31 pH unit absolute range for the forereef and backreef respectively; Figure 5-4). In addition, the reef zones have opposing seasonal cycles, whereby the forereef pH is greater during warmer months (r^2=0.19, p=0.1), in contrast to the backreef pH, which is greater during colder months (r^2=0.25, p=0.039, Figure 5-4, Figure 5-5).

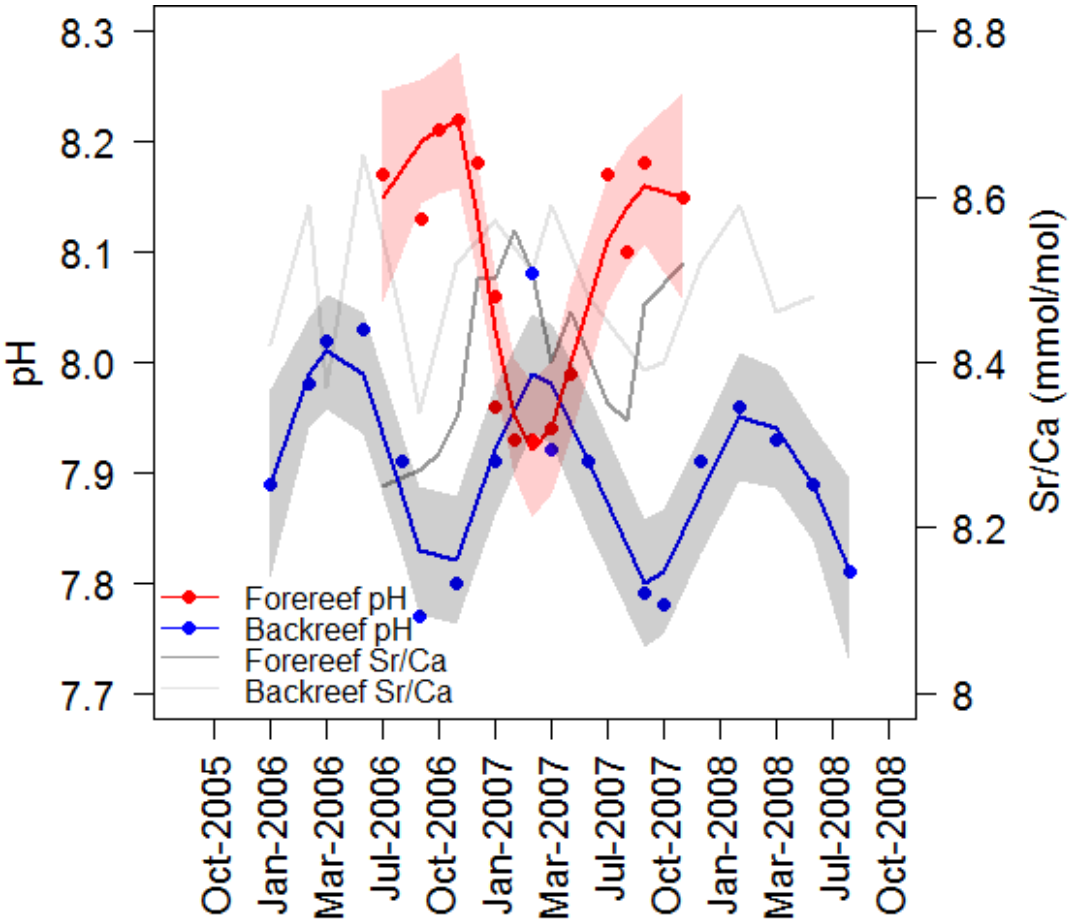

Figure 5-4. Forereef (red) and backreef (blue) seawater pH (pH_{sw}) reconstructed from the sub-annual boron isotopic composition of the FR-12 and BR-06 corals. The forereef monthly pH_{sw} demonstrates its highest pH around September, whereas the bimonthly backreef pH_{sw} demonstrates its highest pH during the spring. The data points are fitted with a LOESS smoother and the error bands represent 2 standard error confidence intervals on the smoother. Sr/Ca ratios are also plotted in grey to demonstrate temperature variation with seasonality (high Sr/Ca = low temperatures, low Sr/Ca = high temperatures).

Given the pH of the reef zones overlap in the months of January, March and April in 2008, the differences in elemental ratios and pH difference between the forereef and backreef were calculated for this time interval of similar pH. The Sr/Ca and Li/Mg were found to be significantly correlated with pH and a 0.11 and 0.14 mmol/mol difference remains, respectively (Figure 5-6).

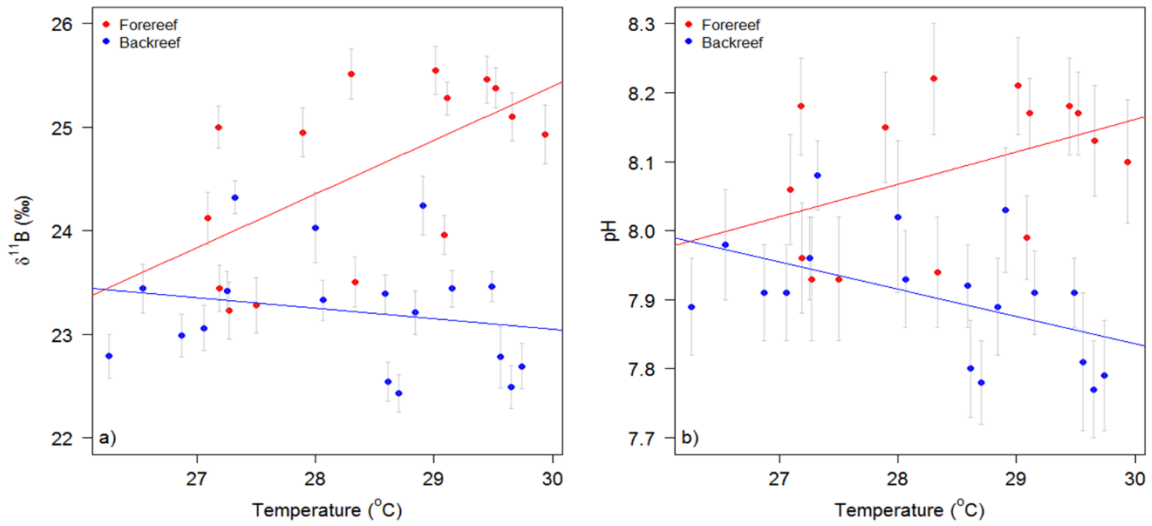

Figure 5-5. a) The $\delta^{11}B$ of the forereef coral FR-12 (red) is positively correlated with sea surface temperatures (SST), and the backreef BR-06 coral (blue) has an insignificant inverse correlation with SST. Error bars represent 2 standard errors of the averaged $\delta^{11}B$ measurement, based on the external reproducibility. b) The pH of the forereef (red) displays an insignificant positive relationship with SST, in contrast to the backreef (blue) which has an insignificant anti-correlation with SST. Error bars represent 2 standard errors on the pH reconstruction, based on the standard error of $\delta^{11}B$.

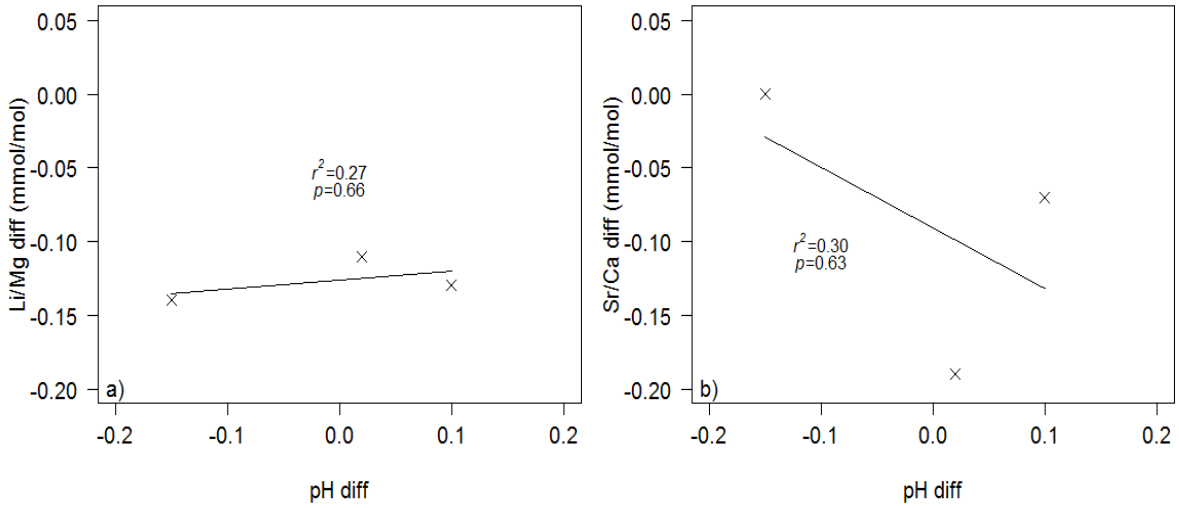

Figure 5-6. Differences between forereef and backreef (a) Li/Mg ratios and (b) Sr/Ca ratios and pH from the months of January, March and April when the pH of the two reef zones overlap show no significant correlation.

5.3.3 pH and temperature effects on skeletal Li/Mg and Sr/Ca ratios

The cultured samples demonstrate an inverse relationship between Sr/Ca and Li/Mg ratios and temperature, but this relationship is only significant for Sr/Ca (p=0.001 and p=0.059 respectively; Figure 5-7a,b), yet both ratios have significant inverse correlations with pH (p=0.001 and p<0.001 respectively; Figure 5-7c,d). The variability of elemental ratios in both the temperature and pH experiments at a given temperature or pH is large, and does not increase with increasing temperature or pH or *vice versa* (Figure 5-9). A similar degree of variation in cultured coral Sr/Ca and Li/Mg ratios is explained by changes in seawater pH (35% to 42%), but Sr/Ca is approximately three times more sensitive to these changes (Sr/Ca slope = -1.090, Li/Mg slope = -0.325; Figure 5-8 c,d; Table 5-2). Twice as much of the variability in Sr/Ca ratios can be attributed to temperature as can be for Li/Mg ratios, and Sr/Ca ratios are more than four times more sensitive to changes in temperature (Sr/Ca slope = -0.115, Li/Mg slope = -0.025; Figure 5-7a,b; Table 5-2).

5.3.4 pH and temperature effects on partition coefficients

The cultured corals reveal that the partition coefficient (K_D) of Li/Mg is up to four times higher than that of Sr/Ca (Figure 5-7e-h) in both the temperature and pH experimental corals. Like the elemental ratios, the K_Ds of Li and Sr are also significantly negatively correlated with tank temperature and pH (Figure 5-7e-h), resulting in higher K_Ds at lower pH or lower temperature. The partition coefficients of Li/Mg in the cultured samples have the highest absolute values (<4) out of the elements investigated, and also demonstrate the largest range across the different pHs, owed to the steep slope (-0.653). Despite the elemental composition of the individual artificial seawater tank being the denominator, the K_Ds within each experiment are scattered. A Welch's unequal variance t-test found the K_D of Li/Mg to be significantly different between corals from the tanks at 28°C and pH 8.07 (mean=2.90 and 3.85 respectively, p>0.001), despite them having almost identical conditions. No significant difference was found between the K_D of Sr/Ca for the same experiments.

The K_D of Sr/Ca and Li/Mg in the forereef coral samples follows the negative correlation expected from the pH culturing experiment, yet this is not the case in the backreef corals, which display significant positive trends with pH (Figure 5-11). The field samples also show that the K_D Sr/Ca is less sensitive to changes in pH than Li/Mg K_D (Figure 5-8g,h), which is the opposite to what is observed in the cultured samples (Figure 5-8c,d). The slope of the relationship between the K_D Sr/Ca in the cultured samples (-1.090) is twice as steep

as that in the forereef field samples (-0.058). The backreef field samples display the same sensitivity albeit in the opposite direction (0.058).

The K_Ds of the bimonthly field samples differ from those of the cultured samples, even within the same pH range (as predicted by the linear equation), most notably, the absolute K_Ds of both Li/Mg and Sr/Ca are higher in the cultured samples than the field samples. For instance, the backreef corals experienced a pH range of 7.77 to 8.08, whereby the range in K_D Sr/Ca was 0.94 to 0.98 as opposed to 1.05 to 1.09 in the cultured corals. The K_DLi/Mg in the same field samples ranged from 2.61 to 3, as opposed to 3.32 to 3.53 in the cultured corals. The forereef field corals experienced a pH range of 7.93 to 8.22, contributing to a K_D Li/Mg range of 2.16 to 2.81 and a K_D Sr/Ca range of 0.93 to 0.97. Over this range of pH using the cultured calibration, a range in K_D Li/Mg would be the equivalent of 3.32 to 3.42, three times as much as the 1.04 to 1.07 range in K_D Sr/Ca.

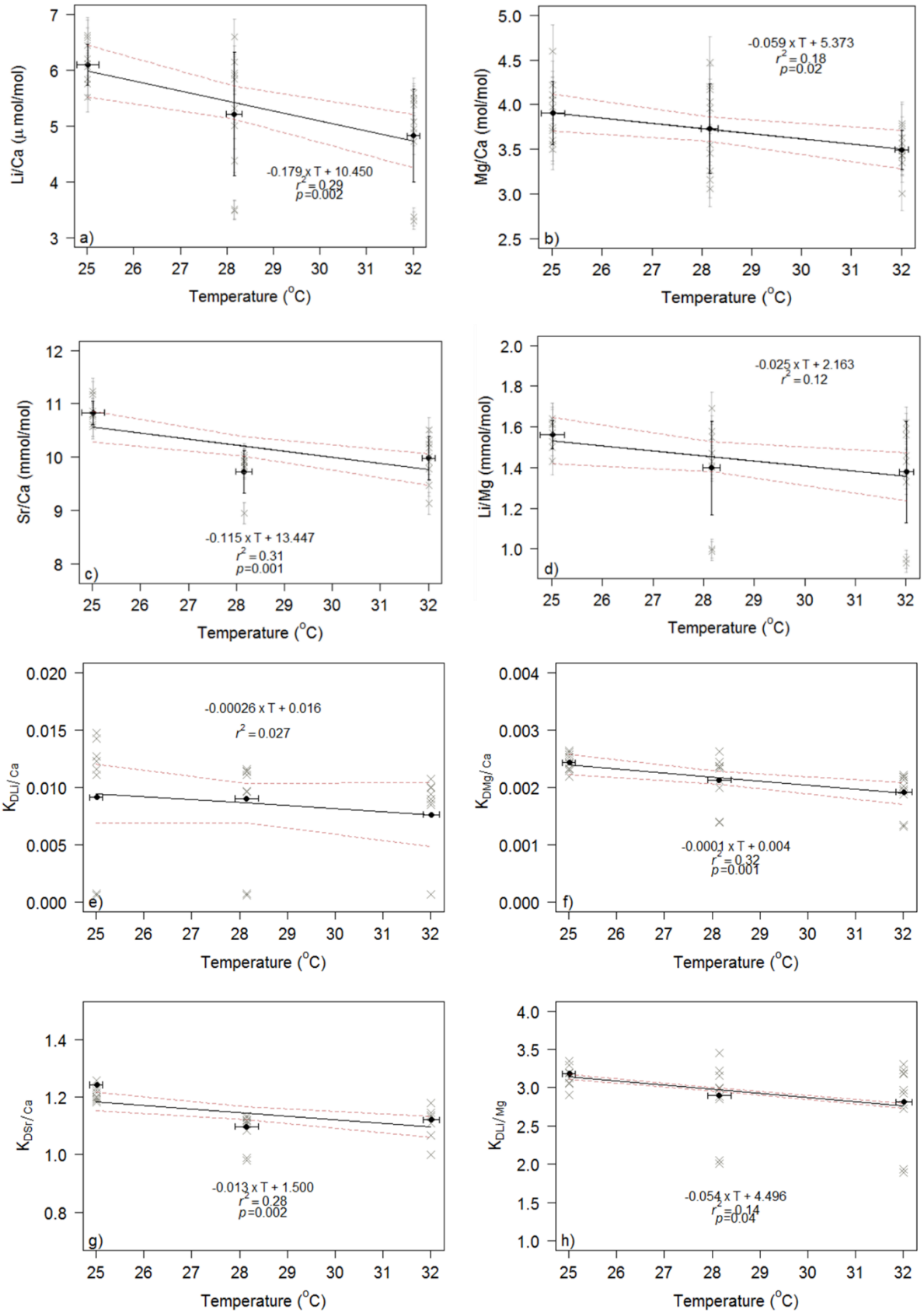
Li/Ca (µ mol/mol)
-0.179 x T + 10.450
r^2 = 0.29
p=0.002
a)
Temperature (°C)
Mg/Ca (mol/mol)
-0.059 x T + 5.373
r^2 = 0.18
p=0.02
b)
Temperature (°C)
Sr/Ca (mmol/mol)
-0.115 x T + 13.447
r^2 = 0.31
p=0.001
c)
Temperature (°C)
Li/Mg (mmol/mol)
-0.025 x T + 2.163
r^2 = 0.12
d)
Temperature (°C)
$K_{DLi/Ca}$
-0.00026 x T + 0.016
r^2 = 0.027
e)
Temperature (°C)
$K_{DMg/Ca}$
-0.0001 x T + 0.004
r^2 = 0.32
p=0.001
f)
Temperature (°C)
$K_{DSr/Ca}$
-0.013 x T + 1.500
r^2 = 0.28
p=0.002
g)
Temperature (°C)
$K_{DLi/Mg}$
-0.054 x T + 4.496
r^2 = 0.14
p=0.04
h)
Temperature (°C)

Figure 5-7. Temperature calibrations using the elemental ratios and partition coefficients (K_D) of *Siderastrea siderea* cultured at 25.01, 28.16 and 32.01°C. (a) Li/Ca-temperature. (b) Mg/Ca-temperature (c) Sr/Ca-temperature. (d) Li/Mg-temperature. Crosses represent each individual measurement and have 2σ external precision errors. Closed circles represent the averaged values from different reef zones and tanks. Error bars show 2 standard deviations on both the average ratio and temperature or pH measurement. Red dashed lines mark the 95% confidence boundaries. e) K_D Li/Ca-temperature. f) K_D Sr/Ca-temperature. g) K_D Sr/Ca-temperature. h) K_D Li/Mg-temperature. Note the different y-axis scales for the partition coefficients.

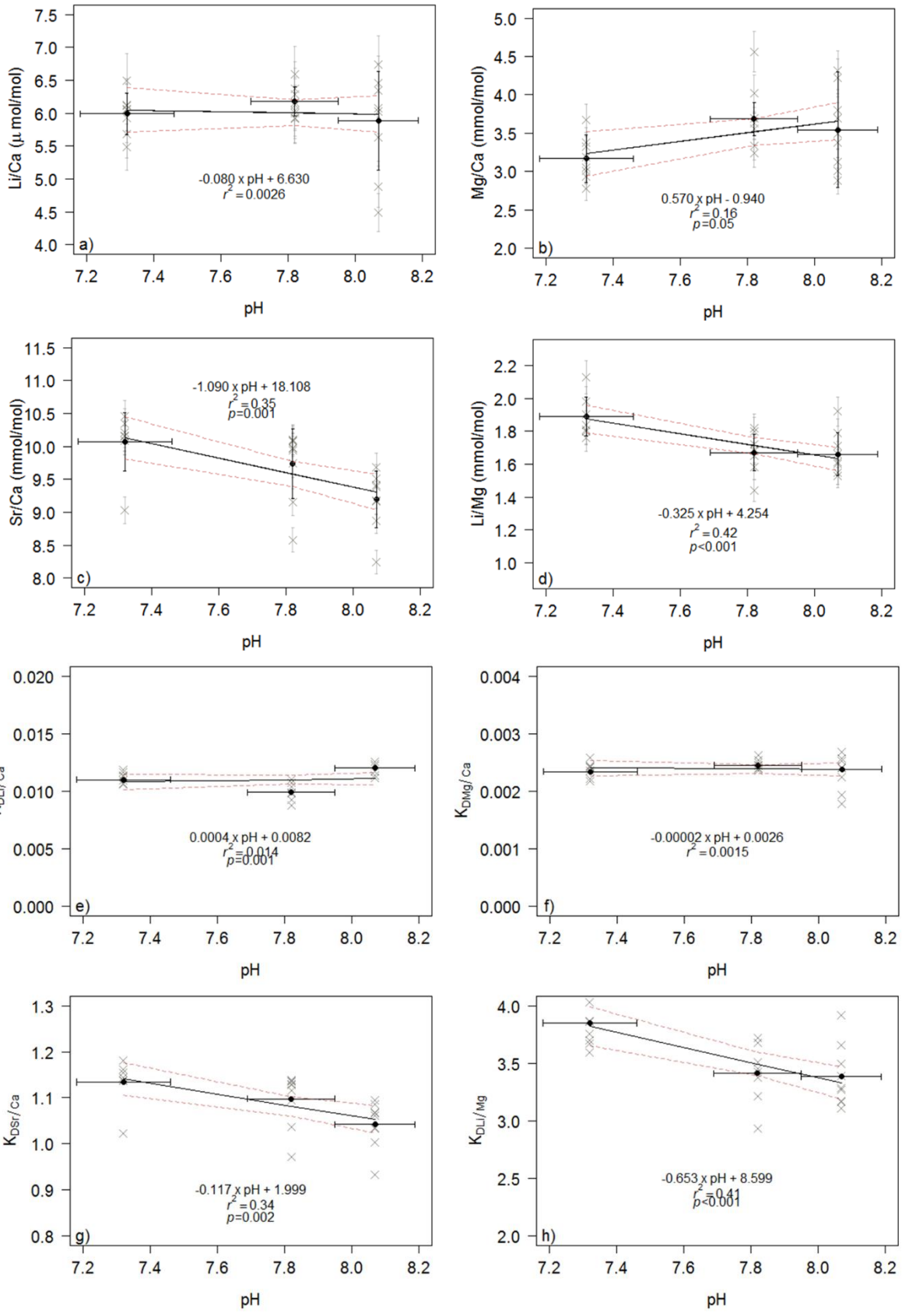
Li/Ca (µmol/mol)
-0.080 x pH + 6.630
r^2 = 0.0026
a)
Mg/Ca (mmol/mol)
0.570 x pH - 0.940
r^2 = 0.16
p=0.05
b)
Sr/Ca (mmol/mol)
-1.090 x pH + 18.108
r^2 = 0.35
p=0.001
c)
Li/Mg (mmol/mol)
-0.325 x pH + 4.254
r^2 = 0.42
p<0.001
d)
$K_{DLi/Ca}$
0.0004 x pH + 0.0082
r^2 = 0.014
p=0.001
e)
$K_{DMg/Ca}$
-0.00002 x pH + 0.0026
r^2 = 0.0015
f)
$K_{DSr/Ca}$
-0.117 x pH + 1.999
r^2 = 0.34
p=0.002
g)
$K_{DLi/Mg}$
-0.653 x pH + 8.599
r^2 = 0.41
p<0.001
h)
pH

Figure 5-8. pH calibrations using the elemental ratios and partition coefficients (K_D) of *Siderastrea siderea* cultured in artificial seawater at pHs 7.32, 7.82 and 8.07 at 28°C. (a) Li/Ca-temperature. (b) Mg/Ca-temperature (c) Sr/Ca-temperature. (d) Li/Mg-temperature. Crosses represent each individual measurement and have 2σ external precision errors. Closed circles represent the averaged values from different reef zones and tanks. Error bars show 2 standard deviations on both the average ratio and temperature or pH measurement. Red dashed lines mark the 95% confidence boundaries. e) K_D Li/Ca-temperature. f) K_D Sr/Ca-temperature. g) K_D Sr/Ca-temperature. h) K_D Li/Mg-temperature. Note the different y-axis scales for the partition coefficients.

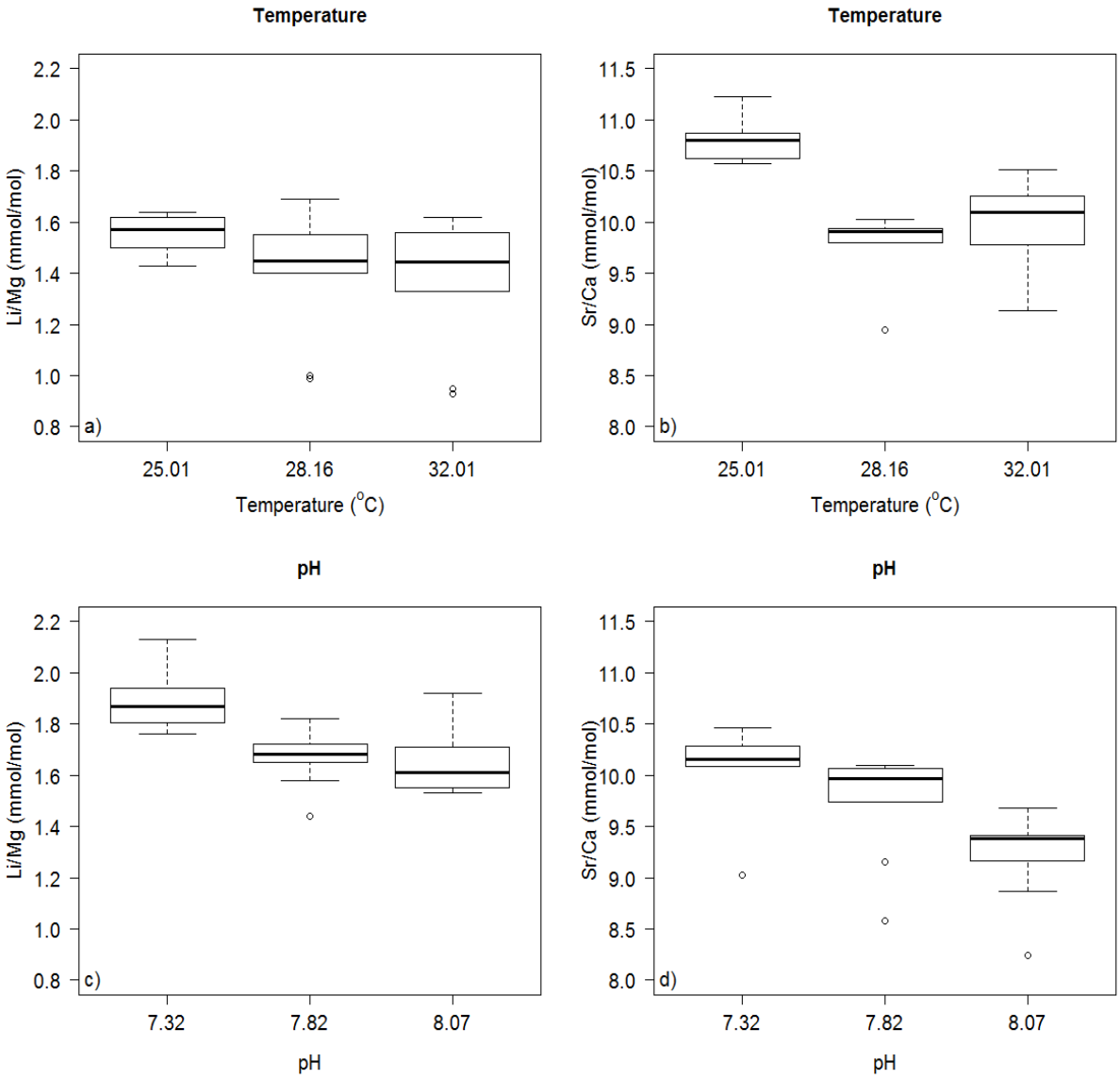

Figure 5-9. Box and whisker plots demonstrate the range of elemental ratio variability within each culture experiment (*n*=10 for each temperature experiment, *n*=8 for pH 7.32, *n*=9 for 7.82 and *n*=9 8.07). a) Li/Mg ratios and (b) Sr/Ca ratios in the temperature variation experiment. c) Li/Mg ratios and (d) Sr/Ca ratios in the pH variation experiment. Bold black line represents the median value; box represents the interquartile range; open circles are outliers.

In agreement with the cultured samples (Figure 5-7), the relationships of the field coral Li/Mg and Sr/Ca ratios with pH_{sw} in the forereef are also negatively correlated (Figure 5-10a,b), and the slopes are within error of each other (-0.367 ± 0.256 and -0.510 ± 0.221 respectively; Table 5-2) and the Li/Mg-pH slope matches that of the cultured samples (-0.367 ± 0.256 and -0.325 ± 0.078 respectively; Table 5-2). Despite the similarities in the slopes, the forereef Li/Mg-pH coefficient of determination (0.14) is half that of the cultured

Li/Mg-pH (0.42), and both the forereef (0.29) and cultured Sr/Ca-pH (0.35) calibrations, meaning the forereef Li/Mg ratios are not significantly dependent on pH (p=0.13; Table 5-1).

The positive correlation between backreef field Li/Mg and Sr/Ca with pH_{sw} from $\delta^{11}B$ contradicts the relationships observed in forereef field corals and the cultured samples. Nevertheless, the slope of the backreef field samples (0.350 ± 0.147) demonstrate an equal sensitivity of Li/Mg to pH as observed in the cultured and forereef samples, albeit in the opposite direction (Figure 5-10). Further to this, the same amount of variation in Li/Mg ratios can be attributed to pH (30%) as the forereef samples, and both the Li/Mg and Sr/Ca ratios in the cultured *S. siderea* (Table 5-2).

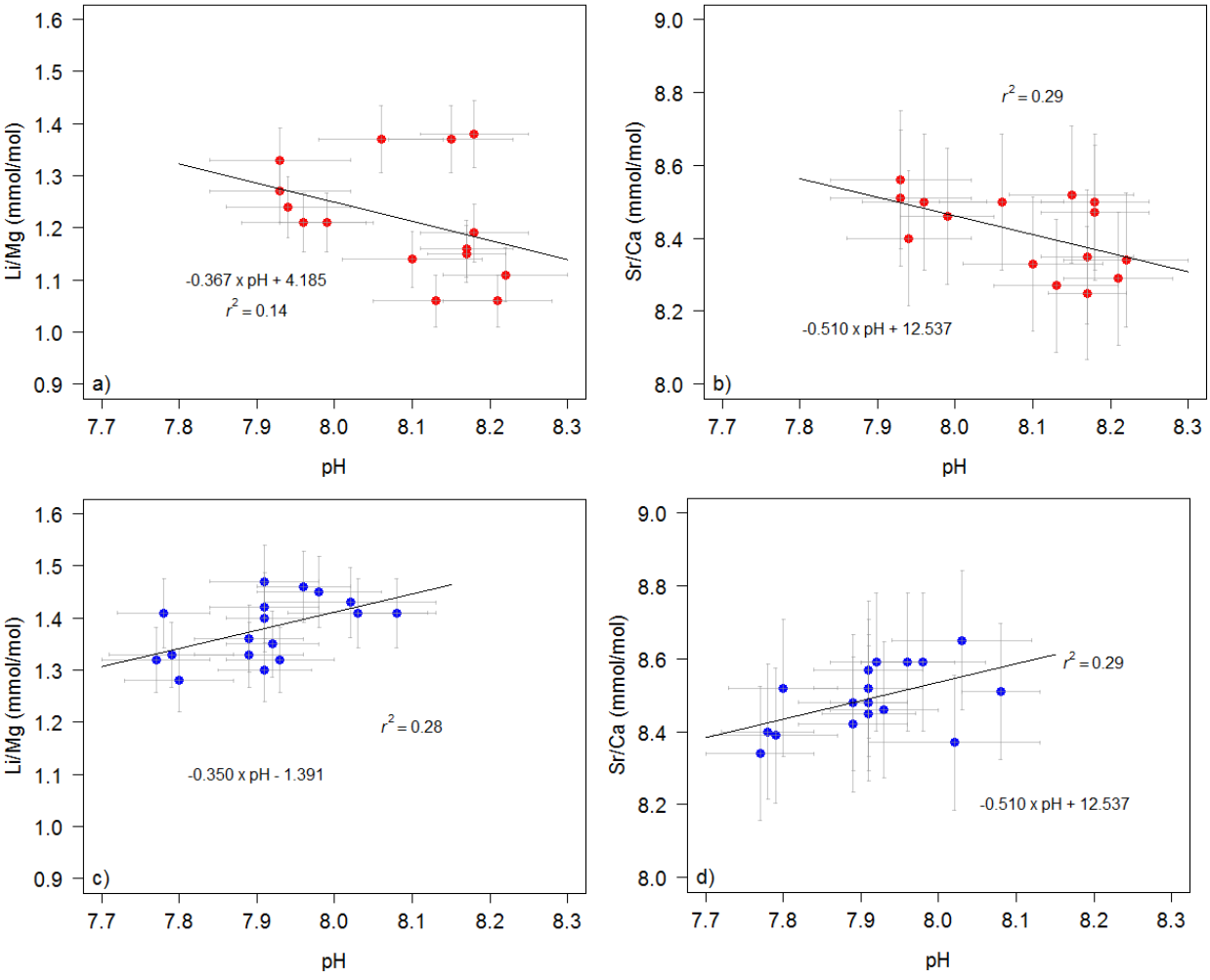

Figure 5-10. pH dependency of Li/Mg and Sr/Ca in field samples from the forereef FR-12 (red) and backreef BR-06 (blue) corals. a) Forereef Li/Mg ratios and b) forereef Sr/Ca ratios display a negative relationship with pH. c) Backreef Li/Mg ratios and d) Sr/Ca ratios display a positive relationship with pH. The elemental ratios originate from the monthly (FR-12) or bimonthly (BR-06) sampling and the error bars represent the 2σ external reproducibility. The pH is reconstructed from the boron isotopic composition of each of the coral cores.

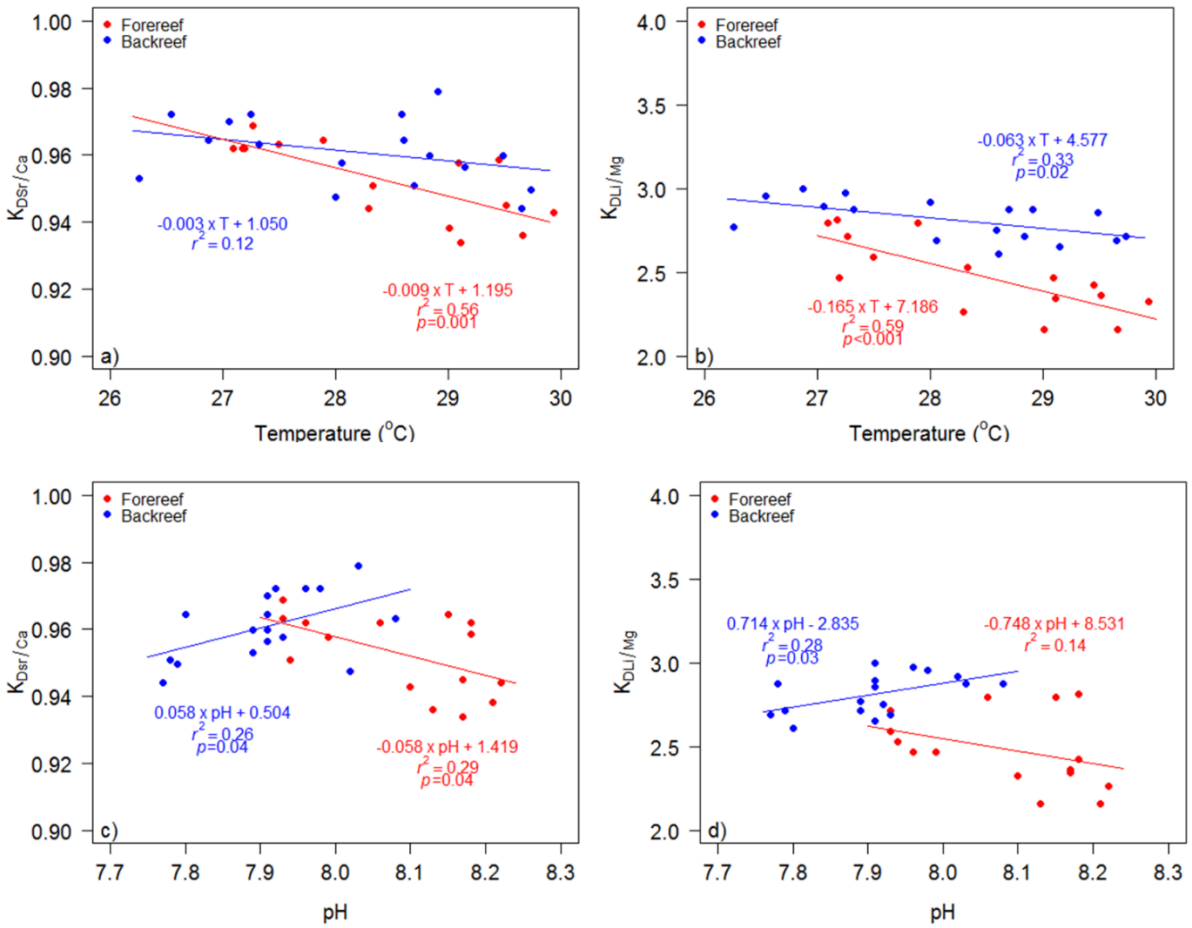

Figure 5-11. Relationships between partition coefficients (K_D) of the forereef (red) and backreef (blue) bimonthly field samples. a) K_D Sr/Ca vs. temperature. b) K_D Li/Ca vs. temperature. c) K_D Sr/Ca vs. pH. d) K_D Li/Mg vs. pH.

Table 5-2. Regression statistics for the linear regressions of Li/Mg and Sr/Ca ratio calibrations with pH in both the cultured and field samples. Calibrations are in the form $y = m \times \text{pH} + c$.

Calibration	***c***	**± 2se**	***m***	**± 2se**	r^2	***p***
Forereef field Li/Mg	4.185	2.070	-0.367	0.256	0.14	0.18
Backreef field Li/Mg	-1.391	1.159	0.350	0.147	0.28	0.03
Forereef field Sr/Ca	12.537	1.784	-0.510	0.221	0.29	0.038
Backreef field Sr/Ca	4.457	1.754	0.510	0.222	0.26	0.04
S. siderea culture Li/Mg	4.254	0.608	-0.325	0.078	0.42	<<0.01
S. siderea culture Sr/Ca	18.108	2.348	-1.090	0.303	0.35	<0.01

5.3.5 pH effects on Li/Mg- and Sr/Ca-SST proxies in *S. siderea*

Correcting the initial elemental ratios of the field samples for any pH influenced elemental incorporation allows for new, pH corrected SST proxy calibrations to be generated (Figure 5-12). In the corrected forereef Sr/Ca-SST calibration, all SST dependency has been eradicated from the initial correlation (Figure 5-12b), with the slope decreasing from -0.075 ± 0.019 to -0.004 ± 0.034. This contrasts with backreef Sr/Ca composition becoming twice as sensitive to SST (-0.028 ± 0.019 to -0.068 ± 0.032) following the pH correction. However, if the maximum uncertainties of the corrected calibrations are considered, the forereef and backreef Sr/Ca-SST calibrations just about fall within error of each other. Additionally, the corrected backreef Sr/Ca-SST sensitivity becomes more similar to the cultured sample sensitivity, whereas in the forereef it becomes less similar to the cultures, and neither of these corrected SST calibrations are within the uncertainty of the culture calibration (Table 5-3). The changes in the sensitivity of Li/Mg to SST were more subtle, with the slope decreasing by 25% from -0.081 ± 0.019 to -0.060 ± 0.021 in the forereef, and increasing by 30% in the backreef from -0.031 ± 0.011 to -0.044 ± 0.014. Nonetheless, the pH correction has brought the forereef and backreef Li/Mg sensitivity to within uncertainty, and also to within uncertainty of the culture SST calibration.

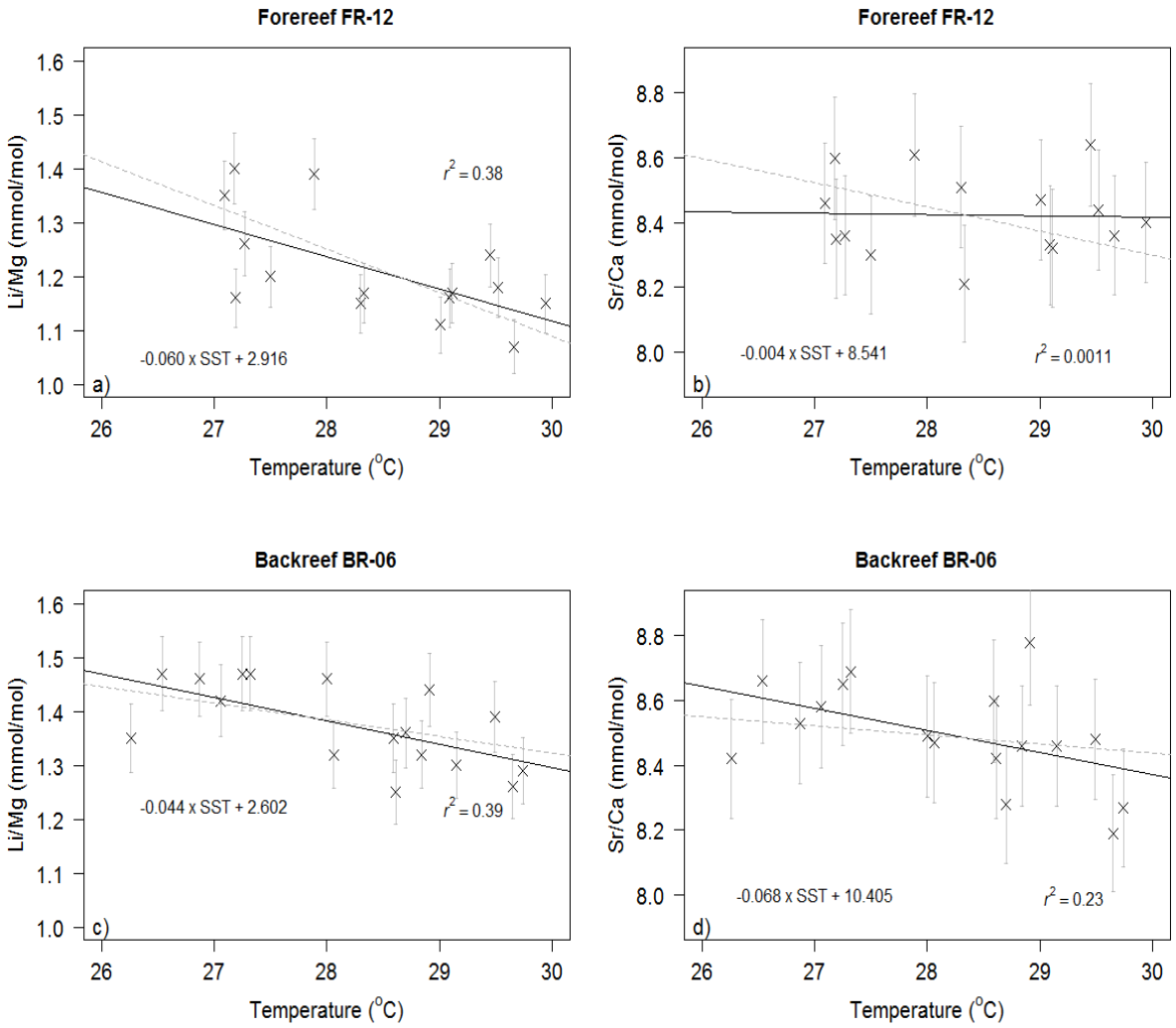

Figure 5-12. Forereef and backreef field-based calibrations of Sr/Ca and Li/Mg sea surface temperature proxies in *Siderastrea siderea* corrected for the influence of pH as determined by cultured samples. a) Forereef FR-12 Li/Mg. b) Forereef FR-12 Sr/Ca. c) Backreef BR-06 Li/Mg. d) Backreef BR-06 Sr/Ca. Crosses indicate individual samples with 2σ external reproducibility errors. Black lines represent the best linear fit through the pH corrected data, grey dashed lines indicate where the best linear fit would be for the original sea surface temperature calibrations.

Table 5-3. Regression statistics for the forereef and backreef sea surface temperature calibrations fitted with a linear regression in the form Li/Mg = $m \times SST(°C) + c$. The original calibrations are formed directly from the measured monthly (FR-12) or bimonthly (BR-06) elemental ratios. The corrected calibrations are constructed from elemental ratios which have been corrected for the influence of pH.

Calibration	***c***	**± 2se**	***m***	**± 2se**	r^2	***p***
Culture						
Li/Mg	2.163	0.366	-0.025	0.013	0.12	0.06
Sr/Ca	13.443	0.915	-0.115	0.032	0.31	0.001
Original field						
Forereef Li/Mg	3.525	0.537	-0.081	0.019	0.59	0.001
Backreef Li/Mg	2.245	0.318	-0.031	0.011	0.33	0.02
Forereef Sr/Ca	10.555	0.529	-0.075	0.019	0.56	0.001
Backreef Sr/Ca	9.278	0.545	-0.028	0.019	0.12	0.17
Corrected field						
Forereef Li/Mg	2.916	0.599	-0.060	0.021	0.38	0.01
Backreef Li/Mg	2.602	0.399	-0.044	0.014	0.39	0.01
Forereef Sr/Ca	8.541	0.962	-0.004	0.034	0.001	0.91
Backreef Sr/Ca	10.405	0.900	-0.068	0.032	0.23	0.05

Despite the slopes for the forereef and backreef Li/Mg-SST relationships becoming more similar after the pH correction, the absolute values of these two reef zones remain significantly different (mean FR=1.21 mmol/mol, mean BR=1.68 mmol/mol, $p<<0.001$; Figure 5-12a,c). Even when the extreme ranges in uncertainty on the culture calibration are considered, the potential range of intercept values for the forereef and backreef do not overlap (Table 5-4), despite the good agreement in the slopes. On the other hand, the difference in Sr/Ca slopes between the reef zones increased (Table 5-3, Figure 5-12), but the absolute values became more similar (mean FR=8.42, mean BR=8.50, $p=0.16$), and the Sr/Ca-SST relationship becomes positive. When considering the reef zones individually, it is evident that the potential range of pH corrected SST calibrations in the backreef are very similar, especially for Li/Mg (Table 5-4). In the forereef, there is also only a small range in corrected Li/Mg-SST calibrations, but this breaks down for Sr/Ca, where the maximum uncertainties in the Sr/Ca-pH culture calibration would generate a positive correlation between Sr/Ca and SST (Table 5-4).

Table 5-4. Range of linear regressions for the corrected Li/Mg and Sr/Ca calibrations against sea surface temperature given the maximum uncertainties on the cultured coral elemental ratio-pH calibrations. Regressions are in the form Li/Mg = m × SST(°C) + c.

Calibration	c	m	r^2
Forereef Li/Mg (steep)	2.759	-0.053	0.29
Forereef Li/Mg (shallow)	3.071	-0.065	0.44
Backreef Li/Mg (steep)	2.649	-0.045	0.37
Backreef Li/Mg (shallow)	2.523	-0.041	0.38
Forereef Sr/Ca (steep)	8.015	0.015	0.01
Forereef Sr/Ca (shallow)	9.104	-0.024	0.06
Backreef Sr/Ca (steep)	10.662	-0.077	0.23
Backreef Sr/Ca (shallow)	10.068	-0.056	0.21

The residuals between elemental ratios calculated from the original SST calibration and the ratios calculated from the pH corrected calibration were plotted against the pH as a means of determining how much influence pH has on the ratios when the SST signal was removed. The sensitivity of both reef zones are within error of each other for the separate ratios, but the slopes in the Sr/Ca residuals are steeper than in the Li/Mg residuals (Figure 5-13). The residual elemental ratios are inversely correlated with pH but the relationship is not significant (p=0.053).

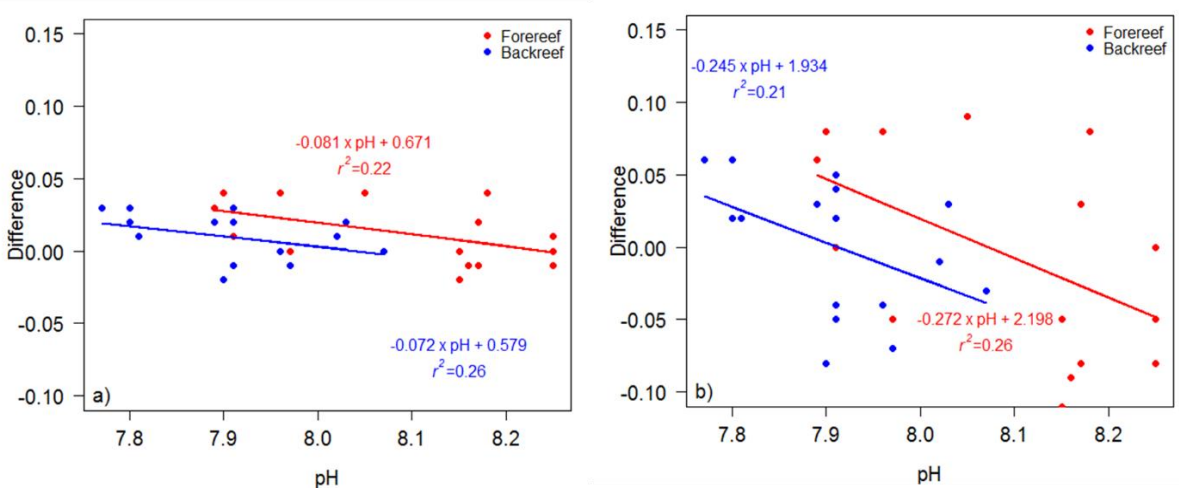

Figure 5-13. Relationship of residual (a) Li/Mg and (b) Sr/Ca ratios after the ratios calculated from the pH corrected SST calibrations had been removed from the ratios calculated from the uncorrected SST calibrations against pH. Residuals in the forereef are in red, and residuals in the backreef are in blue.

The influence of both temperature and pH can be combined using a multivariable regression (Table 5-5), and this improves the coefficient of determination of backreef Li/Mg

from r^2=0.33 to r^2=0.44 (SST only, to multivariable respectively; Table 5-3, Table 5-5), or the backreef Li/Mg-pH correlations from r^2=0.28 in the field and r^2=0.42 in the cultures to r^2=0.44 for the multivariable respectively (Table 5-2, Table 5-5). For Sr/Ca, the multivariate model only improved the Sr/Ca-field SST calibration (from r^2=0.12 to r^2=0.28). The multivariable correlation of determination for forereef Li/Mg does not improve relative to the original SST calibration, but it is improved relative to both the field and cultured pH calibrations (r^2=0.58, r^2=0.14 and r^2=0.42 respectively; Table 5-5, Table 5-2). Combining the effects of SST and pH doubled the amount of forereef Sr/Ca variation explained by these variables as opposed to considering field pH alone (r^2=0.29 to r^2=0.59; Table 5-2, Table 5-5), but only a minor improvement on the Sr/Ca culture pH calibration, and no changes to the Sr/Ca-SST calibration (r^2=0.56) were achieved.

Table 5-5. Multivariable linear regression statistics for the multiple parameter forereef and backreef calibrations. Calibrations are in the form: elemental ratio = ((x_1 × SST) + (x_2 × pH)) + c.

Calibration	c	x_1	x_2	r^2	p
Forereef Li/Mg	3.691	-0.079	-0.028	0.58	0.006
Forereef Sr/Ca	11.638	-0.064	-0.173	0.59	0.005
Backreef Li/Mg	0.094	-0.014	0.245	0.44	0.016
Backreef Sr/Ca	5.267	-0.014	0.475	0.28	0.099

5.3.6 Calcification effects

The calcification rates of the cultured corals were measured in both the temperature and pH varied tanks by using an empirically calibrated buoyant weight technique (see *Castillo et al.*, 2014) as it is thought that the effect of pH on element incorporation in coral may occur via the influence of pH on coral calcification (*Tanaka et al.*, 2015). The calcification rate of corals varied within single experiments, where a greater range was observed across the range of temperature conditions (<134 mg/cm^2/90 day; Figure 5-14). Overall, a parabolic relationship exists between both pH or temperature and calcification rate (subject of the study by *Castillo et al.*, 2014).

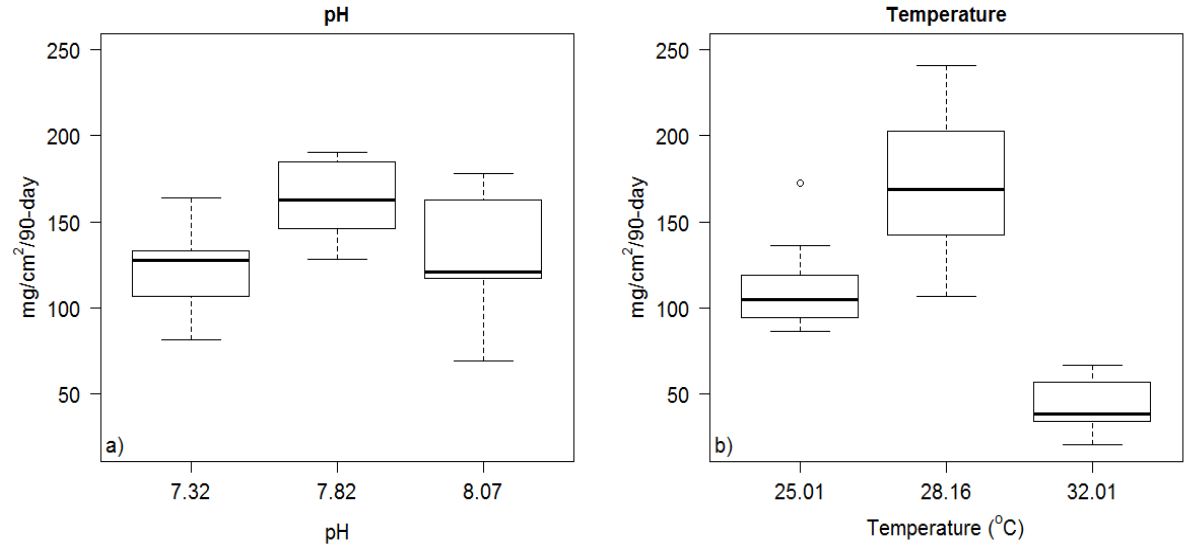

Figure 5-14. Variability in calcification rates in the (a) pH varied cultures and (b) the temperature varied cultures.

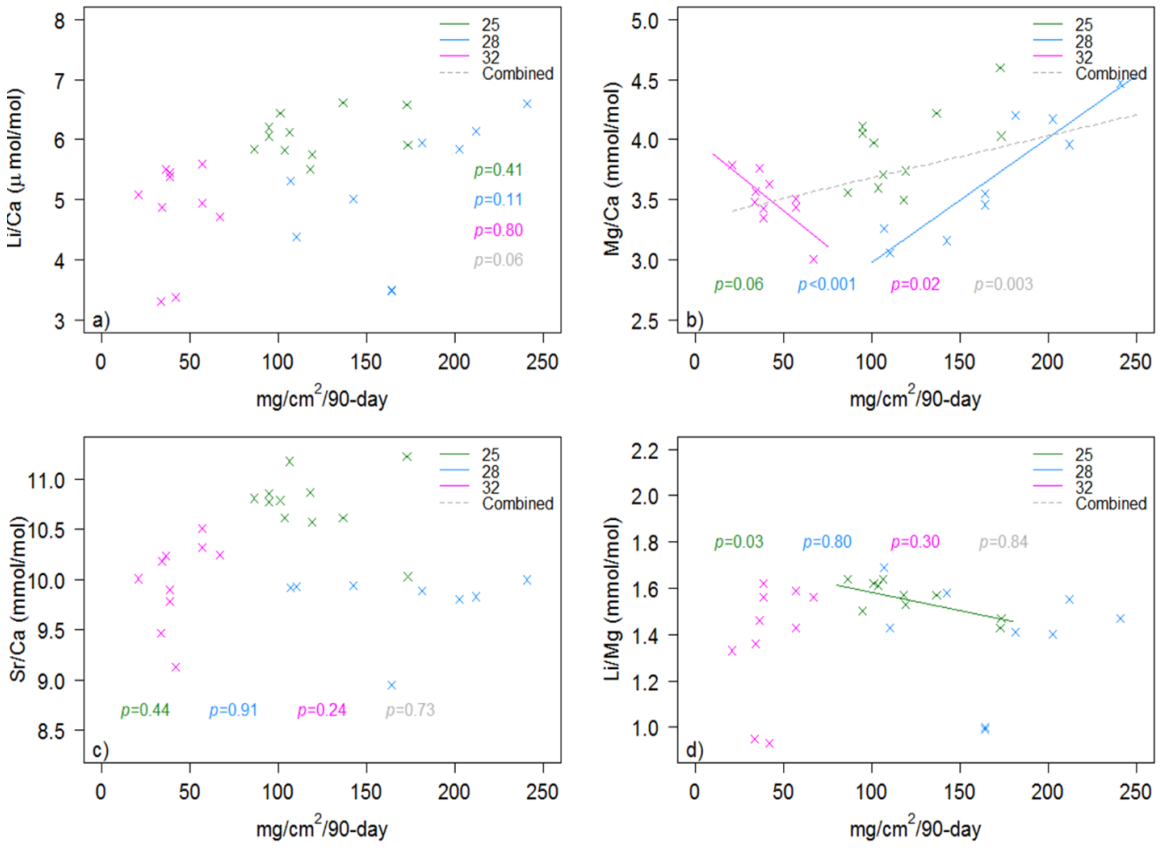

Figure 5-15. Calcification rates and elemental ratios from *S. siderea* cultured at 25°C, 28°C and 32°C. a) Li/Ca ratios. b) Mg/Ca ratios. c) Sr/Ca ratios. d) Li/Mg ratios. Data where there is a significant correlation between the elemental ratio and calcification rate is fitted with a line of best fit.

Significant relationships were found between Mg/Ca and calcification in both the 28°C (p=0.02) and 32°C cultures (<0.001), indicating that this relationship gets stronger with increasing temperatures. However, Mg/Ca ratios and calcification share are negatively correlated, as opposed to the strongly positively correlated relationship that exists in the cultures from 32°C. A significant negative relationship was also found between Li/Mg and calcification rate at 25ºC (r^2=0.43, p=0.03). No significant relationsips were observed between either Li/Ca or Sr/Ca ratios and calcification rate.

Li/Ca significantly increases with increasing calcification rates in the pH 7.82 cultures (r^2=0.43, p=0.05). Mg/Ca also has a strongly significant positive relationship with calcification, but only in the pH 8.07 cultures (r^2=0.43, p=0.03). If the calcification rates from each pH experiment are combined, a significant inverse correlation is observed between Li/Mg ratios and calcification rate in corals cultured under varying pH conditions (r^2=0.24, p=0.02; Figure 5-15a), and furthermore, the residuals from the cultured Li/Mg-pH calibrations are significantly correlated with pH (Figure 5-13), but this is more than likely a consequence of Li/Mg and calcification rate being independent of each other, but both dependent on pH (Figure 5-7, Figure 5-14).

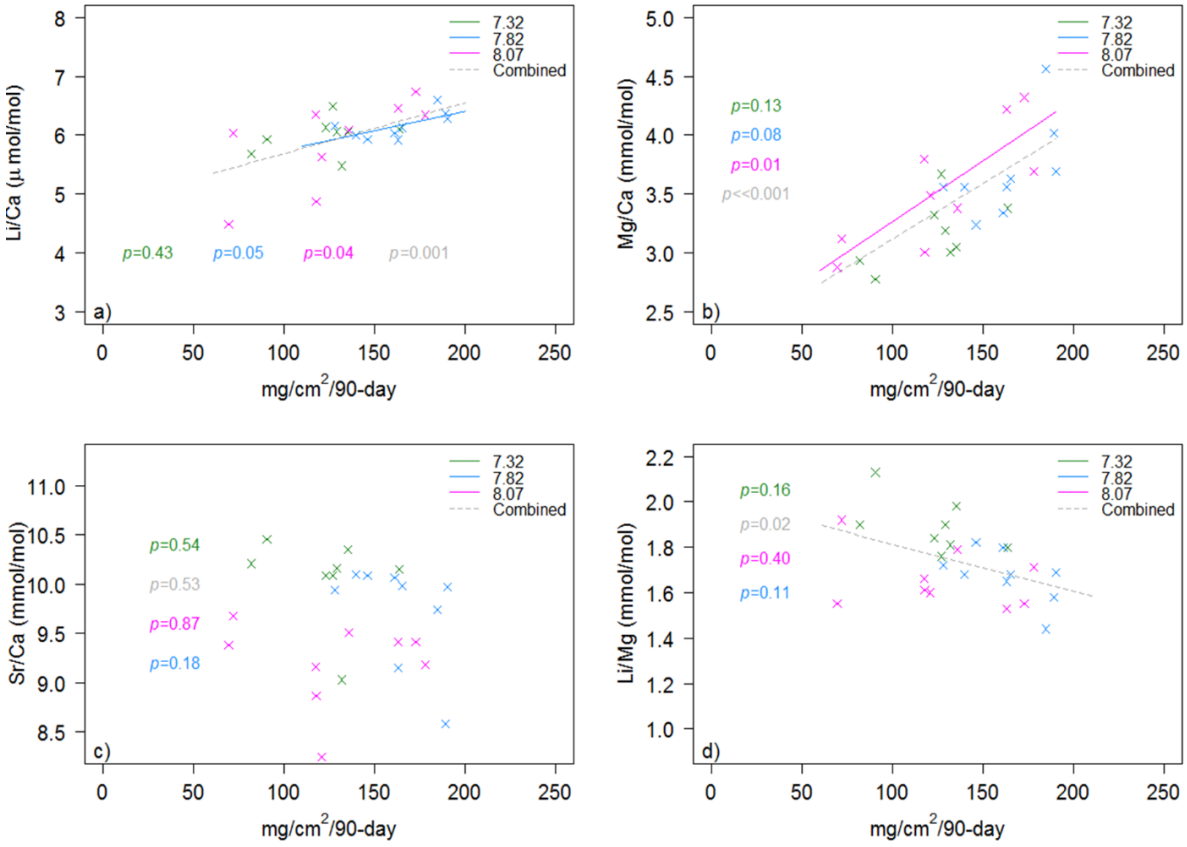

Figure 5-16. Calcification rates and elemental ratios from *S. siderea* cultured at pHs 7.32, 7.82, 8.07. a) Li/Ca ratios. b) Mg/Ca ratios. c) Sr/Ca ratios. d) Li/Mg ratios. Data where there is a significant correlation between the elemental ratio and calcification rate is fitted with a line of best fit.

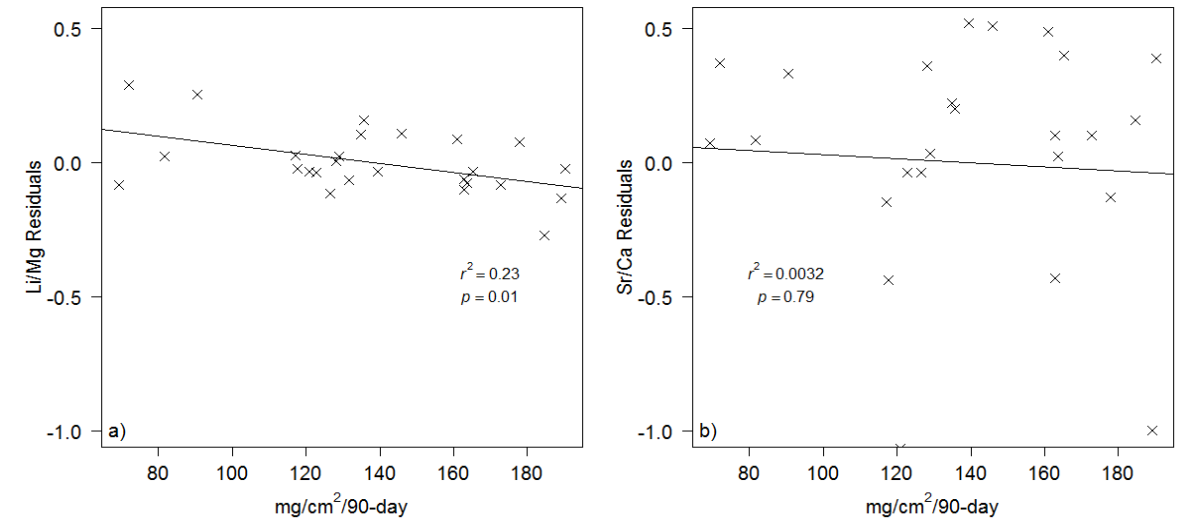

Figure 5-17. Residuals from the linear models of elemental ratios against pH in cultured *S. siderea* samples. a) Li/Mg residuals are significantly inversely correlated with calcification rate. b) Residual Sr/Ca ratios are not significantly correlated with pH.

5.3.7 Skeletal microstructure impacts on elemental ratios

Two theca walls of the backreef BR-06 coral were sub-sampled during this study, and are referred to as either "theca 1", indicating the theca wall sub-sampled at a monthly resolution (see Chapter 4), or "theca 2", indicating the theca wall sub-sampled at a bimonthly resolution for the purpose of boron isotope analysis in this chapter (Figure 5-3). In Figure 5-18, it is evident that the absolute Li/Mg values (not pH corrected) are different between the two theca walls (theca walls overlap between January 2006 and August 2008), however, the resulting linear calibration of the bimonthly samples is within error of the calibration from theca 1 (Li/Mg = -0.033(±0.014) × SST + 2.458(±0.406); Table 3-2, Chapter 3). This difference is driven by variations in Li/Ca ratios (Figure 5-18a), which are significantly different between the two theca (p<<0.001). The Sr/Ca ratios replicate more consistently than Li/Mg ratios between theca walls, and again, the bimonthly subsampled theca 2 generates a near identical Sr/Ca-SST calibration.

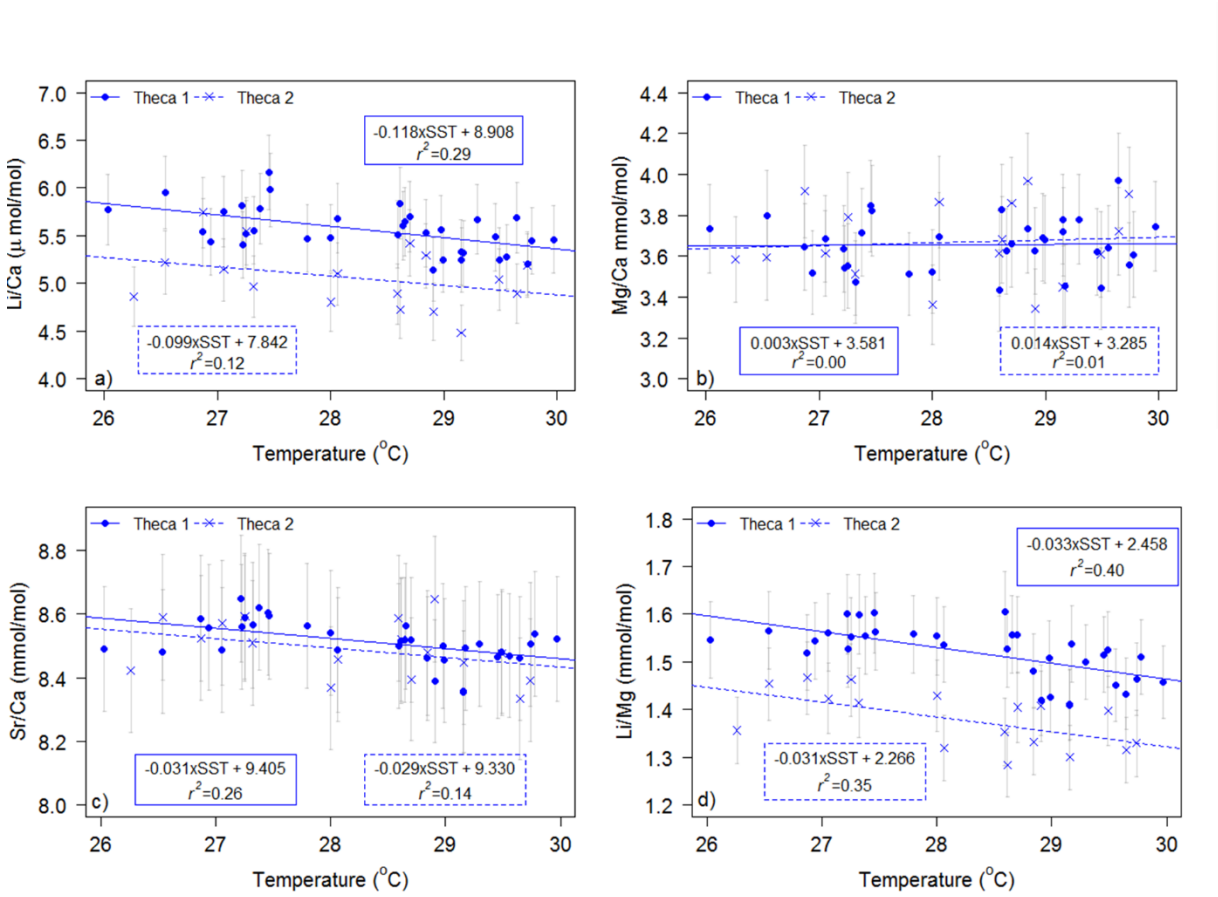

Figure 5-18. a) Linear calibrations of Li/Ca-SST. b) Mg/Ca-SST. c) Sr/Ca-SST and d) Li/Mg-SST from two individual theca walls of the backreef BR-06 coral. The closed circles and solid line represent the samples from the theca wall sub-sampled at a monthly resolution, and the crosses and dashed line represent the samples from a different theca wall sub-sampled at a bimonthly resolution.

Four samples from two columellas (A,B), which host the centers of calcification (COC), were micromilled from the FR-12 coral, adjacent to the top of the theca wall sampling path (Figure 5-3). Each COC sample is equivalent to approximately two months, so the elemental ratios of two theca wall samples were averaged to represent one COC sample. In the Apr-Jun samples, the Li/Mg and Sr/Ca ratios of both COC samples and the theca sample are within external precision. In the Jul-Sep samples, the Sr/Ca ratios are within external precision, but the Li/Mg ratios of the COCs are not within error of each other, or with the theca sample.

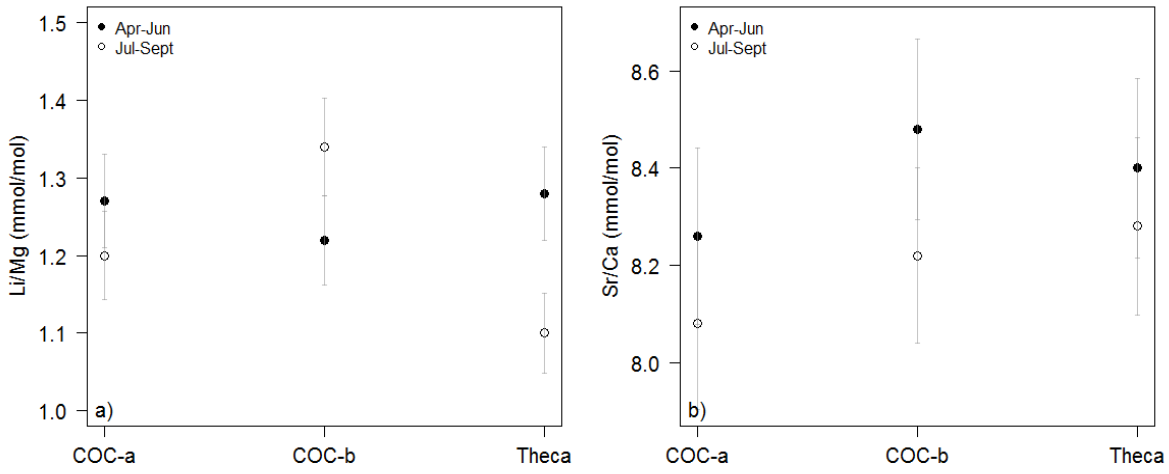

Figure 5-19. Samples from two columellas (hosting centres of calcification; COCs) are compared to theca wall samples in terms of their (a) Li/Mg composition and (b) Sr/Ca composition. Closed circles represent samples from April to June 2007, open circles represent samples from July to September 2007. Error bars represent 2σ external error.

5.4 Discussion

5.4.1 Seasonal cycles in seawater pH in the Sapodilla Cayes

Interannual pH variations are common in coral reef environments due to seasonal fluctuations in net community calcification and net primary productivity (e.g. *Bates et al.*, 2010). As demonstrated by studies using pH loggers, the pH range of coral reefs can be from 7.65 in the upwelling regions of the Pacific Ocean (*Manzello*, 2010), up to 8.4 in Japan (*Kayanne et al.*, 2005) and the Great Barrier Reef (*Santos et al.*, 2011), and average values of 8 to 8.2 in the Red Sea and Hawaii (*Silverman et al.*, 2007; *Gray et al.*, 2012a). The seasonal pH range calculated from both the FR-12 forereef and BR-06 backreef corals are

within the presently observed range. Corresponding seasonal variations in the $\delta^{11}B$ of coral skeletons have previously been identified by *Hemming et al.,* (1998), where it was observed that $\delta^{11}B$ displays a seasonal variation, with the heaviest $\delta^{11}B$ corresponding to the highest skeletal density from the time of highest primary production, which was argued would increase pH_{sw}. Using the annually resolved $\delta^{11}B$ data (Chapter 3), the pH calculated in the forereef (in 2008) was 8.12, whereas in the backreef (in 2006) it is 7.88. Despite the consensus that theca walls should be directly sub-sampled (e.g. the bimonthly samples) rather than bulk sampling homogenised skeletal material (e.g. the cultured samples) in order to avoid undesirable impacts from vital effects (e.g. pH up-regulation), the average reconstructed pH from the sub-annual forereef and backreef samples (8.18 and 7.92 respectively) are within the uncertainty of the reconstructed pH from the relevant annual sample.

It is also noteworthy that the high resolution $\delta^{11}B$ samples show a decreasing pH trend even over the short time-series in both reef zones (Figure 5-4). Using values from the LOESS smoother, the peaks in forereef pH decreased by 0.02 pH units (2006-2007), and the peaks in backreef pH decreased by 0.02 (2006-2007) and 0.04 pH units (2007-2008). These changes are ten times more rapid than the average open ocean rate of change, similar to the rate of acidification we would expect per decade rather than per year (-0.017 to -0.019 pH units per decade; *Bates et al.,* 2010), but part of this signal could be caused by interannual variability. This suggests that the anticipated ocean acidification signal is possibly being exacerbated by a more localised reef process that decreases pH, such as calcification.

Forereef environments are typically associated with low variations in environmental conditions, such as temperature and pH, as a result of more direct contact with deeper, open ocean water. The low variance of this environment has often been thought to provide these corals with less resilience to climate change and the associated rapidly changing conditions (*Barshis et al.,* 2010; *Castillo et al.,* 2011; *Comeau et al.,* 2014; *Schoepf et al.,* 2015). However, not only do the pH reconstructions here point to larger seasonal variations in forereef pH (~0.3 pH units) than in the backreef (~0.15 pH units, and more characteristic of other coral reefs e.g. *Kayanne et al.,* (2005) and *Silverman et al.,* (2007); Figure 5-4), but forereef and backreef cultures of *S. siderea* have previously been shown to have equal calcification responses to increases in temperature and pCO_2 conditions (*Castillo et al.,* 2014).

In the MBRS, there must be specific local drivers of the seasonal forereef and backreef pH cycles (Figure 5-4) since the backreef reaches its maximum pH during the spring (~March); and the forereef reaches its maximum pH at the end of the summer (~September).

Additionally, the backreef has a lower pH relative to the open ocean (~8.1), similar to observations from Flinders Reef in the Great Barrier Reef, Australia (*Pelejero et al.,* 2005). The positive correlation between forereef pH and SST is not statistically significant (p=0.1, Figure 5-4, Figure 5-5) and is therefore not consistent with the understanding that higher temperatures increase the rate of calcification (to a certain threshold; e.g. *Castillo et al.*, 2014) and therefore the amount of CO_2 produced, according to Equation 5-5.

$$Ca^{2+} + 2HCO_3^- \rightarrow CaCO_3 + H_2O + CO_2 \qquad \text{Equation. 5-5}$$

A transect of pH reconstructions from $\delta^{11}B$ across the Great Barrier Reef found that pH is positively correlated with rainfall and river plume discharge (*D'Olivo et al.*, 2015), so based on these findings, one might expect the forereef pH_{sw} to be highest during or after the rainy season, rather than directly before it, because high riverine inputs promote phytoplankton activity, which utilises dissolved CO_2 and increases the pH_{sw}. River water plumes following flood events can have either lower $\delta^{11}B$ values (14.13‰ to 28‰; *D'Olivo et al.*, 2015), or higher $\delta^{11}B$ values (+42.8‰) than seawater. Without any river water samples, it is difficult to explore if Honduran rivers impart a low $\delta^{11}B$ onto water within the MBRS relative to seawater (39.61‰; *Foster et al.*, 2010), and whether the forereef signal in Figure 5-4 may be a direct consequence of the boron isotopic composition of the river water. The residence of boron in seawater (*Lemarchand et al.*, 2002) suggests such far-field influences are unlikely. Furthermore, satellite observations suggest that salinity only fluctuates between approximately 36 psu and 37 psu (Appendix A-1), which would only result in a 0.008 variation in reconstructed pH from coral, well within the 0.07 pH unit error from the $\delta^{11}B$ measurements. Therefore, the pH variability is unlikely to be driven by resulting changes in salinity. and corals growing in regions with low salinity variability have previously been shown to possess a seasonal variability in $\delta^{11}B$ (*D'Olivo et al.*, 2015).

5.4.2 Impacts of pH on elemental ratios

The pH effect on the elemental ratios and partition coefficients is evident in Figure 5-8, Figure 5-10 and Figure 5-11. The observation that the partition coefficients of Sr/Ca and Li/Mg in the backreef field samples have an opposing relationship with pH (Figure 5-11) than what is expected from the cultured samples (Figure 5-8), which were temperature controlled, extends the evidence that temperature is not the only controlling parameter on elemental incorporation into coral skeletons.

The culture experimentsdemonstrate that Li/Mg has a negative relationship with pH (high pH = low Li/Mg; Figure 5-7), therefore in the summer when SST is high (low Li/Mg) and pH is low (high Li/Mg), there is a reduced temperature effect on Li/Mg. This could potentially explain the low sensitivity of Li/Mg to SST in the backreef coral compared to that observed in the forereef where we see high pH in the summer (Table 5-3), but it is worth noting that the variability in backreef and forereef variability (0.2 mmol/mol and 0.4 mmol/mol over the natural variation in pH (~0.25 pH units) is comparable with the Li/Mg range in a single culture experiment (0.3 mmol/mol to 0.4 mmol/mol). A significant negative correlation was also found between pH and Sr/Ca ratios (r^2=0.33, p<0.01; Table 5-2), matching the Sr/Ca-pH relationship found in the *Acropora digitifera* culturing study of *Tanaka et al.*, (2015), but in disagreement with the varying carbonate ion culturing experiment (CO_3^{2-}; pH 7.9 to 8.5) of *Gagnon et al.*, (2013) in *Stylophora pistillata*. Moreover, the Sr/Ca ratios of *S. pistillata* are more sensitive to changes in temperature than seawater carbonate chemistry, whereas in *S. siderea*, although forereef corals are also more sensitive to temperature than pH in the field, backreef corals have a greater sensitivity to field pH than temperature. The sensitivity of *S. siderea* Sr/Ca displayed in the cultured samples is double that observed in the field (forereef slopes of -1.090 ± 0.303 and -0.510 ± 0.221 respectively), and therefore *S. siderea* Sr/Ca ratios can be considered more sensitive to changes in pH_{sw} than temperature. Li/Mg ratios also demonstrated a significant negative correlation with pH (r^2=0.38, p<0.01; Table 5-2) at a constant temperature, which does not agree with the findings of *Montagna et al.*, (2014), where Li/Mg ratios across a range of species were found to be correlated with ΔCO_3^{2-} between the different environments, but this was argued to be a result of the strong correlations between CO_3^{2-} and temperature.

The potential pH control on Li/Mg and Sr/Ca is a candidate to also explain both the increased scatter in the lower temperature data for the Li/Mg-SST calibration set of *Montagna et al.*, (2014) and its non-linear nature. For example, cold-water corals such as *D. dianthus* live in deeper seawater where temperature is lower but an ambient pH is also low (e.g. 7.6 to 7.8; *Anagnostou et al.*, 2012), compared to an average of ~7.9 to 8.1 for tropical corals in this study. This seasonal pH variability will be folded into any simple calibration between observed seasonal SST variability and the Li/Mg ratio. As a result, any calibration based on seasonal temperatures will only hold true beyond the calibration interval if seasonal pH variability remains constant through time.

The most striking outcome of the pH corrections is that the variation in temperature sensitivity between the two reef zones was successfully resolved, resulting in the corrected Li/Mg-SST linear calibrations becoming within error of each other and the coefficients of

determination becoming very similar (r^2=0.38 and r^2=0.39 in the forereef and backreef respectively; Figure 5-12a,c and Table 5-3). Along with the forereef corrected Li/Mg-SST calibration becoming more similar to that of the backreef, it also becomes more similar to the culture derived calibration. The similarities between the corrected field Li/Mg-SST calibrations and the culture calibration means that as much ratio variability from pH has been accounted for as the culture calibration allows, particularly since the corrected calibrations generated from the extreme range in uncertainty of the culture calibrations do not have a large impact on the corrections (Table 5-4). However, since the absolute Li/Mg ratios of the backreef remain significantly lower than the forereef after the pH correction, (even within the extreme uncertainty range; Table 5-4), and in the cultures the ratios within each individual pH treatment vary by up to 0.3 mmol/mol, coupled with pH accounting for only 42% of the variability at a constant temperature, a third parameter must also be influencing Li/Mg ratios. The possibility of calcification rate influencing Li/Mg ratios is explored below in section 5.4.4.

Although correcting the SST calibrations for the influence of pH on Sr/Ca ratios revealed larger changes in Sr/Ca sensitivity to pH compared to Li/Mg, indicative of pH having a greater control over Sr/Ca ratios (Figure 5-12), such comparisons cannot be made confidently, due to the large uncertainty on both the slope and intercept of the cultured Sr/Ca-pH calibration (±0.3 and ±2.35 respectively; Table 5-2, Figure 5-7b).

Given the observed relationship between pH and Li/Mg in cultured *S. siderea* (Figure 5-7), long term changes in pH have the potential to significantly influence the SST reconstructed with the Li/Mg proxy. For instance, a decrease of pH from 8.1 to 8.0 pH units in the backreef since the 1920s would be expected to cause an increase of 0.04 mmol/mol of Li/Mg. Using the backreef Li/Mg-SST calibration, the Li/Mg ratio at 28^{o}C is 1.53 mmol/mol, so an increase of 0.04 mmol/mol would therefore only be equal to an apparent SST increase of 0.2°C (it is worth noting here that 0.04 mmol/mol is well within error of the calibration).

When multiple environmental parameters are expected to have changed over time (such as SST and pH through ocean warming and acidification), particularly if both of these parameters influence a proxy such as Li/Mg, a multivariable model may be able to resolve the difficulties above. Here, the impacts of SST and pH on Li/Mg and Sr/Ca were combined using a multivariable model, regressing each elemental ratio against both pH and SST simultaneously (Table 5-5). The resulting calibrations are unique to each reef zone, mostly due to the opposing elemental ratio-pH correlation between the two reef zones. The amount of variability that can be attributed to these combined effects is equal to or greater than considering those parameters singularly; for example, SST and pH are responsible for 33%

and 28% of the variability in their own right, but when considered in tandem up to 44% of variability can be explained by simultaneous changes in these parameters. Theoretically, if the pH cycle has not changed over a time-series, using these multivariable calibrations in conjunction with the δ^{11}B-pH proxy should generate more successful SST reconstructions from Li/Mg and Sr/Ca because the change in pH from ocean acidification will be accounted for through the seasonal range in pH. Unfortunately, the multivariable calibrations cannot yet be tested because there are no downcore sub-annually resolved samples.

So far, three lines of enquiry indicate that Li/Mg and Sr/Ca are partly influenced by parameters other than temperature and pH: (i) While the multivariable calibrations describe more elemental variation than temperature and pH individually, there is still <60% of scatter (for the significant calibrations; Table 5-5) unaccounted for. (ii) The difference between the forereef and backreef Li/Mg or Sr/Ca ratios where the sub-annual pH overlapped did not correlate with the difference in pH (Figure 5-6). (iii) Residuals between corrected and non-corrected ratios were not significantly correlated with pH (Figure 5-13), despite the significant inverse relationships between pH and measured ratios in both cultured and field samples. In *Fowell et al*., (2016), it was suggested that the discrepancy between forereef and backreef Li/Mg ratio derived SST reconstructions was potentially a consequence of these reef zones not sharing the same seawater pH. The difference in Li/Mg ratios themselves is driven by a difference in Mg/Ca ratios, which are on average 0.5 mmol/mol lower in the backreef. Following that study, the boron isotopic composition of the same corals showed that the pH of the backreef is indeed significantly lower than the forereef (Chapter 3). Here, the Mg/Ca ratios in the cultured corals exhibit a pH sensitivity 7 times greater than that of Li/Ca (Figure 5-8), making it feasible that differences in pH plays a role in the differences between forereef and backreef Li/Mg ratios. The cultures show a positive relationship between Mg/Ca and pH (Figure 5-8), so therefore the lower Mg/Ca ratios in the backreef field samples follow the expected trend from the lower seawater pH in this reef zone. Although the relationship between Mg/Ca ratios and pH can explain the difference in Li/Mg ratios, it does not answer the question of why there is such a large error associated with backreef Li/Mg-SSTs.

5.4.3 Potential microstructure effects on Li/Mg

Sr/Ca ratios have been shown to be reproducible in different theca walls of the same *S. siderea* colony (DeLong *et al*., 2014), and by using the near replicate samples from the backreef BR-06 core, it is established here that this also seems to be the case in our backreef

S. siderea coral (Figure 5-18). This, however, was not the case for Li/Mg, where we report that theca 1 has an average Li/Mg ratio of 1.52 mmol/mol, and theca 2 has an average of 1.38 mmol/mol, the difference between (~10%) which is significant ($p<<0.001$). This difference in Li/Mg ratios is driven by a significant difference in Li/Ca ratios between theca 1 and theca 2 (mean = 5.56 µmol/mol and 5.06 µmol/mol respectively, $p<<0.001$). Replicate theca analyses in *Porites* coral by Hathorne *et al*. (2013b) found the Li/Ca ratios of contemporaneous sampling transects to be mostly within error of each other, even over sections of anaomalously high ratios. The difference with our results is that we do not observe simultaneously high Mg/Ca ratios, which remain the same between theca 1 and theca 1 (Figure 5-18). This absence of higher Mg/Ca ratios in theca 1 makes it unlikely that a higher Li/Ca ratios in theca 1 are a result of unintentional incorporation of COC material (Hathorne *et al*., 2013b). Despite the differences in absolute Li/Mg ratios, the slope of the Li/Mg-SST correlation is the same in both sample sets (Figure 5-18a). In Chapter 4, it was discussed that the Li/Mg-SST calibration from the backreef failed to accurately reconstruct historic SSTs from downcore samples. This problem would not be solved by using the calibration from theca 2, because the scatter and the slope are comparable to theca 1. However, with this in mind, using samples from a different theca wall downcore may have contributed to some of the offset between the backreef Li/Mg-SST reconstructions and HadISST, but since this was also the case for the Sr/Ca based SSTs (which as noted earlier, have previously been demonstrated to replicate consistently across theca walls in *Siderastrea siderea*; *DeLong et al.,* 2011), and the sensitivity of Li/Mg to SST in theca 1 and theca 2 are comparable, this is not likely to be the main issue.

If the problem is approached on the skeletal microscale, the impact of including material from the centres of calcification in the columella can be considered. Unlike the cold-water coral *Lophelia pertusa*, which shows no change in Li/Mg composition between the theca wall and columella (which hosts the centres of calcification; COCs) (*Montagna et al.*, 2014), a comparison study by *Meibom et al.*, (2006) discovered that in the tropical coral *Colopophyllia sp* the Li/Ca and Mg/Ca were enriched 120% and 100% respectively in the COCs relative to the fibrous aragonite as opposed to only a 10 to 15% enrichment of Sr/Ca. COC data in this study is very limited, lacking a full sampling path, and does not allow the impact of COC sampling to be confidently quantified. Nevertheless, the maximum difference between a COC and theca sample (Jul-Sep) in terms of Li/Mg is 0.24 mmol/mol (Figure 5-19), making the COC ~20% more enriched than the theca wall as a result of ~10% more Li/Ca and ~10% less Mg/Ca. If the COCs can enrich Li/Mg up to 20% in *S. siderea*, this is enough to explain the offset between backreef theca 1 and theca 2. However, there

was no difference between either of the COC samples and the theca wall sample from Apr-Jun, implying an inconsistent offset occurs, which does not fit with the consistent offset between theca 1 and theca 2 in BR-06 (Figure 5-18). Therefore, incorporation of COC material may increase the Li/Mg ratio of theca wall samples in *S. siderea* but a more thorough investigation needs to be completed, so it is recommended that the practice of sampling theca walls in high-resolution studies is continued.

5.4.4 Impacts of cultured coral calcification rate on elemental ratios

Despite growth under tightly controlled conditions, the cultured samples exhibit considerable variability for Sr/Ca and Li/Mg (Figure 5-9) within a given experiment in both the temperature and pH experiments, implying that another factor(s) influences Li, Mg, and Sr uptake into the coral skeleton within the bounds of the experimental conditions. Some of this scatter is likely a result of pH variations between the different tanks, yet all the samples here have been treated under the assumption that they experienced and archived the mean pH for each experiment. Although significant parabolic relationships were found between calcification rate and temperature or pH by *Castillo et al.*, (2014), there is a large variation in calcification rates within each treatment, but there is no apparent correlation between the range of calcification and the range of conditions to which the corals were exposed (Figure 5-14). On average, the calcification rate of the corals cultured at 32°C is 75% less than those at 28.16°C. Therefore the geochemical data from the samples cultured at 32°C must be treated cautiously, given that the slower calcification rate may be a stress response to the high temperature (e.g. *De'ath et al*., 2009), and that calcification rate has previously been shown to impact Sr/Ca ratios (*Cohen et al.*, 2001; *Gaetani and Cohen*, 2006), although this is not thought to be the case in *S. siderea* (*DeLong et al*., 2016).

Despite there being no significant correlations between Li/Ca or Mg/Ca and calcification in the 25°C cultures, one exists between Li/Mg ratios and calcification at 25°C. There were, however, calcification rate effects on Mg/Ca ratios in the remaining pH cultures. This was anticipated, given that Rayleigh Fraction should cause Mg/Ca ratios to increase with faster precipitation because Mg^{2+} ions become more available relative to Ca as Ca is removed from the calcifying fluid, because the K_D Mg/Ca is <1. This was the case in the 28°C cultures, but the 32°C cultures displayed the opposite trend (Figure 5-15).

Based on transcriptomic evidence, one might have expected to see a correlation between Li/Mg and calcification rate, such as that observed when the data from each individual pH experiments are combined and Li/Mg ratios are significantly anticorrelated

with calcification rate in the pH variation experiment (Figure 5-15c). This is because *S. siderea* grown under higher pCO_2 conditions (lower pH) expressed more H^+ membrane transporter genes and an ATP synthesis coupled proton transport gene, both of which are vital for removing excess H^+ ions from the ECF than colonies grown at lower pCO_2 conditions or higher temperatures (*Davies et al.*, 2016). Nevertheless, calcification rate is not correlated with Li/Mg ratios within the individual experiments (Figure 5-15a,c), supporting the suggestion that the Li/Mg-SST proxy removes the effects of skeletal growth, as anticipated by Rayleigh fractionation models (and noted by *Gagnon et al.*, 2007 and *Montagna et al.*, 2014). However, there is one exception to this finding, given that the Li/Mg ratios in the 25°C experiment were significantly negatively correlated with calcification rate (Figure 5-15a). This could be caused by a greater expression of proton pumping genes expressed at 25°C than 32°C (*Davies et al.*, 2016) and this is only significant in Li/Mg because Sr has a larger ionic radius than either Li or Mg (*Shannon*, 1976), so it may be the case that if the pool of calcifying fluid becomes more open (or "leaky"), smaller ions may become more readily incorporated into the aragonite lattice.

Sr/Ca was not found to have a significant relationship with calcification ($p>0.5$) in either of the experiments, agreeing with the findings in the field samples of *Alibert and McCulloch*, 1997, *Swart et al*., 2002, and *DeLong et al*., 2011, and inorganically precipitated aragonite (*Mucci et al.*, 1989), but disagreeing with the inverse correlation in the species *Stylophora pistillata* (*Ferrier-Pagès et al.*, 2002).

5.5 Conclusions and recommendations of further study

This study provides the most comprehensive assessment of potential secondary impacts on the Li/Mg-SST proxy in coral to date, focussing on the influence of pH, and comparing the results to the popular Sr/Ca-SST proxy. Sub-annual measurements of $\delta^{11}B$ revealed opposing correlations between pH and Li/Mg in the forereef and backreef zones, where the correlation is positive in the FR-12 coral and inverse in the BR-06 coral. Using elemental ratio-pH calibrations based on *S. siderea* cultures from a pH range of 7.32, 7.82 and 8.07, and the $\delta^{11}B$ based pH reconstructions of the field samples, the SST calibrations were corrected for the influence of pH on both Li/Mg and Sr/Ca ratios in forereef and backreef coral. Once the influence of pH on these ratios had been removed, the corrected SST calibrations of both reef zones became within error of each other, despite a persistent significant difference between forereef and backreef Li/Mg absolute values.

Multivariable calibrations combining the influence of SST and pH, which were shown to correlate equally or more strongly to Li/Mg and Sr/Ca ratios, may hold the key to reconstructing more accurate historic temperatures across a time-series where ocean acidification has caused pH to decline. However, in the current absence of downcore pH reconstructions at a sub-annual resolution, these calibrations remain untested, and also still leave a large amount of variation in the elemental data that cannot be ascribed to either temperature or pH.

Microstructure variations were identified as an additional possible cause of Li/Mg scatter due to the consistent offset of Li/Mg ratios between two separate theca walls. Li/Mg is potentially enriched by up to 20% in columella COC samples but this was not reproducible and therefore an in depth study of the spatial variability on the scale of individual colonies of coral, including more analyses of COCs, is required to fully quantify the potential microstructure effects on Li/Mg ratios and the impact that unintentional incorporation of these into the theca samples may have.

Finally, calcification rate was also investigated as a potential influential factor on elemental ratios, but neither Li/Mg ratios nor Sr/Ca ratios were identified as being significantly correlated with calcification rate when either the pH or temperature of the culture media was varied. The only exception was the significant inverse relationship between Li/Mg ratios and calcification rates at 25°C, potentially suggesting that an increase in proton pumping at lower temperatures (*Davies et al.*, 2016) causes the calcifying fluid to become less isolated, allowing ions with small ionic radii to be incorporated into the skeleton more easily.

Although progress has been made in developing an understanding of the influence of pH, calcification rate and microskeletal structures on Li/Mg ratios, the latter two are not yet fully quantified and need to be studied in more detail in addition to other potential controlling factors not explored here. After assessing the potential influences of the Li/Mg-SST proxy, it is recommended to be used with caution and preferably in tandem with other proxies such as the δ^{11}B-pH proxy so that multivariable calibrations can be tested and applied.

Chapter 6: Conclusion

6.1 Thesis summary

To summarise, this thesis has made novel contributions to the field of coral geochemistry and our understanding of how corals are responding to anthropogenic stressors. In Chapter 3, using the first century-long record of the boron isotopic composition of *S. siderea* colonies, riverine inputs of terrigenous nutrients were shown to mask the ocean acidification signal in the forereef while a decline in extension rates in this reef zone were observed. This indicates that ocean acidification is not a major driver of changes in coral calcification in Belize. In chapter 4, the first calibration of the Li/Mg-sea surface temperature (SST) proxy in *S. siderea* was generated in a forereef and backreef colony, demonstrating that Li/Mg is a credible addition to the SST proxy toolbox. However, the significant difference between the SST reconstructions for the forereef and backreef indicate a secondary parameter affects this proxy, the impact of which can be reduced by applying a multi-elemental proxy. Chapter 5 presents the first multi-year monthly resolved boron isotope time-series of corals and are used as part of an extensive investigation into secondary influences on the Li/Mg-SST proxy, and identified a significant influence of pH on both Li/Mg and Sr/Ca ratios. However, this did not describe all of the remaining variability that remained from the temperature correlation, leaving a third (or more) parameter(s) still in question, suggesting that multi-proxy reconstructions present a more accurate alternative than single-proxy based climate reconstructions.

6.2 Main conclusions

6.2.1 Chapter 3: Declining coral extension in Belize decoupled from ocean acidification

The aim of chapter 3 was to use annually resolved $\delta^{11}B$ measurements to reconstruct a century-long record of pH reconstructions in the Sapodilla Cayes, Belize. This was successfully performed in two different sections of the reef – the forereef and the backreef. Through doing this, it was revealed that there was no recorded decrease in the forereef pH, despite an observed decrease in extension rates. This was in stark contrast with the backreef, which acidified by ~0.15 pH units without causing any decline in extension rates. To

investigate possible causes of these spatial differences, monthly resolved Ba/Ca ratios were measured, and they demonstrate that the amount of terrigenous sediment deposited in the forereef has significantly increased over a century, likely as a direct consequence of increased land clearance, agriculture and population – not as a result of change in precipitation volumes. The significantly larger availability of nutrients in the forereef stimulated an increase in macroalgae cover and therefore an increase in the use of inorganic carbon, driving up local pH. The most significant finding of this chapter was therefore the lack of correlation between ocean acidification and coral extension, implying that ocean acidification is not a major driver of coral growth in this region.

6.2.2 Chapter 4: Intra-reef variations in Li/Mg and Sr/Ca sea surface temperature proxies in the Caribbean reef-building coral *Siderastrea siderea*

Chapter 4 aimed to test the applicability of the Li/Mg-SST proxy and compare it to the traditional Sr/Ca-SST proxy in the coral *S. siderea*. This study found that the Li/Mg-SST proxy works equal to or better than the Sr/Ca-SST proxy in forereef, and can be used to reconstruct historic temperatures not significantly different to the HadISST record and to an accuracy of 1.5°C, demonstrating that Li/Mg is a useful addition to the SST proxy toolbox in some circumstances. However, neither of the SST proxies worked equally well in backreef corals. Here, SST reconstruction accuracies were limited to 2.7 and 4°C for Li/Mg and Sr/Ca respectively, in conjunction with absolute reconstructed values ranging between 15 and 35°C, which is not representative of the HadISST and would likely prove fatal to coral. However, multi-proxy SSTs (combining Li/Mg and Sr/Ca ratios, or Li/Ca, Mg/Ca, Sr/Ca ratios) can increase reconstruction precision by <0.4°C against single proxy calibrations in the forereef, and <2.2°C in the backreef.

6.2.3 Chapter 5: Examining the effect of pH on Li/Mg- and Sr/Ca-SST proxies: insights from culture and sub-annual boron isotope data

Chapter 5 aimed to determine the secondary impact on the Li/Mg-SST proxy identified in Chapter 4. The most thoroughly investigated variable was pH, and this was explored using monthly to seasonally resolved $\delta^{11}B$ field samples and cultured samples. The $\delta^{11}B$ measurements revealed a seasonal cycle in pH in both reef zones, although the seasonal

range in the forereef was the largest and correlated positively with SST in contrast to the backreef pH. Correlations between pH and Li/Mg and Sr/Ca existed in both the field and cultured samples, but Sr/Ca is more sensitive to pH changes than Li/Mg is. Using the elemental ratio-pH calibrations in the cultured samples, the field SST proxies can be corrected for changes in pH (as calculated from $\delta^{11}B$). This brought the SST calibrations for Li/Mg in both reef zones to be within error of each other, and in the case of Sr/Ca, the backreef calibration becomes more similar to the cultured elemental ratio-SST calibration. However, combining SST and pH in multivariable calibrations did not account for all the variability in either Li/Mg or Sr/Ca, and potentially differences in microskeletal sampling or calcification rate were not significant and therefore do not cause the remainder of variability.

6.3 Further study

6.3.1 Mesoamerican Barrier Reef System observations for improved proxy calibrations

The study of the Sapodilla Cayes corals is not only limited by a lack of measurements of the carbonate system, water quality and terrestrial inputs, but also in ecological data such as reef survey transect data that could identify any difference in coral cover and species (both coral and fish) abundance between the different reef zones. Further studies of this area should take full advantage of new sensor technology by deploying loggers across the forereef and backreef of the Mesoamerican Barrier Reef System and in the estuaries of the most influential Guatemalan rivers. It is now possible to purchase sensors that can simultaneously measure pH, salinity, temperature, chlorophyll and phosphorous, and if these were deployed on the reef for a minimum of 12 months we would be able to constrain the variability in these parameters and investigate how such cycles impact geochemical proxies such as $\delta^{11}B$, Li/Mg and Sr/Ca, or use the data to attempt to calibrate the $\delta^{11}B$ pH proxy or nutrient and primary production proxies. By collecting an abundance of environmental data, it may become possible to identify which parameter is responsible for causing the different sensitivity of Li/Mg and Sr/Ca to SST in the forereef and backreef coral, or the process responsible for the rapid acidification signal in the backreef coral.

6.3.2 Nutrient profiles of the Mesoamerican Barrier Reef

To improve our understanding of how nutrification is influencing coral calcification and differences in pH across the MBRS, a complete assessment of nutrient availability in the water column and sediment needs to be made. Seawater sample collections should be made from the mouths of the major Honduras, Guatemala and Belize rivers and across different parts of the reef in the Sapodilla Cayes for nitrate,phosphate, Ba and other trace metal analyses. These results would allow us to map the concentrations and pathways of the various nutrients across the reef. In conjunction, reef transects that identify the macro- and turf algae at a species level and total algae cover should be a priority and may also be combined with fish surveys (although *Suchley et al.*, (2016) did not find any correlation between herbivorous fish numbers and increasing macroalgae coverage in the MBRS) to determine what, if any, the difference between these parameters is between the forereef and backreef zones. Additionally, the annual samples from the cores used in this study (and more) should be analysed for their $\delta^{15}N$ composition. Previous studies in corals have shown that the skeletal $\delta^{15}N$ composition is an effective monitor of the organic matter in coral skeletons ($\delta^{15}N_{coral}$), which can vary with that of nitrogenous sources and track changes in fertilizer use through agricultural runoff into reef waters as a decline in $\delta^{15}N_{coral}$ (*Uchida et al.*, 2008; *Yamazaki et al.*, 2011). Potentially, samples of macroalgae could be collected for nitrogen isotope analysis as a way to determine what the main source of nitrogen is in each region, for example, macroalgae which utilise sewage derived nitrogen are more enriched than macroalgae which uses atmospheric nitrogen (*Lapointe et al.*, 2005).

6.3.3 Bermuda samples

As an addition to the Belize samples, a number of cores were collected from Bermuda. A full description of the sampling strategy is provided in Appendix C, but to summarise, three individual colonies of three coral species were cored (*Porites astreoides*, *Diploria strigosa*, *Diploria labyrinthiformis*), and two replicate cores were drilled from each colony. Bermuda was selected as a sampling site for a number of reasons; firstly, extensive local observations of the carbonate system and SST are available, which present the opportunity to calibrate multiple environmental proxies. Secondly, limited industry and agriculture may suggest low levels of chronic pollution, so any changes in calcification rates over time are likely to be a direct result of ocean acidification or ocean warming and subsequent ecosystem changes. Thirdly, corals in Bermuda are already growing close to the limits of aragonite saturation,

so assessing their response to climate change over the last century may provide a framework for other corals. The main goal of the Bermuda samples was to extend the Bermuda Atlantic Time-series (BATS), generating geochemical reconstructions beyond the 1983 starting point of BATS using well-constrained calibrations generated from samples at the top of the core. The aims of the study using the Bermuda coral samples are therefore to calibrate the boron isotope ($\delta^{11}B$) pH proxy and Li/Mg- and Sr/Ca SST proxies in multiple coral species. By applying these geochemical to make climate reconstructions, it would be possible to being to determine the changes in calcification rate and begin to form projections of the changes in seawater chemistry and coral calcification we might expect to see in the future.

The *Porites astreoides* core 1B dates from 1949 to 2014, and core 3B ranges from 1969 to 2014 (Figure 6-1). Two to three years were sampled at a bimonthly to seasonal resolution from the top of the core (~2011 to 2014), the middle (~1986 to 1989; the beginning of the BATS record) and the downcore (~1974-1977) of two of the *Porites* cores (slabs need to be X-rayed now they have been milled in order to confirm the years). The multielemental ratios of each of these samples were measured, and using the Sr/Ca and Li/Mg ratios, the seasonal cycles of the samples were identified. The samples representative of winter growth (identified by high Sr/Ca ratios) were selected to be analysed for their $\delta^{11}B$. From Figure 6-2 it is evident that seasonal cycles have been captured in some sections of the cores, but less successfully in other sections, particularly in the oldest samples. Part of the problem may be the relatively low sampling resolution, and these measurements should be repeated in other *P. astreoides* cores that were collected, and also assess the variation between different species by performing the same measurements on the faster growing *Diploria sp.* samples. The $\delta^{11}B$ of the two cores show opposing trends in long term pH variability, as core 1B shows an increase in $\delta^{11}B$, in contrast to core 3B which shows a decrease in $\delta^{11}B$ (Figure 6-3).

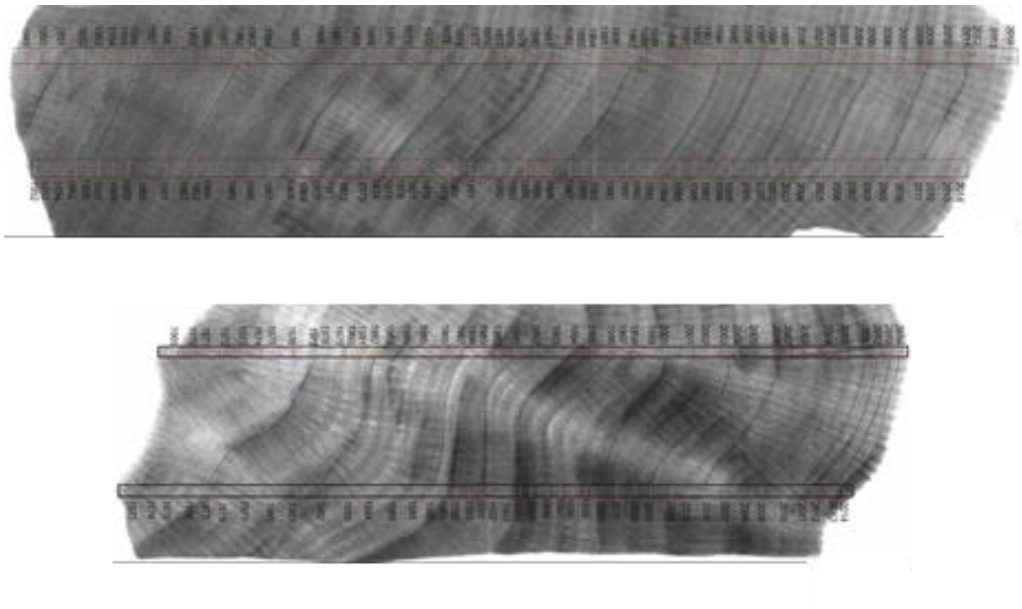

Figure 6-1. Dated X-rays of *Porites astreoides* slabs. a) Core 1B. b) Core 3B.

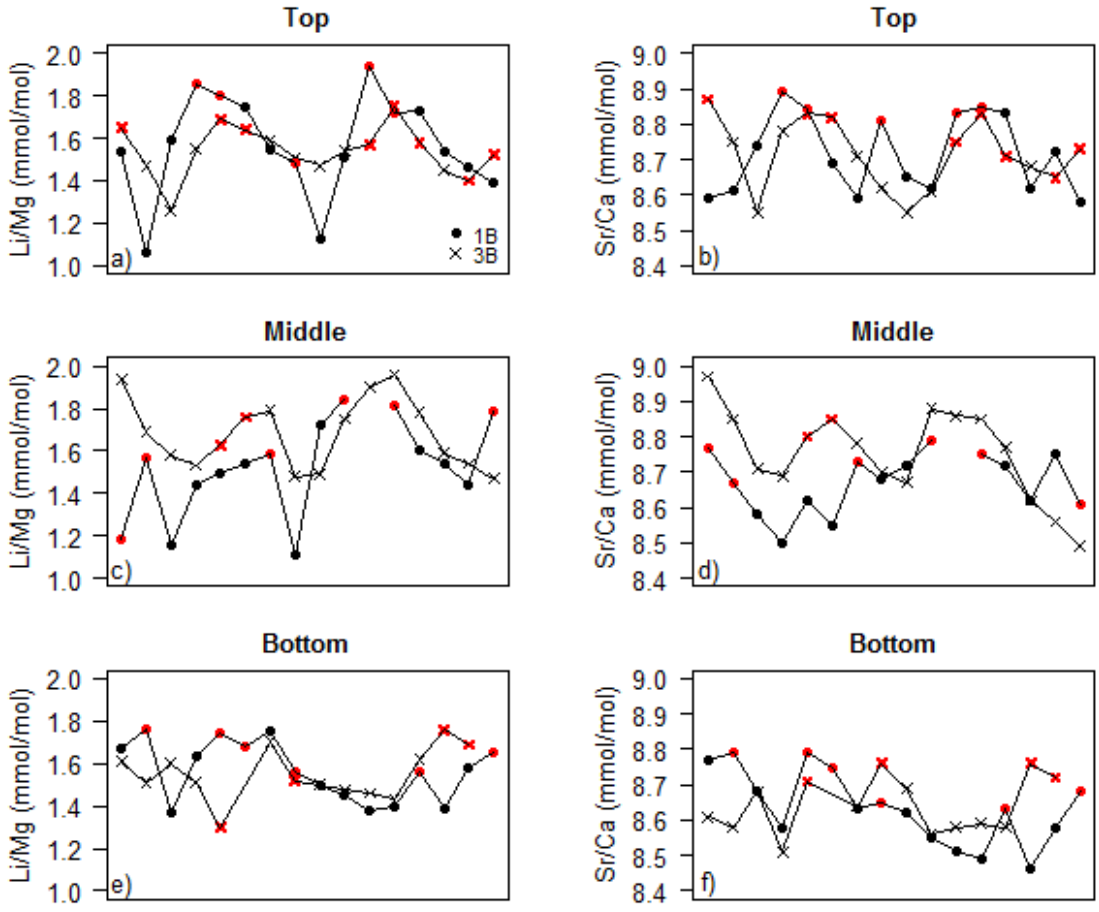

Figure 6-2. Li/Mg and Sr/Ca ratios from the top (~2011-2014), middle (~1986-1989) and bottom (~1974-1977) sections of the *Porites astreoides* cores 1B (circles) and 3B (crosses). The red symbols indicate the samples selected to be analysed for their boron isotopic composition.

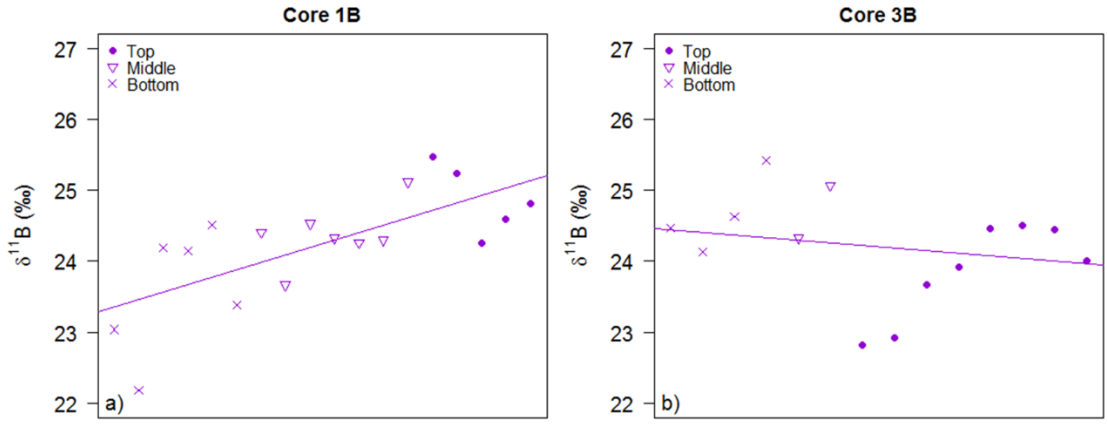

Figure 6-3. Boron isotopic composition of *Porites astreoides* cores (a) 1B and (b) 3B. Crosses represent downcore samples, triangles represent 1980s samples, and circles represent 2013 samples.

The coral cores should also be CT scanned to determine the density and calcification rate and investigate whether the skeletal structure has changed over time, and quantify any rate of change, allowing an apparent link between ocean acidification and declining coral calcification (*Bates et al.*, 2010) to be investigated.

6.3.4 Calibrate the δ^{11}B-pH proxy

The δ^{11}B-pH proxy has been successfully calibrated in various *Porites* species, *S. pistillata* and others, but no calibration has been generated for *S. siderea*, so throughout this thesis, calibrations from the species *Porites cylindrica* (*Hönisch et al.*, 2004) was used and this is likely to have introduced errors in our absolute pH values (but will not have affected the relative difference between the reef zones or throughout the time-series or the reported rate of change). Once we have species-specific calibrations (or indeed, reef zone calibrations) of the δ^{11}B-pH proxy in *S. siderea*, it would be possible to quantify the absolute pH change across the MBRS over the last century, rather than rely on the relative change between the beginning and the end of the record, allowing our results to be more comfortably assessed against other pH reconstructions from reefs across the globe.

Alternatively, rather than a different colony in separate tanks of unique pH, the calibration could be performed using a single colony, providing a longer growth time was allowed. This could be done by making a coral with a traceable isotopic signature, culturing it at a particular pH until enough calcification had occurred to sample, then change the isotopic signature of the seawater and change the pH conditions and so on until the control had been cultured at a full pH range.

Calibrations could be made using *in situ* measurements and field samples, or culturing a number of individuals in aquaria of different conditions, or culturing single colonies for a longer period of time and adjusting the conditions and isotopic composition of the seawater every few months. It would also be interesting to compare the different techniques using a single species. An attempt has already been made to generate a δ^{11}B-pH calibration using cultured samples of *S. siderea*, but there was too much δ^{11}B variability between tanks of the same treatment to generate a calibration (Figure 6-4; M. Henehan, unpublished data), potentially due to the composition of the artificial seawater and the inadvertent sampling of pre-culture material grown in natural seawater. As anticipated, *S. siderea* δ^{11}B is offset from the borate ion curve, indicating vital effects such as pH-upregulation are affecting the skeletal δ^{11}B, but the δ^{11}B is currently much higher than other species. Future culturing experiments would benefit from using natural seawater rather than artificial seawater.

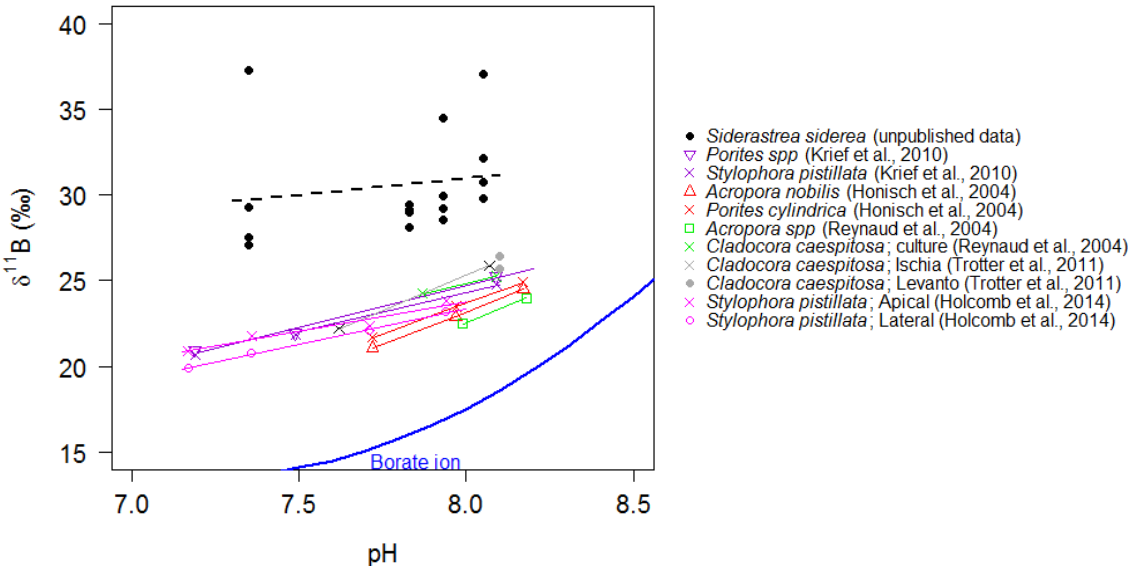

Figure 6-4. Preliminary boron isotope data from cultured *Siderastrea siderea* (black circles) in comparison to existing calibrations of other tropical coral species.

6.3.5 Determine the extent of pH-upregulation in *S. siderea* and assess the impact of observed climate change on this mechanism

The coral species *S. siderea* appears to possess high levels of resilience to the impacts of climate change, and part of this may be a result of pH-upregulation. However, this has not yet been quantified in *S. siderea*, and without a species-specific δ^{11}B-pH proxy, it has not been possible to determine this during the course of this PhD. Given the apparent lack of impact from ocean acidification on backreef colonies of *S. siderea*, pH-upregulation is

anticipated to play a major role in this, but what is the energetic cost of this to the coral, how sustainable is it, and are backreef corals capable of larger internal pH changes than forereef corals? This could either be determined using *in situ* pH data from field observations to calibrate the δ^{11}B-pH proxy as discussed above, or alternatively, forereef and backreef colonies could be cultured under controlled conditions and their internal pH could be measured using pH indicator dyes or microprobes. In addition to the importance of pH_{cf} for the calcification process itself, understanding how pH_{cf} relates to seawater pH is also of critical importance for the development of seawater pH proxies. For the corals themselves, understanding how this mechanism changes during chronic acidification will provide a vital insight into how coral calcification will respond to predicted levels of ocean acidification in the twenty first century.

6.3.6 Determine possible changes in the seasonal pH cycle over the twentieth century

In Chapter 5, it was revealed that the forereef and backreef pH cycles are controlled by different primary parameters. It would be possible to establish if the opposing relationships between pH and SST in the forereef and backreef are due to anthropogenic stressors such as nutrification by sampling downcore at high resolution and analysing the boron isotopic composition to see if the pH cycles are synchronised between the two reef zones during times when humans had a smaller impact on the reef.

6.4 Concluding remarks

This PhD has made significant contributions to the understanding of the suitability of geochemical proxies in corals to reconstruct century long records of ocean acidification and ocean warming. This study is the first to use Li/Mg ratios from *Siderastrea siderea* to reconstruct historic SST and it was successful in terms of generating reconstructed SSTs with either equal or greater precision to those from Sr/Ca ratios. However, the assessment of the reconstructed temperatures from two different reef zones and cultured samples highlights the significant impact of secondary parameters on this proxy that, despite the thorough examination seen here, are still not fully understood. By using a suite of climate proxies, this project has demonstrated the resilience of the coral *S. siderea* to current levels of ocean acidification and ocean warming, but vulnerability to chronic terrestrial pollution. This

drives home the notion that the response of corals to climate change is regional, and that to protect them in the future, policy and management needs to limit global greenhouse gas emissions and improve regional watershed management.

Appendices

Appendix A Supporting information for Chapter 3

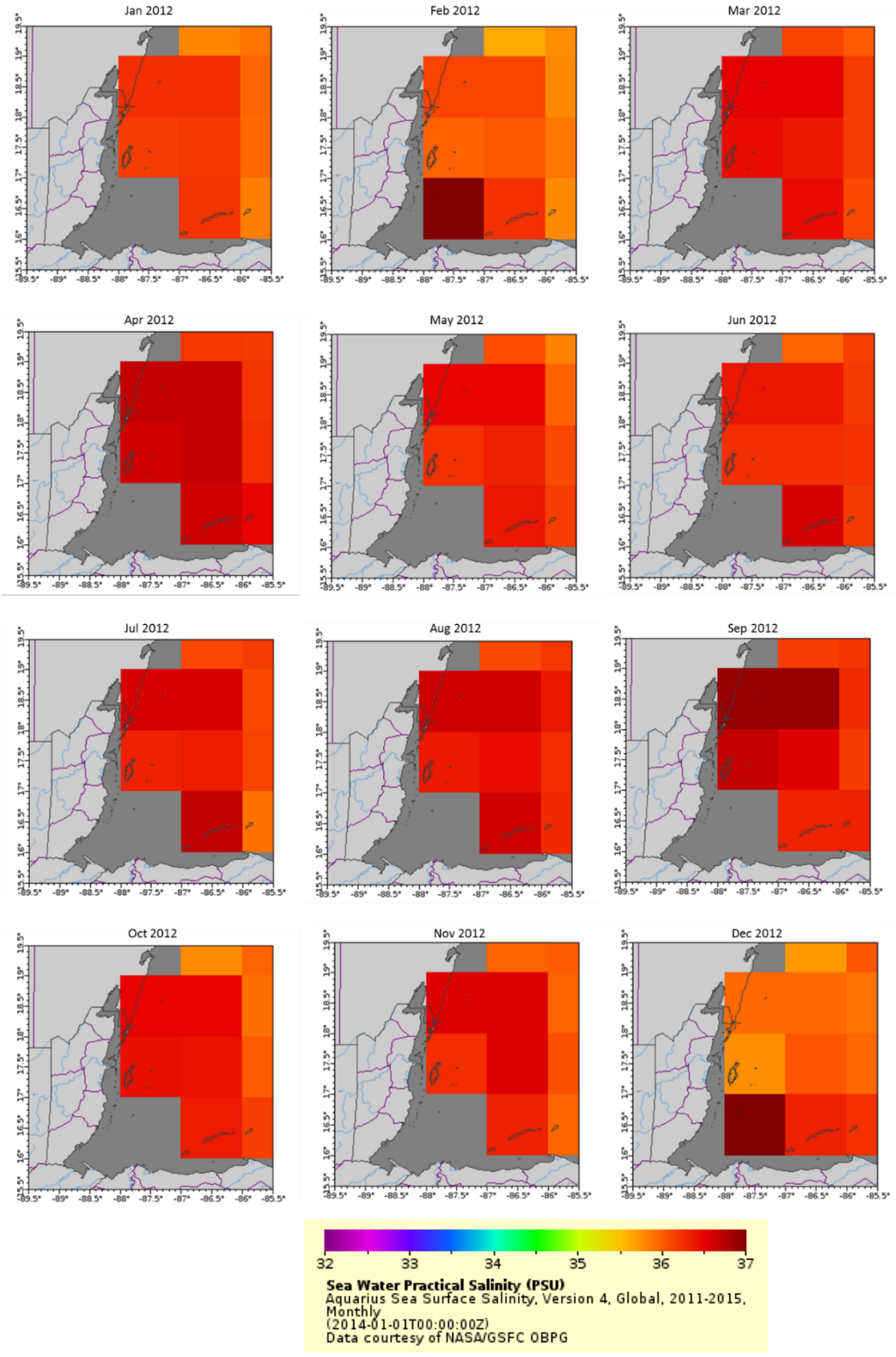

Figure A-1. Monthly sea surface salinity from the Caribbean Sea near to Belize as measured by the Aquarius satellite (Version 4) between January and December 2012. The grid square closest to the sampling site only contains data for the months of February and December 2012.

Appendix B Supporting information for Chapter 4

Text B1

The standard set-up for the Element ICP-MS at the University of Southampton includes an additional ammonia (NH_3) gas introduced into the spray chamber at a flow rate of 0.07 ml min^{-1} simultaneously with the sample gas to make the internal environment more basic (*Al-Ammar et al.*, 2000; *Ni*, 2006). This is necessary for obtaining precise, reproducible B/Ca ratios (although these are not the subject of this particular study) by facilitating instrumental B-wash out (*Al-Ammar et al.*, 2000; *Ni*, 2006).

Whilst the addition of NH_3 gas improves the B-washout it introduces an additional interference on ^{7}Li by $^{14}N^{++}$. This however can be adequately resolved in low resolution mode by moving the analyte mass window to focus on a section of the $^{7}Li^{+}$ peak where the interference is reduced. The peak center was chosen to be a mass (typically ~7.015 amu) which would allow for some minor drift (Figure A1). Combined with careful background determination this ensured a minimal impact of $^{14}N^{++}$ on ^{7}Li.

Text B2

To determine if our cleaning protocol alters the trace element ratios of coral, a cleaning test was performed on JCp. Four 5 mg samples of JCp were subjected to the full coral cleaning procedure (section 2.3.2), and an additional four 5 mg samples were directly dissolved in 0.5 M HNO_3. The trace elemental composition of these samples were determined using the Element ICP-MS (section 2.3.3), and bracketed against the external standard BSGS (*Ni*, 2006; *Ni et al.*, 2007). To correct for the mean difference between JCp bracketed against BSGS or the external standard used in this study, the Li/Ca and Mg/Ca ratios were decreased by 3.6% and 6.12% respectively, and the Li/Mg and Sr/Ca ratios were increased by 3.42% and 0.79% respectively. As stated in the main text, the Li/Ca and Mg/Ca ratios declined 25% as a result of cleaning, but the Li/Mg ratios are not impacted by this procedure and equally, the Sr/Ca ratios are consistent between cleaned and uncleaned samples (Figure A2).

Figures

Figure B1

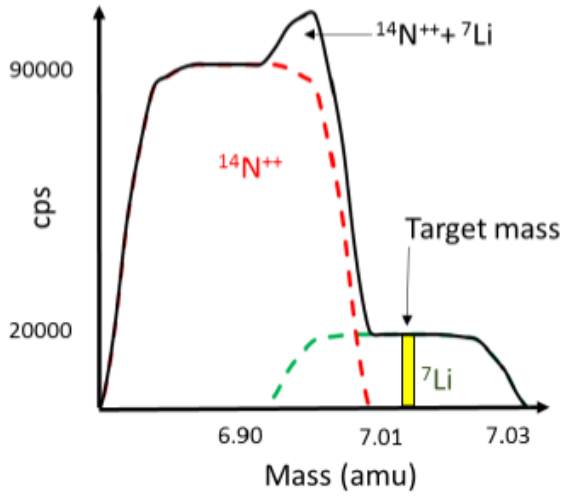

Figure B1. Schematic of the isobaric interference on ^{7}Li from $^{14}N^{++}$. A typical ^{7}Li peak (green dotted curve) has ~20,000cps (0.1 ppb) when ^{115}In and ^{138}U sensitivity is 200 x 10^{3} cps per 0.1 ppb. The red dotted curve reveals the $^{14}N^{++}$ isobaric interference located at the left (lower mass) of the ^{7}Li peak with an intensity of ~90,000 cps for the same tuning conditions as above, when additional gas (NH_3) is set to 0.070 ml min^{-1}. The area where these overlap causes a $^{7}Li^{+14}N^{++}$ spike. Note that the ^{7}Li blank is insignificant compared to the signal (typically ~200 cps or 1 ppt).

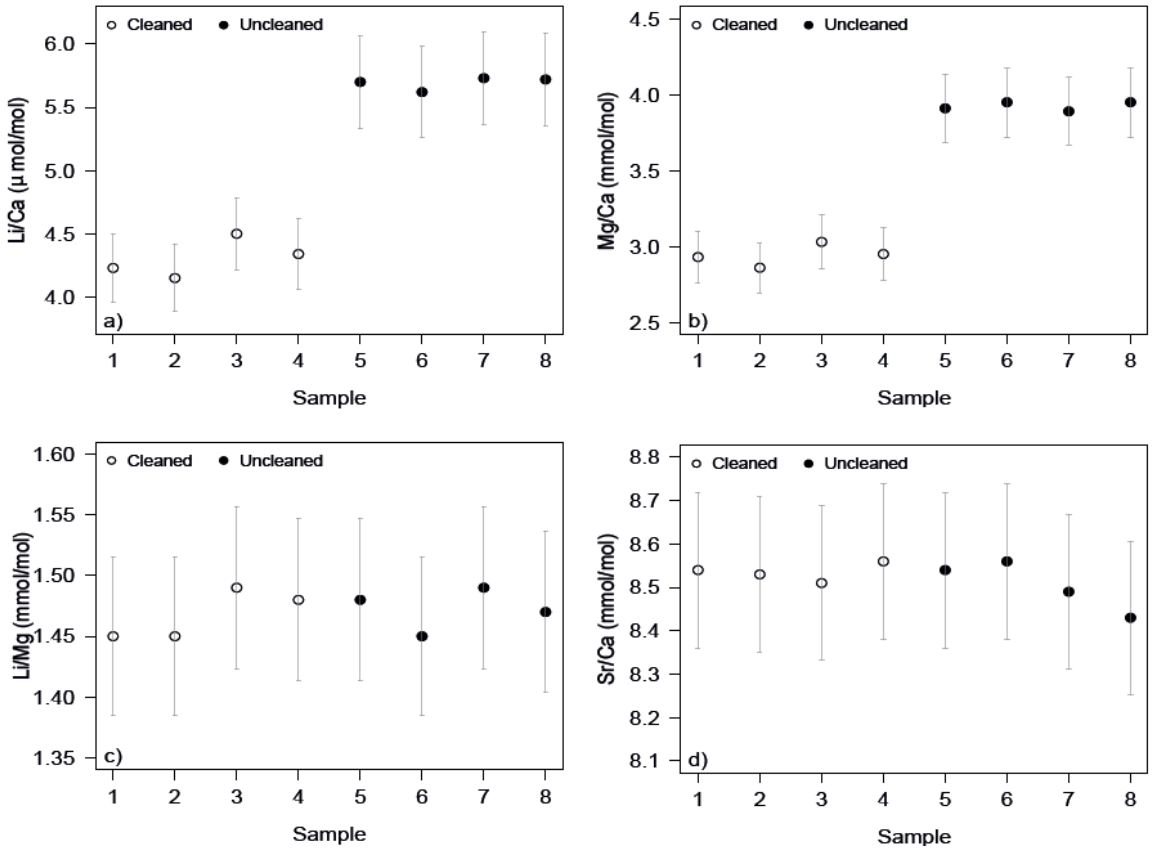

Figure B2. Results of JCp-1 elemental analysis after samples were either cleaned (open circles) or directly dissolved in 0.5 M HNO_3 without being cleaned. (a) Li/Ca and (b) Mg/Ca ratios are lower in cleaned samples, in contrast to (c) Li/Mg and (d) Sr/Ca ratios which are unaffected by the cleaning process. Error bars represent the 2σ external precision based on long term measurements of JCp-1 bracketed against the Cardiff University multi-element standard.

Table B1. Inner reef and outer reef data logger temperature, and Reynolds sea surface temperature composites for the forereef and backreef regions, and HadISST1 (2002-2008).

Date	Inshore logger (°C)	Offshore logger (°C)	Reynolds forereef (°C)	Reynolds backreef (°C)	HadISST (°C)
Jan-02			26.41	26.43	26.82
Feb-02			26.73	26.72	26.71
Mar-02			27.00	27.10	26.93
Apr-02			27.98	28.18	28.00
May-02			28.58	28.73	28.49
Jun-02			30.07	30.29	28.95
Jul-02	29.33	29.33	29.34	29.46	28.84
Aug-02	29.56	29.51	29.58	29.68	28.99
Sep-02	29.93	29.82	30.21	30.36	29.37
Oct-02	29.39	29.40	29.36	29.36	29.27
Nov-02	28.49	28.46	28.49	28.59	28.22
Dec-02	27.07	27.28	27.33	27.33	27.41
Jan-03	25.60	25.93	26.04	25.80	26.39
Feb-03	26.04	26.14	26.40	26.31	26.50
Mar-03	28.19	27.91	27.99	28.18	27.02
Apr-03	28.06	27.79	27.94	28.04	27.71
May-03	29.48	29.08	28.88	28.95	28.32
Jun-03	30.47	30.06	29.86	30.04	28.74
Jul-03	29.85	29.72	29.20	29.37	28.89
Aug-03	29.78	29.70	29.46	29.49	29.24
Sep-03	30.48	30.35	30.02	30.12	29.49
Oct-03	30.14	30.02	29.5	29.47	29.01
Nov-03	28.77	28.67	28.61	28.53	28.24
Dec-03	26.86	26.98	27.00	26.90	27.27
Jan-04	25.53	26.09	26.22	26.05	26.63
Feb-04	26.76	26.64	26.71	26.71	26.51
Mar-04	26.88	26.79	26.78	26.83	26.83
Apr-04	28.16	27.92	28.06	28.14	27.75
May-04	28.79	28.56	28.43	28.48	28.26
Jun-04	29.40	29.26	29.13	29.24	28.73
Jul-04		29.35	28.83	28.88	29.03
Aug-04		29.99	30.04	30.04	29.39
Sep-04		30.32	29.74	29.85	29.47
Oct-04		29.83	29.16	29.12	29.02
Nov-04		28.40	28.11	28.05	28.18
Dec-04	26.81	27.34	27.34	27.28	27.34
Jan-05	26.32	26.40	26.45	26.33	26.49
Feb-05	25.99	26.26	26.43	26.37	26.44

Mar-05	27.57	27.52	27.30	27.46	26.75
Apr-05	28.69	28.27	27.92	28.10	27.77
May-05	29.59	29.27	29.38	29.66	28.54
Jun-05	30.46	30.15	30.15	30.29	28.85
Jul-05	30.44	30.13	30.19	30.22	29.13
Aug-05	29.80	29.69	29.98	29.95	29.32
Sep-05			29.84	29.91	29.47
Oct-05			29.2	29.24	28.77
Nov-05			27.54	27.50	27.86
Dec-05			26.91	26.85	27.08
Jan-06			26.41	26.38	26.45
Feb-06			26.08	26.00	26.31
Mar-06			26.85	26.95	26.62
Apr-06			27.95	28.04	27.63
May-06			28.74	28.89	28.35
Jun-06			28.87	28.92	28.39
Jul-06			29.21	29.16	28.98
Aug-06		29.97	29.25	29.15	29.37
Sep-06		30.14	29.79	29.72	29.36
Oct-06	29.87	29.47	29.15	29.17	28.98
Nov-06	28.30	28.50	28.38	28.37	28.11
Dec-06	27.23	27.14	27.01	26.94	27.45
Jan-07	26.98	27.14	27.13	27.14	26.84
Feb-07	27.24	27.25	27.27	27.29	26.97
Mar-07	27.53	27.46	27.27	27.35	27.08
Apr-07	28.48	28.29	28.10	28.24	27.93
May-07	29.55	29.22	28.88	28.96	28.56
Jun-07	29.92	29.72	29.40	29.41	29.17
Jul-07	29.84	29.78	29.59	29.58	28.97
Aug-07	30.01	29.71	29.95	30.00	29.28
Sep-07	29.84	29.41	29.52	29.45	29.31
Oct-07	29.39	29.04	29.36	29.45	29.23
Nov-07	28.18	27.45	27.81	27.84	28.18
Dec-07	26.90	26.91	27.06	27.00	27.77
Jan-08	26.49	26.54	26.82	26.71	26.74
Feb-08	27.25	27.17	27.19	27.28	26.96
Mar-08	27.49	27.32	27.10	27.21	27.33
Apr-08	28.34	28.06	27.69	27.78	28.00
May-08	29.37	29.10	28.81	29.00	28.14
Jun-08	29.20	28.94	28.76	28.85	28.69
Jul-08	29.12	29.10	28.63	28.62	28.86
Aug-08	29.99	29.78	29.79	29.86	29.41
Sep-08	30.56	30.29	29.99	30.05	29.43
Oct-08	28.51	28.36	28.39	28.31	28.85
Nov-08	27.11	27.15	27.24	27.16	27.80
Dec-08	26.27	26.32	26.27	26.17	26.94

Table B2. Gravimetric elemental ratios and average measured elemental ratios of the University of Southampton consistency standards.

	SECS1		SECS2		SECS3	
	Gravimetric	Average measured	Gravimetric	Average measured	Gravimetric	Average measured
Li/Ca (µmol/mol)	12.48	11.82	23.98	23.68	40.02	37.47
n		11		20		16
2σ		0.39		0.67		0.83
%RSD (2σ)		3.30		2.83		2.22
Mg/Ca (mmol/mol)	1.00	1.03	3.00	2.97	6.99	6.80
n		13		21		16
2σ		0.03		0.10		0.12
%RSD (2σ)		2.91		3.37		1.76
Sr/Ca (mmol/mol)	0.50	0.50	1.00	0.99	2.00	1.97
n		13		22		16
2σ		0.02		0.03		0.04
%RSD (2σ)		4.00		3.03		2.03
Li/Mg (mmol/mol)	12.48	11.50	7.99	7.96	5.73	5.51
n		11		19		16
2σ		0.47		0.19		0.09
%RSD (2σ)		4.09		2.39		1.63

Table B3. Coretop Li/Mg and Sr/Ca ratios from the forereef (FR-12) and backreef (BR-06) corals used to make the Li/Mg- and Sr/Ca-SST calibrations. The backreef Li/Mg ratio for July 2008 was not included in the calibration.

Zone	Date	Li/Mg (mmol/mol)	Sr/Ca (mmol/mol)	Li/Ca (µmol/mol)	Mg/Ca (mmol/mol)	Interpolated Reynolds SST (°C)
Backreef	Sep-08	1.46	8.52	5.46	3.75	29.97
Backreef	Aug-08	1.45	8.47	5.28	3.64	29.56
Backreef	Jul-08		8.52	5.61		28.64
Backreef	Jun-08	1.48	8.46	5.53	3.73	28.84
Backreef	May-08	1.51	8.50	5.57	3.69	28.98
Backreef	Apr-08	1.54	8.49	5.68	3.70	28.06
Backreef	Mar-08	1.56	8.62	5.78	3.72	27.38
Backreef	Feb-08	1.55	8.59	5.52	3.55	27.25
Backreef	Jan-08	1.54	8.56	5.44	3.52	26.94
Backreef	Dec-07	1.52	8.59	5.54	3.65	26.87
Backreef	Nov-07	1.60	8.61	6.16	3.85	27.46
Backreef	Oct-07	1.56	8.52	5.70	3.66	28.70
Backreef	Sep-07	1.51	8.47	5.49	3.62	29.45
Backreef	Aug-07	1.46	8.51	5.21	3.56	29.74
Backreef	Jul-07	1.51	8.54	5.45	3.61	29.78
Backreef	Jun-07	1.53	8.48	5.25	3.44	29.49
Backreef	May-07	1.54	8.49	5.32	3.46	29.18
Backreef	Apr-07	1.61	8.50	5.51	3.43	28.59
Backreef	Mar-07	1.56	8.56	5.47	3.51	27.79
Backreef	Mar-07	1.60	8.57	5.56	3.47	27.32
Backreef	Feb-07	1.60	8.65	5.82	3.63	27.22
Backreef	Jan-07	1.56	8.49	5.75	3.68	27.06
Backreef	Dec-06	1.56	8.59	5.98	3.82	27.47
Backreef	Nov-06	1.53	8.51	5.84	3.83	28.61
Backreef	Oct-06	1.50	8.51	5.67	3.78	29.29
Backreef	Sep-06	1.43	8.46	5.69	3.97	29.65
Backreef	Aug-06	1.41	8.35	5.33	3.78	29.15
Backreef	Jul-06	1.41	8.36	5.25	3.72	29.15
Backreef	Jun-06	1.43	8.46	5.25	3.68	28.99
Backreef	May-06	1.42	8.39	5.14	3.62	28.91
Backreef	May-06	1.56	8.56	5.64	3.62	28.65
Backreef	Apr-06	1.55	8.54	5.48	3.52	28.00
Backreef	Mar-06	1.53	8.56	5.41	3.54	27.22
Backreef	Mar-06	1.57	8.48	5.95	3.80	26.54
Backreef	Feb-06	1.55	8.49	5.77	3.74	26.03
Forereef	Sep-08	1.08	8.24	5.07	4.68	29.94
Forereef	Jul-08	1.11	8.33	4.98	4.48	28.88

Forereef	Jun-08	1.22	8.33	5.41	4.44	28.78
Forereef	Apr-08	1.34	8.46	5.59	4.19	27.63
Forereef	Feb-08	1.39	8.56	5.33	3.83	27.17
Forereef	Jan-08	1.37	8.56	5.39	3.93	26.93
Forereef	Nov-07	1.37	8.52	5.39	3.93	27.89
Forereef	Sep-07	1.19	8.47	5.25	4.40	29.45
Forereef	Aug-07	1.14	8.33	5.13	4.51	29.94
Forereef	Jul-07	1.16	8.35	5.18	4.45	29.52
Forereef	May-07	1.21	8.46	5.39	4.44	29.09
Forereef	Apr-07	1.24	8.40	5.29	4.28	28.33
Forereef	Mar-07	1.27	8.51	5.30	4.18	27.50
Forereef	Feb-07	1.33	8.56	5.45	4.10	27.27
Forereef	Jan-07	1.21	8.50	4.35	3.60	27.19
Forereef	Jan-07	1.37	8.50	4.97	3.63	27.09
Forereef	Dec-06	1.38	8.50	5.33	3.85	27.18
Forereef	Nov-06	1.11	8.34	4.98	4.50	28.30
Forereef	Oct-06	1.06	8.29	4.87	4.58	29.01
Forereef	Sep-06	1.06	8.27	4.89	4.63	29.66
Forereef	Aug-06	1.01	8.17	4.80	4.73	29.28
Forereef	Jul-06	1.15	8.25	5.04	4.37	29.11
Forereef	May-06	1.26	8.48	4.72	3.76	28.75
Forereef	Mar-06	1.33	8.55	4.61	3.46	26.96
Forereef	Jan-06	1.44	8.66	4.81	3.33	26.56

Table B4. Downcore (1921-1926) Li/Mg and Sr/Ca ratios in both the forereef (FR-12) and backreef (BR-06) corals, and the resulting sea surface temperature reconstructions.

Zone	Date	Li/Mg (mmol/mol)	Sr/Ca (mmol/mol)	Li/Ca (µmol/mol)	Mg/Ca (mmol/mol)	Li/Mg-SST (°C)	Sr/Ca-SST (°C)	MLR1-SST (°C)	MLR2-SST (°C)
Backreef	Jan-26	1.48	8.32	5.39	3.65	29.64	34.97	28.99	28.98
Backreef	Dec-25	1.47	8.46	5.56	3.78	29.94	30.45	28.94	28.80
Backreef	Nov-25	1.53	8.55	5.40	3.53	28.12	27.55	28.18	28.39
Backreef	Oct-25	1.50	8.50	5.40	3.59	29.03	29.16	28.57	28.64
Backreef	Sep-25	1.48	8.53	4.87	3.29	29.64	28.19	28.76	29.33
Backreef	Jul-25	1.51	8.52	4.75	3.14	28.73	28.52	28.43	29.20
Backreef	Jun-25	1.53	8.51	5.13	3.34	28.12	28.84	28.22	28.65
Backreef	May-25	1.50	8.50	5.22	3.47	29.03	29.16	28.57	28.81
Backreef	Apr-25	1.52	8.59	5.12	3.37	28.42	26.26	28.24	28.73
Backreef	Dec-24	1.50	8.51	5.45	3.64	29.03	28.84	28.55	28.63
Backreef	Oct-24	1.40	8.44	5.35	3.83	32.06	31.10	29.74	29.72
Backreef	Oct-24	1.45	8.42	5.48	3.77	30.55	31.74	29.21	29.08
Backreef	Sep-24	1.39	8.43	5.15	3.70	32.36	31.42	29.87	29.97
Backreef	Sep-24	1.32	8.39	4.93	3.73	34.48	32.71	30.69	30.81
Backreef	Sep-24	1.33	8.40	4.77	3.58	34.18	32.39	30.57	30.82
Backreef	Aug-24	1.32	8.43	4.77	3.61	34.48	31.42	30.64	30.92
Backreef	Aug-24	1.37	8.49	5.02	3.66	32.97	29.48	30.02	30.21
Backreef	Jun-24	1.42	8.45	4.92	3.46	31.45	30.77	29.51	29.83
Backreef	May-24	1.37	8.52	5.08	3.71	32.97	28.52	29.99	30.20
Backreef	May-24	1.51	8.64	5.07	3.36	28.73	24.65	28.30	28.87
Backreef	Apr-24	1.57	8.69	5.09	3.24	26.91	23.03	27.58	28.31
Backreef	Apr-24	1.60	8.64	5.24	3.26	26.00	24.65	27.30	27.92
Backreef	Dec-23	1.62	8.54	5.38	3.32	25.39	27.87	27.19	27.69
Backreef	Sep-23	1.51	8.55	4.65	3.09	28.73	27.55	28.40	29.34
Backreef	May-23	1.61	8.66	4.99	3.09	25.70	24.00	27.17	28.14
Backreef	May-23	1.59	8.62	5.14	3.24	26.30	25.29	27.43	28.19
Backreef	Apr-23	1.60	8.77	5.37	3.36	26.00	20.45	27.16	27.75
Backreef	Jan-23	1.66	8.56	5.38	3.23	24.18	27.23	26.72	27.35
Backreef	Dec-22	1.63	8.64	5.24	3.20	25.09	24.65	26.97	27.69
Backreef	Nov-22	1.59	8.68	5.05	3.17	26.30	23.35	27.37	28.20
Forereef	Dec-25	1.29	8.34	5.58	4.33	27.83	29.04	28.30	28.40
Forereef	Nov-25	1.22	8.38	5.00	4.10	28.57	28.60	28.48	28.27
Forereef	Sep-25	1.25	8.45	5.15	4.12	28.25	27.90	28.14	28.13
Forereef	Jun-25	1.32	8.31	5.23	3.96	27.53	29.40	28.27	27.92
Forereef	Apr-25	1.30	8.42	5.01	3.87	27.77	28.18	28.01	27.72
Forereef	Feb-25	1.45	8.75	5.39	3.71	26.13	24.80	26.29	26.75
Forereef	Jan-25	1.41	8.54	5.04	3.59	26.63	26.95	27.15	26.98
Forereef	Nov-24	1.27	8.48	5.00	3.95	28.06	27.60	27.96	27.82
Forereef	Jul-24	1.31	8.37	5.13	3.91	27.61	28.72	28.10	27.80
Forereef	May-24	1.27	8.45	5.28	4.15	28.00	27.97	28.05	28.10
Forereef	Apr-24	1.35	8.47	5.73	4.24	27.21	27.71	27.63	27.96
Forereef	Apr-24	1.38	8.49	5.69	4.12	26.90	27.51	27.43	27.73
Forereef	Mar-24	1.42	8.63	5.68	4.01	26.48	26.06	26.82	27.33
Forereef	Mar-24	1.49	8.61	5.62	3.77	25.75	26.27	26.57	26.90
Forereef	Jan-24	1.43	8.62	5.66	3.95	26.38	26.16	26.81	27.24
Forereef	Dec-23	1.39	8.61	5.99	4.32	26.79	26.27	27.02	27.79
Forereef	Nov-23	1.35	8.51	5.82	4.32	27.21	27.30	27.50	28.03
Forereef	Nov-23	1.30	8.49	5.66	4.37	27.73	27.51	27.79	28.26
Forereef	Sep-23	1.19	8.51	5.32	4.45	28.88	27.30	28.22	28.63
Forereef	Jul-23	1.21	8.39	5.35	4.44	28.67	28.54	28.50	28.72
Forereef	May-23	1.28	8.56	5.55	4.33	27.94	26.78	27.66	28.16
Forereef	Apr-23	1.30	8.56	5.48	4.21	27.73	26.78	27.57	27.95
Forereef	Mar-23	1.40	8.61	5.58	3.99	26.69	26.27	26.97	27.38
Forereef	Feb-23	1.39	8.53	5.26	3.79	26.79	27.09	27.26	27.27

Forereef	Jan-23	1.43	8.63	5.49	3.85	26.38	26.06	26.78	27.12
Forereef	Jan-23	1.41	8.59	5.37	3.81	26.58	26.47	26.99	27.17
Forereef	Oct-22	1.20	8.41	5.15	4.29	28.77	28.33	28.49	28.53
Forereef	Aug-22	1.23	8.41	5.29	4.30	28.46	28.33	28.35	28.45
Forereef	Jun-22	1.24	8.32	5.35	4.30	28.35	29.26	28.59	28.53
Forereef	May-22	1.32	8.53	5.28	3.99	27.52	27.09	27.58	27.68
Forereef	Apr-22	1.32	8.55	5.30	4.02	27.52	26.89	27.52	27.70
Forereef	Apr-22	1.35	8.50	5.36	3.96	27.21	27.40	27.54	27.60
Forereef	Mar-22	1.39	8.53	5.42	3.91	26.79	27.09	27.26	27.41
Forereef	Feb-22	1.37	8.52	5.48	3.99	27.00	27.20	27.38	27.56
Forereef	Jan-22	1.41	8.58	5.70	4.05	26.58	26.58	27.02	27.47
Forereef	Jan-22	1.40	8.56	5.73	4.08	26.69	26.78	27.13	27.53
Forereef	Dec-21	1.35	8.55	5.61	4.15	27.21	26.89	27.38	27.77
Forereef	Nov-21	1.32	8.37	5.59	4.22	27.52	28.74	28.07	28.15

Table B5. Historic HadISST1 data, encompassing the forereef and backreef zones between 1921 and 1926.

Date	HadISST (°C)
Jan-26	26.82
Dec-25	27.55
Nov-25	28.31
Oct-25	29.36
Sep-25	29.64
Aug-25	29.14
Jul-25	28.56
Jun-25	28.19
May-25	28.02
Apr-25	27.57
Mar-25	26.48
Feb-25	26.33
Jan-25	26.47
Dec-24	27.16
Nov-24	27.73
Oct-24	28.41
Sep-24	28.94
Aug-24	28.83
Jul-24	28.76
Jun-24	28.5
May-24	27.98
Apr-24	27.03
Mar-24	26.34
Feb-24	26.45
Jan-24	26.56
Dec-23	27.16
Nov-23	27.64
Oct-23	28.63
Sep-23	28.98
Aug-23	28.75
Jul-23	28.53
Jun-23	28.32
May-23	27.97
Apr-23	27.51
Mar-23	26.44
Feb-23	26.32
Jan-23	26.29
Dec-22	26.94
Nov-22	27.34

Oct-22	28.77
Sep-22	28.89
Aug-22	28.81
Jul-22	28.54
Jun-22	28.27
May-22	27.92
Apr-22	27.34
Mar-22	26.66
Feb-22	26.59
Jan-22	26.38
Dec-21	27.16
Nov-21	27.81
Oct-21	28.45
Sep-21	29.18
Aug-21	28.87
Jul-21	28.83

Appendix C Coral sampling in Bermuda

Sampling was facilitated by the Bermuda Institute of Ocean Science (BIOS) and occurred between 13th November and 19th December 2014. Permits were granted from both the BIOS Collecting and Experimental Ethics Policy committee, and also CITES permits from the Bermudan Government.

Seawater samples were collected along a transit from BIOS to the Bermuda Ocean Acidification and Coral Reef Investigation (BEACON) monitoring buoy at Hog Reef (Figure B-1) approximately every 2 miles for the purpose of analysing the boron isotopic composition of seawater. A Niskin bottle was cast over the back of the RV Rumliner to a depth of 1m and fired. The coordinates of the transect seawater samples were as follows:

TSW 1: 32.36118N, 64.71951W
TSW2: 32.40025N, 64.76255W
TSW 3: 32.43828N, 64.80619W
TSW 4: 32.45684N, 64.83434W

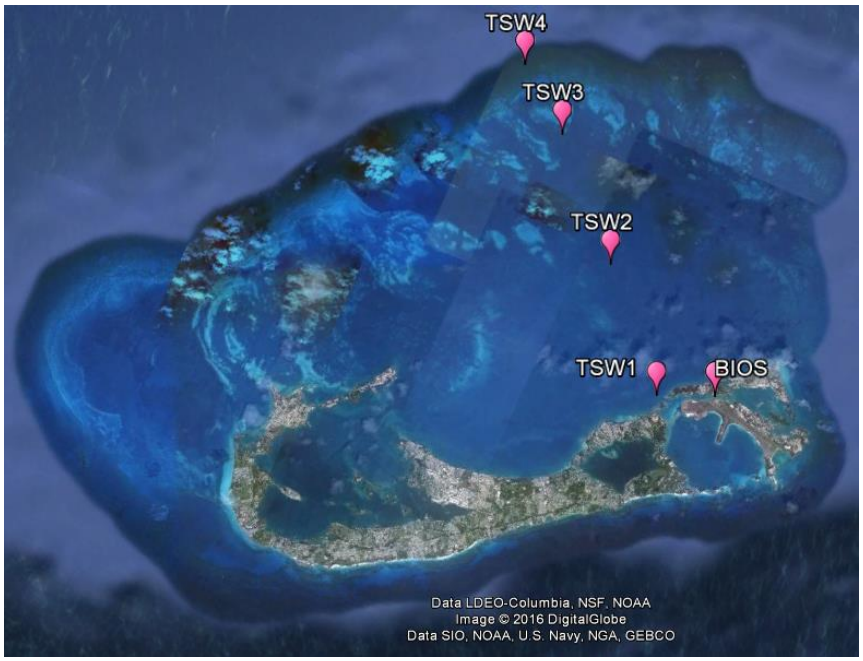

Figure C-1. Map of seawater sampling transect between the Bermuda Institute of Ocean Science and the BEACON monitoring buoy at Hog Reef. Transect samples were collected at a depth of 1 m. Seawater samples were also collected next to the cored coral colonies. Corals were cored within 12 m of the BEACON monitoring buoy at 32.46°N, 64.83°W.

Collected water was allowed to drain for 30 seconds before rinsing the 7 ml acid cleaned Teflon beakers 5 times. The beaker was then allowed to fill, trying to minimise the number of bubbles in the seawater. Whilst the beakers were being filled, care was taken not to touch the insides, and hands were not passed over open beakers to avoid the introduction of air-borne boron. Nitrile gloves were worn at all times. A water sample was also collected next to the first colony of each species before any drilling was performed in order to minimise the number of particulates in the sample. Lids were partially unscrewed at the surface to make it possible to open the beakers under pressure. Nitrile gloves were worn and the beaker was fully opened underwater and allowed to flush before being re-capped. Upon return to the lab at BIOS, beakers and associated bags were rinsed in MQ water and Parafilmed before drying. All seawater samples were acidified with 120 µl 0.5 M HNO_3 per 5 ml seawater upon return to the clean lab at NOCS.

An inflatable raft was used to load scuba cylinders, and was tied to the BEACON buoy. These tanks were then tied to a rope and dropped down to a diver and laid to rest on a sandy clearing in the reef. Empty cylinders were released and collected by a snorkeller and secured onto the raft (Figure C-2).

Figure C-2. Raft containing full scuba cylinders attached to the (BEACON) monitoring buoy.

Before any corals were drilled, the site was surveyed and ideal colonies were marked with weights. The colonies chosen to sample had no current visible disease or bleaching, and were assumed to not overlap a different colony during the top 15cm. Corals identified for sampling were between 10 m and 12 m below the sea surface and *Diploria labyrinthiformis*, *Diploria strigosa* and *Porites astreoides* species were chosen. Three individuals from each species were cored two times (Figure C-3a,d). Each core had a 5 cm diameter and the lengths

ranged from 8 to 15 cm. A 1 horse power hand held pneumatic air drill with a custom made 5 cm x 15 cm diamond core bit, powered by scuba cylinders was used to drill the coral (Figure B-3b). Cores were drilled down the maximum growth axis. For some colonies, several attempts were made before a groove was made in the coral ready to drill. Each core required 1 to 2 12 litre compressed air scuba cylinders. After the core had been drilled, it was chiselled out of the coral using a mallet and an aluminium pipe which had been cut into a leaver (Figure C-3c).

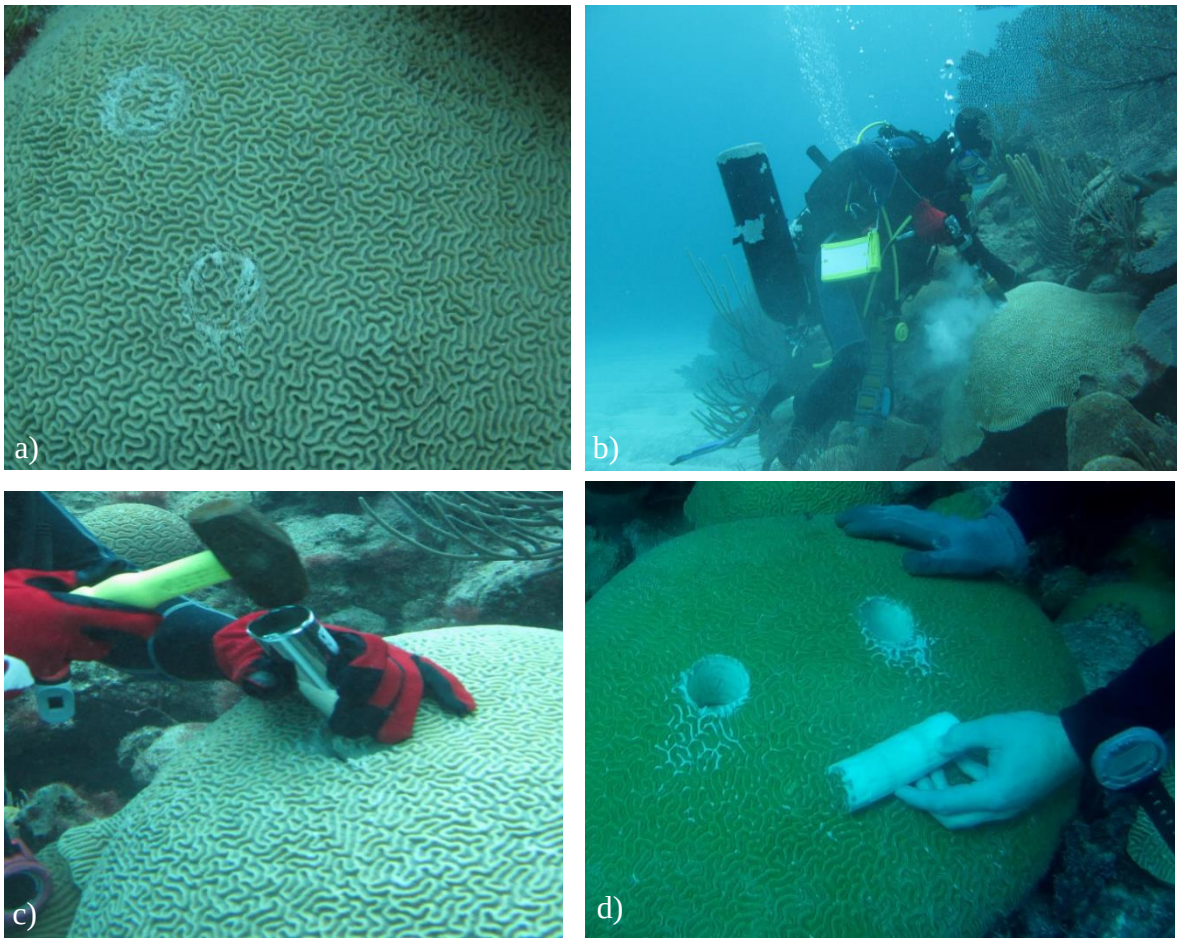

Figure C-3. a) Initial grooves in a *Diploria strogosa* colony. b) Drilling in progress. c) Some of the cores had to be chiselled out to break the bottom of the core from the coral. d) Replicate core holes can be seen in this *Diploria labyrinthiformis* colony, and one of the cores. The white marks around the coring sites are damage to the external tissue layer caused by the drill slipping whilst making the grooves.

Two dives were completed on 13th November 2014. The first dive allowed the recovery of *Diploria labyrinthiformis* colony 1 A and B, *Diploria labyrnthiformis* colony 2 A. The second dive allowed the recovery of *Diploria labyrinthiformis* colony 2 B, and colony 3 A and B. *Porites atreoides* 1 A was drilled in dive 2 but was not recovered until a third dive that occurred for the purpose of recovering all the equipment from the sea bed.

During the dives, photographs were taken of the selected colonies before and after coring, in addition to the labelled core in the bag next to the sampled coral. Cement plugs were made by pouring cement mix into small plastic cups, which had been cut down to match the size of the anticipated hole (approx. 5.5 cm diameter). Once the cement had dried, the plastic cup was removed. The cement plugs were inserted into all of the core holes in December to prevent any boring organisms inhabiting the holes, and to allow the cement to become colonised by symbionts to enable the coral to continue to grow.

Before the cores were returned to the UK, the outermost tissue layers of the corals were removed using a WaterPik (Figure C-4), before being left to soak in pure ethanol for 5 minutes and then rinsed, soaked and re-rinsed in deionised water. Upon return to NOCS, the coral cores were sliced along their major growth axis, into a slab 6mm thick.

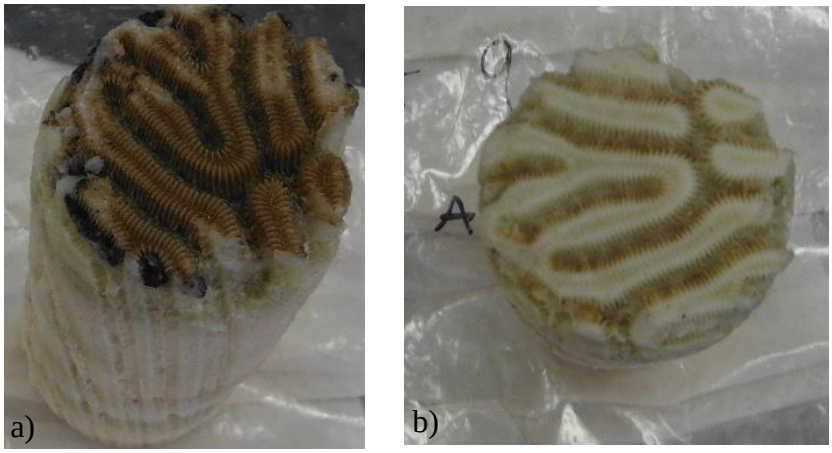

Figure C-4. *Diploria labyrinthiformis* core (a) before and (b) after having the tissue layer removed with a WaterPik.

Bibliography

Abram, N. J., H. V. McGregor, J. E. Tierney, M. N. Evans, N. P. McKay, and D. S. Kaufman (2016), Early onset of industrial-era warming across the oceans and continents, *Nature*, *536*(7617), 411-418.

Achituv, Y., and Z. Dubinsky (1990), Carbon budgets in marine mutualistic associations between microalgae and cnidarians, *Comparative physiology*, *5*, 36-48.

Adkins, J. F., E. A. Boyle, W. B. Curry, and A. Lutringer (2003), Stable isotopes in deep-sea corals and a new mechanism for "vital effects", *Geochimica et Cosmochimica Acta*, *67*(6), 1129–1143.

Al-Ammar, A. S., R. K. Gupta, and R. M. Barnes (2000), Elimination of boron memory effect in inductively coupled plasma-mass spectrometry by ammonia gas injection into the spray chamber during analysis, *Spectrochimica Acta Part B*, *55*, 629-635.

Al-Horani, F. A., S. M. Al-Moghrabi, and D. d. Beer (2003), The mechanism of calcification and its relation to photosynthesis and respiration in the scleractinian coral *Galaxea fascicularis*, *Marine Biology*, *142*, 419–426.

Albright, R., J. Benthuysen, N. Cantin, K. Caldeira, and K. Anthony (2015), Coral reef metabolism and carbon chemistry dynamics of a coral reef flat, *Geophysical Research Letters*, *42*(10), 3980-3988.

Alibert, C., and M. T. McCulloch (1997), Strontium/calcium ratios in modern *Porites* corals from the Great Barrier Reef as a proxy for sea surface temperature: Calibration of the thermometer and monitoring of ENSO, *Palaeocenography*, *12*(3), 345-363.

Alibert, C., and L. Kinsley (2008), A 170- year Sr/Ca and Ba/Ca coral record from the western Pacific warm pool: 1. What can we learn from an unusual coral record?, *Journal of Geophysical Research: Oceans*, *113*(C4).

Alibert, C., L. Kinsley, S. J. Fallon, M. T. McCulloch, R. Berkelmans, and F. McAllister (2003), Source of trace element variability in Great Barrier Reef corals affected by the Burdekin flood plumes, *Geochimica et Cosmochimica Acta*, *67*(2), 231-246.

Allemand, D., É. Tambutté, D. Zoccola, and S. Tambutté (2011), Coral calcification, cells to reefs, in *Coral reefs: an ecosystem in transition*, edited by Z. Dubinsky and N. Stambler, pp. 119-150, Springer, Netherlands.

Allemand, D., C. Ferrier-Pagès, P. Furla, F. Houlbrèque, S. Puverel, S. Reynaud, É. Tambutté, S. Tambutté, and D. Zoccola (2004), Biomineralisation in reef-building corals: from molecular mechanisms to environmental control, *Comptes Rendus Palevol*, *3*(6-7), 453-467.

Allen, R. J. (2015), A 21st century northward tropical precipitation shift caused by future anthropogenic aerosol reductions, *Journal of Geophysical Research: Atmospheres*, *120*(18), 9087-9102.

Allison, N., A. A. Finch, M. Newville, and S. R. Sutton (2005), Strontium in coral aragonite: 3. Sr coordination and geochemistry in relation to skeletal architecture, *Geochimica et Cosmochimica Acta*, *69*(15), 3801-3811.

Alpert, A. E., A. L. Cohen, D. W. Oppo, T. M. DeCarlo, J. M. Gove, and C. W. Young (2016), Comparison of equatorial Pacific sea surface temperature variability and trends with Sr/Ca records from multiple corals, *Paleoceanography*, *31*(2), 252–265.

Anagnostou, E., K. F. Huang, C. F. You, E. L. Sikes, and R. M. Sherrell (2012), Evaluation of boron isotope ratio as a pH proxy in the deep sea coral *Desmophyllum dianthus*: Evidence of physiological pH adjustment, *Earth and Planetary Science Letters*, *349-350*, 251-260.

Anand, P., H. Elderfield, and M. H. Conte (2003), Calibration of Mg/Ca thermometry in planktonic foraminifera from a sediment trap time series, *Paleoceanography*, *18*(2), 1050.

Anderson, D. M., E. M. Mauk, E. R. Wahl, C. Morrill, A. J. Wagner, D. Easterling, and T. Rutishauser (2013), Global warming in an independent record of the past 130 years, *Geophysical Research Letters*, *40*, 189–193.

Andersson, A., I. Kuffner, F. Mackenzie, P. Jokiel, K. Rodgers, and A. Tan (2009), Net loss of $CaCO_3$ from a subtropical calcifying community due to seawater acidification: mesocosm-scale experimental evidence, *Biogeosciences*, *6*(8), 1811-1823.

Andersson, A. J., and D. Gledhill (2013), Ocean acidification and coral reefs: effects on breakdown, dissolution, and net ecosystem calcification, *Annual Review of Marine Science*, *5*, 321-348.

Andersson, A. J., F. T. Mackenzie, and L. M. Ver (2003), Solution of shallow-water carbonates: An insignificant buffer against rising atmospheric CO_2, *Geology*, *31*(6), 513-516.

Andersson, A. J., K. L. Yeakel, N. R. Bates, and S. J. de Putron (2014), Partial offsets in ocean acidification from changing coral reef biogeochemistry, *Nature Climate Change*, *4*(1), 56-61.

Andréfouët, S., P. Mumby, M. McField, C. Hu, and F. Muller-Karger (2002), Revisiting coral reef connectivity, *Coral Reefs*, *21*(1), 43-48.

Anthony, K., G. Diaz-Pulido, N. Verlinden, B. Tilbrook, and A. Andersson (2013), Benthic buffers and boosters of ocean acidification on coral reefs, *Biogeosciences*, *10*(7), 4897-4909.

Anthony, K. R., D. I. Kline, G. Diaz-Pulido, S. Dove, and O. Hoegh-Guldberg (2008a), Ocean acidification causes bleaching and productivity loss in coral reef builders, *Proceedings of the National Academy of Sciences of the United States of America*, *105*(45), 17442-17446.

Anthony, K. R. N., J. A. Kleypas, and J.-P. Gattuso (2011), Coral reefs modify their seawater carbon chemistry – implications for impacts of ocean acidification, *Global Change Biology*, *17*(12), 3655-3666.

Anthony, K. R. N., D. I. Kline, G. Diaz-Pulido, S. Dove, and O. Hoegh-Guldberg (2008b), Ocean acidification causes bleaching and productivity loss in coral reef builders, *Proceedings of the National Academy of Sciences*, *105*(45), 17442-17446.

Archer, C., and D. Vance (2004), Mass discrimination correction in multiple-collector plasma source mass spectrometry: an example using Cu and Zn isotopes, *Journal of Analytical Atomic Spectrometry*, *19*(5), 656-665.

Aronson, R., W. Precht, M. Toscano, and K. Koltes (2002), The 1998 bleaching event and its aftermath on a coral reef in Belize, *Marine Biology*, *141*(3), 435-447.

Aronson, R. B., W. F. Precht, I. G. Macintyre, and T. J. Murdoch (2000), Ecosystems: Coral bleach-out in Belize, *Nature*, *405*(6782), 36-36.

Atkinson, M., B. Carlson, and G. Crow (1995), Coral growth in high-nutrient, low-pH seawater: a case study of corals cultured at the Waikiki Aquarium, Honolulu, Hawaii, *Coral Reefs*, *14*(4), 215-223.

Baird, A., and P. Marshall (2002), Mortality, growth and reproduction in scleractinian corals following bleaching on the Great Barrier Reef, *Marine Ecology Progress Series*, *237*, 133-141.

Baker, A. C., P. W. Glynn, and B. Riegl (2008), Climate change and coral reef bleaching: An ecological assessment of long-term impacts, recovery trends and future outlook, *Estuarine, Coastal and Shelf Science*, *80*(4), 435-471.

Barbaste, M., K. Robinson, S. Guilfoyle, B. Medina, and R. Lobinski (2002), Precise determination of the strontium isotope ratios in wine by inductively coupled plasma sector field multicollector mass spectrometry (ICP-SF-MC-MS), *Journal of Analytical Atomic Spectrometry*, *17*(2), 135-137.

Barker, N. H., and C. M. Roberts (2004), Scuba diver behaviour and the management of diving impacts on coral reefs, *Biological Conservation*, *120*(4), 481-489.

Barker, S., M. Greaves, and H. Elderfield (2003), A study of cleaning procedures used for foraminiferal Mg/Ca paleothermometry, *Geochemistry Geophysics Geosystems*, *4*(9), 8407.

Barnes, D., and M. Devereux (1984), Productivity and calcification on a coral reef: a survey using pH and oxygen electrode techniques, *Journal of Experimental Marine Biology and Ecology*, *79*(3), 213-231.

Barshis, D., J. Stillman, R. Gates, R. Toonen, L. Smith, and C. Birkeland (2010), Protein expression and genetic structure of the coral *Porites lobata* in an environmentally extreme Samoan back reef: does host genotype limit phenotypic plasticity?, *Molecular Ecology*, *19*(8), 1705-1720.

Bates, N., M. Best, K. Neely, R. Garley, A. Dickson, and R. Johnson (2012), Detecting anthropogenic carbon dioxide uptake and ocean acidification in the North Atlantic Ocean, *Biogeosciences*, *9*(7), 2509-2522.

Bates, N. R., L. Samuels, and L. Merlivat (2001), Biogeochemical and physical factors influencing seawater fCO_2 and air- sea CO_2 exchange on the Bermuda coral reef, *Limnology and Oceanography*, *46*(4), 833-846.

Bates, N. R., A. Amat, and A. J. Andersson (2010), Feedbacks and responses of coral calcification on the Bermuda reef system to seasonal changes in biological processes and ocean acidification, *Biogeosciences*, *7*(8), 2509-2530.

Bates, N. R., Y. M. Astor, M. J. Church, K. Currie, J. E. Dore, M. Gonzalez-Davila, L. Lorenzoni, F. Muller-Karger, J. Olafsson, and J. Magdalena Santana-Casiano (2014), A time-series view of changing surface ocean chemistry due to ocean uptake of anthropogenic CO_2 and ocean acidification, *Oceanography*, *27*(1), 126-141.

Beck, J. W., R. L. Edwards, E. Ito, F. W. Taylor, J. Recy, F. Rougerie, P. Joannot, and C. Henin (1992), Sea-surface temperature from coral skeletal strontium/calcium ratios, *Science*, *257*(5070), 644-647.

Berkelmans, R., G. De'ath, S. Kininmonth, and W. J. Skirving (2004), A comparison of the 1998 and 2002 coral bleaching events on the Great Barrier Reef: spatial correlation, patterns, and predictions, *Coral Reefs*, *23*(1), 74-83.

Bourke, L., E. Selig, and M. Spalding (2002), *Reefs at Risk in Southeast Asia*, Cambridge.
Boyer, T., J. Antonov, O. Baranova, H. Garcia, D. Johnson, R. Locarnini, A. Mishonov, D. Seidov, I. Smolyar, and M. Zweng (2009), World ocean database 2009, vol. 1, Introduction, NOAA Atlas NESDIS, vol. 66, edited by S, edited, Levitus.

Brassell, S. C., G. Eglinton, I. T. Marlowe, U. Pflaumann, and M. Sarnthein (1986), Molecular stratigraphy: A new tool for climatic assessment, *Nature*, *320*, 129–133.

Brodie, J., F. Kroon, B. Schaffelke, E. Wolanski, S. Lewis, M. Devlin, I. Bohnet, Z. Bainbridge, J. Waterhouse, and A. Davis (2012), Terrestrial pollutant runoff to the Great Barrier Reef: an update of issues, priorities and management responses, *Marine Pollution Bulletin*, *65*(4), 81-100.

Broecker, W. S., C. Langdon, T. Takahashi, and T.-H. Peng (2001), Factors controlling the rate of $CaCO_3$ precipitation on Great Bahama Bank, *Global Biogeochemical Cycles*, *15*(3), 589-596.

Bronnimann, S., A. M. Fischer, E. Rozanov, P. Poli, G. P. Compo, and P. D. Sardeshmukh (2015), Southward shift of the northern tropical belt from 1945 to 1980, *Nature Geosci*, *8*(12), 969-974.

Bruckner, A. W., R. J. Bruckner, and P. Sollins, (2000), Parrot fish predation on live coral: "spot biting" and "focused biting", *Coral Reefs*, *19*, 50.

Bruggemann, J. H., M. J. H. van Oppen, A. M. Breeman (1994), Foraging by the stoplight parrotfish *Sparisoma viride*. I. Intake and assimilation of food, protein and energy, *Marine Ecology Progression Series*, *106*, 41-55.

Bruno, J. F., and E. R. Selig (2007), Regional decline of coral cover in the Indo-Pacific: timing, extent, and subregional comparisons, *PLoS One*, *2*(8), e711.

Bruno, J. F., E. R. Selig, K. S. Casey, C. A. Page, B. L. Willis, C. D. Harvell, H. Sweatman, and A. M. Melendy (2007), Thermal stress and coral cover as drivers of coral disease outbreaks, *PLoS Biology*, *5*(6), e124.

Bryant, D., L. Burke, J. McManus, M. Spalding, D. Hinrichsen, and C. Wilkinson (1998), Reefs at risk: a map-based indicator of threats to the worlds coral reefs, *DEFENDERS*, *74*(3), 6-15.

Burke, L., and Z. Sugg (2006), Hydrologic modeling of watersheds discharging adjacent to the Mesoamerican Reef, *World Resources Institute, Washington, DC*.

Burke, L., K. Reytar, M. Spalding, and A. Perry (2011), *Reefs at risk revisited*.
Cahyarini, S. Y., M. Pfeiffer, and W.-C. Dullo (2009), Improving SST reconstructions from coral Sr/Ca records: multiple corals from Tahiti (French Polynesia), *International Journal of Earth Sciences*, *98*(1), 31-40.

Cahyarini, S. Y., M. Pfeiffer, I. S. Nurhati, E. Aldrian, W. C. Dullo, and S. Hetzinger (2014), Twentieth century sea surface temperature and salinity variations at Timor inferred from paired coral $\delta^{18}O$ and Sr/Ca measurements, *Journal of Geophysical Research: Oceans*, *119*(7), 4593-4604.

Caldeira, K., and M. E. Wickett (2003), Anthropogenic carbon and ocean pH, *Nature*, *425*, 365.

Canadell, J. G., C. L. Quéré, M. R. Raupach, C. B. Field, E. T. Buitenhuis, P. Ciais, T. J. Conway, N. P. Gillett, R. A. Houghton, and G. Marland (2007), Contributions to accelerating atmospheric CO_2 growth from economic activity, carbon intensity, and efficiency of natural sinks, *Proceedings of the National Academy of Sciences of the United States of America*, *104*(47), 18866–18870.

Cantin, N. E., A. L. Cohen, K. B. Karnauskas, A. M. Tarrant, and D. C. McCorkle (2010), Ocean warming slows coral growth in the central Red Sea, *Science*, *329*(5989), 322-325.

Carilli, J. E., R. D. Norris, B. Black, S. M. Walsh, and M. McField (2010), Century- scale records of coral growth rates indicate that local stressors reduce coral thermal tolerance threshold, *Global Change Biology*, *16*(4), 1247-1257.

Carilli, J. E., H. V. McGregor, J. J. Gaudry, S. D. Donner, M. K. Gagan, S. Stevenson, H. Wong, and D. Fink (2014), Equatorial Pacific coral geochemical records show recent weakening of the Walker Circulation, *Paleoceanography*, *29*(11), 1031-1045.

Caroselli, E., F. Zaccanti, G. Mattioli, G. Falini, O. Levy, Z. Dubinsky, and S. Goffredo (2012), Growth and demography of the solitary scleractinian coral *Leptopsammia pruvoti* along a sea surface temperature gradient in the Mediterranean Sea, *PLoS One*, *7*(6), e37848.

Carpenter, K. E., M. Abrar, G. Aeby, R. B. Aronson, S. Banks, A. Bruckner, A. Chiriboga, J. Cortés, J. C. Delbeek, and L. DeVantier (2008), One-third of reef-building corals face elevated extinction risk from climate change and local impacts, *Science*, *321*(5888), 560-563.

Carricart-Ganivet, J., L. Vásquez-Bedoya, N. Cabanillas-Terán, and P. Blanchon (2013), Gender-related differences in the apparent timing of skeletal density bands in the reef-building coral *Siderastrea siderea*, *Coral Reefs*, *32*(3), 769-777.

Carriquiry, J. D., and G. Horta-Puga (2010), The Ba/Ca record of corals from the Southern Gulf of Mexico: contributions from land-use changes, fluvial discharge and oil-drilling muds, *Marine Pollution Bulletin*, *60*(9), 1625-1630.

Case, D. H., L. Robinson, F., M. E. Auro, and A. C. Gagnon (2010), Environmental and biological controls on Mg and Li in deep-sea scleractinian corals, *Earth and Planetary Science Letters*, *300*, 215–225.

Castillo, K., and B. Helmuth (2005), Influence of thermal history on the response of *Montastraea annularis* to short-term temperature exposure, *Marine Biology*, *148*(2), 261-270.

Castillo, K. D., and F. P. Lima (2010), Comparison of in situ and satellite-derived (MODIS-Aqua/Terra)
methods for assessing temperatures on coral reefs, *Limnol. Oceanogr. Methods*, *8*, 107-117.

Castillo, K. D., J. B. Ries, and J. M. Weiss (2011), Declining coral skeletal extension for forereef colonies of *Siderastrea siderea* on the Mesoamerican Barrier Reef System, Southern Belize, *PLoS One*, *6*(2), e14615.

Castillo, K. D., J. B. Ries, J. M. Weiss, and F. P. Lima (2012), Decline of forereef corals in response to recent warming linked to history of thermal exposure, *Nature Climate Change*, *2*(10), 756-760.

Castillo, K. D., J. B. Ries, J. F. Bruno, and I. T. Westfield (2014), The reef-building coral *Siderastrea siderea* exhibits parabolic responses to ocean acidification and warming, *Proceedings of the Royal Society of London B: Biological Sciences*, *281*(1797), 20141856.

Catanzaro, E. J. (1970), *Boric acid: isotopic and assay standard reference materials*, National Bureau of Standards, Institute for Materials Research.

Cesar, H., L. Burke, and L. Pet-Soede (2003), The economics of worldwide coral reef degradation.

Chandler R. and M. Scott (2011), Statistical Methods for Trend Detection and Analysis in the Environmental Sciences, Wiley.

Chazottes, V., T. Le Campion-Alsumard, M. Peyrot-Clausade, and P. Cuet (2002), The effects of eutrophication-related alterations to coral reef communities on agents and rates of bioerosion (Reunion Island, Indian Ocean), *Coral Reefs*, *21*(4), 375-390.

Chérubin, L., C. Kuchinke, and C. Paris (2008), Ocean circulation and terrestrial runoff dynamics in the Mesoamerican region from spectral optimization of SeaWiFS data and a high resolution simulation, *Coral Reefs*, *27*(3), 503-519.

Cohen, A. L., and M. Holcomb (2009), Why corals care about ocean acidification: Uncovering the mechanism, *Oceanography*, *22*(4).

Cohen, A. L., G. D. Layne, S. R. Hart, and P. S. Lobel (2001), Kinetic control of skeletal Sr/Ca in a symbiotic coral: Implications for the paleotemperature proxy, *Paleoceanography*, *16*(1), 20-26.

Cohen, A. L., K. E. Owens, G. D. Layne, and N. Shimizu (2002), The effect of algal symbionts on the accuracy of Sr/Ca paleotemperatures from coral, *Science*, *296*, 331-333.

Cohen, A. L., G. A. Gaetani, T. Lundälv, B. H. Corliss, and R. Y. George (2006), Compositional variability in a cold-water scleractinian, *Lophelia pertusa*: New insights into "vital effects", *Geochemistry, Geophysics, Geosystems*, *7*, 12.

Cohen, A. L., D. C. McCorkle, S. d. Putron, G. A. Gaetani, and K. A. Rose (2009a), Morphological and compositional changes in the skeletons of new coral recruits reared in acidified seawater: Insights into the biomineralization response to ocean acidification, *Geochemistry, Geophysics, Geosystems*, *10*(7), Q07005.

Cohen, A. L., D. C. McCorkle, S. de Putron, G. A. Gaetani, and K. A. Rose (2009b), Morphological and compositional changes in the skeletons of new coral recruits reared in acidified seawater: Insights into the biomineralization response to ocean acidification, *Geochemistry Geophysics Geosystems*, *10*(7).

Collins, M., S.-I. An, W. Cai, A. Ganachaud, E. Guilyardi, F.-F. Jin, M. Jochum, M. Lengaigne, S. Power, and A. Timmermann (2010), The impact of global warming on the tropical Pacific Ocean and El Niño, *Nature Geoscience*, *3*(6), 391-397.

Comeau, S., P. J. Edmunds, N. B. Spindel, and R. C. Carpenter (2014), Diel pCO_2 oscillations modulate the response of the coral *Acropora hyacinthus* to ocean acidification, *Marine Ecology Progress Series*, *501*, 99-111.

Corrège, T. (2006), Sea surface temperature and salinity reconstruction from coral geochemical tracers, *Palaeogeography, Palaeoclimatology, Palaeoecology*, *232*, 408–428.

Cox, C. E., C. D. Jones, J. P. Wares, K. D. Castillo, M. D. McField, and J. F. Bruno (2013), Genetic testing reveals some mislabeling but general compliance with a ban on herbivorous fish harvesting in Belize, *Conservation Letters*, *6*(2), 132-140.

Cubasch, U., D. Wuebbles, D. Chen, M. C. Facchini, D. Frame, N. Mahowald, and J.-G. Winther (2013), Climate Change 2013: The Physical Science Basis, Introduction. IPCC WGI Fifth Assessment Report.

D'Olivo, J., M. T. McCulloch, S. Eggins, and J. Trotter (2015), Coral records of reef-water pH across the central Great Barrier Reef, Australia: assessing the influence of river runoff on inshore reefs, *Biogeosciences*, *12*(4), 1223-1236.

Davenport, J., and J. L. Davenport (2006), The impact of tourism and personal leisure transport on coastal environments: a review, *Estuarine, Coastal and Shelf Science*, *67*(1), 280-292.

Davies, S. W., A. Marchetti, J. B. Ries, and K. D. Castillo (2016), Thermal and pCO_2 stress elicit divergent transcriptomic responses in a resilient coral, *Frontiers in Marine Science*, *3*, 112.

De'ath, G., J. M. Lough, and K. E. Fabricius (2009), Declining coral calcification on the Great Barrier Reef, *Science*, *323*(5910), 116-119.

de Villiers, S., G. T. Shen, and B. K. Nelson (1994), The Sr/Ca-temperature relationship in coralline aragonite: Influence of variability in and skeletal growth parameters, *Geochimica et Cosmochimica Acta*, *58*, 197-208.

DeLong, K. L., T. M. Quinn, and F. W. Taylor (2007), Reconstructing twentieth- century sea surface temperature variability in the southwest Pacific: A replication study using multiple coral Sr/Ca records from New Caledonia, *Paleoceanography*, *22*(4).

DeLong, K. L., J. A. Flannery, C. R. Maupin, R. Z. Poore, and T. M. Quinn (2011), A coral Sr/Ca calibration and replication study of two massive corals from the Gulf of Mexico, *Palaeogeography, Palaeoclimatology, Palaeoecology*, *307* 117–128.

DeLong, K. L., J. A. Flannery, R. Z. Poore, T. M. Quinn, C. R. Maupin, K. Lin, and C.-C. Shen (2014), A reconstruction of sea surface temperature variability in the southeastern Gulf of Mexico from 1734-2008 CE using cross-dated Sr/Ca records from the coral *Siderastrea siderea*, *Paleoceanography*, *29*(5), 403–422.

Diaz-Pulido, G., C. Cornwall, P. Gartrell, C. Hurd, and D. V. Tran (2016), Strategies of dissolved inorganic carbon use in macroalgae across a gradient of terrestrial influence: implications for the Great Barrier Reef in the context of ocean acidification, *Coral Reefs*, 1-15.

Dickson, A. D. (1990), Thermodynamics of the dissociation of boric acid in synthetic seawater from 273.15 to 318.15 K, *Deep-Sea Research*, *37*(5), 755-766.

Dissard, D., E. Douville, S. Reynaud, A. Juillet-Leclerc, P. Montagna, P. Louvat, and M. McCulloch (2012), Light and temperature effects on $\delta^{11}B$ and B/Ca ratios of the zooxanthellate coral *Acropora sp.*: results from culturing experiments, *Biogeosciences*, *9*(11), 4589-4605.

Doney, S. C., V. J. Fabry, R. A. Feely, and J. Kleypas (2009), Ocean Acidification: The Other CO_2 Problem, *Annual Review of Marine Science*, *1*, 169-192.

Donner, S. D., T. R. Knutson, and M. Oppenheimer (2007), Model-based assessment of the role of human-induced climate change in the 2005 Caribbean coral bleaching event, *Proceedings of the National Academy of Sciences*, *104*(13), 5483-5488.

Eakin, C. M., J. A. Morgan, S. F. Heron, T. B. Smith, G. Liu, L. Alvarez-Filip, B. Baca, E. Bartels, C. Bastidas, and C. Bouchon (2010), Caribbean corals in crisis: record thermal stress, bleaching, and mortality in 2005, *PLoS One*, *5*(11), e13969.

Edmunds, P., and P. S. Davies (1986), An energy budget for *Porites porites* (Scleractinia), *Marine Biology*, *92*(3), 339-347.

Enfield, D. B., and E. J. Alfaro (1999), The dependence of Caribbean rainfall on the interaction of the tropical Atlantic and Pacific Oceans, *Journal of Climate*, *12*(7), 2093-2103.

G. Esslemont, R.A. Russel, W.A. Maher (2004), Coral record of harbour dredging: Townsville, Australia, *Journnal of Marine Systems*, *52*(1-4), 51-64.

Ezer, T., D. V. Thattai, B. Kjerfve, and W. D. Heyman (2005), On the variability of the flow along the Meso-American Barrier Reef system: a numerical model study of the influence of the Caribbean current and eddies, *Ocean Dynamics*, *55*(5-6), 458-475.

Fabricius, K., G. De'ath, L. McCook, E. Turak, and D. M. Williams (2005), Changes in algal, coral and fish assemblages along water quality gradients on the inshore Great Barrier Reef, *Marine Pollution Bulletin*, *51*(1), 384-398.

Fabricius, K. E. (2005), Effects of terrestrial runoff on the ecology of corals and coral reefs: review and synthesis, *Marine Pollution Bulletin*, *50*(2), 125-146.

Fallon, S. J., M. T. McCulloch, and C. Alibert (2003), Examining water temperature proxies in *Porites* corals from the Great Barrier Reef: a cross-shelf comparison, *Coral Reefs*, *22*, 389–404.

FAO (2012), *The State of World Fisheries and Aquaculture*, Rome.

Feely, R. A., C. L. Sabine, K. Lee, W. Berelson, J. Kleypas, V. J. Fabry, and F. J. Millero (2004), Impact of Anthropogenic CO_2 on the $CaCO_3$ System in the Ocean, *Science*, *305*, 362-366.

Felis, T., A. Suzuki, H. Kuhnert, M. Dima, G. Lohmann, and H. Kawahata (2009), Subtropical coral reveals abrupt early-twentieth-century freshening in the western North Pacific Ocean, *Geology*, *37*(6), 527-530.

Felis, T., G. Lohmann, H. Kuhnert, S. J. Lorenz, D. Scholz, J. Pätzold, S. A. Al-Rousan, and S. M. Al-Moghrabi (2004), Increased seasonality in Middle East temperatures during the last interglacial period, *Nature*, *429*, 164-168.

Ferrier-Pagès, C., F. Boisson, D. Allemand, and E. Tambutté (2002), Kinetics of strontium uptake in the scleractinian coral *Stylophora pistillata*, *Marine Ecology Progress Series*, *245*, 93-100.

Finch, A. A., and N. Allison (2008), Mg structural state in coral aragonite and implications for the paleoenvironmental proxy, *Geophysical Research Letters*, *35*(8).

Fleitmann, D., R. B. Dunbar, M. McCulloch, M. Mudelsee, M. Vuille, T. R. McClanahan, J. E. Cole, and S. Eggins (2007), East African soil erosion recorded in a 300 year old coral colony from Kenya, *Geophysical Research Letters*, *34*(4).

Folland, C., and D. Parker (1995), Correction of instrumental biases in historical sea surface temperature data, *Quarterly Journal of the Royal Meteorological Society*, *121*(522), 319-367.

Foster, G. (2008), Seawater pH, pCO_2 and $[CO_3^{2-}]$ variations in the Caribbean Sea over the last 130 kyr: A boron isotope and B/Ca study of planktic foraminifera, *Earth and Planetary Science Letters*, *271*(1), 254-266.

Foster, G. L., and J. W. Rae (2016), Reconstructing ocean pH with boron isotopes in foraminifera, *Annual Review of Earth and Planetary Sciences*, *44*, 207-237.

Foster, G. L., P. A. E. Pogge von Strandmann, and J. W. B. Rae (2010), Boron and magnesium isotopic composition of seawater, *Geochemistry Geophysics Geosystems*, *11*(8), Q08015.

Foster, G. L., B. Hönisch, G. Paris, G. S. Dwyer, J. W. Rae, T. Elliott, J. Gaillardet, N. G. Hemming, P. Louvat, and A. Vengosh (2013), Interlaboratory comparison of boron isotope analyses of boric acid, seawater and marine $CaCO_3$ by MC-ICPMS and NTIMS, *Chemical Geology*, *358*, 1-14.

Fowell, S. E., K. Sandford, J. A. Stewart, K. D. Castillo, J. B. Ries, and G. L. Foster (2016), Intrareef variations in Li/Mg and Sr/Ca sea surface temperature proxies in the Caribbean reef-building coral *Siderastrea siderea*, *Paleoceanography*, *31*(10), 1315-1329.

Gaetani, G. A., and A. L. Cohen (2006), Element partitioning during precipitation of aragonite from seawater: A framework for understanding paleoproxies, *Geochimica et Cosmochimica Acta*, *70*, 4617-4634.

Gaetani, G. A., A. L. Cohen, Z. Wang, and J. Crusius (2011), Rayleigh-based, multi-element coral thermometry: A biomineralization approach to developing climate proxies, *Geochimica et Cosmochimica Acta*, *75*, 1920–1932.

Gagan, M. K., G. B. Dunbar, and A. Suzuki (2012), The effect of skeletal mass accumulation in *Porites* on coral Sr/Ca and $\delta^{18}O$ paleothermometry, *Paleoceanography*, *27*(1), PA1203.

Gagan, M. K., L. K. Ayliffe, D. Hopley, J. A. Cali, G. E. Mortimer, J. Chappell, M. T. McCulloch, and M. J. Head (1998), Temperature and surface-ocean water balance of the mid-Holocene tropical western Pacific, *Science*, *279*(5353), 1014-1018.

Gagnon, A. C., J. Adkins, and J. Erez (2012), Seawater transport during coral biomineralization, *Earth and Planetary Science Letters*, *329-330*, 150-161.

Gagnon, A. C., J. F. Adkins, D. P. Fernandez, and L. F. Robinson (2007), Sr/Ca and Mg/Ca vital effects correlated with skeletal architecture in a scleractinian deep-sea coral and the role of Rayleigh fractionation, *Earth and Planetary Science Letters*, *261*(1-2), 280–295.

Gagnon, A. C., J. F. Adkins, J. Erez, J. M. Eiler, and Y. Guan (2013), Sr/Ca sensitivity to aragonite saturation state in cultured subsamples from a single colony of coral: Mechanism of biomineralization during ocean acidification, *Geochimica et Cosmochimica Acta*, *105*(0), 240-254.

Galer, S. J. (1999), Optimal double and triple spiking for high precision lead isotopic measurement, *Chemical Geology*, *157*(3), 255-274.

Gardner, T. A., I. M. Côté, J. A. Gill, A. Grant, and A. R. Watkinson (2003), Long-term region-wide declines in Caribbean corals, *Science*, *301*(5635), 958-960.

Gattuso, J.-P., D. Allemand, and M. Frankignoulle (1999), Photosynthesis and calcification at cellular, organismal and community levels in coral reefs: a review on interactions and control by carbonate chemistry, *American zoologist*, *39*(1), 160-183.

Gattuso, J-P., and H. Lavigne (2009), Approaches and software tools to investigate the impact of ocean acidification, *Biogeosciences*, *6*, 2121–2133.

Gattuso, J.-P., A. Magnan, R. Billé, W. Cheung, E. Howes, F. Joos, D. Allemand, L. Bopp, S. Cooley, and C. Eakin (2015), Contrasting futures for ocean and society from different anthropogenic CO_2 emissions scenarios, *Science*, *349*(6243), aac4722.

GBRMPA (2016), Great Barrier Reef Coral Mortality, edited.

Georgiou, L., J. Falter, J. Trotter, D. I. Kline, M. Holcomb, S. G. Dove, O. Hoegh-Guldberg, and M. McCulloch (2015), pH homeostasis during coral calcification in a free ocean CO_2 enrichment (FOCE) experiment, Heron Island reef flat, Great Barrier Reef, *Proceedings of the National Academy of Sciences*, *112*(43), 13219-13224.

Giannini, A., Y. Kushnir, and M. A. Cane (2000), Interannual variability of Caribbean rainfall, ENSO, and the Atlantic Ocean, *Journal of Climate*, *13*(2), 297-311.

Glenn, E., D. Comarazamy, J. E. González, and T. Smith (2015), Detection of recent regional sea surface temperature warming in the Caribbean and surrounding region, *Geophysical Research Letters*, *42*(16), 6785-6792.

Glynn, P. W. (1996), Coral reef bleaching: facts, hypotheses and implications, *Global change biology*, *2*(6), 495-509.

Goreau, T., and A. Macfarlane (1990), Reduced growth rate of *Montastrea annularis* following the 1987–1988 coral-bleaching event, *Coral Reefs*, *8*(4), 211-215.

Goreau, T., T. McClanahan, R. Hayes, and A. Strong (2000), Conservation of coral reefs after the 1998 global bleaching event, *Conservation Biology*, *14*(1), 5-15.

Gould, J., D. Roemmich, S. Wijffels, H. Freeland, M. Ignaszewsky, X. Jianping, S. Pouliquen, Y. Desaubies, U. Send, and K. Radhakrishnan (2004), Argo profiling floats bring new era of *in situ* ocean observations, *Eos*, *85*(19), 179-184.

Graham, N. A. J., S. Jennings, M. A. MacNeil, D. Mouillot, and S. K. Wilson (2015), Predicting climate-driven regime shifts versus rebound potential in coral reefs, *Nature*, *518*(7537), 94-97.

Gray, S. E., M. D. DeGrandpre, C. Langdon, and J. E. Corredor (2012a), Short- term and seasonal pH, pCO_2 and saturation state variability in a coral- reef ecosystem, *Global Biogeochemical Cycles*, *26*(3).

Gray, S. E. C., M. D. DeGrandpre, T. S. Moore, T. R. Martz, G. E. Friederich, and K. S. Johnson (2011), Applications of in situ pH measurements for inorganic carbon calculations, *Marine Chemistry*, *125*(1), 82-90.

Grove, C. A., S. Kasper, J. Zinke, M. Pfeiffer, D. Garbe- Schönberg, and G. J. A. Brummer (2013), Confounding effects of coral growth and high SST variability on skeletal Sr/Ca: Implications for coral paleothermometry, *Geochemistry, Geophysics, Geosystems*, *14*(4), 1277-1293.

Guerrot, C., R. Millot, M. Robert, and P. Négrel (2011), Accurate and High- Precision Determination of Boron Isotopic Ratios at Low Concentration by MC- ICP- MS (Neptune), *Geostandards and Geoanalytical Research*, *35*(2), 275-284.

Hagens, M, and J. J. Middelburg (2016), Attributing seasonal pH variability in surface ocean waters to governing factors, *Geophysical Research Letters, 43*(24), 12528-12527

Hall, N., K. Berry, L. Rintoul, and M. Hoogenboom (2015), Microplastic ingestion by scleractinian corals, *Marine Biology, 162*(3), 725-732.

Hanor, J. S., L-H. Chan (1977), Non-conservative behavior of barium during mixing of Mississippi River and Gulf of Mexico waters, *Earth and Planetary Science Letters, 37*(2), 242-250.

Hart, S. R., A. L. Cohen, P. Ramsay (1997), Microscale analysis of Sr/Ca and Ba/Ca in *Porites, Proceedings of the 8th International Coral Reef Symposium*, 2

Hastenrath, S. (1976), Variations in low-latitude circulation and extreme climatic events in the tropical Americas, *Journal of the Atmospheric Sciences, 33*(2), 202-215.

Hathorne, E., A. C. Gagnon, T. Felis, J. F. Adkins, R. Asami, W. Boer, N. Caillon, D. Case, K. M. Cobb, E. Douville, P. deMenocal, A. Eisenhauer, D. Garbe-Schönberg, W. Geibert, S. Goldstein, K. Hughen, M. Inoue, H. Kawahata, M. Kölling, F. L. Cornec, B. K. Linsley, H. V. McGregor, P. Montagna, I. S. Nurhati, T. M. Quinn, J. Raddatz, H. Rebaubier, L. Robinson, F., A. Sadekov, R. M. Sherrell, D. Sinclair, A. W. Tudhope, G. Wei, H. Wong, H. C. Wu, and C.-F. You (2013a), Interlaboratory study for coral Sr/Ca and other element/Ca ratio measurements, *Geochemistry, Geophysics, Geosystems, 14*, 3730–3750.

Hathorne, E. C., T. Felis, A. Suzuki, H. Kawahata, and G. Cabioch (2013b), Lithium in the aragonite skeletons of massive *Porites* corals: A new tool to reconstruct tropical sea surface temperatures, *Palaeoceanography, 28*, 143–152.

Hawkins, J. P., and C. M. Roberts (2004), Effects of artisanal fishing on Caribbean coral reefs, *Conservation Biology, 18*(1), 215-226.

Hemming, N., T. Guilderson, and R. Fairbanks (1998), Seasonal variations in the boron isotopic composition of coral: A productivity signal?, *Global Biogeochemical Cycles, 12*(4), 581-586.

Hemming, N. G., and G. N. Hanson (1992), Boron isotopic composition and concentration in modern marine carbonates, *Geochimica et Cosmochimica Acta, 56*, 537-543.

Henehan, M. J., J. W. Rae, G. L. Foster, J. Erez, K. C. Prentice, M. Kucera, H. C. Bostock, M. A. Martínez-Botí, J. A. Milton, and P. A. Wilson (2013), Calibration of the boron isotope proxy in the planktonic foraminifera *Globigerinoides ruber* for use in palaeo-CO_2 reconstruction, *Earth and Planetary Science Letters, 364*, 111-122.

Hodgson, G. (1990), Sediment and the settlement of larvae of the reef coral *Pocillopora damicornis*, *Coral Reefs, 9*(1), 41-43.

Hoegh-Guldberg, O. (1999), Climate change, coral bleaching and the future of the world's coral reefs, *Marine and Freshwater Research, 50*(8), 839-866.

Hoegh-Guldberg, O., P. J. Mumby, A. J. Hooten, R. S. Steneck, P. Greenfield, E. Gomez, C. D. Harvell, P. F. Sale, A. J. Edwards, K. Caldeira, N. Knowlton, C. M. Eakin, R. Iglesias-Prieto, N. Muthiga, R. H. Bradbury, A. Dubi, and M. E. Hatziolos (2007), Coral reefs under rapid climate change and ocean acidification, *Science*, *318*(5857), 1737-1742.

Hofmann, G. E., J. E. Smith, K. S. Johnson, U. Send, L. A. Levin, F. Micheli, A. Paytan, N. N. Price, B. Peterson, and Y. Takeshita (2011), High-frequency dynamics of ocean pH: a multi-ecosystem comparison, *PLoS One*, *6*(12), e28983.

Houlbrèque, F., and C. Ferrier-Pagès (2009), Heterotrophy in scleractinian corals, *Biological Reviews*, *84*(1), 1-17.

Holcomb, M., D. C. McCorkle, and A. L. Cohen (2010), Long-term effects of nutrient and CO_2 enrichment on the temperate coral *Astrangia poculata* (Ellis and Solander, 1786), *Journal of Experimental Marine Biology and Ecology*, *386*(1-2), 27-33.

Holcomb, M., A. Venn, E. Tambutte, S. Tambutte, D. Allemand, J. Trotter, and M. McCulloch (2014), Coral calcifying fluid pH dictates response to ocean acidification, *Scientific reports*, *4*, 5207.

Hönisch, B., N. G. Hemming, A. G. Grottoli, A. Amat, G. N. Hanson, and J. Bijma (2004), Assessing scleractinian corals as recorders for paleo-pH: Empirical calibration and vital effects, *Geochimica et Cosmochimica Acta*, *68*(18), 3675-3685.

Horvath, K. M., K. D. Castillo, P. Armstrong, I. T. Westfield, T. Courtney, and J. B. Ries (2016), Next-century ocean acidification and warming both reduce calcification rate, but only acidification alters skeletal morphology of reef-building coral *Siderastrea siderea*, *Scientific Reports*, *6*, 29613.

Hughes, T. P. (1994), Catastrophes, phase shifts, and large-scale degradation of a Caribbean coral reef, *Science-AAAS-Weekly Paper Edition*, *265*(5178), 1547-1551.

Hughes, T. P., A. H. Baird, D. R. Bellwood, M. Card, S. R. Connolly, C. Folke, R. Grosberg, O. Hoegh-Guldberg, J. Jackson, and J. Kleypas (2003), Climate change, human impacts, and the resilience of coral reefs, *Science*, *301*(5635), 929-933.

Hume, B., C. D'angelo, J. Burt, A. C. Baker, B. Riegl, and J. Wiedenmann (2013), Corals from the Persian/Arabian Gulf as models for thermotolerant reef-builders: prevalence of clade C3 *Symbiodinium*, host fluorescence and *ex situ* temperature tolerance, *Marine Pollution Bulletin*, *72*(2), 313-322.

Iglesias-Rodriguez, D. M., P. R. Halloran, R. E. M. Riackaby, I. R. Hall, E. Colmenero-Hidalgo, J. R. Gittins, D. R. H. Green, T. Tyrrell, S. J. Gibbs, P. v. Dassow, E. Rehm, E. V. Armbrust, and K. P. Boessenkool (2008), Phytoplankton Calcification in a High-CO_2 World, *Science*, *320*, 336-340.

Ip, Y. K., and A. L. L. Lim (1991), Are calcium and strontium transported by the same mechanism in the hermatypic coral *Galaxea fascicularis*, *Journal of Experimental Biology*, *159*, 507-513.

IPCC (2007), Climate Change 2007: Synthesis Report. Contribution of Working Groups I, II and III to the Fourth Assessment Report of the Intergovernmental Panel on Climate Change*Rep.*, IPCC, Geneva, Switzerland.

Iwasaki, S., M. Inoue, A. Suzuki, O. Sasaki, H. Kano, A. Iguchi, K. Sakai, and H. Kawahata (2016), The role of symbiotic algae in the formation of the coral polyp skeleton: 3- D morphological study based on X- ray micro- computed tomography, *Geochemistry, Geophysics, Geosystems*.

Izuka, S. K. (1988), Relationship of magnesium and other minor elements in tests of *Cassidulina-subglobos*a and *Cassidulina-oriangulata* to physical oceanic properties, *Journal of Foraminiferal Research*, *18*(2), 151-157.

John, S. G., and J. F. Adkins (2010), Analysis of dissolved iron isotopes in seawater, *Marine Chemistry*, *119*(1), 65-76.
Johnson, D. (2002), Environmentally sustainable cruise tourism: a reality check, *Marine Policy*, *26*(4), 261-270.

Jones, G. P., M. I. McCormick, M. Srinivasan, and J. V. Eagle (2004), Coral decline threatens fish biodiversity in marine reserves, *Proceedings of the National Academy of Sciences of the United States of America*, *101*(21), 8251-8253.

Jones, P., K. Trenberth, P. Ambenje, R. Bojariu, D. Easterling, T. Klein, D. Parker, J. Renwick, M. Rusticucci, and B. Soden (2007), Observations: surface and atmospheric climate change, *IPCC, Climate change*, 235-336.

Kakihana, H., M. Kotaka, S. Satoh, M. Nomura, and M. Okamoto (1977), Fundamental studies of the ion-exchange separation of boron isotopes, *Bulletin of the Chemical Society of Japan*, *50*(1), 158-163.

Kayanne, H., H. Hata, K. Nozaki, K. Kato, A. Negishi, H. Saito, H. Yamano, T. Isamu, H. Kimoto, and M. Tsuda (2002), Submergible system to measure seawater pCO_2 on a shallow sea floor, *Marine Technology Society Journal*, *36*(1), 23-28.

Kayanne, H., H. Hata, S. Kudo, H. Yamano, A. Watanabe, Y. Ikeda, K. Nozaki, K. Kato, A. Negishi, and H. Saito (2005), Seasonal and bleaching- induced changes in coral reef metabolism and CO_2 flux, *Global Biogeochemical Cycles*, *19*(3).

Keeling, C. D., S. C. Piper, R. B. Bacastow, M. Wahlen, T. P. Whorf, M. Heimann, and H. A. Meijer (2005), Atmospheric CO_2 and $^{13}CO_2$ exchange with the terrestrial biosphere and oceans from 1978 to 2000: observations and carbon cycle implications, in *A history of atmospheric CO_2 and its effects on plants, animals, and ecosystems*, edited, pp. 83-113, Springer.

Kennedy, J. J., N. A. Rayner, R. O. Smith, D. E. Parker, and M. Saunby (2011), Reassessing biases and other uncertainties in sea surface temperature observations measured in situ since 1850: 2. Biases and homogenization, *Journal of Geophysical Research*, *116*(D12), 27

Keywan, R., S. Rao, V. Krey, C. Cho, V. Chirkov, G. Fischer, G. Kindermann, N. Nakicenovic, and P. Rafaj (2011), RCP 8.5—A scenario of comparatively high greenhouse gas emissions, *Climatic Change*, *109*, 33-57.

Kiessling, W., and C. Simpson (2011), On the potential for ocean acidification to be a general cause of ancient reef crises, *Global Change Biology*, *17*(1), 56-67.

Kiss, E. (1988), Ion-exchange separation and spectrophotometric determination of boron in geological materials, *Analytica Chimica Acta*, *211*, 243-256.

Kleypas, J. A. (1999), Geochemical consequences of increased atmospheric carbon dioxide on coral reefs, *Science*, *284*(5411), 118-120.
Kleypas, J. A., and K. K. Yates (2009), Coral reefs and ocean acidification, *Oceanography*.

Kleypas, J. A., G. Danabasoglu, and J. M. Lough (2008), Potential role of the ocean thermostat in determining regional differences in coral reef bleaching events, *Geophysical Research Letters*, *35*(3).

Kleypas, J. A., K. Anthony, and J. P. Gattuso (2011), Coral reefs modify their seawater carbon chemistry–case study from a barrier reef (Moorea, French Polynesia), *Global Change Biology*, *17*(12), 3667-3678.

Kleypas, J. A., R. A. Feely, V. J. Fabry, C. Langdon, C. L. Sabine, and L. L. Robbins (2005), Impacts of ocean acidification on coral reefs and other marine calcifiers: a guide for future research, paper presented at Report of a workshop held 18–20 April 2005, St. Petersburg, Florida, sponsored by the National Science Foundation, National Oceanic and Atmospheric Administration, and the U.S. Geological Survey: http://www.healthyreefs.org/pdf/communicati.pdf.

Kline, D. I., L. Teneva, K. Schneider, T. Miard, A. Chai, M. Marker, K. Headley, B. Opdyke, M. Nash, M. Valetich, J. K. Caves, B. D. Russell, S. D. Connell, B. J. Kirkwood, P. Brewer, E. Peltzer, J. Silverman, K. Caldeira, R. B. Dunbar, J. R. Koseff, S. G. Monismith, B. G. Mitchell, S. Dove, and O. Hoegh-Guldberg (2012), A short-term *in situ* CO_2 enrichment experiment on Heron Island (GBR), *Scientific Reports*, *2*, 413.

Klochko, K., A. J. Kaufman, W. Yao, R. H. Byrne, and J. A. Tossell (2006), Experimental measurement of boron isotope fractionation in seawater, *Earth and Planetary Science Letters*, *248*(1-2), 276-285.

Klochko, K., G. D. Cody, J. A. Tossell, P. Dera, and A. J. Kaufman (2009), Re-evaluating boron speciation in biogenic calcite and aragonite using ^{11}B MAS NMR, *Geochimica et Cosmochimica Acta*, *73*(7), 1890-1900.

Knaff, J. A. (1997), Implications of summertime sea level pressure anomalies in the tropical Atlantic region, *Journal of Climate*, *10*(4), 789-804.

Kramer, P., M. McField, F. Álvarez, L. , I. Drysdale, M. Rueda Flores, A. Giró, and R. Pott (2015), Report Card for the Mesoamerican Reef *Rep.*

Krief, S., E. J. Hendy, M. Fine, R. Yam, A. Meibom, G. L. Foster, and A. Shemesh (2010), Physiological and isotopic responses of scleractinian corals to ocean acidification, *Geochimica et Cosmochimica Acta*, *74*(17), 4988-5001.

Kuffner, I. B., P. L. Jokiel, K. u. S. Rodgers, A. J. Andersson, and F. T. Mackenzie (2012), An apparent "vital effect" of calcification rate on the Sr/Ca temperature proxy in the reef coral *Montipora capitata*, *Geochemistry, Geophysics, Geosystems*, *13*(8).

Lamb, J. B., J. D. True, S. Piromvaragorn, and B. L. Willis (2014), Scuba diving damage and intensity of tourist activities increases coral disease prevalence, *Biological Conservation*, *178*, 88-96.

Langdon, C., and M. Atkinson (2005), Effect of elevated pCO_2 on photosynthesis and calcification of corals and interactions with seasonal change in temperature/irradiance and nutrient enrichment, *Journal of Geophysical Research: Oceans*, *110*(C9).

Lapointe, B. E., P. J. Barile, M. M. Littler, and D. S. Littler (2005), Macroalgal blooms on southeast Florida coral reefs: II. Cross-shelf discrimination of nitrogen sources indicates widespread assimilation of sewage nitrogen, *Harmful Algae*, *4*(6), 1106-1122.

Larpnun, R., C. Scott, and P. Surasawadi (2011), Practical coral reef management on a small island: Controlling sediment on Koh Tao, Thailand, *Catchment Management and Coral Reef Conservation: a practical guide for coastal resource managers to reduce damage from catchment areas based on best practice case studies*, *88*.

Lavigne, H., and J. P. Gattuso (2010), Seacarb: Seawater Carbonate Chemistry with R. R Package Version 2.3.5, edited.

Le Quéré, C., T. Takahashi, E. T. Buitenhuis, C. Rödenbeck, and S. C. Sutherland (2010), Impact of climate change and variability on the global oceanic sink of CO_2, *Global Biogeochemical Cycles*, *24*(4), GB4007.

Lea, D. W., G. T. Shen, and E. A. Boyle (1989), Coralline barium records temporal variability in equatorial Pacific upwelling, *Nature*, *340*(6232), 373-376.

Leder, J. J., A. M. Szmant, and P. K. Swart (1991), The effect of prolonged "bleaching" on skeletal banding and stable isotopic composition in *Montastrea annularis*, *Coral Reefs*, *10*(1), 19-27.

Lemarchand, D., J. Gaillardet, C. Göpel, and G. Manhes (2002), An optimized procedure for boron separation and mass spectrometry analysis for river samples, *Chemical Geology*, *182*(2), 323-334.

Levitus, S., J. I. Antonov, T. P. Boyer, O. K. Baranova, H. E. Garcia, R. A. Locarnini, A. V. Mishonov, J. Reagan, D. Seidov, and E. S. Yarosh (2012), World ocean heat content and thermosteric sea level change (0–2000 m), 1955–2010, *Geophysical Research Letters*, *39*(10).

Lewis, B. M., L. D. Nothdurft, and L. N. Nothdurft (2016), Expulsion of *Symbiodinium* by pulsed inflation under hyperthermal stress in *Heliofungia actiniformis*, *Coral Reefs*, 1-1.

Lewis, S. E., J. E. Brodie, Z. T. Bainbridge, K. W. Rohde, A. M. Davis, B. L. Masters, M. Maughan, M. J. Devlin, J. F. Mueller, and B. Schaffelke (2009), Herbicides: a new threat to the Great Barrier Reef, *Environmental Pollution*, *157*(8), 2470-2484.

Linsley, B., G. Wellington, D. Schrag, L. Ren, M. Salinger, and A. Tudhope (2004), Geochemical evidence from corals for changes in the amplitude and spatial pattern of South Pacific interdecadal climate variability over the last 300 years, *Climate Dynamics*, *22*(1), 1-11.

Liu, G., A. E. Strong, and W. Skirving (2003), Remote sensing of sea surface temperatures during 2002 Barrier Reef coral bleaching, *Eos, Transactions American Geophysical Union*, *84*(15), 137-141.

Liu, Y., W. Liu, Z. Peng, Y. Xiao, G. Wei, W. Sun, J. He, G. Liu, and C.-L. Chou (2009), Instability of seawater pH in the South China Sea during the mid-late Holocene: Evidence from boron isotopic composition of corals, *Geochimica et Cosmochimica Acta*, *73*(5), 1264-1272.

Liu, Y., Z. Peng, R. Zhou, S. Song, W. Liu, C.-F. You, Y.-P. Lin, K. Yu, C.-C. Wu, and G. Wei (2014), Acceleration of modern acidification in the South China Sea driven by anthropogenic CO_2, *Scientific reports*, *4*.

Lough, J., and D. Barnes (2000), Environmental controls on growth of the massive coral *Porites*, *Journal of Experimental Marine Biology and Ecology*, *245*(2), 225-243.

Lugo-Fernández, A., H. H. Roberts, and J. N. Suhayda (1998), Wave transformations across a Caribbean fringing-barrier coral reef, *Continental Shelf Research*, *18*(10), 1099-1124.

Lüthi, D., M. Le Floch, B. Bereiter, T. Blunier, and J.-M. Barnola (2008), High-resolution carbon dioxide concentration record 650,000-800,000 years before present, *Nature*, *453*, 379–382.

Mann, K., and J. Lazier (1996), Dynamics of marine ecosystems: Blackwell Science Cambridge, edited, Massachusetts.

Mantua, N. J., and S. R. Hare (2002), The Pacific decadal oscillation, *Journal of Oceanography*, *58*(1), 35-44.

Manzello, D. P. (2010), Ocean acidification hotspots: Spatiotemporal dynamics of the seawater CO_2 system of eastern Pacific coral reefs, *Limnology and Oceanography*, *55*(1), 239-248.

Marriott, C. S., G. M. Henderson, N. S. Belshaw, and A. W. Tudhope (2004a), Temperature dependence of δ^7Li, δ^{44}Ca and Li/Ca during growth of calcium carbonate, *Earth and Planetary Science Letters*, *222*(2), 615–624.

Marriott, C. S., G. M. Henderson, R. Crompton, M. Staubwasser, and S. Shaw (2004b), Effect of mineralogy, salinity, and temperature on Li/Ca and Li isotope composition of calcium carbonate, *Chemical Geology*, *212*(1-2), 5–15.

Marshall, J. F., and M. T. McCulloch (2002), An assessment of the Sr/Ca ratio in shallow water hermatypic corals as a proxy for sea surface temperature, *Geochimica et Cosmochimica Acta*, *66*(18), 3263-3280.

Martin, P., N. F. Goodkin, J. A. Stewart, G. L. Foster, E. L. Sikes, H. K. White, S. Hennige, and J. M. Roberts (2016), Deep- sea coral δ^{13}C: A tool to reconstruct the difference between seawater pH and δ^{11}B- derived calcifying fluid pH, *Geophysical Research Letters*, *43*(1), 299-308.

Martínez-Botí, M., G. Marino, G. Foster, P. Ziveri, M. Henehan, J. Rae, P. G. Mortyn, and D. Vance (2015), Boron isotope evidence for oceanic carbon dioxide leakage during the last deglaciation, *Nature*, *518*(7538), 219-222.

Martz, T. R., J. J. Carr, C. R. French, and M. D. DeGrandpre (2003), A submersible autonomous sensor for spectrophotometric pH measurements of natural waters, *Analytical Chemistry*, *75*(8), 1844-1850.

Marubini, F., and P. Davies (1996), Nitrate increases zooxanthellae population density and reduces skeletogenesis in corals, *Marine Biology*, *127*(2), 319-328.

Marubini, F., and M. Atkinson (1999), Effects of lowered pH and elevated nitrate on coral calcification, *Marine Ecology Progress Series*, *188*, 117-121.

Marubini, F., H. Barnett, C. Langdon, and M. Atkinson (2001), Dependence of calcification on light and carbonate ion concentration for the hermatypic coral *Porites compressa*, *Marine Ecology*
Progress Series, *220*, 153-162.

Marubini, F., C. Ferrier-Pagès, P. Furla, and D. Allemand (2008), Coral calcification responds to seawater acidification: a working hypothesis towards a physiological mechanism, *Coral Reefs*, *27*(3), 491-499.

Maupin, C., R., T. M. Quinn, and R. B. Halley (2008), Extracting a climate signal from the skeletal geochemistry of the Caribbean coral *Siderastrea siderea*, *Geochemistry, Geophysics, Geosystems*, *9*(12), Q12012.

McClanahan, T., R. Aronson, W. Precht, and N. Muthiga (1999), Fleshy algae dominate remote coral reefs of Belize, *Coral Reefs*, *18*(1), 61-62.

McClanahan, T. A., and N. A. Muthiga (1998), An ecological shift in a remote coral atoll of Belize over 25 years, *Environmental Conservation*, *25*(02), 122-130.

McConnaughy, T. (1989), ^{13}C and ^{18}O isotopic disequilibrium in biological carbonates: I. Patterns, *Geochimica et Cosmochimica Acta*, *53*, 151-162.

McCook, L., J. Jompa, and G. Diaz-Pulido (2001), Competition between corals and algae on coral reefs: a review of evidence and mechanisms, *Coral Reefs*, *19*(4), 400-417.

McCulloch, M., J. Falter, J. Trotter, and P. Montagna (2012a), Coral resilience to ocean acidification and global warming through pH up-regulation, *Nature Climate Change*, *2*, 623-627.

McCulloch, M., S. Fallon, T. Wyndham, E. Hendy, J. Lough, and D. Barnes (2003), Coral record of increased sediment flux to the inner Great Barrier Reef since European settlement, *Nature*, *421*(6924), 727-730.

McCulloch, M., J. Trotter, P. Montagna, J. Falter, R. Dunbar, A. Freiwald, G. Försterra, M. López Correa, C. Maier, A. Rüggeberg, and M. Taviani (2012b), Resilience of cold-water scleractinian corals to ocean acidification: Boron isotopic systematics of pH and saturation state up-regulation, *Geochimica et Cosmochimica Acta*, *87*, 21-34.

McCulloch, M. T., M. Holcomb, K. Rankenburg, and J. A. Trotter (2014), Rapid, high-precision measurements of boron isotopic compositions in marine carbonates, *Rapid Communications in Mass Spectrometry*, *28*(24), 2704-2712.

McCulloch, M. T., M. K. Gagan, G. E. Mortimer, A. Chivas, R. , and P. J. Isdale (1994), A high-resolution Sr/Ca and $\delta^{18}O$ coral record from the Great Barrier Reef, Australia, and the 1982–1983 El Niño, *Geochimica et Cosmochimica Acta*, *58*(12), 2747-2754.

McCulloch, M. T., A. W. Tudhope, T. M. Esat, G. E. Mortimer, J. Chappell, B. Pillans, A. R. Chivas, and A. Omura (1999), Coral record of equatorial sea-surface temperatures during the penultimate deglaciation at Huon Peninsula, *Science*, *283*(5399), 202-204.

McGregor, H. V., and M. K. Gagan (2003), Diagenesis and geochemistry of Porites corals from Papua New Guinea: implications for paleoclimate reconstruction, *Geochimica et Cosmochimica Acta*, *67*(12), 2147-2156.

McManus, W. J., J. Reyes, B. Rodolfo, and J. Nañola, L. Cleto (1997), Effects of some destructive fishing methods on coral cover and potential rates of recovery, *Environmental Management*, *21*(1), 69-78.

McPhaden, M. J. (1999), Genesis and Evolution of the 1997-98 El Niño, *Science*, *283*(5404), 950-954.

Meibom, A., H. Yurimoto, J.-P. Cuif, I. Domart-Coulon, F. Houlbreque, B. Constantz, Y. Dauphin, E. Tambutté, S. Tambutté, D. Allemand, J. Wooden, and R. B. Dunbar (2006), Vital effects in coral skeletal composition display strict three-dimensional control, *Geophysical Research Letters*, *33*, L11608.

Mendes, J., and J. Woodley (2002), Effect of the 1995-1996 bleaching event on polyp tissue depth, growth, reproduction and skeletal band formation in *Montastraea annularis*, *Marine Ecology Progress Series*, *235*, 93-102.

Mitsuguchi, T., E. Matsumoto, O. Abe, T. Uchida, and P. J. Isdale (1996), Mg/Ca thermometry in coral skeletons, *Science*, *274*(5289), 961-963.

Mitsuguchi, T., P. X. Dang, H. Kitagawa, T. Uchida, and Y. Shibata (2008), Coral Sr/Ca and Mg/Ca records in Con Dao Island off the Mekong Delta: Assessment of their potential for monitoring ENSO and East Asian monsoon, *Global and Planetary Change*, *63*(4), 341–352.

Montaggioni, L. F., F. Le Cornec, T. Corrège, and G. Cabioch (2006), Coral barium/calcium record of mid-Holocene upwelling activity in New Caledonia, South-West Pacific, *Palaeogeography, Palaeoclimatology, Palaeoecology*, *237*(2), 436-455.

Montagna, P., M. McCulloch, E. Douville, M. López Correa, J. Trotter, R. Rodolfo-Metalpa, D. Dissard, C. Ferrier-Pagès, N. Frank, A. Freiwald, S. Goldstein, C. Mazzoli, S. Reynaud, A. Rüggeberg, S. Russo, and M. Taviani (2014), Li/Mg systematics in scleractinian corals: Calibration of the thermometer, *Geochimica et Cosmochimica Acta*, *132*(0), 288-310.

Morice, C. P., J. J. Kennedy, N. A. Rayner, and P. D. Jones (2012), Quantifying uncertainties in global and regional temperature change using an ensemble of observational estimates: The HadCRUT4 data set, *Journal of Geophysical Research: Atmospheres*, *117*(D8).

Morse, J. W., A. J. Andersson, and F. T. Mackenzie (2006), Initial responses of carbonate-rich shelf sediments to rising atmospheric pCO_2 and "ocean acidification": role of high Mg-calcites, *Geochimica et Cosmochimica Acta*, *70*(23), 5814-5830.

Moya, A., S. Tambutté, A. Bertucci, E. Tambutté, S. Lotto, D. Vullo, C. T. Supuran, D. Allemand, and D. Zoccolo (2008), Carbonic anhydrase in the scleractinian coral *Stylophora pistillata*: Characterization, localization, and role in biomineralization, *Journal of Biological Chemistry*, *283*, 25475-25484.

Moyer, R., and A. Grottoli (2011), Coral skeletal carbon isotopes ($\delta^{13}C$ and $\Delta^{14}C$) record the delivery of terrestrial carbon to the coastal waters of Puerto Rico, *Coral Reefs*, *30*(3), 791-802.

Mucci, A., R. Canuel, and S. Zhong (1989), The solubility of calcite and aragonite in sulfate-free seawater and the seeded growth kinetics and composition of the precipitates at 25°C, *Chemical Geology*, *74*(3-4), 309-320.

Muller, E., C. S. Rogers, A. S. Spitzack, and R. Van Woesik (2008), Bleaching increases likelihood of disease on *Acropora palmata* (Lamarck) in Hawksnest Bay, St John, US Virgin Islands, *Coral Reefs*, *27*(1), 191-195.

Mumby, P.J. (2009), Herbivory versus corallivory: are parrotfish good or bad for Caribbean coral reefs? *Coral Reefs*, *28*(3): 683-690.

Muscatine, L. (1990), The role of symbiotic algae in carbon and energy flux in reef corals, *Ecosystems of the world*, *25*, 75-87.

Muscatine, L., L. McCloskey, and R. Marian (1981), Estimating the daily contribution of carbon from zooxanthellae to coral animal respiration, *Oceanography*, *26*(4).

Muscatine, L. and J. Porter (1977), Reef corals: Mutualistic symbioses adapted to nutrient poor environments, *BioScience*, *27*(7), 454-460.

Muscatine, L., J. Porter, and I. Kaplan (1989), Resource partitioning by reef corals as determined from stable isotope composition, *Marine Biology*, *100*(2), 185-193.

Ni, Y. (2006), Evaluation of boron isotopes and trace abundances in planktonic foraminifers as palaeo-oceanographic proxies, 217 pp, University of Bristol, University of Bristol.

Ni, Y., G. L. Foster, T. Bailey, T. Elliott, D. N. Schmidt, P. Pearson, B. Haley, and C. Coath (2007), A core top assessment of proxies for the ocean carbonate system in surface-dwelling foraminifers, *Paleoceanography*, *22*(3).

NMFS (2006), National Marine Fisheries Service, Status report on the continental United States distinct population segment of the *Epinepheuls itajara*, edited by NOAA, Silver Spring, MD.

Nurhati, I. S., K. M. Cobb, C. D. Charles, and R. B. Dunbar (2009), Late 20th century warming and freshening in the central tropical Pacific, *Geophysical Research Letters*, *36*(21).

Ogden, J., and N. Ogden (1998), Reconnaissance survey of the coral reefs and associated ecosystems of Cayos Cochinos, Honduras, *Revista de biología tropical*, *46*, 67-74.

Okai, T., A. Suzuki, H. Kawahata, S. Terashima, and N. Imai (2002), Preparation of a New Geological Survey of Japan Geochemical Reference Material: Coral JCp-1, *Geostandards Newsletter*, *26*(1), 95-99.

Orr, J. C., V. J. Fabry, O. Aumont, L. Bopp, S. C. Doney, R. A. Feely, A. Gnanadesikan, N. Gruber, A. Ishida, F. Joos, R. M. Key, K. Lindsay, E. Maier-Reimer, R. Matear, P. Monfray, A. Mouchat, R. G. Najjar, G.-K. Plattner, K. B. Rodgers, C. L. Sabine, J. L. Sarmiento, R. Schlitzer, R. D. Slater, I. J. Totterdell, M.-F. Weirig, Y. Yamanaka, and A. Yool (2005), Anthropogenic ocean acidification over the twenty-first century and its impact on calcifying organisms, *Nature*, *437*(29), 681-686.

Pandolfi, J. M. (2015), Incorporating uncertainty in predicting the future response of coral reefs to climate change, *Annual Review of Ecology, Evolution, and Systematics*, *46*, 281-303.

Pandolfi, J. M., S. R. Connolly, D. J. Marshall, and A. L. Cohen (2011), Projecting coral reef futures under global warming and ocean acidification, *Science*, *333*(6041), 418-422.

Pandolfi, J. M., R. H. Bradbury, E. Sala, T. P. Hughes, K. A. Bjorndal, R. G. Cooke, D. McArdle, L. McClenachan, M. J. Newman, and G. Paredes (2003), Global trajectories of the long-term decline of coral reef ecosystems, *Science*, *301*(5635), 955-958.

Paris, C., and L. Chérubin (2008), River-reef connectivity in the Meso-American Region, *Coral Reefs*, *27*(4), 773-781.

Patterson, K. L., J. W. Porter, K. B. Ritchie, S. W. Polson, E. Mueller, E. C. Peters, D. L. Santavy, and G. W. Smith (2002), The etiology of white pox, a lethal disease of the Caribbean elkhorn coral, *Acropora palmata*, *Proceedings of the National Academy of Sciences*, *99*(13), 8725-8730.

Pelejero, C., E. Calvo, M. T. McCulloch, J. F. Marshall, M. K. Gagan, J. M. Lough, and B. N. Opdyke (2005), Preindustrial to modern interdecadal variability in coral reef pH, *Science*, *309*(5744), 2204-2207.

Penland, C., and L. Matrosova (1998), Prediction of tropical Atlantic sea surface temperatures using linear inverse modeling, *Journal of Climate*, *11*(3), 483-496.

Penman, D. E., B. Hönisch, R. E. Zeebe, E. Thomas, and J. C. Zachos (2014), Rapid and sustained surface ocean acidification during the Paleocene- Eocene Thermal Maximum, *Paleoceanography*, *29*(5), 357-369.

Pfeiffer, M., W.-C. Dullo, J. Zinke, and D. Garbe-Schönberg (2009), Three monthly coral Sr/Ca records from the Chagos Archipelago covering the period of 1950–1995 AD: reproducibility and implications for quantitative reconstructions of sea surface temperature variations, *International Journal of Earth Sciences*, *98*(1), 53-66.

Prins, H., and J. Elzenga (1989), Bicarbonate utilization: function and mechanism, *Aquatic Botany*, *34*(1), 59-83.

Prouty, N., M. E. Field, J. D. Stock, S. D. Jupiter, and M. McCulloch. (2010), Coral Ba/Ca records of sediment input to the fringing reef of the southshore of Moloka'i, Hawai'i over the last several decades, *Marine Pollution Bulletin*, *60*, 1822–1835

Prouty, N., K. Hughen, and J. Carilli (2008), Geochemical signature of land-based activities in Caribbean coral surface samples, *Coral Reefs*, *27*(4), 727-742.

Provoost, P., S. van Heuven, K. Soetaert, R. W. P. M. Laane, and J. J. Middelburg (2010), Seasonal and long-term changes in pH in the Dutch coastal zone, *Biogeosciences*, *7*(11), 3869-3878.

Quinn, T. M., and F. W. Taylor (2006), SST artifacts in coral proxy records produced by early marine diagenesis in a modern coral from Rabaul, Papua New Guinea, *Geophysical Research Letters*, *33*(4).

Quinn, T. M., T. J. Crowley, F. W. Taylor, C. Henin, P. Joannot, and Y. Join (1998), A multicentury stable isotope record from a New Caledonia coral: Interannual and decadal sea surface temperature variability in the southwest Pacific since 1657 AD, *Paleoceanography*, *13*(4), 412-426.

R Development Core Team (2013), R: A Language and Environment for Statistical Computing, edited, R Foundation for Statistical Computing, Vienna, Austria.

Raddatz, J., V. Liebetrau, A. Rüggeberg, E. Hathorne, A. Krabbenhöft, A. Eisenhauer, F. Böhm, H. Vollstaedt, J. Fietzke, M. López Correa, A. Freiwald, and W.-C. Dullo (2013), Stable Sr-isotope, Sr/Ca, Mg/Ca, Li/Ca and Mg/Li ratios in the scleractinian cold-water coral *Lophelia pertusa*, *Chemical Geology*, *352*.

Rae, J. W. B. (2011), Boron isotopes in benthic foraminifera: measurement, calibration and glacial CO_2, University of Bristol.

Raupach, M., G. Marland, P. Ciais, C. Le Quéré, J. Canadell, G. Klepper, and C. Field (2007), Global and regional drivers of accelerating CO_2 emissions, *Proceedings of the National Academy of Sciences of the United States of America*, *104*(24), 10288-10293.

Rayner, N., P. Brohan, D. Parker, C. Folland, J. Kennedy, M. Vanicek, T. Ansell, and S. Tett (2006), Improved analyses of changes and uncertainties in sea surface temperature measured in situ since the mid-nineteenth century: The HadSST2 dataset, *Journal of Climate*, *19*(3), 446-469.

Rayner, N. A., D. E. Parker, E. B. Horton, C. K. Folland, L. V. Alexander, and D. P. Rowell (2003), Global analyses of sea surface temperature, sea ice, and night marine air temperature since the late nineteenth century, *Journal of Geophysical Research*, *108*(D14).

Rayner, N. A., P. Brohan, D. E. Parker, C. K. Folland, J. J. Kennedy, M. Vanicek, T. J. Ansell, and S. F. B. Tett (2005), Improved analyses of changes and uncertainties in sea surface temperature measured *in situ* since the Mid-Nineteenth Century: The HadSST2 Dataset, *Journal of Climate*, *19*, 446-469.

Reichelt-Brushett, A., and P. Harrison (1999), The effect of copper, zinc and cadmium on fertilization success of gametes from scleractinian reef corals, *Marine Pollution Bulletin*, *38*(3), 182-187.

Rérolle, V. M., C. F. Floquet, A. J. Harris, M. C. Mowlem, R. R. Bellerby, and E. P. Achterberg (2013), Development of a colorimetric microfluidic pH sensor for autonomous seawater measurements, *Analytica Chimica Acta*, *786*, 124-131.

Restrepo, J. D., P. Zapata, J. M. Díaz, J. Garzón-Ferreira, and C. B. García (2006), Fluvial fluxes into the Caribbean Sea and their impact on coastal ecosystems: The Magdalena River, Colombia, *Global and Planetary Change*, *50*(1), 33-49.

Reynaud, S., N. G. Hemming, A. Juillet-Leclerc, and J.-P. Gattuso (2004), Effect of pCO_2 and temperature on the boron isotopic composition of the zooxanthellate coral *Acropora* sp., *Coral Reefs*, *23*, 539–546.

Reynaud, S., N. Leclercq, S. Romaine-Lioud, C. Ferrier-Pagés, J. Jaubert, and J.-P. Gattuso (2003), Interacting effects of CO_2 partial pressure and temperature on photosynthesis and calcification in a scleractinian coral, *Global Change Biology*, *9*(11), 1660-1668.

Reynaud, S., C. Ferrier-Pagès, A. Meibom, S. Mostefaoui, R. Mortlock, R. Fairbanks, and D. Allemand (2007), Light and temperature effects on Sr/Ca and Mg/Ca ratios in the scleractinian coral *Acropora sp*, *Geochimica et Cosmochimica Acta*, *71*(2), 354–362.

Reynolds, R. W., N. A. Rayner, T. M. Smith, D. C. Stokes, and W. Wang (2002), An improved *in situ* and satellite SST analysis for climate, *Journal of Climate*, *15*(13), 1609-1625.

Rhein, M. a., S. Rintoul, S. Aoki, E. Campos, D. Chambers, R. Feely, S. Gulev, G. Johnson, S. Josey, and A. Kostianoy (2013), Observations: ocean, *Climate change*, 255-315.

Ridgwell, A., and R. E. Zeebe (2005), The role of the global carbonate cycle in the regulation and evolution of the Earth system, *Earth and Planetary Science Letters*, *234*(3), 299-315.

Riegl, B. M., S. J. Purkis, A. S. Al-Cibahy, M. A. Abdel-Moati, and O. Hoegh-Guldberg (2011), Present limits to heat-adaptability in corals and population-level responses to climate extremes, *PLoS One*, *6*(9), e24802.

Ries, J. B. (2011), A physicochemical framework for interpreting the biological calcification response to CO_2-induced ocean acidification, *Geochimica et Cosmochimica Acta*, *75*(14), 4053-4064.

Ries, J. B., A. L. Cohen, and D. C. McCorkle (2009), Marine calcifiers exhibit mixed responses to CO_2-induced ocean acidification, *Geology*, *37*(12), 1131-1134.

Ries, J. B., A. L. Cohen, and D. C. McCorkle (2010), A nonlinear calcification response to CO_2-induced ocean acidification by the coral *Oculina arbuscula*, *Coral Reefs*, *29*(3), 661-674.

Rivest, E. B., and T. C. Gouhier (2015), Complex environmental forcing across the biogeographical range of coral populations, *PLoS One*, *10*(3), e0121742.

Rodolfo-Metalpa, R., F. Houlbreque, E. Tambutte, F. Boisson, C. Baggini, F. P. Patti, R. Jeffree, M. Fine, A. Foggo, J. P. Gattuso, and J. M. Hall-Spencer (2011), Coral and mollusc resistance to ocean acidification adversely affected by warming, *Nature Clim. Change*, *1*(6), 308-312.

Rodrigues, L. J., and A. G. Grottoli (2006), Calcification rate and the stable carbon, oxygen, and nitrogen isotopes in the skeleton, host tissue, and zooxanthellae of bleached and recovering Hawaiian corals, *Geochimica et Cosmochimica Acta*, *70*(11), 2781-2789.

Rogers, C. S. (1979), The effect of shading on coral reef structure and function, *Journal of Experimental Marine Biology and Ecology*, *41*(3), 269-288.

Rogers, C. S. (1990), Responses of coral reefs and reef organisms to sedimentation, *Marine ecology progress series. Oldendorf*, *62*(1), 185-202.

Rollion-Bard, C., M. Chaussidon, and C. France-Lanord (2011), Biological control of internal pH in scleractinian corals: Implications on paleo-pH and paleo-temperature reconstructions, *Comptes Rendus Geoscience*, *343*(6), 397-405.

Rosenheim, B. E., P. K. Swart, S. R. Thorrold, P. Willenz, L. Berry, and C. Latkoczy (2004), High-resolution Sr/Ca records in sclerosponges calibrated to temperature *in situ*, *Geology*, *32*(2), 145-148.

Rosenthal, Y., M. P. Field, and R. M. Sherrell (1999), Precise determination of Element/Calcium ratios in calcareous samples using sector field Inductively Coupled Plasma Mass Spectrometry, *Analytical Chemistry*, *71*, 3248-3253.

Rosner, M., R. L. Romer, and A. Meixner (2005), Air handling in clean laboratory environments: the reason for anomalously high boron background levels, *Analytical and Bioanalytical Chemistry*, *382*(1), 120-124.

Rüggeberg, A., J. Fietzke, V. Liebetrau, A. Eisenhauer, W.-C. Dullo, and A. Freiwald (2008), Stable strontium isotopes (δ 88/86 Sr) in cold-water corals—A new proxy for reconstruction of intermediate ocean water temperatures, *Earth and Planetary Science Letters*, *269*(3), 570-575.

Rustad, J. R., E. J. Bylaska, V. E. Jackson, and D. A. Dixon (2010), Calculation of boron-isotope fractionation between B (OH) 3 (aq) and, *Geochimica et Cosmochimica Acta*, *74*(10), 2843-2850.

Sabine, C. L., R. A. Feely, N. Gruber, R. M. Key, K. Lee, J. L. Bullister, R. Wanninkhof, C. S. Wong, D.
W. Wallace, B. Tilbrook, F. J. Millero, T. H. Peng, A. Kozyr, T. Ono, and A. F. Rios (2004), The oceanic sink for anthropogenic CO_2, *Science*, *305*(5682), 367-371.

Saenger, C., A. L. Cohen, D. W. Oppo, and D. Hubbard (2008), Interpreting sea surface temperature from strontium/calcium ratios in *Montastrea* corals: Link with growth rate and implications for proxy reconstructions, *Paleoceanography*, *23*(3), PA3102.

Sala, E., E. Ballesteros, and R. M. Starr (2001), Rapid Decline of Nassau Grouper Spawning Aggregations in Belize: Fishery Management and Conservation Needs, *Fisheries*, *26*(10), 23-30.

Santos, I. R., R. N. Glud, D. Maher, D. Erler, and B. D. Eyre (2011), Diel coral reef acidification driven by porewater advection in permeable carbonate sands, Heron Island, Great Barrier Reef, *Geophysical Research Letters*, *38*(3).

Sanyal, A., J. Bijma, H. Spero, and D. W. Lea (2001), Relationship between pH and the boron isotopic composition. Implications for the boron isotope as a paleo-pH proxy, *Palaeogeography*, *16*(5), 515-519.

Sanyal, A., N. G. Hemming, W. S. Broecker, D. W. Lea, H. J. Spero, and G. N. Hanson (1996), Oceanic pH control on the boron isotopic composition of foraminifera: Evidence from culture experiments, *Paleoceanography*, *11*(5), 513.

Saphier, A. D., and T. C. Hoffmann (2005), Forecasting models to quantify three anthropogenic stresses on coral reefs from marine recreation: Anchor damage, diver contact and copper emission from antifouling paint, *Marine Pollution Bulletin*, *51*(5), 590-598.

Sayani, H. R., K. M. Cobb, A. L. Cohen, W. C. Elliott, I. S. Nurhati, R. B. Dunbar, K. A. Rose, and L. K. Zaunbrecher (2011), Effects of diagenesis on paleoclimate reconstructions from modern and young fossil corals, *Geochimica et Cosmochimica Acta*, *75*(21), 6361-6373.

Schlesinger, M. E., and N. Ramankutty (1994), An oscillation in the global climate system of period 65-70 years, *Nature*, *367*(6465), 723-726.

Schmidt, C., M. Kucera, and S. Uthicke (2014), Combined effects of warming and ocean acidification on coral reef foraminifera *Marginopora vertebralis* and *Heterostegina depressa*, *Coral Reefs*, *33*(3), 805-818.

Schneider, K., and J. Erez (2006), The effect of carbonate chemistry on calcification and photosynthesis in the hermatypic coral *Acropora eurystoma*, *Limnol. Oceanogr., 51 (3) 1293., 1284*.

Schoepf, V., M. Stat, J. L. Falter, and M. T. McCulloch (2015), Limits to the thermal tolerance of corals adapted to a highly fluctuating, naturally extreme temperature environment, *Scientific reports*, *5*, 17639.

Schouten, S., E. C. Hopmans, E. Schefuss, and J. S. Sinninghe Damsté (2002), Distributional variations in marine crenarchaeotal membrane lipids: A new tool for reconstructing ancient sea water temperatures? , *Earth Planetary Science Letters*, *204*, 265-274.

Seidel, M. P., M. D. DeGrandpre, and A. G. Dickson (2008), A sensor for *in situ* indicator-based measurements of seawater pH, *Marine Chemistry*, *109*(1), 18-28.

Shannon, R. D. (1976), Revised effective ionic radii and systematic studies of interatomic distances in halides and chalcogenides, *Acta Crystallographica Section A: Crystal Physics, Diffraction, Theoretical and General Crystallography*, *32*(5), 751-767.

Sheng, J., L. Wang, S. Andréfouët, C. Hu, B. G. Hatcher, F. E. Muller- Karger, B. Kjerfve, W. D. Heyman, and B. Yang (2007), Upper ocean response of the Mesoamerican barrier reef system to Hurricane

Mitch and coastal freshwater inputs: A study using Sea- viewing Wide Field- of- view Sensor (SeaWiFS) ocean color data and a nested- grid ocean circulation model, *Journal of Geophysical Research: Oceans*, *112*, C07016.

Shimoda, T., T. Ichikawa, and Y. Matsukawa (1998), Nutrient conditions and their effects on coral growth in reefs around Ryukyu Islands, *Bulletin of the National Research Institute of Fisheries Science*, *10*(12), 71-80.

Shinjo, R., R. Asami, K.-F. Huang, C.-F. You, and Y. Iryu (2013), Ocean acidification trend in the tropical North Pacific since the mid-20th century reconstructed from a coral archive, *Marine Geology*, *342*, 58-64.

Silverman, J., B. Lazar, and J. Erez (2007), Effect of aragonite saturation, temperature, and nutrients on the community calcification rate of a coral reef, *Journal of Geophysical Research: Oceans*, *112*(C5).

Silverman, J., B. Lazar, L. Cao, K. Caldeira, and J. Erez (2009), Coral reefs may start dissolving when atmospheric CO_2 doubles, *Geophysical Research Letters*, *36*(5), L05606.

Sinclair, D. J. (2005), Correlated trace element "vital effects" in tropical corals: a new geochemical tool for probing biomineralization, *Geochimica et Cosmochimica Acta*, *69*(13), 3265-3284.

Sinclair, D. J. (2005), Non-river flood barium signals in the skeletons of corals from coastal Queensland, Australia, *Earth and Planetary Science Letters*, *237*(3-4), 354-469.

Sinclair, D. J., and M. T. McCulloch (2004), Corals record low mobile barium concentrations in the Burdekin River during the 1974 flood: evidence for limited Ba supply to rivers?, *Palaeogeography, Palaeoclimatology, Palaeoecology*, *214*(1), 155-174.

Sinclair, D. J., and M. J. Risk (2006), A numerical model of trace-element coprecipitation in a physicochemical calcification system: Application to coral biomineralization and trace-element 'vital effects', *Geochimica et Cosmochimica Acta*, *70*(15), 3855-3868.

Smith, D. J., D. J. Suggett, and N. R. Baker (2005), Is photoinhibition of zooxanthellae photosynthesis the primary cause of thermal bleaching in corals?, *Global Change Biology*, *11*(1), 1-11.

Smith, J. E., N. N. Price, C. E. Nelson, and A. F. Haas (2013), Coupled changes in oxygen concentration and pH caused by metabolism of benthic coral reef organisms, *Marine Biology*, *160*(9), 2437-2447.

Smith, J. E., H. P. Schwarcz, M. J. Risk, T. A. McCONNAUGHEY, and N. Keller (2000), Paleotemperatures from deep-sea corals: overcoming 'vital effects', *Palaios*, *15*(1), 25-32.

Smith, T. M., R. W. Reynolds, T. C. Peterson, and J. Lawrimore (2008), Improvements to NOAA's historical merged land–ocean surface temperature analysis (1880–2006), *Journal of Climate*, *21*, 2283–2296.

Soto, I., S. Andréfouët, C. Hu, F. Muller-Karger, C. Wall, J. Sheng, and B. Hatcher (2009), Physical connectivity in the Mesoamerican Barrier Reef System inferred from 9 years of ocean color observations, *Coral Reefs*, *28*(2), 415-425.

Spalding, M., C. Ravilious, and E. P. Green (2001), *World atlas of coral reefs*, Univ of California Press.

Steinacher, M., T. L. Frolicher, G. K. Plattner, and S. C. Doney (2009), Imminent ocean acidification in the Arctic projected with the NCAR global coupled carbon cycle-climate model, *Biogeosciences*, *6*, 515-533.

Stephens, M. P., G. Samuels, D. B. Olson, R. A. Fine, and T. Takahashi (1995), Sea- air flux of CO_2 in the North Pacific using shipboard and satellite data, *Journal of Geophysical Research: Oceans*, *100*(C7), 13571-13583.

Suchley, A., M. D. McField, and L. Alvarez-Filip (2016), Rapidly increasing macroalgal cover not related to herbivorous fishes on Mesoamerican reefs, *PeerJ*, *4*, e2084.

Sutherland, K. P., J. W. Porter, J. W. Turner, B. J. Thomas, E. E. Looney, T. P. Luna, M. K. Meyers, J. C. Futch, and E. K. Lipp (2010), Human sewage identified as likely source of white pox disease of the threatened Caribbean elkhorn coral, *Acropora palmata*, *Environmental microbiology*, *12*(5), 1122-1131.

Suzuki, A., and H. Kawahata (2003), Carbon budget of coral reef systems: an overview of observations in fringing reefs, barrier reefs and atolls in the Indo- Pacific regions, *Tellus B*, *55*(2), 428-444.

Swart, P. K. (1983), Carbon and oxygen isotope fractionation in scleractinian corals: a review, *Earth-Science Reviews*, *19*(1), 51-80.

Swart, P. K., H. Elderfield, and M. J. Greaves (2002), A high-resolution calibration of Sr/Ca thermometry using the Caribbean coral *Montastraea annularis*, *Geochemistry, Geophysics, Geosystems*, *3*(11), 1–11.

Swart, P. K., L. Greer, B. E. Rosenheim, C. S. Moses, A. J. Waite, A. Winter, R. E. Dodge, and K. Helmle (2010), The $\delta^{13}C$ Suess effect in scleractinian corals mirror changes in the anthropogenic CO_2 inventory of the surface oceans, *Geophysical Research Letters*, *37*(5).

Szmant, A., and N. Gassman (1990), The effects of prolonged "bleaching" on the tissue biomass and reproduction of the reef coral *Montastrea annularis*, *Coral Reefs*, *8*(4), 217-224.

Szmant, A. M. (2002), Nutrient enrichment on coral reefs: is it a major cause of coral reef decline?, *Estuaries*, *25*(4), 743-766.

Takahashi, T., S. C. Sutherland, D. W. Chipman, J. G. Goddard, C. Ho, T. Newberger, C. Sweeney, and D. R. Munro (2014), Climatological distributions of pH, pCO_2, total CO_2, alkalinity, and $CaCO_3$ saturation in the global surface ocean, and temporal changes at selected locations, *Marine Chemistry*, *164*, 95125.

Tambutté, S., M. Holcomb, C. Ferrier-Pagès, S. Reynaud, É. Tambutté, D. Zoccola, and D. Allemand (2011), Coral biomineralization: From the gene to the environment, *Journal of Experimental Marine Biology and Ecology*, *408*(1-2), 58-78.

Tan, S. H., and G. Horlick (1987), Matrix-effect observations in inductively coupled plasma mass spectrometry, *Journal of Analytical Atomic Spectrometry*, *2*(8), 745-763.

Tanaka, K., M. Holcomb, A. Takahashi, H. Kurihara, R. Asami, R. Shinjo, K. Sowa, K. Rankenburg, T. Watanabe, and M. McCulloch (2015), Response of *Acropora digitifera* to ocean acidification: constraints from $\delta^{11}B$, Sr, Mg, and Ba compositions of aragonitic skeletons cultured under variable seawater pH, *Coral Reefs*, *34*(4), 1139-1149.

Tang, L., J. Sheng, B. G. Hatcher, and P. F. Sale (2006), Numerical study of circulation, dispersion, and hydrodynamic connectivity of surface waters on the Belize shelf, *Journal of Geophysical Research: Oceans*, *111*(C1).

Tarrant, A., M. Atkinson, and S. Atkinson (2004), Effects of steroidal estrogens on coral growth and reproduction, *Marine Ecology Progress Series*, *269*, 121-129.

Taylor, M. A., D. B. Enfield, and A. A. Chen (2002), Influence of the tropical Atlantic versus the
tropical Pacific on Caribbean rainfall, *Journal of Geophysical Research: Oceans*, *107*(C9).

Tchernov, D., H. Kvitt, L. Haramaty, T. S. Bibby, M. Y. Gorbunov, H. Rosenfeld, and P. G. Falkowski (2011), Apoptosis and the selective survival of host animals following thermal bleaching in zooxanthellate corals, *Proceedings of the National Academy of Sciences*, *108*(24), 9905-9909.

Thresher, R. E., B. Tilbrook, S. Fallon, N. C. Wilson, J. Adkins (2011), Effects of chronic low saturation levels on the distribution, growth and skeletal chemistry of deep-sea corals and other seamount megabenthos, *Marine Ecology Progress Series*, *442*, 87-99.

Tierney, J. E., N. J. Abram, K. J. Anchukaitis, M. N. Evans, C. Giry, K. H. Kilbourne, C. P. Saenger, H. C. Wu, and J. Zinke (2015), Tropical sea surface temperatures for the past four centuries reconstructed from coral archives, *Paleoceanography*, *30*(3), 226-252.

Tilman, D., J. Fargione, B. Wolff, C. D'Antonio, A. Dobson, R. Howarth, D. Schindler, W. H. Schlesinger, D. Simberloff, and D. Swackhamer (2001), Forecasting agriculturally driven global environmental change, *Science*, *292*(5515), 281-284.

Tratalos, J. A., and T. J. Austin (2001), Impacts of recreational SCUBA diving on coral communities of the Caribbean island of Grand Cayman, *Biological Conservation*, *102*(1), 67-75.

Trotter, J., P. Montagna, M. McCulloch, S. Silenzi, S. Reynaud, G. Mortimer, S. Martin, C. Ferrier-Pagès, J.-P. Gattuso, and R. Rodolfo-Metalpa (2011), Quantifying the pH 'vital effect' in the temperate zooxanthellate coral *Cladocora caespitosa*: Validation of the boron seawater pH proxy, *Earth and Planetary Science Letters*, *303*(3-4), 163-173.

Tudhope, A. W., D. W. Lea, G. B. Shimmield, C. P. Chilcott, and S. Head (1996), Monsoon climate and Arabian Sea coastal upwelling recorded in massive corals from Southern Oman

Uchida, A., M. Nishizawa, K. Shirai, H. Iijima, H. Kayanne, N. Takahata, and Y. Sano (2008), High sensitivity measurements of nitrogen isotopic ratios in coral skeletons from Palau, western Pacific: Temporal resolution and seasonal variation of nitrogen sources, *Geochemical Journal*, *42*(3), 255-262.

Urey, H. C. (1947), The thermodynamic properties of isotopic substances, *Journal of the Chemical Society*, 562-581.

Urey, H. C., H. A. Lowenstam, S. Epstein, and C. R. McKinney (1951), Measurement of paleotemperatures and temperatures of the Upper Cretaceous of England, Denmark, and the southeastern United States, *Geological Society of America Bulletin*, *62*(4), 399-416.

van Dam, J. W., A. P. Negri, S. Uthicke, and J. F. Mueller (2011), Chemical pollution on coral reefs: exposure and ecological effects, *Ecological Impact of Toxic Chemicals.*, 187-211.

Van Hooidonk, R., J. Maynard, and S. Planes (2013), Temporary refugia for coral reefs in a warming world, *Nature Climate Change*, *3*(5), 508-511.

van Woesik, R., K. van Woesik, L. van Woesik, and S. van Woesik (2013), Effects of ocean acidification on the dissolution rates of reef-coral skeletons, *PeerJ*, *1*, e208.

Vega Thurber, R. L., D. E. Burkepile, C. Fuchs, A. A. Shantz, R. McMinds, and J. R. Zaneveld (2014), Chronic nutrient enrichment increases prevalence and severity of coral disease and bleaching, *Global change biology*, *20*(2), 544-554.

Vengosh, A., Y. Kolodny, A. Starinsky, A. R. Chivas, and M. T. McCulloch (1991), Coprecipitation and isotopic fractionation of boron in modern biogenic carbonates, *Geochimica et Cosmochimica Acta*, *55*(10), 2901-2910.

Venn, A., E. Tambutté, M. Holcomb, D. Allemand, and S. Tambutté (2011), Live tissue imaging shows reef corals elevate pH under their calcifying tissue relative to seawater, *PLoS One*, *6*(5), e20013.

Venn, A., E. Tambutté, M. Holcomb, J. Laurent, D. Allemand, and S. Tambutté (2013), Impact of seawater acidification on pH at the tissue-skeleton interface and calcification in reef corals, *Proceedings of the National Academy of Sciences of the United States of America*, *110*(5), 1634-1639.

Vitousek, P. M., H. A. Mooney, J. Lubchenco, and J. M. Melillo (1997), Human domination of Earth's ecosystems, *Science*, *277*(5325), 494-499.

Waliser, D. E., and C. Gautier (1993), A satellite-derived climatology of the ITCZ, *Journal of Climate*, *6*(11), 2162-2174.

Wang, B.-S., C.-F. You, K.-F. Huang, S.-F. Wu, S. K. Aggarwal, C.-H. Chung, and P.-Y. Lin (2010), Direct separation of boron from Na-and Ca-rich matrices by sublimation for stable isotope measurement by MC-ICP-MS, *Talanta*, *82*(4), 1378-1384.

Watson, E. B. (1996), Surface enrichment and trace-element uptake during crystal growth, *Geochimica et Cosmochimica Acta*, *60*(24), 5013-5020.

Weber, J. N. (1973), Incorporation of strontium into reef coral skeletal carbonate, *Geochimica et Cosmochimica Acta*, *37*(9), 2173-2190.

Weber, M., D. de Beer, C. Lott, L. Polerecky, K. Kohls, R. M. M. Abed, T. G., Ferdelman, and K. E. Fabricius (2012), Mechanisms of damage to corals exposed to sedimentation, *Proceedings of the National Academy of Science, 109*(24), E1558-E1567.

Wei, G., M. T. McCulloch, G. Mortimer, W. Deng, and L. Xie (2009), Evidence for ocean acidification in the Great Barrier Reef of Australia, *Geochimica et Cosmochimica Acta*, *73*(8), 2332-2346.

Wei, G., Z. Wang, T. Ke, Y. Liu, W. Deng, X. Chen, J. Xu, T. Zeng, and L. Xie (2015), Decadal variability in seawater pH in the West Pacific: Evidence from coral $\delta^{11}B$ records, *Journal of Geophysical Research: Oceans*, *120*(11), 7166-7181.

Weterings, R. (2011), A GIS-based assessment of threats to the natural environment on Koh Tao, Thailand, *Kasetsart J.(Nat. Sci.), 755*, 743-755.

Wiedenmann, J., C. D'Angelo, E. G. Smith, A. N. Hunt, F.-E. Legiret, A. D. Postle, and E. P. Achterberg (2013), Nutrient enrichment can increase the susceptibility of reef corals to bleaching, *Nature Climate Change*, *3*(2), 160-164.

Wilcox, L. J., A. J. Charlton-Perez, and L. J. Gray (2012), Trends in Austral jet position in ensembles of high- and low-top CMIP5 models, *Journal of Geophysical Research, 117*, D13115.

Wilkinson, C. (2008), Global coral reef monitoring network: status of coral reefs of the world in 2008, *Australian Institute of Marine Science, Townsville*.

Wittenberg, M., and W. Hunte (1992), Effects of eutrophication and sedimentation on juvenile corals, *Marine Biology*, *112*(1), 131-138.

Wollast, R., R. Garrels, and F. Mackenzie (1980), Calcite-seawater reactions in ocean surface waters, *Am. J. Sci*, *280*(9), 831-848.

Wolter, K., and M. S. Timlin (1998), Measuring the strength of ENSO events: how does 1997/98 rank? *Weather*, *53*(9), 315-324.

Woodruff, S. D., S. J. Worley, S. J. Lubker, Z. Ji, J. E. Freeman, D. I. Berry, P. Brohan, E. C. Kent, R. W. Reynolds, R. O. Smith, and C. Wilkinson (2011), ICOADS Release 2.5: extensions and enhancements to the surface marine meteorological archive, *International Journal of Climatology*, *31*(7), 951–967.

Wooldridge, S. A. (2009), Water quality and coral bleaching thresholds: Formalising the linkage for the inshore reefs of the Great Barrier Reef, Australia, *Marine Pollution Bulletin*, *58*(5), 745-751.

Wootton, J. T., and C. A. Pfister (2012), Carbon system measurements and potential climatic drivers at a site of rapidly declining ocean pH, *PLoS One*, *7*(12), e53396.

Yamazaki, A., T. Watanabe, and U. Tsunogai (2011), Nitrogen isotopes of organic nitrogen in reef coral skeletons as a proxy of tropical nutrient dynamics, *Geophysical Research Letters*, *38*(19).

Yates, K., and R. Halley (2006), CO_3^{2-} concentration and pCO_2 thresholds for calcification and dissolution on the Molokai reef flat, Hawaii, *Biogeosciences Discussions*, *3*(1), 123-154.

Zak, M. R., M. Cabido, and J. G. Hodgson (2004), Do subtropical seasonal forests in the Gran Chaco, Argentina, have a future?, *Biological conservation*, *120*(4), 589-598.

Zakai, D., and N. E. Chadwick-Furman (2002), Impacts of intensive recreational diving on reef corals at Eilat, northern Red Sea, *Biological Conservation*, *105*(2), 179-187.

Zeebe, R. E. (1999), An explanation of the effect of seawater carbonate concentration on foraminiferal oxygen isotopes, *Geochimica et Cosmochimica Acta*, *63*(13), 2001-2007.

Zeebe, R. E., and D. Wolf-Gladrow (2001), *CO_2 in seawater : equilibrium, kinetics and isotopes.*, Elsevier Science, Amsterdam.

Zeebe, R. E., and A. Sanyal (2002), Comparison of two potential strategies of planktonic foraminifera for house building: Mg^{2+} or H^+ removal?, *Geochimica et Cosmochimica Acta*, *66*(7), 1159 –1169.

Zeebe, R. E., A. Ridgwell, and J. C. Zachos (2016), Anthropogenic carbon release rate unprecedented during the past 66 million years, *Nature Geoscience*, *9*(4), 325-329.

Zoccola, D., E. Tambutté, E. Kulhanek, S. Puverel, J. C. Scimeca, D. Allemand, and S. Tambutté (2004), Molecular cloning and localization of a PMCA P-type calcium ATPase from the coral *Stylophora pistillata*, *Biochimica et Biophysica Acta*, *1663*(1-2), 117-126.